Studying α-Synuclein pathology using iPSC-derived dopaminergic neurons

Federico Zambon

Balliol College

Department of Physiology, Anatomy and Genetics University of Oxford

Hilary Term 2017

A thesis submitted for the degree of Doctor of Philosophy

Abstract

Parkinson's disease (PD) is characterised by the loss of dopaminergic neurons in the *Substantia Nigra pars compacta* in the midbrain and the presence of intracellular aggregates, known as Lewy bodies (LBs), in the surviving neurons. The aetiology of PD is unknown but a causative role for α-Synuclein (SNCA) has been proposed. Although the function of αSyn is not well understood, a number of pathological mechanisms associated with αSyn toxicity have been proposed. In this study, nine induced pluripotent stem cells (iPSCs) lines from healthy individuals and PD patients carrying the A53T *SNCA* mutation or a triplication of *SNCA* were differentiated to dopaminergic neurons (iDAn). All iPSC lines differentiated with similar efficiency to iDAn, indicating that they could be used for phenotypic analysis. Quantification of αSyn expression showed increased αSyn intracellular staining and the novel detection of increased αSyn oligomerization in PD iDAn. Analysis of mitochondrial respiration found a decrease in basal respiration, maximal respiration, ATP production and spare capacity in PD iDAn, but not in undifferentiated iPSCs, indicating the cell-type specificity of these defects. Decreased phosphorylation of dynamin-1-like protein at Ser616 ($DRP1^{Ser616}$) and increased levels of Peroxisome proliferator-activated receptor gamma coactivator 1-α (PGC-1α) in A53T *SNCA* iDAn suggest a new pathological mechanism linking αSyn to the imbalance in mitochondria homeostasis. Markers of endoplasmic reticulum (ER) stress were found to be up-regulated, along with increased β-Glucocerebrosidase (GBA) activity, perturbation of autophagy and decreased expression of fatty acids binding protein 7 (FAPB7) in PD iDAn. Lastly, lentiviral vectors for RNAi-

mediated knockdown of αSyn were developed and these reduced αSyn protein levels in iDAn, resulting in increased expression of FABP7. These results describe a novel functional link between αSyn and FABP7. This work demonstrates that iDAn are a promising and relevant *in vitro* cell model for studying cellular dysfunctions in PD pathology, and the phenotypic analysis of A53T *SNCA* and *SNCA* triplication iDAn enabled the detection of novel pathological mechanisms associated with PD.

Declaration

I confirm that the work presented in this thesis is my own and performed by the author at the University of Oxford. Where information has been derived from other sources, I confirm that this has been indicated in the thesis. This work has not been submitted for any other degree in this or any other University.

Acknowledgements

Completing a PhD is hard work and it would have been impossible without the support of many people who encouraged and challenged me, making me a better person and hopefully a better scientist.

I wish to thank my supervisors Prof Richard Wade-Martins and Dr Sally Cowley for their mentoring throughout the past 4 years and for the opportunity to join their labs and take part in a very challenging and stimulating project. Their knowledge and support have always been very valuable to push me forward to the next experiment or to make me stop and look at the results from different prospective. I also need to thank Jane, for her incredible patience in dealing with my endless requests for more cells, and Federica and Walther for generating the iPSC lines used in this work.

The Wade-Martins lab has been an amazing place to work and I have a lot of people to thank for their constant support and encouragement and for listening to me complaining everyday. Liz and Òscar, for their inspiring passion for science and all the time and patience they dedicated to me. Brent and Hugo, for discussing experiments and science, even when we totally disagreed with each other, and for sharing their knowledge with me. Becky, Charmaine, and Mang Ching for being awesome colleagues and friends, I do not know what I would have done without you. Heather, for all the discussions about experiments that did not work and how much we wished we did not choose to do a PhD with iPSCs.

And all present and past members of the lab for always being supportive and helpful, for their advices and for making every day in the lab a lot more fun: Alastair, Amy, Ben, Dana, Dayne, Gabriela, Helle, Kathie, Maria, Michele, Milena, Natalie, Nora, Ruth, Sarah, Siv and Tara.

A special thank you goes to two very important people to me. To Debora, for being my best friend and always being there for me, despite the distance. And to James for reminding me that happiness can be found even in the darkest of times, if only one remembers to turn on the light.

Last, but most importantly, I want to thank my parents Claudio and Gianna, my brother Luca and my aunt Loreta for their constant support. Even if they probably still do not known what I have been doing everyday for the past four years in a lab in Oxford, they have always made sure that I was eating properly. And to my grandparents, I wish you could all be here and I hope I have made you proud.

This past four year have changed my life so for so many reasons. I seem to have developed a love/hate relationship with science, but looking back I feel it was all worth it. I will always cherish the memories I made with all the amazing people I met in Oxford.

Publications and conference presentations

Beevers J, Lai MC, Booth HA, **Zambon F**, Parkkinen L, Vowles J, Cowley SA, Wade-Martins R, Caffrey TM. 'MAPT genetic variation alters isoform expression affecting axonal transport in iPSC-derived dopamine neurons' (Submitted for review).

Haenseler W, **Zambon F**, Lee H, Vowles J, Rinaldi F, Duggal G, Houlden H, Gwinn K, Wray S, Luk KC, Wade-Martins R, James WS, Cowley SA. 'Excess α-Synuclein compromises phagocytosis in iPSC-macrophages' (Submitted for review).

Zambon F, Booth H, Hartfield E, Fernandes H, Haenseler W, Vowles J, Cowley S, Wade-Martins R. Studying α-Synuclein pathology in A53T-*SNCA* iPSC-derived dopaminergic neurons. (Selected poster presentation). Parkinson's Diseases UK Conference 2014 - York, United Kingdom, 2014.

Zambon F, Booth H, Hartfield E, Fernandes H, Haenseler W, Vowles J, Cowley S, Wade-Martins R. Mitochondrial respiration dysfunction in A53T *SNCA* iPSC-derived dopaminergic neurons. (Selected poster presentation). Mitochondria: balancing health and disease - London, United Kingdom, 2016.

Zambon F, Ryan B, Fernandes H, Haenseler W, Vowles J, Cowley S & Wade-Martins R. Phenotypic analysis of A53T SNCA iPSC-derived dopaminergic neurons. (Selected podium presentation). Society for Neuroscience Conference 2016. San Diego, United States of America, 2016.

Table of contents

Abbreviations

$^{-/-}$ = Knock Out (also KO)
(db)cAMP= N6,2′-O-dibutyryl 3′,5′-cyclic adenosine monophosphate
αSyn= SNCA or a-Synuclein
6-OHDA= 6-hydroxydopamine
AA= Ascorbic acid
AADC= Aromatic L-amino acid decarboxylase
AAV= Adeno-associated virus
AD= Autosomal dominant or Alzheimer's disease
ANOVA= Analysis of variance
AR= Autosomal recessive
ATF4= Activating transcription factor 4
ATF6= Activating transcription factor 6
ATP= Adenosine triphosphate
BCA= Bicinchoninic acid assay
BDNF= Brain derived neurotrophic factor
BiP/GRP78= Binding immunoglobulin protein/78 kDa glucose-regulated protein
BMP= Bone morphogenetic proteins
cAMP= Cyclic adenosine monophosphate
CBE= Conduritol B epoxide
CHOP= C/EBP homologous protein
CMA= Chaperone-mediated autophagy
CMV= Cytomegalovirus
CNS= Central nervous system
CNV= Copy number variant
CoxI= Complex I (mitochondria)
cPPT= Central polypurine tract
CRISPR= Clustered regularly interspaced short palindromic repeat
CSPα= Cysteine string protein α
DA= Dopamine
DAn= Dopaminergic neurons
DAPT= N-[N-(3,5-difluorophenacetyl-L-alanyl)]-(S)-phenylglycine t-butyl ester
DAT= Dopamine transporter
DBS= Deep brain stimulation
ddH2O= Double distilled H_2O

DIV= Days *in vitro*
DLB= Dementia with Lewy bodies
DMEM= Dulbecco modified Eagle's medium
DMSO= Dimethyl sulfoxide
DNA= Deoxyribonucleic acid
DNAse= Deoxyribonuclease
DRP1= Dynamin-1-like protein
dsRNA= Double stranded RNA
EB= Embryoid body
ECAR= Extracellular acidification rate
eF1α= Elongation factor 1-α
eFI2a= Eukaryotic translation initiation factor 2a
eGFP= Enhanced green fluorescent protein
eoPD= Early onset Parkinson's disease
ePhys= Electrophysiology
ER= Endoplasmic reticulum
ERAD= Endoplasmic reticulum associated degradation
ESC= Embryonic stem sell
ETC= Electron transport chain
EtOH= Ethanol
FA= Fatty acid
FABP= Fatty acid-binding protein
FACS= Fluorescence-activated cell sorting
FBS= Fetal bovine serum
FCCP= p-triflouromethoxyphenylhydrazone
FGF8a= Fibroblast growth factor 8a
FOXA2= Forkhead box A2
FP= Floor plate
GBA= β-Glucocerebrosidase
gDNA= Genomic DNA
GDNF= Glia derived neurotrophic factor
GIRK2= G protein-coupled inwardly-rectifying potassium channel
GSK3β= Glycogen synthase kinase 3β
GWAS= Genome-wide association study
HIV-1= Human immunodeficiency virus type 1
HSC70= Heat shock 70 kDa protein 8
iDAn= iPSC-derived dopaminergic neurons
iPD= Idiopathic Parkinson's disease
iPSC= Induced pluripotent stem cell
IRE1α= Inositol-requiring enzyme 1α
KD= Knock-down

kDa= kilo dalton
KO= Knock out (also $^{-/-}$)
L-DOPA= 3,4-dihydroxy-L-phenylalanine
LAMP1= Lysosomal-associated membrane protein 1
LAMP2A= Lysosome-associated membrane protein 2a
LB= Lewy body
LMX1A= LIM homeobox transcription factor 1α
LN= Lewy neurite
LRRK2= Leucine-rich repeats kinase 2
LTR= Long terminal repeat
LV= Lentivirus
MAO= Monoamine oxidase A
MAPT= Microtubule-associated protein tau
MEF= Mouse embryonic fibroblast
MEF2C= Myocyte-specific enhancer factor 2C
MeOH= Methanol
miRNA= MicroRNA
MOI= Multiplicity of infection
MPP^+= 1-methyl-4-phenylpyridinium
MPPP= 1-methyl-4-phenyl-4-propionoxypiperidine
MPTP= 1-methyl-4-phenyl-1,2,3,6-tetrahydropyridine
mRNA= Messenger RNA
MSA= Multiple system atrophy
NAC= Non-amyloid β component
NAD+/NADH= Nicotinamide adenine dinucleotide (oxidised/reduced)
NADP+/NADPH= Nicotinamide adenine dinucleotide phosphate (oxidised/reduced)
NPC= Neuronal progenitor cell
OCR= Oxygen consumption rate
p62= Ubiquitin-binding protein p62
PCR= Polymerase chain reaction
PD= Parkinson's disease
PDI= Protein disulfide isomerase
PGC-1α= Peroxisome proliferator-activated receptor gamma coactivator 1-α
PINK1= PTEN-induced putative kinase 1
PITX3= Pituitary homeobox 3
PLA= Proximity ligation assay
PolyA= Polyadenylation sequence
Pre-miRNA= Precursor miRNAs
Pri-miRNA= Primary miRNA
PTM= Post-translational modification
PUFA= Polyunsaturated fatty acids

PVDF= Polyvinylidene difluoride
RBD= REM sleep behavior disorder
REM= Rapid eye movement
RISC= RNA-induced silencing complex
RNA= Ribonucleic acid
RNAi= RNA interference
RNApolII= RNA polymerase II
RNApolIII= RNA polymerase III
RNAse= ribonuclease
ROCK= Rho-associated protein kinase
ROCKi= ROCK inhibitor (Y-27632)
ROS= Reactive oxygen specie
rpm= Rotations per minute
RRE= Rev response elements
rRNA= Ribosomal RNA
RT= Room remperature
SEM= Standard error of the mean
sgRNA= Single guide RNA
SHH= Sonic hedgehog
shRNA= Short hairpin RNA
siRNA= Small interfering RNA
SNARE= Soluble NSF attachment protein receptor
SNAP-25= Synaptosome associated protein 25
SNCA= αSyn or α-Synuclein
SNP= Single nucleotide Polymorphism
SNpc= Substantia Nigra pars compacta
SOC= Super Optimal Broth
ssRNA= Single stranded RNA
TGFβ3= Transforming growth factor β-3
TH= Tyrosine hydroxylase
ThS= Thioflavin S
ThT= Thioflavin T
tRNA= Transfer RNA
TUJ1= β3-tubulin
UPR= Unfolded protein responce
UTR= Untranslated region
VAMP2= Vesicle-associated membrane protein 2
VMAT2= Vesicular monoamine transporter 2
vmDAn= Ventral midbrain dopaminergic neurons
VTA= Ventricular tegmental area
VAMP2= Vesicle-associated membrane protein 2

XBP1= X-box binding protein 1

x *g*= Relative centrifugal force expressed in units of gravity

List of figures

List of tables

Chapter 1

Introduction

1.1|Parkinson's Disease

1.1.1|Introduction

Parkinson's Disease (PD) is the second most common neurodegenerative disorder with adulthood onset (Lars and Rudolph 2005). It was first described by James Parkinson in 1817 in his essay entitled *"An essay on the shaking palsy"*, where he detailed the characteristic involuntary tremors of the limbs and bradykinesia with no apparent loss of senses and intellect. Although cases of juvenile PD have been reported, the disorder develops less frequently under 50 years of age, whilst the risk significantly increases over 60 (de Lau and Breteler 2006). Early symptoms are generally misinterpreted for ageing, leading to a 2-3 years delay between onset and diagnosis (Lees, Hardy, and Revesz 2009). Although first described two centuries ago, there is still no cure or reliable biomarker for PD and the aetiology is unknown (Dauer and Przedborski 2003). A study published in 1995 based on the elderly population in the Netherlands suggested that the overall disease's prevalence in the population was 1.4%, with a gradual increase from 0.3% for people between 55 and 64 years of age up to 5% in the female population aged 95 to 99 (Rijk et al. 1997). The increase in longevity, especially in industrialised countries, has the effect of incrementing the economic burden towards the treatment of PD. Data gathered from PD clinics in Germany reported that in 1995 the average cost of a PD patient upon diagnosis was about

£750 ($1,130) per annum, accompanied by several patients who progressively stopped working with disease worsening despite L-DOPA treatment. Based on PD prevalence, the disease was estimated to cost about $2 billion annually in medical bills in Germany alone (Dodel et al. 1998). It is forecast that by 2030 between 8.7 and 9.3 million individuals over 50 years of age will be diagnosed with PD worldwide (Dorsey et al. 2007). PD is a debilitating and costly pathology and it is therefore essential to understand the early pathological mechanisms that cause its onset to develop effective treatments.

This section aims to discuss PD pathology from the genetics to the pathological and clinical phenotype, to put it into context with the study of its pathological mechanisms using iPSC-derived dopaminergic neurons.

1.1.2|Pathological and clinical features

One of the hallmarks of PD is the selective loss of dopaminergic neurons (DAn) in the *Substantia nigra pars compacta* (*SNpc*) in the midbrain. This loss of dopaminergic innervation from the midbrain to the dorsal striatum, a part of the brain that primarily coordinates motor function, is responsible for the motor symptoms of PD (Dauer and Przedborski 2003). Genetic and toxin-based PD animal models support this feature and are characterised by a selective loss of DAn in the *SNpc* (Janezic et al. 2013; Lo Bianco et al. 2002; Tatton and Kish 1997; Betarbet et al. 2000; Manning-Bog et al. 2003). Historically, DAn were identified by immunohistochemistry for the expression of key enzymes for dopamine (DA) metabolism such as tyrosine hydroxylase (TH) and aromatic amino acid decarboxylase (AADC). DA is synthesised from tyrosine in the form of L-DOPA by TH and then converted to DA by AADC; DA then accumulates inside neurotransmitter vesicles via the vesicular monoamine transporter 2 (VMAT2) and is then, once released, taken up by the DA transporter (DAT) on the cell surface (Venda et al. 2010). The midbrain contains

two major groups of DAn: A9 neurons in the *SNpc* which project to the striatum and A10 neurons in the ventral tegmental area (VTA) which project to limbic and cortical areas. DAn in the midbrain are also characterised depending on their morphology and protein expression: A10 neurons are rounder in shape, express the calcium binding protein, Calbindin, and have low levels of DAT; conversely, A9 neurons are more densely packed, calbindin-negative and uniquely express the inward rectifier potassium channel GIRK2 (Björklund and Dunnett 2007). Among all the different subpopulations of DAn, the most affected by PD are the A9 neurons, whereas A10 neurons are less implicated (German et al. 1989; McRitchie, Cartwright, and Halliday 1997; Uhl, Hedreen, and Price 1985). DA depletion caused by the neurodegeneration of the *SNpc* is found to be most striking in the putamen in the dorsal striatum (Kish, Shannak, and Hornykiewicz 1988). As a consequence, at the onset of motor symptoms, when ~60% of the DAn in the *SN*pc have been lost, a depletion of ~80% of striatal DA content has occurred (Dauer and Przedborski 2003).

Another hallmark of PD is the presence of intracellular inclusions in the surviving neurons, termed "Lewy bodies" (LBs). These are spherical and eosinophilic protein aggregates found in all PD affected brain regions and mostly composed of the protein α-Synclein (αSyn) (Spillantini et al. 1997; Spillantini et al. 1998). Lewy neurites (LNs) have also been described as αSyn inclusions found in the neurites, as compared to LBs (Braak et al. 1999), which could be part of an early pathological stage since they are present in patients that have yet to develop LBs (Braak et al. 2003). Other proteins have been found in LBs, including ubiquitin (Spillantini et al. 1997), 14-3-3 proteins (Kawamoto et al. 2002), heat shock cognate 71 kDa protein (HSC70) (Leverenz et al. 2007), ER stress markers (Slodzinski et al. 2009) and GBA (Goker-Alpan et al. 2010). Independent reports have also suggested that tau, a protein heavily implicated in Alzheimer's disease, and its

phosphorylated forms may co-localise with αSyn in LBs, especially at their periphery (Arima et al. 1999; Ishizawa et al. 2003). Nevertheless, PD is not the only neurodegenerative disorder characterised by αSyn inclusions, since these have been documented in Dementia with Lewy Bodies (DLB) and Multiple System Atrophy (MSA) cases. This notion led researchers to collectively refer to neurodegenerative disease affected by α-Synuclein (SNCA or αSyn) pathology as synucleinopathies (Spillantini and Goedert 2000).

Even though PD is generally described as a disease characterised by the loss of DAn in the *SNpc*, this is an incomplete assumption. The pathology extends to virtually the whole brain, especially in the later stages of the disease, which accounts for a variety of non-motor symptoms in PD, as described by Braak and colleagues. It is thought that the pathology begins in the olfactory bulb at the stages 1 and 2, which can precede by a few years the onset of motor symptoms, with patients reporting impaired sense of smell long before diagnosis. Stages 3 and 4 follow that with the development of pathology in the basal ganglia, particularly with αSyn pathology in the *SNpc*. At these stages, LBs and LNs can be detected in PD patients and this coincides with the onset of motor symptoms. Lastly, stages 5 and 6 concur with the involvement of cortical areas and limbic structures that can underlie the appearance of impaired cognition, which is more common in the later stages of the disease (Braak et al. 2003). Recently, work by Roberts and colleagues described a technique based on the Proximity Ligation Assay that allows the discrimination of αSyn oligomers from monomeric or fibrillar species (αSyn PLA). For the first time, this work gave new insights into previously undetected pathology in brain regions of PD patients that were thought to be only mildly affected by the disease, like the cingulate cortex and medulla (Roberts, Wade-Martins, and Alegre-Abarrategui 2015).

The most common clinical symptom is motor dysfunction, which includes tremors

at rest, postural instability, rigidity and bradykinesia that arise as a consequence of the loss of DAn in the *SNpc* and dopaminergic innervation in the striatum (Jankovic 2008). Non-motor symptoms include autonomic nervous system dysfunction, for example cardiovascular or gastrointestinal manifestations, rapid eye movement disorders (REM), dementia, hyposmia, anxiety and depression (Dickson et al. 2009). Non-motor symptoms can precede the onset of PD diagnosis by up to four decades and predominantly do not respond to treatments that are effective for motor symptoms (Meissner 2012). Dementia was found to be present in ~40% of the PD patients and psychological assessments found that various other cognition and intellect impairments are very common. Recent studies involving patients affected by REM sleep behaviour disorder (RBD) have found them to be more prone to develop neurodegenerative diseases, especially synucleinopathies, including PD and DLB. RBD is thought to be the palindromic stage of these diseases and these patients are important for early intervention or disease modifying strategies, especially for PD (Iranzo et al. 2014; Dos Santos, Barreto, and Kohlmeier 2014). Overall, clinical diagnosis is generally done after the onset of the disease, when ~60% of the neurons are already lost (Dauer and Przedborski 2003; Fearnley and Lees 1991) and can only be confirmed by *post-mortem* examination.

1.1.3|The genetic basis of Parkinson's Disease

Over the past 20 years, rare single nucleotide mutations and copy number variants have been linked to PD. They account for 3-5% of the sporadic cases, compared to about 30% of the familial forms (Klein and Westenberger 2012). Loci of PD-related genes have been historically labelled *PARK* genes and chronologically numbered. The initial discovery of most of the genes linked to PD was done via genetic linkage analysis of kindreds identified by a familial aggregation of the disease and subsequent confirmation by sequencing; this

led to the discovery of rare but highly penetrant mutations. Alternatively, most recent discoveries utilised exome or whole-genome sequencing and genome wide association studies (GWAS) to identify even rarer polymorphisms or variants between control and patient groups (Trinh and Farrer 2013).

To date, between 13 and 18 *PARK* loci have been identified, although only five have been confirmed as pathogenic for PD. Some discrepancies arise from the fact that some loci were either erroneously labelled, like in the case of *PARK4*, or others have not been confirmed or replicated in subsequent studies (Klein and Westenberger 2012; Lesage and Brice 2009) (Table 1.1).

Gene	Locus	PARK	Protein	Function	Inheritence	Pathology	Identification	Remarks
SNCA	4q21-22	1	αSyn	*Chaperone for SNARE proteins*	AD	eoPD	Linkage analysis	Point mutations, CNVs and Rep1
Parkin	6q25.2-q27	2	Parkin	E3 ubiquitin ligase (mitophagy)	AR	eoPD	Linkage analysis	Nonsense, missense, splice site mutations & insersions/deletions
Unknown	*2p13*	*3*				*iPD*	*Linkage analysis*	
SNCA	4q21-q23	4	αSyn		AD	eoPD	Linkage analysis	Erroneous labelling, identical to *PARK1*
UCHL1	4p13	5	UCHL1	Deubiquitinating enzyme		PD	Candidate gene	
PINK1	1p35-p36	6	PINK1		AR	eoPD	Linkage analysis	Missense or nonsense
DJ-1	1p36	7	DJ-1	Ser/Thr-protein kinase (mitophagy)	AR	eoPD	Linkage analysis	Point mutations or exons deletions
LRRK2	12q12	8	LRRK2	*Kinase with GTPase activity*	AD	iPD	Linkage analysis	More than 50 point mutations
ATP13A2	1p36	9	ATP13A2	(Putative) P-type transport ATPase	AR	KRS & PD	Linkage analysis	Homozygous and compound heterozygous
Unknown	*1p32*	*10*			*RF*	*iPD*	*Linkage analysis*	
Unknown	*2q36-27*	*11*				*loPD*	*Linkage analysis*	
Unknown	*Xq21-q25*	*12*			*RF*	*iPD*	*Linkage analysis*	
HTRA2	2p12	13	HtrA2	Serine protease (mitochondria dependent apoptosis)	RF	iPD	Candidate gene	
PLA2G6	22q13.1	14	PLA2G6	Ca-independent phospholipase A2 (Fatty acids metabolism)	AR	eoPD	Linkage analysis	Homozygous and compound heterozygous
FXBO7	22q12-q13	15	FXBO7	F-box-containing *protein*	AR	eoPD	Linkage analysis	Truncation, Homozygous and compound heterozygous
Unknown	*1q32*	*16*			*RF*	*iPD*	*GWAS*	
VPS35	16q11.2	17	VSP35	Retrograde transport of proteins from endosomes to the trans-Golgi network (retromer complex)	AD	iPD	Exome sequencing	Point mutations
EIF4G1	3q27.1	18	EIF4G1	*mRNA processing*		iPD	Linkage analysis	
GBA	1q22	NA	GBA	Glycolipid metabolism	RF	iPD	GWAS	Heterozygous GD-associated mutations
MAPT	17q21.31	NA	Tau	Microtubules stabilisation	RF	iPD	GWAS	H2 haplotype is protective

Table 1.1|List of genes and proteins proposed to be associated with PD

AD= Autosomal Dominant; AR= Autosomal Recessive; eoPD= early onset PD; iPD= idiopathic PD; PD= Parkinson's Disease; KRS= Kufor–Rakeb Syndrome; GWAS= Genome-Wide Association Study; CNV= Copy Number Variation; GD= Gaucher's Disease; RF= Risk Factor.

The two most common autosomal dominant (AD) genes associated with PD are *SNCA* and *LRRK2*, characterised by early-onset (eoPD) or typical PD respectively. The *SNCA* locus (*PARK1*- 4q21-q23) was the first to be associated to PD in 1997 in an Italian kindred with a family history of PD (Polymeropoulos et al. 1996). Following that, multiple reports have described rare point mutations causing eoPD: A53T (Polymeropoulos et al. 1997), A30P (Krüger et al. 1998), E46K (Zarranz et al. 2004), H50Q (Appel-Cresswell et al. 2013; Proukakis et al. 2013), G51D (Lesage et al. 2013) and A53E (Petra et al. 2014; Pasanen et al. 2014). Furthermore, copy number variants (CNVs) are now known to cause PD, including duplications (Chartier-Harlin et al. 2004; Ibáñez et al. 2004) and triplications (Singleton et al. 2003; Olgiati et al. 2015). CNVs in the *SNCA* gene seem to be predominantly characteristic of Asian PD patients, whereas point mutations are over-represented in individuals with a Caucasian background (Nuytemans et al. 2010). Mutations in the *LRRK2* (*PARK8*) gene have been described to cause mid-to-late onset PD with a slow progression and represent the most common cause among familial PD cases. The frequency of these mutations seems to depend on the ethnic background, ranging from 1% worldwide to 20% and 40% in the Arab and Ashkenazi Jewish population respectively (Nuytemans et al. 2010). The first linkage of the *LRRK2* locus (PARK 8 - 12p11.2-q13.1) with PD was described in 2002 in a Japanese family with an autosomal dominant form of the disease closely resembling iPD (Funayama et al. 2002). Subsequently, various *LRRK2* mutations were described in 46 families, including I2020T and R1441C (Zimprich et al. 2004). Afterwards, the G2019S mutation was found to be present in 1.6% of sporadic PD patients (Gilks et al. 2005). Due to the presence of 51 exons in *LRRK2*, more than 50 different missense and nonsense mutations have been reported to date (Nuytemans et al. 2010).

The three most studied and characterised PD genes with autosomal recessive (AR)

inheritance are *PRKN* (*PARK2* - 6q26), *PINK1* (*PARK6* - 1p35-36) and *DJ-1* (*PARK7* - 1p36). The *PRKN* (*PARK2*) locus was first described in a consanguineous Japanese family with autosomal recessive juvenile PD in 1998 and mutations in this gene are now known to be the most common cause of juvenile PD (Kitada et al. 1998; Klein and Westenberger 2012). They are also quite heterogeneous with nonsense, missense or splice site mutations and insertions/deletions spanning the entire locus, and are over-represented among patients of Asian and Latin-American genetic background (Nuytemans et al. 2010). In a screen for *PARK2* mutations in eoPD patients in an European cohort, mutations in the *PARK6* were identified instead (Valente et al. 2001). *PINK1 (PARK6)* mutations are the second most common cause of eoPD and, contrary to *PARK2*, are often either missense or nonsense (Klein and Westenberger 2012) and generally evenly distributed among different ethnic groups (Nuytemans et al. 2010). Lastly, *DJ-1* (PARK7) mutations only account for 1-2% of eoPD with only a few point mutations or exon deletions reported to date (Klein and Westenberger 2012) and they appear to be more common in the Asian population (Nuytemans et al. 2010).

The latest GWAS or exome sequencing studies have vastly contributed to the association of new loci or single nucleotide polymorphisms (SNPs) with PD. In 2009, two independent studies applied a GWAS approach to the study of genetic risk factors for PD in a Japanese and European cohort. *SNCA* (αSyn) and *MAPT* (tau) loci were strongly associated with PD in both studies (Simón-Sánchez et al. 2009; Satake et al. 2009). Data from recent large-scale meta-analysis studies further confirmed the association of *SNCA* and *MAPT* and identified *GBA* as a PD risk gene (Nalls et al. 2014; Pankratz et al. 2012). Interestingly, the association of *MAPT* and *GBA* with the disease at the GWAS scale corroborated previous reports indicating that the H1 *MAPT* haplotype is a PD risk factor (Vandrovcova et al. 2009), whereas *GBA* heterozygous mutations are common among

sporadic PD patients (Sidransky et al. 2009). Overall, the heterozygous N370S and L444P mutations in *GBA* are the most common, especially in Ashkenazi Jewish patients, and are characterised by early onset and atypical PD (Sidransky et al. 2009). Mutations in *GBA* were found in ~4% of the cases in a British PD patients cohort characterised by the early onset of the disease, αSyn pathology and dementia (Neumann et al. 2009).

Lastly, recent reports associated other genes with monogenic forms of PD or Parkinsonism and include: *PARK9* (*ATP13A2*), *PARK14 (PLA2G6)* and *PARK15* (*FBXO7*) and *PARK17* (*VPS35*). *ATP13A2* mutations are associated with Kufor-Rakeb syndrome, a neurodegenerative disorder characterised by eoPD with pyramidal degeneration and dementia (Ramirez et al. 2006). Gene mapping and mutation analysis found an association between *PLA2G6* with a Parkinson-like syndrome in patients with adult-onset, affected by dystonia-parkinsonism, involvement of the pyramidal tracts and cerebral and cerebellar atrophy (Paisan-Ruiz et al. 2009). Recessive mutations in *FBX07,* in the form of truncation or compound heterozygous mutation, were shown to cause neurodegeneration in an Italian and Dutch family. The pathology had an early onset of Parkinsonism, affected the extrapyramidal and pyramidal tracts and L-DOPA treatment had variable effect (Di Fonzo et al. 2009). Lastly, autosomal dominant *VPS35* point mutations were described in a Swiss family affected by late-onset PD that was responsive to L-DOPA treatments (Vilariño-Güell et al. 2011).

1.1.4|Aetiology

The aetiology of PD is still not well understood, despite insights from both the genetics and environmental clues. Apart from the monogenic cases and genetic risk factors, it is likely that PD onset is a result of a complex interaction between the exposure to environmental causative agents and a predisposition at the genetic level. Above all, ageing is the biggest

risk factors for PD, probably because most of the intracellular mechanisms aiming to govern cellular homeostasis decrease in their efficiency with age (Reeve, Simcox, and Turnbull 2014). In 1979, a drug abuser who accidentally had an intravenous injection of 1-methyl-4-phenyl-1,2,3,6-tetrahydropyridine (MPTP) instead of the opioid 1-methyl-4-phenyl-4-propionoxy-piperidine (MPPP) developed symptoms closely resembling those of PD. The patient was responsive to treatments aimed at stimulating DA receptors and a *post-mortem* analysis revealed neuronal loss in the *SNpc* (Davis et al. 1979). In 1983, another report on four individuals found the same pathological hallmarks as a consequence of this drug abuse (Langston et al. 1983). Since then, other studies reported how particular drugs or toxins can induce symptomatology very similar to PD. These agents were found to be common among pesticides and cause mitochondrial dysfunction and oxidative stress (Tanner et al. 2011). One of these agents, Rotenone, an insecticidal/pesticidal chemical that causes inhibition of mitochondrial complex I activity, was found to be a risk factor for developing PD from both environmental or occupational exposure in the US population (Dhillon et al. 2008). Chronic exposure to Rotenone in rats was later found to cause degeneration of nigrostriatal dopaminergic neurons and accumulation of cytoplasmic inclusions composed of αSyn (Betarbet et al. 2000). Exposure to the herbicide Paraquat, another mitochondrial inhibitor, was reported to be associated with the development of PD (Liou et al. 1997) and later shown to cause neurodegeneration of dopaminergic neurons and accumulation of αSyn in mice (Manning-Bog et al. 2003). Exposure to metals, especially from occupational sources, has been investigated as a PD risk factor as well. Independent studies have shown that chronic exposure to copper, manganese or iron is a risk factor for PD (Gorell et al. 1997; Aschner et al. 2009). Although being a negative association, cigarette smoke was associated with a reduced incidence of PD, both among current and past smokers (Checkoway et al. 2002). However, no clear effect was detected

on disease progression between smoking and non-smoking PD patients (Alves et al. 2004). Caffeine consumption was not shown to segregate PD patients from healthy controls (Checkoway et al. 2002) but it might improve PD symptoms (Postuma et al. 2012; Prediger 2010).

1.1.5|Current and future treatments

So far, the only available treatments for PD aim to ameliorate the symptoms but do not halt the progression of the disease. The most common drug treatment is the administration of levodopa (L-DOPA) to replenish DA levels in the striatum. L-DOPA supplementation bypasses TH and gets converted to DA by AADC. However, since the introduction of this drug, various side effects have been reported (Barbeau 1969). High doses of L-DOPA can increase the risk of levodopa-induced dyskinesia and ultimately affect quality of life for PD patients (Thanvi, Lo, and Robinson 2007). Dyskinesia is thought to be caused by the intermittent administration and effect of L-DOPA, which in turn causes stimulation of DA receptors in the brain in a non-physiological dosage and manner (Bibbiani et al. 2005). Since DA is degraded by monoamine oxidase (MAO) *in vivo*, MAO inhibitors are often used as adjunctive therapy together with L-DOPA. The two most common molecules are rasagiline and selegiline and were also shown to have disease-modifying effects on their own, making them an even more attractive therapy (Fernandez and Chen 2007).

One of the alternatives to the pharmacological treatment of PD is deep brain stimulation (DBS) that works by the implantation of a stimulating electrode in the globus pallidus or subthalamic nucleus; this aims to disrupt the unbalanced neuronal activity that triggers PD motor symptoms. Moreover, DBS allows a lower dosage of L-DOPA together with a reduced rate of dyskinesia onset (Breit, Schulz, and Benabid 2004). Despite DBS decreasing PD symptoms, as any other therapy for PD, it still does not halt the progressive

degeneration of neurons in the patient brains (Shulman, De Jager, and Feany 2011).

Techniques and studies concerning grafting of DAn from human embryonic brains started to become popular towards the end of the twentieth century, mostly to overcome the side effects of L-DOPA. Pioneering work done by Lindvall and colleagues at the University of Lund (Sweden) showed the proof of principle whereby patients who received a graft displayed modest improvements in their speed of movements and the magnitude of the effect of L-DOPA (Lindvall et al. 1989). Upon refinement of the procedure, four new patients displayed an improvement starting from 6 weeks post-grafting that remained stable after 1 year (Lindvall et al. 1992). Since then, numerous clinical trials of PD cell-therapy have been undertaken but with variable results. This is mostly due to the presence of placebo effects among patients receiving L-DOPA, the variability in the length of the follow-ups post-grafting, the difference in age and stage of the disease among the patients and ultimately the fact that some patients developed graft-induced dyskinesia (Barker et al. 2013). One of the major drawbacks of this treatment came from long-term follow-ups reporting the presence of pathology in grafted neurons. At a *post-mortem* examination fourteen years post-transplant, a patient displayed a loss of DAT immuno-reactivity alongside the presence of aggregated αSyn in the grafted neurons (Kordower et al. 2008). Despite the initial survival and the innervation of the grafted neurons in the host putamen, evidence pointed towards spreading of the disease to the grafted cells and the onset of pathological hallmarks that were indistinguishable from those found in the host *SNpc* (Li et al. 2008). This pioneered the idea that αSyn pathology could spread from host-to-graft in a prion-like fashion (Luk et al. 2009; Masuda-Suzukake et al. 2013).

Since the advent of the induced pluripotent stem cell (iPSC) technology, much effort has been put into developing procedures for autologous iPSC-derived neurons transplantation. So far, cross-species transplants of human cells into PD animal models

have proven to be effective. Work done in the Studer laboratory demonstrated the applicability of grafts of embryonic stem cells (ESC)-derived ventral midbrain DAn precursors in animal models of PD. The transplanted neurons formed grafts containing $TH^+/FOXA2^+$ cells that were able to functionally rescue 6-hydroxy dopamine (6-OHDA) lesions in mouse, rat and monkey (Kriks et al. 2011). Similarly, a study by Kirkeby and colleagues found that, upon optimisation of the differentiation protocol for the patterning towards ventral midbrain neurons, human iPSC-derived DAn were successfully transplanted in the striatum of adult rats. These neurons displayed identical morphology, projections and expression profile as the human fetal midbrain neurons grafted alongside (Kirkeby et al. 2012). Recently, autologous iPSC-derived DAn were successfully transplanted into non-human primates and were shown to survive for at least one year without immune-suppression (Sundberg et al. 2013). Similarly, functional improvement was reported upon autologous transplant in a MPTP non-human primate model (Hallett et al. 2015). Nevertheless, tumorigenicity is probably the biggest hurdle for this type of approach, especially for iPSCs. Refinement of reprogramming techniques, especially with the aim of avoiding the use of oncogenes during the reprogramming and generating cells that more closely resemble ESCs, will be essential (Ben-David and Benvenisty 2011).

1.2|α-Synuclein

1.2.1|Introduction

It is widely accepted that the protein α-Synuclein (SNCA or αSyn) has a central role in Parkinson's Disease (PD). Mutations and copy number variants in the *SNCA* gene encoding for the protein αSyn are linked to PD, whereas GWASs have repeatedly reported this locus as the strongest risk factor. The hallmark of PD cellular pathology is the accumulation of misfolded αSyn in DAn in the form of LBs, both in sporadic and familial cases (Spillantini et al. 1997). The aetiology of PD is still not well understood but evidence for a causative role for αSyn suggests a wide involvement in the disease.

This section reports the relevant experimental evidence regarding αSyn function and dysfunction in both health and PD. This will be applicable in the context of studying iPSC-derived DAn (iDAn) carrying mutations or copy number variants in the *SNCA* gene and the pathological mechanisms associated with αSyn. It is also important to consider and discuss what has already been reported in the field using iDAn to highlight common or divergent pathological mechanisms. There is a continuum in αSyn involvement in PD, from the genetics to the specific cell type that is most vulnerable in the disease and the putative intracellular roles and partners for this protein. It is important to keep in mind all the aspects regarding this protein that we know very little about and yet is cardinal in PD.

1.2.2|Architecture, splicing and genetics of the *SNCA* locus

The *SNCA* gene is situated on chromosome 4 (4q21-q23) and was the first genetic locus associated to PD via genetic linkage studies of a kindred showing autosomal dominant transmission of the disease (Polymeropoulos et al. 1996). The full length transcript

(SNCA-140) contains all six exons of *SNCA* (Uéda et al. 1993), whereas the differential splicing of exon 3 and 5 causes in-frame deletions and results in the expression of the shorter isoforms SNCA-112 (-ex3), SNCA-126 (-ex5) and SNCA-89 (-ex3 and -ex5) (Beyer et al. 2008). In the promoter region of *SNCA* (~10 kb upstream of the translation start site) lays a polymorphic micro-satellite (Rep1) with a mixed sequence repeat that was firstly associated with Alzheimer's disease (Xia, Rohan de Silva, et al. 1996) and subsequently confirmed as a PD risk factor (Farrer, Maraganore, and Lockhart 2001; Krüger and Vieira-Saecker 1999). More recently, a large-scale analysis showed how the 263 bp allele of Rep1 is associated with an increased risk of PD, compared to the 259 bp, but does not change the age of onset. Overall, the Rep1 allele variability in *SNCA* could explain up to 3% of PD risk in the general population, indicating that this locus is not solely linked to PD in a rare autosomal dominant fashion (Maraganore, Andrade, and Elbaz 2006). Increasing lines of evidence also suggest that polymorphisms in the 3' region of *SNCA* are associated with PD and could affect αSyn expression (Mueller et al. 2005; McCarthy et al. 2011). Recent work used CRISPR/Cas9 gene editing to generate isogenic ESC lines to study the effect of GWAS hits on the *SNCA* gene and evaluate their effect on αSyn expression in ESC-derived neurons. A single nucleotide polymorphism (SNP) in the enhancer in intron-4 of *SNCA* was shown to regulate αSyn expression, with the risk variant associated to the G allele, whereas Rep1 was reported to have no effects (Soldner et al. 2016).

In the last two decades, many point mutations and copy number variants of *SNCA* have been linked to PD. The *SNCA* locus was first linked to PD in 1996 in a large Italian kindred with familial history of the disease with early onset (Polymeropoulos et al. 1996). The following year, sequencing of the fourth exon of *SNCA* found a single base pair change (G to A), creating an alanine to threonine (A53T) amino acid change in the protein sequence, in the same family and three other unrelated kindreds of Greek origin with

familial PD (Polymeropoulos et al. 1997). Since then, other point mutations and copy number variants of this locus have been linked to PD. A G to C mutation in exon 3 causing an alanine to proline mutation (A30P) was found in patients of a family of German origin with PD history (Krüger et al. 1998) and a mutation from G to A causing the replacement of glutamic acid to lysine residues (E46K) was described in a Spanish family affected by PD (Zarranz et al. 2004). Recently, three novel *SNCA* mutations have been reported. A mutation in exon 4 causing the H50Q substitution was reported in a patient with familial history of L-DOPA responsive PD (Proukakis et al. 2013). Exome sequencing of three PD patients found a single base change causing the G51D mutation that was associated with early onset and death within a few years, with pathology extending beyond the basal ganglia to the pyramidal tract (Lesage et al. 2013). Lastly, the A53E mutation was described in a Finnish patient displaying both PD and multiple system atrophy (MSA) and extensive αSyn pathology in both neurons and glia (Pasanen et al. 2014). Copy number variants of the *SNCA* locus have also been linked to PD, including duplications (Chartier-Harlin et al. 2004; Ibáñez et al. 2004) and triplications (Singleton et al. 2003; Olgiati et al. 2015), indicating that gene dosage can also play an important role in PD aetiology.

Analysis of data from the Human Expression Atlas (ebi.ac.uk) shows that *SNCA* expression is at its highest in the brain but can also be readily detected in red blood cells (Miller et al. 2004). αSyn is expressed in most of the brain regions accounting for up to 1% of the total proteins in the brain (Iwai et al. 1995) and has been reported to be expressed, or at least in the case of PD patients, in the enteric nervous system (Shannon et al. 2012). RNA sequencing data of different cell types within the brain showed that neurons are by far the cell type that expresses the most total *SNCA* transcripts, followed by oligodendrocyte precursors cells and to a lesser extent astrocytes and microglia (Zhang et al. 2014). Lastly, iPSCs but not ESCs express αSyn (Woodard et al. 2014; Nguyen et al. 2011).

1.2.3|Structure of αSyn

αSyn is a 140 amino acid protein (Uéda et al. 1993) originally discovered as a neuron-specific peptide in the neuromuscular junction of the electric eel (Maroteaux, Campanelli, and Scheller 1988) and as a soluble presynaptic protein implicated in the process of song learning in zebra finch (George et al. 1995). Together with the other two isoforms β and ɣ, αSyn has been described only in vertebrates, with a highly conserved sequence across species (George 2002). It is interesting to note that, apart from humans and very few primates, the A53T substitution is the normal residue in vertebrates and sits in an otherwise well conserved amino acid sequence across species (Hamilton 2004). Neither invertebrates nor single cell organisms, often used as genetic models in PD, display any Synuclein homologues suggesting that it has not evolved as a protein with a crucial cellular function.

The primary structure of αSyn can be divided into three regions: (i) the N-terminus domain comprising the amino acids 1-60; (ii) a central portion between the residues 61 and 95; (iii) the C-terminus composed of the residues 96-140 (Figure 1.1A). The N-terminus sequence is characterised by the presence of five 11 amino acid repeats with the consensus motif KTKEGV (Figure 1.1C). It is also the portion of the protein where all the PD-associated point mutations cluster (A30P, E46K, H50Q, G51D and A53T/E) (Figure 1.1B). The central region of the protein contains two more KTKEGV repeats and a highly hydrophobic stretch of amino acids, known as a non-amyloid component (NAC), named after being purified from amyloid plaques in Alzheimer's disease patient brains (Uéda et al. 1993) (Figure 1.1A,C), which is indispensable for αSyn aggregation (Giasson et al. 2001). Lastly, the C-terminus of αSyn is enriched with negatively charged residues (Giasson et al. 2001) and these are thought to counterbalance the effect of the NAC region on αSyn protein aggregation (Murray et al. 2003).

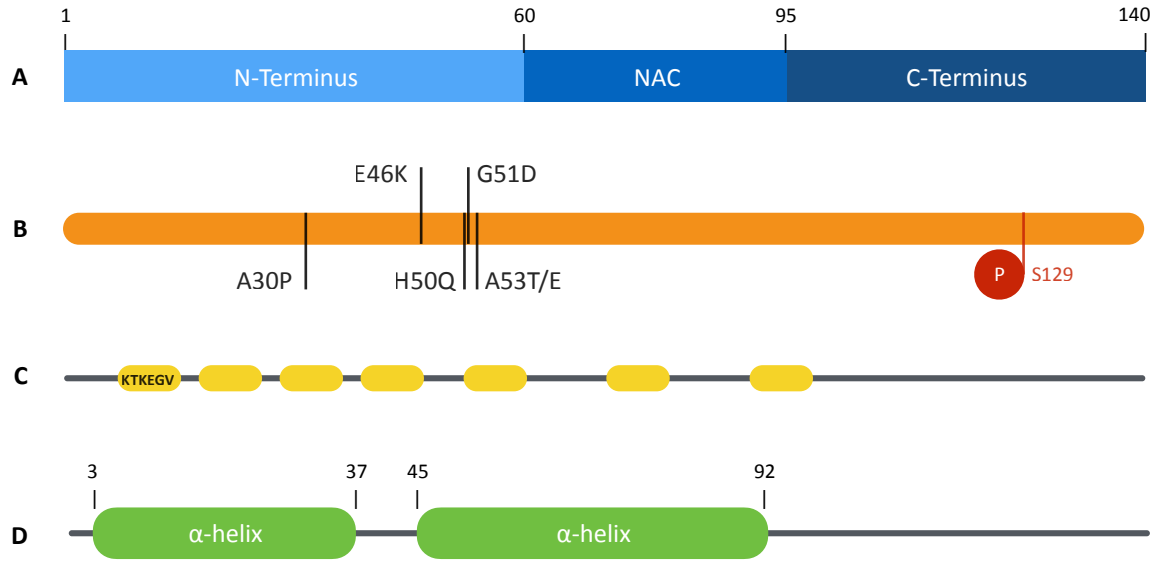

Figure 1.1|Structure of α-Synuclein
(A) Primary structure. **(B)** Mutations and post-transcriptional modification associated with PD. **(C)** Localisation of the KTKEGV motifs. **(D)** Secondary structure upon binding to acidic phospholipids membranes.

The predicted secondary structure of αSyn based on its primary sequence is natively unfolded, which has been observed *in vitro* (Weinreb et al. 1996). Interestingly, αSyn can also adopt an α-helical conformation upon binding to acidic phospholipid membranes (Jo et al. 2000; Davidson et al. 1998), with two curved amphipathic α-helices (Val3-Val37 and Lys45-Thr92) connected by a linker arranged in an anti-parallel manner (Ulmer et al. 2005) (Figure 1.1D). This characteristic secondary structure has a peculiar distribution of polar and non-polar amino acids on opposite sides of the helix, which closely resembles the structure of lipid-binding domains in apolipoproteins (Davidson et al. 1998).

In terms of tertiary structure, αSyn is generally accepted to be a monomeric protein (Burré et al. 2013; Weinreb et al. 1996; Fauvet et al. 2012). This evidence is based on studies where the protein is either expressed and purified from bacterial systems or gets denatured during analysis in samples from cell culture or animal models, where the protein is also over-expressed (Bartels, Choi, and Selkoe 2011). Using non-denaturing conditions to purify the protein from neuronal and non-neuronal cellular systems, including brain tissue,

red blood cells and iPSC-derived DAn, it appears that endogenous αSyn is a tetramer of 58 kDa with an α-helical structure (Bartels, Choi, and Selkoe 2011; Wang, Perovic, and Chittuluru 2011; Dettmer et al. 2015). Moreover, the tetrameric configuration has been observed to be more resistant to aggregation compared to the monomeric recombinant protein (Bartels, Choi, and Selkoe 2011). Although convincing and corroborated by different techniques, these findings were not replicated in other studies, where instead they determined that αSyn is an unfolded monomer lacking any detectable secondary structure (Burré et al. 2013; Fauvet et al. 2012). The discrepancy among the different studies is probably because the tetramer is inherently unstable, especially outside cells, and is lost during cell lysis and subsequent unavoidable dilution of the protein during purification (Dettmer et al. 2013; Luth et al. 2015). To date, the real physiological conformation of αSyn is still poorly understood, despite considerable effort and biochemical studies. Nevertheless, both models could be complementary to each other in a scenario where a continuous balance between the monomeric, α-helical and possibly tetrameric forms of αSyn exist, especially in the context of membrane binding.

It is known that αSyn is prone to self-aggregation into fibrils over a certain period of time at 37°C under shaking conditions (Uversky et al. 2002). The mechanism is nucleation-dependent with an initial lag phase followed by an exponential growth that can be monitored by Thioflavin T (ThT) fluorescence (Uversky and Eliezer 2009). Aggregation of αSyn is reported in some PD models including animals (Kahle 2008; Giasson et al. 2002; Betarbet et al. 2000), cells lines (Outeiro et al. 2008; Roberts, Wade-Martins, and Alegre-Abarrategui 2015) and iPSC-derived DAn (Ryan et al. 2013) but not others (Janezic et al. 2013). Mutant forms of αSyn have been reported to influence the aggregation kinetics, with E46K, A53T, H50Q mutants having an increased aggregation propensity (Ono et al. 2011; Ghosh et al. 2013) whereas A30P, A53E and G51D are less prone to aggregate

compared to the wild type protein (Rutherford et al. 2014; Ono et al. 2011; Fares et al. 2014). The same effect has been described *in vitro* in a cell model (Lázaro et al. 2014). Fibrillar forms of αSyn are reported to have a β-sheet secondary structure (Vilar et al. 2008) but oligomers of different structures and shapes have been reported, including annular protofibrils (Lashuel et al. 2002). Oligomeric αSyn species are thought to be highly toxic to many intracellular processes and organelles (Lashuel et al. 2013) and can even spread between cells (Desplats et al. 2009) and seed the aggregation of intracellular monomeric αSyn (Luk et al. 2009).

Over the last decade, post-transcriptional modifications (PTM) have been reported for αSyn and have all been implicated in affecting its physiological role, in some cases inducing a pathological function. The most common PTM of αSyn in LBs is phosphorylation at the Ser129 residue (Figure 1.1D) (Iwatsubo 2007; Fujiwara et al. 2002; Anderson et al. 2006), which has been shown to increase the propensity of the protein to aggregate *in vitro* (Fujiwara et al. 2002). Other modifications include tyrosine nitration (Giasson et al. 2000), ubiquitination (Tofaris, Layfield, and Spillantini 2001; Hasegawa et al. 2002) and C-terminus truncations (Oueslati, Fournier, and Lashuel 2010; Li et al. 2005).

1.2.4|Cellular function

The elucidation of αSyn physiological function is crucial to understand its pathological role in PD and other synucleinopathies. Despite more than two decades of extraordinary efforts, its precise cellular function is still elusive. Due to its intracellular localisation and supposedly wide range of protein interactions, it has been proposed that αSyn has a role in the regulation of synaptic function and can also act as a signalling molecule.

Research led by Südhof and colleagues has shed light on the molecular mechanisms of αSyn function at the synapse. αSyn is required for the maintenance of SNARE-complex

assembly at the synapse via its interaction with synaptobrevin-2/vesicle-associated membrane protein 2 (VAMP2) (Burré et al. 2010). More recently, αSyn binding and multimerization at cellular membranes was linked to its chaperone function for SNARE proteins (Burré, Sharma, and Südhof 2014). A mouse model lacking the presynaptic protein cysteine-string protein-α (CSPα) was shown to display neurodegeneration due to a decrease in SNARE complexes and the SNARE protein SNAP-25 (Sharma et al. 2012). Interestingly, the phenotype was rescued by αSyn over-expression and required its binding to phospholipids at presynaptic terminals, further confirming its relevant function at the synapse (Sharma et al. 2012; Chandra et al. 2005).

The generation of knockout (KO or $^{-/-}$) animal models further supported a putative role for αSyn in neurotransmission and synaptic release. Nonetheless, they have also shown that αSyn is not an essential protein in brain development and function, as mice lacking the *Snca* gene were viable and with normal development, despite a subtle reduction in DA in the striatum (Abeliovich et al. 2000; Cabin et al. 2002). Importantly, *Snca*$^{-/-}$ mice only display synaptic dysfunction under repetitive stimuli due to a decrease in replenishment of docked vesicles as a consequence of a diminished reserve vesicle pool (Abeliovich et al. 2000; Cabin et al. 2002). Interestingly, *Snca*$^{-/-}$ mice are also more resistant to neurodegeneration caused by MPTP, via a mechanism that does not involve DAT (Dauer et al. 2002; Drolet et al. 2004). Conversely, in double KO (α/βSyn) DA levels are reduced without any apparent impairment of synaptic transmission or DA uptake (Chandra et al. 2004). In a α/γSyn KO mouse model, the increase in DA levels in the striatum upon stimulation was shown not to be linked to DAT function but rather to differences in DA release from synapses (Senior et al. 2008). Triple KO (α/β/γSyn) mice are characterised by age-dependent neurodegeneration associated with increased striatal DA levels and synaptic dysfunction due to decreased excitatory synapse size (Greten-Harrison et al. 2010; Anwar

et al. 2011). With regards to αSyn chaperone activity on SNARE proteins, triple KO mice display SNARE-complex assembly deficits (Burré et al. 2010). These results were further corroborated by additional studies showing that αSyn over-expression causes a reduction in the size and density of vesicles at the synapse, causing a deficit in neurotransmitter release (Nemani et al. 2010).

It has been postulated that αSyn can interact with many intracellular proteins and molecules; however, the cellular models used limit each finding. Ubiquitous cytoplasmic chaperones 14-3-3 proteins (14-3-3s) have been found in LBs (Ubl et al. 2002) and have both physical and functional primary sequence homology with αSyn (Ostrerova et al. 1999). Interestingly, the 14-3-3η isoform was reported to bind and inhibit Parkin; wild-type αSyn, but not the A30P or A53T, can bind to 14-3-3η causing a negative regulation of Parkin inhibition (Sato et al. 2006). Because of the interaction between TH and 14-3-3 proteins, αSyn might be involved in the regulation of DA synthesis as well. In fact, in both rat brains and the mouse MN9D dopaminergic cell line, αSyn can be immuno-precipitated with TH. αSyn over-expression does not alter TH protein level but causes a reduction in TH activity instead (Perez et al. 2002). A similar effect was later shown for AADC as well (Tehranian et al. 2006), whereas αSyn knockdown was found to decrease DAT activity and its localisation at the cellular membrane (Fountaine et al. 2008). Interestingly, αSyn was shown to affect DAT expression by inhibiting its transfer and processing from the ER to the Golgi (Oaks et al. 2013). Lastly, DA-dependent neurotoxicity was linked to the formation of a soluble complex between αSyn and 14-3-3s, that was found to be increased in the *SNpc* of PD patients (Xu et al. 2002).

Much of the hype regarding the interaction between αSyn and LRRK2 came from the fact that αSyn is highly phosphorylated at the Ser129 residue in LBs and some mutant forms of LRRK2, like G2019S, are characterised by increased kinase activity (Greggio

2012). However, few studies have been able to show an interaction and phosphorylation of αSyn by LRRK2 either *in vitro* upon oxidative stress, in DLB and PD brain samples and in a human neuroglioma H4 cell line model for αSyn inclusion formation (Qing, Wong, et al. 2009; Qing, Zhang, et al. 2009; Guerreiro et al. 2013). Moreover, these two proteins might also interact because they localise at the same intracellular location, with LRRK2, like αSyn, shown to associate with intracellular membranes and lipid rafts (Hatano et al. 2007; Alegre-Abarrategui et al. 2009). A synergistic effect of the two proteins on PD pathophysiology has been proposed as well. LRRK2 over-expression causes an exacerbation of the neurodegenerative phenotype of A53T αSyn mice, whereas *Lrrk2* ablation delayed the onset of the phenotype (Lin et al. 2009). Orestein and colleagues found that LRRK2 can cause CMA dysfunction and affect the degradation of wild type αSyn by CMA, in a similar manner to mutant forms of αSyn (Orenstein et al. 2013). On the other hand, LRRK2 and αSyn interaction might occur indirectly via 14-3-3s. Auto-phosphorylation of residues Ser910 and Ser935 in LRRK2 is necessary for the binding of 14-3-3s and it has been shown that decreased phosphorylation of these amino acids due to mutant LRRK2 causes reduced binding of 14-3-3s both in cell and animal models (Nichols et al. 2010). Therefore, it can be postulated that changes in αSyn binding to 14-3-3s may impact on LRRK2 or vice versa.

1.2.5|The relationship between αSyn and mitochondria

The involvement of αSyn in mitochondrial function and dysfunction has been greatly explored since the pathological relevance of mitochondria in PD. Moreover, Parkin and Pink1, two familial recessive PD genes, are involved in mitochondrial homeostasis in both physiological and pathological contexts (Geisler et al. 2010; Poole et al. 2008).

Many studies reported the localisation of αSyn in mitochondria (Nakamura et al.

2011; Shavali et al. 2008; Parihar et al. 2008). Specifically, electron microscopy analysis showed the presence of αSyn in the mitochondrial matrix in brains of PD patient (Devi et al. 2008). More recently, a study in human and mouse models reported that αSyn localises to mitochondria-associated endoplasmic reticulum (ER) membranes (MAMs) rather than to the mitochondria themselves (Guardia-Laguarta et al. 2014). Expression of wild type αSyn in different cellular models was shown to cause fragmentation of mitochondria, but not of any other organelle, probably due to its binding to cardiolipin, the most abundant mitochondrial lipid, in a fission/fusion-independent mechanism (Siddiqui et al. 2012; Nakamura et al. 2011). Oligomeric or prefibrillar αSyn species have also been shown to bind to artificial mitochondria-like membranes *in vitro* and disrupt mitochondrial function (Luth et al. 2014; Nakamura et al. 2011). Activation of macroautophagy due to over-expression of A53T αSyn in primary cortical neurons can induce an up-regulation of mitophagy and consequent bioenergetic impairment (Choubey et al. 2011).

In PD patient brains, complex I (CoxI) activity is significantly reduced in DAn in the *SNpc* (Schapira et al. 1989; Janetzky et al. 1994) and further reports have showed that this is not confined to the midbrain but extends to the frontal cortex as well (Parker, Parks, and Swerdlow 2008). Toxins that inhibit mitochondrial function, especially via CoxI inhibition, have been reported to cause Parkinsonism *in vivo* (Langston et al. 1983; Dhillon et al. 2008). *In vitro*, these toxins reduce the production of ATP and increase the generation of reactive oxygen species (ROS) (Bates et al. 1994; Fountaine et al. 2008). Accumulation of αSyn itself or its aggregated forms was found to specifically compromise CoxI activity (Chinta et al. 2010; Reeve et al. 2015). Unsurprisingly, *Snca*$^{-/-}$ mice are more resistant to MPTP-induced cell toxicity (Dauer et al. 2002; Klivenyi et al. 2006). Furthermore, expression of human wild-type or A53T αSyn is sufficient to restore vulnerability to MPTP (Thomas et al. 2011). In dopaminergic SH-SY5Y neuroblastoma cells, αSyn knockdown

was protective towards MPP^+ toxicity, reducing DAT localisation at the cell surface and activating nitric oxide synthase (NOS) as a protective pathway (Fountaine et al. 2008). However, αSyn knockdown did not directly rescue the effects of MPP^+ on mitochondrial respiration (Ryan et al. 2014).

Peroxisome Proliferator-Activated Receptor (PPAR)-coactivator (PGC-1α) is a transcription factor involved in many intracellular pathways, including mitochondrial biogenesis and metabolism, glucose and fatty acid metabolism and oxidative stress. It is highly expressed in tissues with a high metabolic rate and mitochondrial respiration, including the brain (Liang and Ward 2006). PGC-1α over-expression in mice increases mitochondrial respiration rate and protects against the effect of MPTP (Mudò et al. 2012). In contrast, PGC-1α null mice have abnormal mitochondria and are more sensitive to αSyn over-expression (Ciron et al. 2015; Eschbach et al. 2015). In PD patient brains, genes under the control of PGC-1α were found to be down-regulated whereas activation of PGC-1α in a rat midbrain primary cultures induced the expression of electron transport chain (ETC) enzymes and protected cells from both αSyn and Rotenone toxicity (Zheng et al. 2010). αSyn was shown to bind the PGC-1α promoter in both human and mouse cellular models upon induction of oxidative stress and in the *SNpc* of control and PD patient brains. Expression of wild-type and A53T αSyn reduced PGC-1α promoter activity, mRNA and protein levels *in vitro* (Siddiqui et al. 2012). In iPSC-derived DAn carrying the A53T *SNCA* mutation, PGC-1α activity was decreased compared to an isogenic control. Nitrosative stress was found to be the cause of S-nitrosylation and consequent reduced activity of the myocyte enhancer factor 2C (MEF2C) transcription factor, involved in controlling PGC-1α transcription (Ryan et al. 2013). Pathogenic forms of αSyn clearly have a profound effect on mitochondrial function either via its direct interaction with their membranes and proteins of the ETC or through the disruption of mitochondrial

homeostasis pathways, such as the neuroprotective factor PGC-1α.

1.2.6|The link between αSyn and intracellular degradation pathways

Two different but complementary pathways mainly control intracellular protein and organelle homeostasis. Autophagy, also known as the autophagic-lysosomal pathway, results in the recycling of cytosolic proteins and organelles in the lysosome (Takeshige et al. 1992). Complementary to autophagy, the proteasome regulates protein homeostasis and degradation via its proteolytic activity in the cytoplasm (Etlinger and Goldberg 1977).

To date, much evidence suggests that dysregulation of these degradation pathways is a feature of PD pathology, but it is not known whether this dysfunction is the cause of the onset of the disease or is a consequence. Moreover, conflicting evidence suggests that both the autophagic or proteosomal pathways can degrade αSyn. Originally, the degradation of cytosolic αSyn was thought to predominantly occur via the proteasome (Tofaris, Layfield, and Spillantini 2001; Abeywardana et al. 2013; Tanaka et al. 2001). Interestingly, fibrillar or oligomeric species of αSyn can bind to the proteasome and inhibit its activity (Lindersson et al. 2004) but can also be targeted to the lysosome via a p62-depended mechanism (Watanabe et al. 2012). Alternatively, chaperone-mediated autophagy (CMA) was shown to degrade monomeric αSyn by its binding to the chaperone HSC70 and consequent translocation into the lysosome via LAMP2A. Mutant forms of αSyn were found to inhibit their own degradation and other CMA substrates by irreversibly binding to LAMP2A (Cuervo et al. 2004). Similarly, impairment of macroautophagy by αSyn was also shown to occur via inhibition of Rab1a (Winslow et al. 2010). Overall, a number of studies in the field have acknowledged that αSyn can indeed be degraded by both pathways, mostly depending on the protein burden and cellular homeostasis (Webb et al. 2003; Ebrahimi-Fakhari et al. 2011).

The interaction between αSyn and GBA, which is both a GWAS hit and lysosomal enzyme, has recently suggested potential bidirectional pathological mechanisms. In fact, pharmacological inhibition of GBA with conduritol B epoxide (CBE) causes αSyn accumulation in SH-SY5Y neuroblastoma cells and in mouse midbrains (Manning-Boğ, Schüle, and Langston 2009). Of note, GBA affinity for αSyn is reduced in the PD-associated GBA N370S mutant (Yap et al. 2011). The interaction between GBA and αSyn is thought to be pH-dependent and only occurs at the lysosomal pH of 5.5, via the C-terminus of αSyn. Furthermore, loss of function of the GBA protein can cause the accumulation of αSyn in animal and human cell models, with αSyn alternatively being able to inhibit GBA activity in lysosomes (Mazzulli et al. 2011; Mazzulli, Zunke, Tsunemi, et al. 2016). In a human iPSC-derived DAn model, the heterozygous GBA N370S mutation caused autophagic dysfunction leading to αSyn secretion in the culture media without any apparent intracellular accumulation (Fernandes et al. 2016). Interestingly, treatment of iDAn carrying a triplication of the *SNCA* gene with an activator of GBA activity rescued the accumulation of αSyn in the soma of these cells (Mazzulli, Zunke, Tsunemi, et al. 2016). However, a study by Dermentzaki and colleagues found that they could not detect monomeric or oligomeric αSyn species or impairment of autophagy upon pharmacological GBA inhibition in SH-SY5Y cells or rat primary cortical neurons, suggesting a more complex interaction between this enzyme and PD (Dermentzaki et al. 2013).

Lastly, interplay between αSyn and LRRK2 in autophagic dysfunction has been proposed. Work by Orenstein and colleagues used rodent neuronal cultures and iPSC-derived DAn to elegantly show that LRRK2 is a CMA substrate and its mutant form can compromise this process, with CMA blockage eventually causing the accumulation of αSyn (Orenstein et al. 2013).

1.2.7|The causative role of αSyn with ER stress

The endoplasmic reticulum (ER) is an intracellular compartment involved in many essential processes, including protein folding and glycosylation and lipid synthesis, and is also the major intracellular calcium store. Through the unfolded protein response (UPR), effectors of ER stress pathways are activated in order to overcome harmful intracellular events like the accumulation of misfolded proteins or calcium depletion (Hetz 2012). As in the case of intracellular degradation pathways, it can be speculated that ER stress could be either the cause or consequence of PD pathology.

The ER chaperone BiP/Grp78 is a sensor for unfolded proteins and under normal physiological conditions negatively regulates the effectors of the three UPR pathways; however, upon accumulation of misfolded proteins it dissociates from them. Inositol-requiring kinase 1α (IRE1α) dimerises and autophosphorylates upon dissociation from BiP and causes the unconventional splicing of the transcription factor XBP1, that in turn will induce the expression of other genes regulated by the UPR or involved in the ER-associated degradation (ERAD) of proteins (Lee, Iwakoshi, and Glimcher 2003; Calfon et al. 2002). ATF6 is another UPR effector that, once dissociated from BiP, translocates to the Golgi to be processed to its transcription factor form (ATF6f), which transfers to the nucleus to induce the expression of chaperones and ERAD proteins (Shen et al. 2002). Lastly, release of the negative regulation by BiP from PERK causes the phosphorylation of eIF2α, which ultimately results in a general reduction of mRNA translation, including the transcription of ATF4, involved in the expression of pro-survival genes (Bertolotti et al. 2000). Overall, ER stress can be an immediate and adaptive response that eventually promotes cell survival and restoration of physiological conditions. However, under prolonged UPR activation, cell death is triggered via the mitochondrial apoptosis pathway (Hetz 2012).

In a A53T αSyn mouse model, BiP protein levels and immuno-reactivity were increased, with no changes in ATF4 and total amounts of p-eIF2α or eFI2α, despite both being increased in aged mice. In rat pheochromocytoma cells PC12, the expression of A53T αSyn results in increased phosphorylation of eF12α and up-regulation of BiP (Smith et al. 2005). In a rat model, viral delivery of αSyn causes activation of the PERK pathway with increase in ATF6 and CCAAT-enhancer-binding protein homologous protein (CHOP), whereas over-expression of BiP could revert the phenotype (Gorbatyuk et al. 2012). Lastly, αSyn oligomers could be co-purified with ER membranes, whereas αSyn over-expression in BE(2)M17 neuroblastoma cells activates BiP but not phosphorylation of eF12α (Colla et al. 2012).

Toxin models of PD have also suggested that ER stress is part of the disease pathological mechanism. MPTP treatment in mice causes an up-regulation of BiP and processing of ATF6 into its active form (Egawa et al. 2011). In other studies, both BiP and CHOP were up-regulated in the brains of mice treated with MPTP, as well as BiP and GRP94, another ER chaperone, found to be up-regulated in SHSY-5Y cells upon MPP^+ treatment (Selvaraj et al. 2012).

Some insights into the relationship between ER stress and PD have also come from the use of iPSC-derived neuronal models. Cortical neurons carrying the A53T *SNCA* mutation display increased levels of BiP and protein-disulphide isomerase PDI along with ERAD substrates, including GBA (Chung et al. 2013). Similarly, iPSC-derived DAn carrying the heterozygous N370S GBA mutation are characterised by an up-regulation of UPR markers, including BiP, PDI, and IRE1α (Fernandes et al. 2016).

Lastly, up-regulation of ER stress makers has been reported in PD patient brains *post-mortem*. Phosphorylated forms of both PERK and eIF2α were increased in patient brains compared to controls; interestingly, pPERK was shown to co-localise with αSyn

staining in DAn (Hoozemans et al. 2007). Nitrosylation of PDI was also detected in sporadic PD patient brains and resulted in the inhibition of its catalytic activity and the triggering of UPR (Uehara et al. 2006). BiP was also increased in the *SNpc* of PD patient brains, with a counterintuitive decrease in ATF6. However, further investigation via αSyn over-expression in SH-SY5Y cells demonstrated a decrease in the expression of downstream targets of ATF6, including those for ERAD (Credle et al. 2015).

1.2.8|The impact of αSyn in cellular bioenergetics and lipid metabolism

Some experimental evidence points towards a wider involvement of αSyn in cellular bioenergetics beyond mitochondrial respiration, including fatty acids (FA) and glucose metabolism.

The primary sequence of αSyn contains a motif similar to the one found in fatty acid binding proteins (FABPs) (Sharon et al. 2001). FABPs are a class of proteins that bind and traffic intracellular polyunsaturated fatty acids (PUFAs); at least ten different isoforms have been identified but only three (FABP3, FABP5 and FABP7) are expressed in the brain (Liu et al. 2010). The brain specific isoform FABP7, also known as brain lipid-binding protein (BLBP), was shown to be expressed predominantly during development and rapidly decreasing afterwards (Shimizu et al. 1997). Interestingly, FABP7 levels are increased in the serum of PD patients (Teunissen et al. 2011). *Fabp7*$^{-/-}$ mice are characterised by increased arachidonic acid and palmitate levels in their adult brains (Owada et al. 2006) and elevated high blood glucose levels (Su et al. 2016). Work by Shioda and colleagues reported that FABP3 interacts with αSyn in the mouse *SNpc* and that *Fabp3*$^{-/-}$ mice are resistant to MPTP toxicity and display less αSyn accumulation. Conversely, FABP3 over-expression in PC12 cells causes αSyn oligomerization (Shioda et al. 2014). In *Snca*$^{-/-}$ mice, uptake of palmitate and incorporation into acyl-CoA in the brain is reduced, with a similar effect of FABPs but

without directly binding the fatty acid (Golovko et al. 2005). Exposure of αSyn over-expressing MN9D cells and mouse primary cortical neurons to PUFAs causes the formation of LB-like inclusions containing αSyn (Assayag et al. 2007). Similarly, PUFAs were shown to induce αSyn oligomerization *in vitro* and are elevated in PD brains (Sharon et al. 2003). Furthermore, cardiolipin, the mitochondrial specific phospholipid, is reduced in whole brain of *Snca*$^{-/-}$ mice (Barceló-Coblijn et al. 2007) and this is accompanied by a reduction in mitochondrial function (Ellis et al. 2005), demonstrating a relationship between αSyn, lipids and mitochondria. *In vitro* evidence also suggests that αSyn can also bind to cholesterol (Fantini, Carlus, and Yahi 2011). 24S- and 27S-hydroxycholesterol, two oxidized cholesterol metabolites that are tightly regulated in the brain, decrease the levels of TH expression and increase αSyn expression in SH-SY5Y cells (Prasanthi et al. 2009; Marwarha et al. 2011). Of the two, 24S-hydroxycholesterol is produced by neurons in the brain and is decreased in many neurodegenerative diseases, including PD (Leoni and Caccia 2013).

As mentioned above, other reports have shown a wider impact of αSyn or PD pathology on metabolism and bioenergetics. Positron emission tomography (PET) using 18F-fluorodeoxyglucose found reduced glucose metabolism in the brains of patients diagnosed with PD (Firbank et al. 2016). A metabolomic study found that expression of A53T αSyn or suppression of αSyn expression in mouse brains reduces the metabolic rate in the brain, which in turn compromises energy production (Musgrove et al. 2014). Similarly, A53T αSyn mice have decreased levels of cholesterol, triglycerides and non-esterified fatty acids (NEFA). Blood glucose is unchanged but serum insulin was decreased, together with down-regulation of the NAD-dependent deacetylase Sirtuin-2 (Guerreiro et al. 2016). It has been suggested that A9 DAn are particularly vulnerable compared to other types of neurons because of their high metabolic rate. A9 DAn have a huge axonal

arborisation and synaptic density that demand more energy from metabolic processes like oxidative phosphorylation in the mitochondria. An imbalance in energy demand versus production could therefore determine the onset of PD (Pacelli et al. 2015; Pissadaki and Bolam 2013). Moreover, the typical Ca^{2+} pace-making activity of DAn could even further add to the burden of energy demand in these cells (Chan, Gertler, and Surmeier 2010).

The effect of αSyn on metabolic processes is one of the least studied pathological mechanisms in PD. However, the literature points towards an involvement of αSyn beyond affecting mitochondrial respiration. αSyn direct or indirect effect on PGC-1α may also impact on intracellular bioenergetics since this transcription factor is also involved in the homeostasis of glucose and FA metabolism (Liang and Ward 2006). From an experimental point of view, -omics approaches, including transcriptomics, metabolomics and lipidomics, seem to be the way forward due to the diversity and complexity of intracellular pathways and processes that may be involved.

1.2.9|Evidence for αSyn pathology from iPSC-derived DAn models

The breakthrough in the reprogramming of somatic cells to iPSCs (Takahashi and Yamanaka 2006) and the development and optimisation of protocols for their differentiation to dopaminergic neurons (Chambers et al. 2009; Hartfield et al. 2014; Kirkeby et al. 2012; Kriks et al. 2011; Fasano et al. 2010), opened the possibility of studying PD pathology in a relevant cellular model. Because of its relevance in PD, αSyn has been widely studied in iPSC-derived DAn models, not only in those carrying *SNCA* mutations or copy number variants, but also in LRRK2, GBA, Parkin, Pink1 and idiopathic models. Despite best efforts, each individual study used different control and patient lines, various sources and reprogramming methods, diverse differentiation protocols with considerable differences in the yield of TH^+ neurons (from ~5% to up to ~85%) and

varied time points for the phenotypic analysis (from 30 DIV up to 6 months). Moreover, in some cases, only when isogenic controls were included could statistically significant result be obtained. The scope of this section is to briefly review the outcomes of all the studies where iPSC-derived DAn were used and a phenotype relative to αSyn was reported (see also Table 1.2).

Three studies have so far examined the phenotypes of iPSC-derived DAn carrying a triplication of the *SNCA* gene. These neurons (~10% TH^+, 23–31 DIV) showed increased αSyn mRNA, protein levels and secretion but also displayed heterogeneity in αSyn expression among the neurons (Devine et al. 2011). In line with this, another study (~5-10% TH^+, 50 DIV) showed an increase in αSyn protein levels, oxidative stress markers and susceptibility to H_2O_2 (Byers et al. 2011). Alongside, two further studies focused on the phenotype of neuronal progenitor cells (NPCs), reporting changes in growth, viability, cellular energy metabolism, stress resistance (Flierl et al. 2014) and reduced capacity to differentiate to DAn, decreased neurite outgrowth and lower neuronal activity (Oliveira et al. 2015).

With regard to point mutations in *SNCA*, one iPSC line carrying the A53T mutation and its isogenic control (Soldner et al. 2011) have been used in three different studies, one of which analysed the phenotype in cortical neurons. A53T *SNCA* iPSC-derived DAn (~80-85% TH^+, 35 DIV) were reported to have increased αSyn protein levels and intracellular ThS staining, reduced mitochondrial respiration and increased toxin-induced mitochondrial dysfunction and apoptotic cell death. The phenotype was linked to nitrosative/oxidative stress resulting in S-nitrosylation of MEF2C with consequent inhibition of the PGC1α transcriptional network that controls mitochondria homeostasis (Ryan et al. 2013). The analysis of the same iPSC line differentiated to cortical neurons provided evidence of nitrosative and ER stress and the phenotype was reverted using a

molecule that modulates the activity of the ubiquitin ligase Nedd4 (Chung et al. 2013). Lastly, the work of Dettmer and colleagues provided more supporting evidence of αSyn being present as a native tetramer in neurons, in this case iPSC-derived DAn, and showed that the A53T mutation reduces the αSyn 58/14kDa ratio, which is suggested to increase the propensity to aggregate (Dettmer et al. 2015). More recently, two studies published by Mazzulli and colleagues (~80% TH+, between 90 and 330 DIV), described widespread αSyn pathology in a range of monogenic PD iPSC lines. In *SNCA* triplication and GBA-PD iPSC-derived DAn, αSyn accumulation was associated with a reduction of lysosomal degradation capacity via the disruption of hydrolase trafficking. Interestingly, the phenotype was reverted upon αSyn knockdown (Mazzulli, Zunke, Isacson, et al. 2016). In the second study, αSyn accumulation and ThS$^+$ inclusions in TH$^+$ cells were confirmed in A53T *SNCA*, *SNCA* triplication, GBA heterozygous N370S, *ATP13A2* mutants and idiopathic PD iPSC-derived Dan and the phenotype was reverted upon treatment with a small molecule that increases GBA activity (Mazzulli, Zunke, Tsunemi, et al. 2016).

To date, iPSC-derived neurons carrying *LRRK2* or *GBA* mutations are the most common of all the studies for monogenic PD, probably due to the higher prevalence of these mutations among PD patients. Work by Sánchez-Danés and colleagues in iPSC-derived DAn carrying the G2019S LRRK2 mutation (~15-20% TH$^+$, 42 DIV) reported an increase in cytoplasmic αSyn staining in TH$^+$ neurons (Sánchez-Danés, Richaud-Patin, et al. 2012). This was followed up recently in a transcriptomics study, in which an increase in αSyn at the mRNA level was reported as well (Fernández-Santiago et al. 2015). In the context of LRRK2 and CMA in iPSC-derived DAn (15-20% TH$^+$), an increase in the co-localization between αSyn and LAMP2A was reported (Orenstein et al. 2013). Another study described the increase of αSyn protein levels only when the G2019S LRRK2 lines were compared to their isogenic controls (20-25% TH+, 30–60 DIV), with no difference at

the mRNA level (Reinhardt et al. 2013). Just one study (5% TH+, 60 DIV) reported that G2019S LRRK2 iPSC-derived DAn cultures have increased αSyn protein levels compared a control iPSC and ESC line (Nguyen et al. 2011).

Very interesting data has come from studies using iPSC from individuals carrying heterozygous GBA mutations and idiopathic PD patients. Control iPSC-derived DAn (10% TH^+) were reported to have increased αSyn upon GBA knockdown, whereas αSyn was increased in neurons carrying the heterozygous N370S GBA mutation (Mazzulli 2011). In another study, analysis of heterozygous L444P GBA iPSC-derived DAn (15-20% TH^+, 33DIV) showed increased αSyn protein levels compared to controls, whereas heterozygous N370S GBA neurons had increased αSyn only when compared to its isogenic control (Schöndorf et al. 2014). The analysis of iPSC-derived DAn (80% TH^+ post sort, 36 DIV) from twins carrying the N370S GBA mutation, of which only one was diagnosed with PD, reported again increased protein levels and percentage of TH^+ cells with cytoplasmic staining of αSyn (Woodard et al. 2014). Lastly, work published by Fernandes and colleagues showed that N370S GBA iPSC-derived DAn (15-20% TH^+, 35DIV) did not have any difference in total αSyn protein levels when compared to control lines but secreted more αSyn in the culture media over time (Fernandes et al. 2016).

To date, very little data from studies using idiopathic PD iPSC-derived DAn has been presented, with only two studies (~15-20% TH^+, 42 DIV) on the same lines reporting an increase in the percentage of TH^+ cells with cytoplasmic αSyn staining (Sánchez-Danés, Richaud-Patin, et al. 2012) and an increase in *SNCA* mRNA levels (Fernández-Santiago et al. 2015).

Reference	Year	Genotype	αSyn phenotype	DIV	% TH$^+$
Sanchez-Danes	2011	WT, Idiopathic & G2019S *LRRK2*	Increased αSyn cytoplasmic staining	42	15-20%
Nguyen	2011	H9, WT & G2019S *LRRK2*	Increased protein level	60	5%
Devine	2011	*SNCA* triplication & unaffected sibling	Increased mRNA, protein and release, heterogeneous expression among neurons	23–31	10%
Byers	2011	*SNCA* triplication	Increased protein, increased oxidative stress markers, increased susceptibility to H_2O_2	50	5-10%
Jiang	2011	*Parkin* het ex3-/ ex5- & hom ex3-	Unchanged protein level	70	10%
Seibler	2011	*PINK1* Q456X & V170G	Not assessed	60	6-10%
Mazzulli	2011	*GBA* Heterozygous N370S	Increased αSyn upon GBA KD in WT & increased αSyn in N370S GBA	60	6-10%
Cooper	2012	*LRRK2* G2019S & R1441C	Not assessed	56	1-5%
Imaizumi	2012	*Parkin* ex2-/ ex4- ex6-/ex7	% of αSyn/TH was higher in one of the patient lines	54	10%
Orenstein	2012	*LRRK2* G2019S	Increased αSyn/LAMP2a colocalization	30, 75	15-20%
Reinhardt	2013	*LRRK2* G2019S	Increased protein when comparing G2019S and isogenic	30	20-25%
Sanders	2013	*LRRK2* G2019S	Not assessed	56	1-5%
Ryan	2013	*SNCA* A53T	Increased αSyn, increased P-Ser129, aggregation, increased toxin-induced mitochondrial dysfunction and apoptotic cell death	36	80-85%
Rakovic	2013	*PINK1* V170G	Not assessed		6-10%
Schöndorf	2014	*GBA* Heterozygous N370S & L444P	Increased protein in PD-L444P, decreased αSyn in isogenic lines compared to parental lines	65, 70	15-20%
Woodard	2014	*GBA* Heterozygous N370S	Increased protein in PD-N370S GBA, increased % of αSyn staining in TH+ve cells	32, 34	80% (post sort)
Flierl	2014	*SNCA* triplication	Analysis of NPCs, changes in growth, viability, cellular energy metabolism and stress resistance	-	NPCs
Dettmer	2015	*SNCA* A53T	Reduced αSyn 60/14kDa ratio in PD line	45, 55	NA
Shaltouki	2015	*Parkin* point mutation and deletion	Not assessed	28	~20%
Ohta	2015	*LRRK2* I2020T	No difference	14, 118	~3-5%
Fernández-Santiago	2015	*LRRK2* G2019S	Increased *SNCA* expression at mRNA level	30	15-20%
Oliveira	2015	*SNCA* triplication	Increased protein expression, reduced differentiation efficiency	30, 64 75	2-7%
Chang	2016	*Parkin* Heterozygous ex5-	Increased protein levels	42	50-60%
Fernandes	2016	*GBA* Heterozygous N370S	Unchanged protein levels, increased release in PD-N370S GBA lines	35	15-20%

Reference	Year	Genotype	αSyn phenotype	DIV	% TH$^+$
Mazzulli	2016	*SNCA* triplication and *GBA*-PD	αSyn accumulation, reduced lysosomal degradation capacity, disrupting hydrolase trafficking, knockdown reverted the phenotype	90-330	80%
Mazzulli	2016	A53T *SNCA*, *SNCA* triplication, GBA Heterozygous N370S, ATP13A2 mutants and idiopathic PD	αSyn accumulation, reduction upon treatment with GBA activity modulator and reduction in TH/αSyn and ThS staining in both soma and neurites	60-330	80%
Aflaki	2016	GD *GBA*	Increased protein levels and TH/αSyn staining in some of the lines, reversed by increasing GBA activity	100+	NA
Chung	2016	*Parkin* (V324A) *Pink* (Q456X)	Accumulation, increased TH/αSyn staining	30-45	50-70%

Table 1.2|Summary of papers investigating iDAn with relative αSyn phenotype
NA= Not Accessible; DIV=Days In Vitro.

1.3|Induced pluripotent stem cells and dopaminergic neuron differentiation

1.3.1|Introduction

For many years, scientific research has relied on the use of immortalised cell lines and animal models to study biological processes in both physiological and pathological conditions. Cell and animal models each have their advantages and disadvantages. Immortalised cell lines offer the chance to study intracellular mechanisms in a simplified setting and take advantage of easy genetic manipulation for over-expression, knockdown or reporter genes. On the other hand, animals provide a more relevant physiological environment but, despite the extent in the genetic similarity between human and these animals, some intracellular pathways or disease phenotypes cannot be fully recapitulated.

Immortalised cell lines and animal models have produced a considerable amount of data, giving useful insight on PD pathology. The advent of human induced pluripotent stem cells (iPSCs) brought about the possibility of studying the effect of the genetic background of individuals who developed a disease without the need for any genetic manipulation. Moreover, development of differentiation protocols allowed the analysis of the specific cell type that is most relevant for the pathology (Figure 1.2). However, iPSCs came with the drawbacks of not fully recapitulating the same properties of embryonic stem cells (ESCs) and carrying the same degree of genetic variability that diversifies every human to another. Overall, iPSCs hold great expectations, especially in terms of regenerative medicine, and allow researchers to finally study a relevant genetic disease model in the appropriate cell type in a dish. The aim of this section is to discuss the state-of-art model of iPSCs, differentiation protocols, the advantages, disadvantages and bottlenecks of their use in

research.

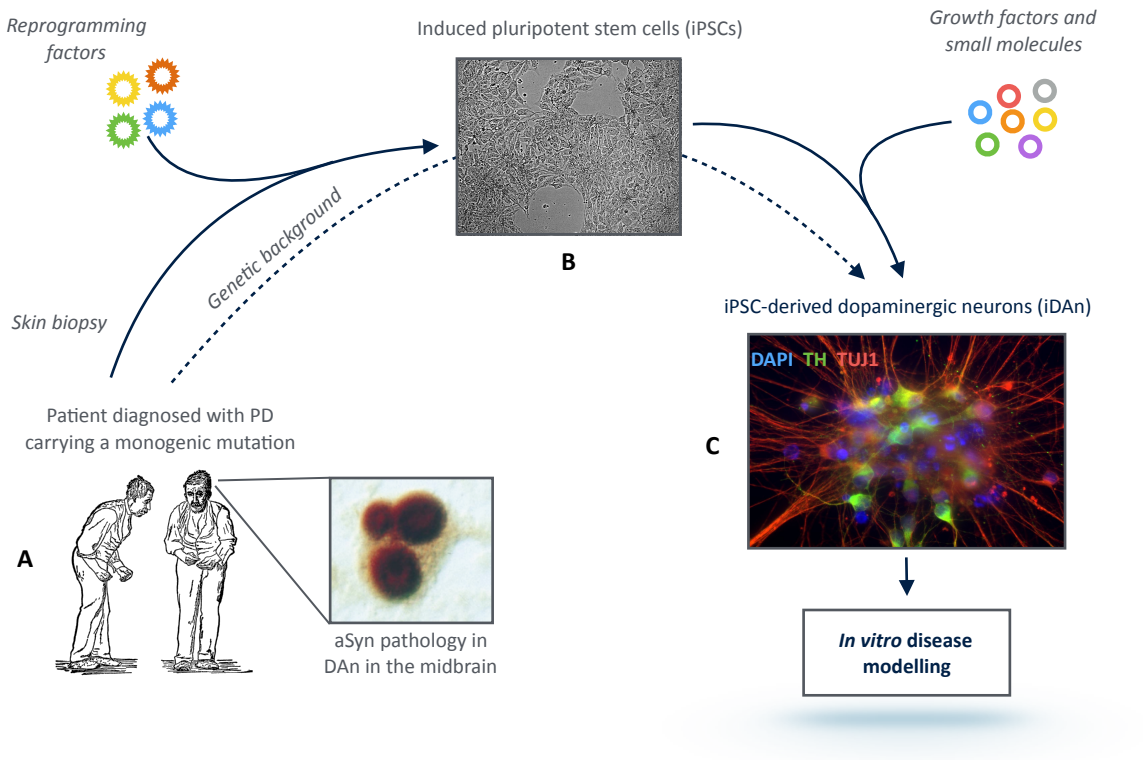

Figure 1.2|iPSC-derived dopaminergic neurons as an *in vitro* cell model of PD
(A) Patients diagnosed with PD carrying a monogenic mutations and displaying αSyn pathology in dopaminergic neurons in the midbrain; Illustration of Parkinson's disease patient by W.R. Gowers published in A Manual of Diseases of the Nervous System (1886); image of neuron containing LBs from Spillantini et al. 1998. **(B)** Representative image of iPSC colony generated from the reprogramming of fibroblasts from a skin biopsy. **(C)** iPSC-derived dopaminergic neurons from a PD patient.

1.3.2|Reprogramming of somatic cells

The discovery of how somatic cells can be reprogrammed to pluripotent stem cells was the result of the pioneering work across a number of different fields. Initial work by John Gurdon at the University of Oxford proposed that nuclei from differentiated somatic cells could be transplanted into unfertilised eggs and direct their differentiation to adult organisms (Gurdon 1962). More than three decades later, Dolly the sheep was the first mammal to be cloned from mammary epithelial cells (Wilmut et al. 1997). These experiments demonstrated how the nuclei of somatic cells retain all the genetic material required to support the development of an entire organism, whereas unfertilised eggs

contain genetic factors that can revert somatic nuclei into a pluripotent stage. Parallel to this, the discovery of MyoD, a transcription factor that can convert fibroblasts to myocytes (Davis, Weintraub, and Lassar 1987), introduced the idea of transcription factors being involved in directing cells towards a certain lineage or type.

Pioneering work in the field of reprogramming of somatic cells by Takahashi and Yamanaka reported for the first time the generation of iPSCs from mouse fibroblasts via the retroviral delivery of four transcription factors from a pool of 24 candidates (Oct3/4, Sox2, c-Myc, and Klf4) (Takahashi and Yamanaka 2006). Later on, this was proven to be applicable for human fibroblasts as well (Takahashi et al. 2007). iPSCs were shown to fulfil all criteria of pluripotency, for example they expressed the pluripotent stem cell marker Nanog and generated all germ layers upon injection into immune-compromised mice. Subsequent studies showed the wide applicability of the technique beyond human fibroblasts as starting material, with studies reporting the generation of iPSCs from lymphocytes (Loh et al. 2009) and adipose cells (Sugii et al. 2010). The delivery of the reprogramming factors was initially achieved using retroviruses (Takahashi et al. 2007) but many other methods have been proposed over the years, especially with the intention of steering away from the potential side effects of viral integration. To date, plasmids (Okita et al. 2011), non-integrating Sendai virus (Fusaki et al. 2009), adenovirus (Stadtfeld et al. 2008), mRNA (Warren et al. 2010), proteins (Kim et al. 2009) and a Cre-loxP system for the excision of the transgenes (Soldner et al. 2009) have all been successfully used to produce iPSCs from somatic cells.

Another approach for the reprogramming of somatic cells is the direct conversion of one cell type to another, eliminating the need for the generation of iPSCs, with the goal of using this technology for *in vivo* applications. Studies have shown that fibroblasts can be directly reprogrammed to neuronal stem cells via the delivery of Sox2 (Ring et al. 2012), or

to dopaminergic neurons with the combined over-expression of three reprogramming transcription factors (Ascl1, Brn2, and Myt1l) and two transcription factors involved in DAn generations (FoxA2 and Lmx1a) (Pfisterer et al. 2011). Interestingly, the expression of three reprogramming factors (Oct4, Sox2 and Nanog) in astrocytes induces the generation of cells expressing neural stem/precursor markers that could then be differentiated into neurons or oligodendrocytes (Corti et al. 2012).

1.3.3|Differentiation of iPSCs to iDAn

Since the introduction of pluripotent stem cell technology, many research groups have started to develop and optimise protocols for their differentiation towards a precise cell lineage. In the context of PD, the focus is to generate the A9 subtype of DAn, which are the cell type most affected by neurodegeneration. Initial attempts to generate human iPSC-derived DAn (iDA) were based on an adaptation of previous protocols generated using mouse ESCs. Early work found that the ectoderm is the default pathway in human ESCs cell-fate acquisition, and the inhibition of the bone morphogenetic proteins (BMPs) is the key point for neuronal induction (Muñoz-Sanjuán and Brivanlou 2002). Multiple studies reported the generation of proliferating neural progenitor cultures (Reubinoff et al. 2001) that could produce midbrain DAn either via the induction of embryoid body (EB) formation (Zhang et al. 2001) or the use of neural-inducing stromal-feeder cell lines (Kawasaki et al. 2002; Perrier et al. 2004; Lee et al. 2007). These protocols generate neuronal precursors organised in rosettes containing monolayers of cells that are positive for the Paired box protein 6 ($PAX6^+$), a key transcription factor in brain development, and can be further differentiated to specific neuronal types. Retinoic acid and sonic hedgehog (SHH) can specify these cells towards a rostral motoneuron phenotype (Lee et al. 2007) whereas SHH and FGF8 can differentiate them to iDAn (Perrier et al. 2004). The ROCK

signalling inhibitor Y-27632 (ROCKi), typically used during the passaging of single-cell stem cells, was found to be key in neuronal differentiation, increasing the efficiency of rosette formation (Watanabe et al. 2007). Nevertheless, these approaches relied on undefined molecules and factors from stromal-feeder cells or the heterogeneous patterning towards all three germ layers induced by the EB formation. Despite these cells showing appropriate functional properties of DAn, they failed to efficiently survive and integrate once grafted *in vivo* (Yang et al. 2008; Ferrari et al. 2006).

A more chemically defined method was published by the Studer laboratory and relied on human recombinant Noggin and SB431542 for a dual inhibition of SMAD signalling to generate a monolayer of neuroectodermal cells, without the need for EB-formation or neural-inducing feeder cells. Moreover, the initial density of ESCs upon induction of differentiation was found to be important to determine caudal-rostral identity of the neuronal precursors, in relation to the CNS *in vivo*. High seeding density resulted in the formation of neuronal rosettes whereas a lower density induced the formation of neural crest–like cells. This protocol was shown to be applicable to iPSC cultures as well and the generation of different neuronal cell-types was achieved by the exposure to different patterning factors and the initial plating of the cells at different densities (Chambers et al. 2009). Subsequently, effort was put into the generation of differentiation protocols aimed at producing floor plate (FP) precursors cells, resembling the region of the CNS from which ventral neuron types, including A9 ventral midbrain DAn (vmDAn), are generated *in vivo* (Isacson, Bjorklund, and Schumacher 2003). The transcription factor Forkhead box A2 (FOXA2) was found to be a robust marker of vmDAn (Ferri et al. 2007), suggesting it could therefore be used as an indicator of the nature of DAn produced by the different protocols. Another study reported that homeoprotein LIM homeobox transcription factor 1α (LMX1A) is another important molecule for the commitment of

cells towards becoming vmDAn in the developing brain (Cai et al. 2009) and was subsequently used to define genuine vmDAn together with FOXA2 (Kriks et al. 2011).

All the early protocols for the differentiation of TH^+ cells via either EBs, rosette formation or the use of stromal-feeder lines were shown to be of a more diencephalic origin, identified by the co-expression of the motoneuron marker Insulin gene enhancer protein (ISL-1) and the dopaminergic marker TH. Very few cells co-expressed both TH and FOXA2 or LMX1A (Cooper et al. 2010). Two protocols were generated to overcome the issue and used LMX1A over-expression to generate correctly specified vmDAn. In both cases, the differentiation protocol included EB formation with (Sánchez-Danés, Consiglio, et al. 2012) or without (Friling et al. 2009) the use of a stromal-feeder cell line to achieve differentiation. SHH had been previously reported to induce ventralisation of neuronal precursors, and an early high-dose exposure was found to induce the up-regulation of the FOXA2 at the expense of the expression of PAX6 and the formation of rosette-like structures. Titration of the concentration and time of exposure of SHH revealed an optimal concentration between 125 and 500 ng/ml from day 1 after neuronal induction with dual-SMAD inhibition. Moreover, it was found that mouse SHH-C25II was 10 times more potent than human SHH-C24II in achieving FP induction (Fasano et al. 2010). Similarly, the correct specification of DAn positive for the midbrain marker FOXA2 also requires FGF8-a and retinoic acid (Cooper et al. 2010). Lastly, the GSK3β inhibitor CHIR99021 is important for the correct specification of FP-derived cells to vmDAn precursors (Kriks et al. 2011; Denham et al. 2012).

After a very fine titration of SHH, CHIR99021 and FGF8, Kriks and colleagues published a protocol for the generation of $FOXA2^+/LMX1A^+$ cells by day 11 after neuronal induction with dual-SMAD inhibition (Kriks et al. 2011). Afterwards, regardless of the type of neuronal induction and patterning, final differentiation into iDAn does not

require any further patterning other than small molecules and growth factors that ensure neuronal maturation and maintenance. Brain-derived neurotrophic factor (BDNF) and glial-derived neurotrophic factor (GDNF) were shown to be neurotrophic factors involved in the maintenance and survival of midbrain DAn (Erickson, Brosenitsch, and Katz 2001). Ascorbic acid was shown to improve the survival of DAn *in vitro*, possibly by counteracting the toxic effects of the auto-oxidation products of endogenous DA (Yan, Studer, and McKay 2001). Dibutyryl cyclic AMP (db-cAMP) was shown to increase the levels of DA and the number of TH^+ neurons in primary neuronal cultures by inducing the differentiation to DAn of neuronal progenitor (Mena et al. 1995), wheareas the Notch inhibitor DAPT (N-[N-(3,5- difluorophenacetyl)-l-alanyl]-S-phenylglycine t-butyl ester) was found to enhance neuronal differentiation in combination with the activation of SHH signalling (Crawford and Roelink 2007). Last, the treatment of neurospheres with TGFβ3 increases the number of TH^+ neurons, consistent with the finding that TGFβ2/TGFβ3 double-KO mice display a reduced number of DAn in the midbrain. (Roussa et al. 2006). All these molecules were reported to promote the differentiation, survival and maintenance of iDAn (Perrier et al. 2004).

Other protocols were then published, based on the previous work by Kirks and colleagues. The protocol published by the Parmar laboratory uses both the dual-SMAD inhibition and EBs formation to generate *bona fide* A9 vmDA from hESCs under chemically defined conditions. Interestingly, FGF8 was nor required for vmDA specification under these experimental conditions (Kirkeby et al. 2012). Work by Doi and colleagues used iPSCs cultured onto human recombinant laminin instead of Matrigel, claiming it increased neuronal differentiation and survival. Afterwards, cells were grown as floating spheres before being plated for final differentiation. Cell sorting for the surface marker CORIN at day 12 was found to generate correctly specified vmDA by day 42, closely resembling fetal

ventral midbrain tissue (Doi et al. 2014). The protocol available in the Wade-Martins laboratory generated by E. Hartfield and colleagues includes the generation of EBs from iPSC cultures and the initiation of neuronal induction via dual-SMAD inhibition. Subsequently, cells within the neuronal rosettes are patterned towards a dopaminergic phenotype via SHH and FGF8-a. Lastly, EBs are manually dissected and replated for final differentiation as discussed above for all the other protocols. DAn in these cultures were shown to express DAT, GIRK2 and VMAT2 and possess Ca^{2+} and electrophysiological properties similar to DAn *in vivo* (Hartfield et al. 2014).

To date there are many different protocols for the differentiation of iPSC to iDAn. They all rely on the same growth factors and small molecules and essentially differ only in their concentration and time of exposure. All protocols achieve dopaminergic differentiation either by the generation of FP precursor cells (Kriks et al. 2011; Xi et al. 2012; Kirkeby et al. 2012), neuronal rosettes (Cooper et al. 2010; Hartfield et al. 2014; Nguyen et al. 2011; Sánchez-Danés, Consiglio, et al. 2012; Byers et al. 2011) or using stromal-feeder cells (Kawasaki et al. 2002; Perrier et al. 2004) with or without EB formation. However, it worth noticing that some of these studies used the H9 hESC line, that has been previously shown to differentiate to neurons much more easily than others (Kim, Lee, et al. 2010; Hu et al. 2010).

1.3.4|Promises and bottlenecks of iPSC-based disease biology

The number of iPSC lines used in a study is clearly determined and limited by the number of patients with a specific rare genetic background. Beyond that, the number of lines used is limited by the cost of iPSC reprogramming, maintenance and differentiation. A further question would be how many clones from a single iPSC line should be enough to be considered informative regarding the effect of a single point mutation within the greater

genetic variability that distinguishes each individual. Lastly, the higher the number of samples and the complexity of the assay, the more challenging the analysis becomes, both in terms of experimental design and statistical analysis.

In the context of neurodegenerative pathologies, the terms "disease in a dish" and "*in vitro* modelling" are somewhat elusive, considering the complexity of the brain and the fact that these conditions generally have an adulthood onset and are phenotypically different among patients. Moreover, it is debatable whether studying a very pure population of a specific type of neuron could resemble the physiological condition in the brain. Yet, this approach is clearly more relevant than using immortalised cells lines of different origin, like human embryonic kidney cells (HEK293) or cervical cancer cells (HeLa), which are often used in the context of PD.

Variability among different iPSC lines, even those generated in the same laboratory or clones of the same line, is well known but poorly understood and even less documented or addressed. It is worth pointing out that each iPSC line clone is generated by manual selection of a single reprogrammed fibroblast, which is then expanded and differentiated to a specific cell type using a cocktail of growth factors and small molecules. Such clonal origin means that any genetic difference present in the fibroblast will have confounding downstream effects. Variability in differentiation propensities of iPSCs is dependent on the donor and not by the cell-type of origin, with transcriptional and epigenetic signatures being the determining factors causing variability in differentiation across iPSC lines (Kyttälä et al. 2016). However, this is in contrast with previous reports claiming that iPSCs maintain a somatic epigenetic signature that causes preferential lineage-specific differentiation (Bar-Nur et al. 2011; Kim, Doi, et al. 2010). Even among different ESC lines, there is a certain preference to differentiate towards a certain cell-type compared to others (Osafune et al. 2008). This suggests that the reprogramming of somatic cells to iPSC

could induce even further variability. For example, iPSCs were shown to have reduced differentiation efficiency when different sets of reprogramming factors were used (Löhle et al. 2012), indicating that the reprogramming strategy might impact the differentiation ability of different iPSC lines. The difference in neuronal differentiation capacity between human iPSCs and ESCs was elegantly compared and showed that iPSCs, despite using the same transcriptional network and responding to the same molecules as ESC, do differentiate to neurons less efficiently and with increased variability (Hu et al. 2010). Overall, it is still debated whether iPSCs are actually different or comparable to ESCs. In spite of everything, it is interesting to point out that man-made iPSCs are exceptionally similar to naturally-existing ESCs (Yamanaka 2012).

A genome-wide expression profile analysis showed that only isogenic iPSC lines have a comparable differentiation outcome to the parental line, whereas a clone of a iPSC line can cluster closer to an unrelated iPSC line than clones of the same line (Reinhardt et al. 2013). The use of isogenic corrected lines has become the gold standard since the development of genome editing technology, of which the latest one is represented by CRISPRs (Mali et al. 2013). Isogenic controls are generally used to overcome the variability among control and disease lines and allow to focus on the effect of a single base change in the genome that could be masked by the genetic variability between donors (Ryan et al. 2013; Soldner et al. 2016; Reinhardt et al. 2013; Schöndorf et al. 2014) or to generate knock-out lines (Shaltouki et al. 2015) to study protein function.

Differentiation protocols seem to play an important role for phenotypic analysis. Molecular characterisation of the final cell population is certainly important, since ubiquitous proteins cause many diseases but affect only a precise cell type, as in the case of αSyn in PD and MSA. In the context of PD, the generation of A9 vmDAn is crucial since other TH^+ neurons in the brain are less affected by the phenotypes. This has been

highlighted by *in vitro* studies comparing DAn generated by either a FP- or a rosette-based protocol, with the latter not generating a phenotype (Chung et al. 2016). Moreover, FP-derived DAn were shown to be more effective for grafting compared to rosette-derived cells (Kriks et al. 2011).

1.4|RNAi

1.4.1|Introduction

The manipulation of gene expression has been greatly explored to evaluate the effects of up- or down-regulation of specific genes to understand their cell function. With regards to down-regulation, the most powerful tool is the generation of knockout animal models in which the ablation of a specific gene leads to the disruption of its expression and therefore function. In *in vitro* human models, this approach is not easily applicable but can be overcome with strategies aiming to target gene expression at the post-transcriptional level. In 1993, a gene (*lin-4*) known to be important for post-embryonic development in C. *elegans* was shown not to encode for a protein but instead an antisense RNA molecule to the mRNA encoding for the protein LIN-14 (Lee, Feinbaum, and Ambros 1993). This phenomenon had been previously described in plants as a down-regulation mechanism by which mRNA expression is not altered but the level of the mRNA produced by a certain gene is reduced (Napoli, Lemieux, and Jorgensen 1990). To date, this mechanism has been exploited in the form of RNA interference (RNAi) to study the function of genes and is characterised by high potency and specificity. In the last decade, RNAi has also become a potential therapeutic approach for a wide range of diseases.

The aim for this section is to illustrate the different ways to use exogenous molecules to achieve down-regulation of specific proteins. Specifically, methods for RNAi in iPSC-derived neurons will be discussed for their relevance of the work reported in chapter 5.

1.4.2|The mechanism of RNAi

RNA interference (RNAi) is the process by which double stranded RNA (dsRNA) initiates

the assembly of a RNA-protein complex that targets a specific gene and results in the reduction of its transcription rate, mRNA stability or translation. MicroRNAs (miRNAs) were discovered as endogenous single-stranded RNA (ssRNA) of 21-24 nucleotides that could bind to a target mRNA (Lee, Feinbaum, and Ambros 1993) and cause silencing either by cleavage or translation inhibition (Doench and Sharp 2004). miRNAs are evolutionally conserved non-coding RNAs that are transcribed from loci normally not annotated with genes, from introns within genes or others are simply clustered in the genome instead (Lagos-Quintana et al. 2001; Lagos-Quintana et al. 2003; Lau et al. 2001). Large primary miRNAs (pri-miRNAs) are transcribed by RNA polymerase II (RNApolII) and then cleaved by enzymes with RNAse activity to generate miRNAs that are about 22 nucleotides in length (Bernstein et al. 2001; Lee et al. 2003). A strand of the miRNA is then loaded into the RNA-induced silencing complex (RISC), which in turn causes RNAi by translational repression due to RISC sequestration of the target mRNAs, guided by the binding of the antisense RNA with a looser complementarity, generally up to 7 nucleotides (Pratt and MacRae 2009).

The endogenous machinery of RNAi can be exploited *in vitro* in two ways. Small interfering RNAs (siRNAs) are exogenous 21 nucleotide RNA duplexes, whereas small hairpin RNAs (shRNA) are transcribed from an exogenous DNA-based plasmid generally integrated into the host genome. siRNA and shRNAs have perfect complementarity to their target mRNA and RISC causes its degradation via nicking the mRNA between the tenth and eleventh base from the 5′-end of the antisense RNA (Pratt and MacRae 2009).

siRNAs are advantageous in terms of affordability, therefore allowing for the screening of large libraries. Work by Elbashir and colleagues reported the applicability of using exogenous RNA duplexes to down-regulate the expression of endogenous proteins in mammalian cell lines (Elbashir et al. 2001). However, their delivery via transfection is

limited in post-mitotic cells, like neurons, and their overall effect is only transient (Paddison et al. 2002).

In comparison, DNA-based plasmids encoding for shRNAs were shown to be a suitable alternative to siRNAs for RNAi. shRNAs have the advantage of sustained long-term expression if the plasmid is retained or integrated in the genome, and can be delivered to hard to transfect cells using viral packaging. Yet, cloning of individual shRNAs and viral packaging is costly and very labour intensive, compared to the transfection of siRNAs. Several constitutive promoters have been used to express shRNAs but the H1 (Brummelkamp, Bernards, and Agami 2002; Sapru et al. 2006; Hasson et al. 2013) and U6 (Schöndorf et al. 2014; Yu, DeRuiter, and Turner 2002) are the most widely adopted. Discrepancies were reported regarding the importance of the length or sequence of the loop (Paddison et al. 2002; Brummelkamp, Bernards, and Agami 2002). Nonetheless, recent work by Jensen and colleagues showed that, despite neither specific sequences or motifs being identified, a screening of different loop sequences found 5'-UGUGCUU-3' to be associated with constructs achieving good knockdown independently from the sense-antisense sequence (Jensen et al. 2012). Most viral constructs contain a fluorescent protein (like eGFP) as a reporter, which is useful for viral titering and to estimate transduction efficiency. In most cases, eGFP is under the control of a strong viral promoter like the Cytomegalovirus promoter (CMV). Unfortunately, it is known that viral promoters can be silenced in stem cells (Norrman et al. 2010), which raises the question of whether this could happen in iPSC-derived cells. One of the most employed promoters is the human elongation factor 1α (eEF1α), which not only is based on a human and not viral sequence but was also shown to sustain strong expression levels in lots of cell types (Qin et al. 2010). In the context of stem cells, mouse ESCs transduced at any stage of the differentiation to neurons with a transgene under the control of the eF1α promoter, showed robust transgene

expression. Nevertheless, mESCs transduced with the same vector showed a significant reduction of transgene expression during *in vitro* differentiation (Hong et al. 2007). The eF1α promoter has been successfully used in iPSCs cultures (Sui et al. 2014) and, although down-regulated during long term culture of undifferentiated iPSCs, was the most stable among other promoters based on human sequences (Norrman et al. 2010).

1.4.3|*In vitro* delivery of RNAi

The most popular way to introduce RNA inside cells is to use carrier molecules (hereafter referred to as transfection), exploiting the ability of nucleic acids to interact with positively charged molecules, such as cationic lipids, to form complexes that are cell-permeable. Ca^{2+}-phosphate co-precipitation has been widely used to deliver siRNAs to cells (Dahm et al. 2008; Donzé and Picard 2002) but the efficiency is generally around 1-5%, especially in primary cells (Xia, Dudek, et al. 1996). Nucleofection relies on a physical method that combines classical electroporation with cell type-specific parameters to deliver genetic material, like siRNAs, to post-mitotic cells like neurons. One of the biggest limitations of this technique is that it can only be applied to cells in suspension, which is something not easily achievable when working with primary or iPSC-derived neurons (Zeitelhofer et al. 2007). Like Ca^{2+}-phosphate co-precipitation, lipofection exploits the ability of negatively charged nucleic acids to bind a positively charged molecule, in this case cationic lipids, to form complexes that are cell-permeable. This technique is considered the gold standard for transfections and has been widely applied to siRNAs and to many different cell types. The lipofection reagent Lipofectamine 2000 has been used to deliver siRNAs to rat primary neurons with an efficiency of ~20-30% (Dalby et al. 2004).

An alternative to the delivery of nucleic acids to cells via chemical or physical methods is the use of viruses (hereafter referred as transduction), employing their capacity

to infect cells and transfer their genetic material. Post-mitotic cells, like neurons, are notoriously challenging to transfect, mostly in terms of achieving high transfection efficiencies. Moreover, they are also very sensitive to changes in the extracellular environment, with transfection solutions causing temporary changes in pH and osmolarity or actual physical stress on the cell membrane during lipofection (Karra and Dahm 2010). The shRNA-based approach takes advantage of the high efficiency given using viral delivery but is also restricted in scale by the generation of DNA constructs and viral particles. Lentiviruses are a type of RNA-based viruses that have been extensively employed to transduced cells to achieve knockdown (Hartfield et al. 2011; Sapru et al. 2006). These viruses are capable of infecting post-mitotic cells and are characterised by high transduction efficiency and low cytotoxicity. The stable integration of their genome into the host allows them to be used for the generation of over- or inducible-expression and knockdown systems (Rahim et al. 2009).

To date, not many studies regarding iPSC-derived neurons have included transfection or transduction at the later stages of the differentiation. Most of the genetic engineering has instead focussed on the manipulation of iPSCs with the creation of isogenic controls (Ryan et al. 2013; Reinhardt et al. 2013; Schöndorf et al. 2014) or reporter lines (Watmuff et al. 2015). However, a few studies have succeeded in applying transfection and transduction techniques to iPSC-derived neurons. Genetic constructs were successfully introduced into iPSC-derived DAn via either nucleofection (Ryan et al. 2013) or lipofection (Chang et al. 2016), whereas lipofection together with an interferon inhibitor was used to deliver a modified mRNA (Miller et al. 2013). Lentiviruses have been used to deliver constructs for the expression of shRNA to different iPSC-derived cell types, including hDAn (Schöndorf et al. 2014; Hasson et al. 2013) and motoneurons (Yang et al. 2014), or proteins (Woodard et al. 2014; Jiang et al. 2012).

1.4.4|Alternative knockdown methods

There are other less common or novel avenues for knocking down proteins that can be explored and are applicable to iPSC-derived neurons, should RNAi not be suitable or effective. It is possible to exploit the cellular machinery involved in the regulation of gene expression, like microRNAs (miRNAs), to knockdown a protein of interest. Specifically for αSyn, miRNA-155, miRNA-7 and miRNA-153 (Doxakis 2010; Fragkouli and Doxakis 2014; Junn et al. 2009) were all shown to decrease protein levels and in some studies confer protection to MPP^+ toxicity in rodent and cellular models. The same mechanism by which the CRISPR technology is used for gene editing can be used to induce knockdown of target proteins at the transcription level (CRISPRi). Upon designing a single guide RNA (sgRNA) that binds the gene of interest in the genome, the Cas9-sgRNA complex binds to the DNA impeding transcription elongation by the RNA polymerase (Gilbert et al. 2013). Peptides can be used to bind a protein of interest and target it for degradation, for example to the lysosome. The "tat-βSyn-degron" peptide relies on three different sequences that allow it to bind αSyn and prime it for degradation via CMA. The "tat" sequence renders the peptide cell permeable, the "degron" sequence corresponds to the CMA-targeting motif (KFERQ) and the βSyn sequence is a short stretch of amino acids of the βSyn protein (36–45) that was shown to interact and bind to αSyn. Both HEK293 cells and rat cortical neurons treated with this peptide showed a decrease in αSyn protein levels (Fan et al. 2014). Lastly, it is possible to pharmacologically decrease αSyn with the compound posiphen that represses αSyn translation via the binding to its 5'-untranslated region, where a sequence similar to the iron-responsive element (IRE) is present (Rogers et al. 2011).

1.5|Aims

The overall aim of this thesis is to investigate the pathological mechanisms associated with αSyn in the context of PD using iPSCs differentiated to iDAn.

This will be detailed in four results chapters:

- Establishment of a protocol for the differentiation of iPSCs to midbrain iDAn (Chapter 3).
- Identification of iPSCs carrying the A53T *SNCA* mutation or a triplication of the *SNCA* gene and the initial characterisation of iDAn derived from these cells (Chapter 4).
- Phenotypic analysis of A53T *SNCA* mutation and *SNCA* Triplication iDAn to elucidate pathological mechanisms linked to αSyn (Chapter 5)
- Knock down of αSyn in iDAn and evaluation of its effect on cell physiology and PD-related phenotypes (Chapter 6)

Chapter 2

Material and methods

2.1|DNA and RNA manipulation

2.1.1|Bacterial cultures

All bacterial cultures were grown in liquid Lysogeny broth or Lysogeny broth-agar plates containing 100 µg/mL Ampicillin. Cultures were performed using a shaking incubator set at 225 rpm and 37°C. Minipreps were prepared using a bench-top microcentrifuge and maxipreps were prepared using an Avanti J-E centrifuge (Beckman Coulter) and a JA10.5 rotor.

2.1.2|Transformation of chemically competent bacteria

DNA constructs were transformed into chemically competent One Shot® TOP10 *E.coli* (Thermo Fisher Scientific - C4040) following the manufacturer's instructions. Briefly, bacteria were thawed on ice before adding 2 µL of Gibson Assembly product previously diluted 1:4 with ddH_2O and left to stand for 30 minutes on ice. They were then heat-shocked at 42°C for 30 seconds before leaving them to stand on ice for 2 minutes. 250 µL of Super Optimal Broth (SOC) medium (Thermo Fisher Scientific - C4040) were added to the tube and bacteria were left to recover at 37°C with 250 rpm shaking for 1 hour. Finally, bacteria were plated onto Lysogeny broth-agar plates containing antibiotic for the selection of the transformed bacteria. Colonies positive for the desired plasmid and insert were

screened via digestion with restriction enzymes of minipreps the day after. For stable stock of transformed bacteria, One Shot® Stbl3™ chemically competent *E.coli* (Thermo Fisher Scientific - C7373) were transformed as described above and then stored at -80°C in 10% DMSO.

2.1.3|Small scale plasmid DNA purification

Single bacterial colonies or DMSO stocks were inoculated into a 1.5 mL starter Lysogeny broth culture containing antibiotics and grown overnight (at least 16 hours). Bacteria suspensions were pelleted at 4000 x *g* for 5 minutes and the supernatant was discarded. Cells were resuspended in 70 µL of STET solution, lysed with 200 µL Solution 2 and neutralised with 150 µL of Solution 3. After incubating the lysate for 5 minutes on ice, debris were pelleted at 16,100 x *g* for 10 minutes and the supernatant was recovered. The DNA was precipitated by adding 250 µL of isopropanol and pelleted at 10,000 x *g* for 10 minutes. After a wash with 250 µL of 70% EtOH wash, the pelleted DNA was left to air-dry and finally resuspended in TE buffer supplemented with 5µg/mL RNAse A.

2.1.4|Large scale plasmid DNA purification

The PureLink® HiPure Plasmid DNA Purification Kit (Thermo Fisher Scientific - K2100) was used for the purification of plasmid DNA for transfection purposes. A single bacterial colony or a sample from a DMSO stock was inoculated into a 1.5 mL starter Lysogeny broth culture and grown for 8 hours (start culture), which was then tipped into a 300 mL Lysogeny broth culture and allowed to grow overnight (at least 16 hours). Bacteria were pelleted by centrifugation at 6000 x *g* for 10 minutes at 4°C. The pellet was resuspended in 10 mL of Buffer R1. Following resuspension, bacteria were lysed in 10 mL of Buffer L7, swirled thoroughly to mix and left to incubate at RT for 5 minutes. Finally, 10 mL of

chilled Buffer N3 were added to neutralise the lysis buffer, mixed by swirling and left to stand on ice for 10 minutes. The tube was then centrifuged for 10 minutes at 10,000 x *g* at 4°C to pellet cellular debris and bacterial genomic DNA. Meanwhile, the column was equilibrated with 15 mL of Buffer EQ1 by allowing the buffer to flow through by gravity. The cleared supernatant was passed through two layers of filtering tissue and then allowed to flow through the column by gravity, followed by a wash with 60 mL Buffer W8. The DNA was eluted with 15 mL of Buffer E4 in 50 mL centrifuge tubes. Eluted DNA was precipitated and pelleted with 10.5 mL of isopropanol and subsequent centrifugation at 4,000 x *g* for 30 minutes at 4 °C. Following centrifugation, the isopropanol was carefully tipped off and the pellet was washed by adding 5 mL of 70% EtOH. After an additional centrifugation at 4,000 x *g* for 10 minutes at 4 °C, the supernatant was discarded and the pellet allowed to air-dry for 10-20 minutes. Finally, the plasmid DNA was resuspended in 250 µL of TE buffer overnight at 4 °C before DNA quantification and storage at -20°C.

2.1.5|Endotoxin-free purification of plasmid DNA using CsCl gradient

This method was used for the purification of plasmid DNA for transfection purposes requiring high amounts of DNA and very low levels of endotoxins (i.e. packaging of lentiviruses in HEK293T cells). A single bacterial colony or a sample from a DMSO stock were inoculated into a 1.5 mL starter Lysogeny broth culture and grown for 8 hours, which were then tipped into a 500 mL Lysogeny broth culture and allowed to grow overnight (at least 16 hours). Bacteria were pelleted by centrifugation at 4,000 x *g* for 10 minutes at 4°C and then resuspended in 18 mL of freshly prepared Solution 1. Following resuspension, 2 mL of freshly prepared Lysozyme Solution were added and swirled thoroughly to mix, before adding 40 mL of Solution 2 to lyse the cells. After incubating at RT for 10 minutes, the lysate was neutralised by adding 20 mL of chilled Solution 3, swirled thoroughly and

left to stand on ice for 10 minutes. The sample was then centrifuged for 10 minutes at 10,000 x *g* at 4°C (Beckman J10.5 rotor) to pellet cellular debris and bacterial genomic DNA. The cleared supernatant was passed through two layers of filtering tissue and collected. The DNA was precipitated by adding 58 mL of isopropanol and pelleted at 10,000 x *g* form 30 minutes at 4°C (Beckman J10.5 rotor). Following centrifugation, the supernatant was carefully tipped off and the pellet was resuspended in 7 mL of TE buffer with gentle swirling. The sample was then transferred into a 50 mL tube containing 7 g of CsCl (Sigma-Aldrich - 289329) and left to dissolve before adding 300µL of 10 mg/mL ethidium bromide solution (Sigma-Aldrich - E1510). After a spin at 4,000 x *g* for 10 minutes at 25°C, the supernatant was carefully loaded into an ultracentrifuge tube (Beckman Coulter - 342413), topped up 1 g/mL of CsCl in TE buffer and spun at 50,000 rpm overnight for 20 hours at 25°C in a 70.1Ti rotor in a Beckman L90-K Ultracentrifuge. The next day, the gradient was examined to determine the presence of an upper band corresponding to nicked/linearised plasmid DNA and a lower band corresponding to supercoiled plasmid DNA. The lower band was carefully removed using a syringe with a 27G needle and loaded into a new ultracentrifuge tube. After topping up with 1 g/mL of CsCl in TE buffer, the sample was spun again at 50,000 rpm for 20 hours at 25°C. The following day the band corresponding to supercoiled plasmid DNA was extracted as described above. The ethidium bromide was removed by at least 5 extraction against a ddH_2O-saturated 1-butanol solution (Sigma-Aldrich - B7906). The sample was then transferred into a clean 50 mL tube and topped up to 10 mL with ddH_2O before adding 40 mL of 100% EtOH to precipitate the DNA. Plasmid DNA was pelleted at 4,000 x *g* for 30 minutes at 4°C. Following centrifugation, the supernatant was carefully tipped off and the pellet washed with 5 mL of 70% EtOH. After an additional centrifugation at 4,000 x *g* for 10 minutes at 4°C, the supernatant was discarded and the pellet allowed to air-dry for

10-20 minutes. Finally, the plasmid DNA was resuspended in 500 µL of TE buffer overnight at 4°C before DNA quantification and storage at -20°C.

2.1.6|Genomic DNA purification

Genomic DNA (gDNA) was extracted from cell pellets and purified using the Illustra genomicPrep Mini Spin Kit (GE Healthcare - 28-9042-75). Briefly, cells were harvested and snap-frozen and stored at -80°C, if necessary. The sample was then lysed with 100 µL of Buffer type 1 before adding 10 µL of Proteinase K (20 mg/ml) and incubated for 15 minutes at 56°C followed by 2 minutes at 70°C; in the meantime, 200 µL of Elution buffer type 5 were warmed to 70°C. To remove any RNA, 5 µL of RNase A (20mg/mL) were added to the sample and left to incubate for 15 minutes at RT. Afterwards, 500 µL of Lysis buffer type 4 were added and left to incubate for further 10 minutes at RT. The sample was then centrifuged at 11,000 x *g* for 1 minute to pellet the cell debris before applying the supernatant to the column provided with the kit. The column was then spun for 1 minute at 11,000 x *g* and the flow-through was discarded. Afterwards, the column was washed with 500 µL of Wash buffer type 6 and spun 3 minutes at 11,000 x *g*. Lastly, the column was transferred to a fresh DNAse- free micro-centrifuge tube and the DNA was eluted with 200 µL of pre-warmed Elution buffer type 5 and a spin for 1 minute at 11,000 x *g*. The purified gDNA was then quantified and stored at -20°C.

2.1.7|Polymerase Chain Reaction (PCR)

All polymerase chain reactions (PCR) were carried out using a BioRad Tetrad 2 Peltier Thermal Cycler. All primers were purchased from Integrated DNA Technologies (Leuven, Belgium). See section 2.7 for primer sequences.

For PCR not requiring proof-reading transcription, the AmpliTaq Gold® DNA Polymerase

with Buffer II and $MgCl_2$ kit (Thermo Fisher Scientific - N8080245) was used. The following reagents and cycling conditions were used:

Component	per rxn
2X KAPA kit	12.5 µL
10µM primers	1µL each
DNA template	varies
ddH2O	up to 25 µL

	Cycles	
	Temperature	Time
	95C	10 minutes
x30	95C	15 seconds
	52 - 68C	30 seconds
	72C	1kb/min
	72C	5 minutes

Table 2.1|Conditions for PCR using AmpliTaq Gold

For PCR requiring proofreading transcription, the KAPA Taq PCR Kit (Kapa Biosystems - KK1006) was used. The following reagents and cycling conditions were used:

Component	per rxn
10X AmpliTaq buffer	2.5 µL
25mM $MgCl_2$	1.5 µL
10mM dNTPs mix	1.25 µL
10µM primers	1 µL each
DNA template	varies
5U/µL AmpliTaq Gold	1µL
ddH_2O	up to 25 µL

	Cycles	
	Temperature	Time
	95C	10 minutes
x30	95C	15 seconds
	52 - 68C	30 seconds
	72C	1kb/min
	72C	5 minutes

Table 2.2|Conditions for PCR using KAPA HiFi PCR Kits

Annealing temperatures and extension times were adjusted according to each reaction to provide optimal specificity. In the case of assessing the optimal temperature for annealing of primers, a gradient between 52°C and 68°C was used. For cloning purposes, 25 ng of template were used, whereas 100 ng of gDNA were used for genotyping purposes.

2.1.8|Agarose gel electrophoresis

Agarose gel electrophoresis was used to resolve and analyse DNA fragments from a PCR or

from a restriction enzymes digestion. Agarose gels were prepared at a concentration of 0.7-2% agarose (w/v), depending on the resolution required, in TBE buffer (Sigma-Aldrich - T4415) containing 0.25 µg/mL of ethidium bromide. Samples were prepared by adding the appropriate volume of 6X DNA Loading Buffer. Electrophoresis was performed using a standard electrophoresis tank (Biorad) at 120V in TBE buffer until the desired separation was achieved. The HyperLadderTM 1 kb (Bioline - BIO-33053) and/or HyperLadderTM 50 bp (Bioline - BIO-33054) were used as size indicators of DNA fragments. Gels were imaged on a Biorad Gel Dock and processed using the Quantity One software (Biorad), if necessary.

2.1.9|Restriction enzymes digests

The digestion of DNA with restriction enzyme(s) was carried out using New England Biolabs (NEB) restriction enzymes; buffers and optimal temperature were selected using the Double Digest Finder tool available in the on the NEB website (www.neb.com). Typically, 200 ng of previously amplified gDNA, 4 µL of a miniprep or 1 µg of plasmid DNA from a maxiprep were used per reaction. The following reagents and cycling conditions were used:

Component	per rxn
10X CutSmart Buffer	2 µL
DNA	varies
Restriction enzyme(s)	5U
ddH_2O	up to 20 µL

Table 2.3|Conditions for restriction enzymes digestion

2.1.10|DNA purification from agarose gel

DNA fragments or PCR amplificates were purified from the agarose gels using the QIAquick Gel Extraction Kit (Qiagen - 28704) following manufacturer's instructions.

Briefly, DNA fragments were excised from the agarose gel using a scalpel and weighed, before adding 3 volumes of Buffer QG, considering that 100 mg of agarose gel are approximately 100 µL. Samples were incubated at 50°C until the agarose gel was completely dissolved, before adding one gel volume of isopropanol. The solution was then loaded onto the column and spun at 16,100 x *g* for 1 minute; the same procedure was repeated twice adding 500 µL of Buffer QG and 750µL of Buffer PE to wash the column. The column was then dried out with a spin at 16,100 x *g* for 1 minute before eluting the DNA with 25 µL of DNAse-free ddH_2O.

2.1.11|Gibson Assembly

Two or more DNA fragments were ligated together using the Gibson Assembly kit (NEB - E2611) following manufacturer's instructions. The concentration of DNA was calculated as $pmol_{DNA}$= (weight in ng) x1,000/(base pairs x 650 daltons). For up to 3 inserts, the reaction was carried on for 15 minutes at 50°C, whereas for up to 6 inserts the reaction was set for 1 hour. Following incubation, assembled products were diluted 4-fold with ddH_2O and stored on ice or at -20°C for subsequent transformation.

Component	1 - 3 inserts	4 - 6 inserts
Gibson Master mix 2X	2.5 µL	2.5 µL
Insert(s)	3X	3X
Vector	1X	1X
Total DNA	0.02-0.5 pmol	0.2- 1 pmol
ddH_2O	up to 20 µL	up to 20 µL

Table 2.4|Conditions for Gibson Assembly

2.1.12|Annealing, dephosphorylation and ligation of DNA fragments

Complementary oligonucleotides were annealed *in vitro* using a BioRad Tetrad 2 Peltier Thermal Cycler. Oligonucleotides were denatured at 95°C for 3 minutes before 70 cycles

of 30 seconds with the temperature decreasing by 1°C at every cycle (final cycle at 25°C). Annealed oligonucleotides where then kept on ice or stored at -20°C. The 5'-end of linear DNA obtained via restriction enzyme(s) digestion was de-phosphorylated before any further cloning to reduce auto-ligation. 1-5 µg of DNA was incubated at 37°C for 15 minutes in a final volume of 20 µL with 2 U of DNA of Antarctic Phosphatase (NEB - M0289S) and 1X Antarctic Phosphatase Reaction Buffer. DNA fragments with complementary ends were ligated at a variable molar ratio depending on the application (1:5-100). DNA fragments were incubated at RT for 20 minutes in a final volume of 10 µL with 1 µL of T4 DNA Ligase (NEB - M0202S) and 1X T4 DNA Ligase Buffer.

2.1.13|Sequencing

Samples for sequencing were prepared accordingly to the BigDye® Terminator Sequencing Kit (Thermo Fisher Scientific - 4337455) in a 96-well plate. Each DNA molecule was sequenced twice with a forward and reverse primers separately. Primer sequences are listed in Table 2.7.

The DNA was then precipitated by adding 2 µL of 125 mM EDTA, 2 µL of 3 M sodium acetate and 50 µL of 100% EtOH and pelleted at 3000 x *g* at 4°C for 30 minutes. After discarding the supernatant, the pellet was washed with 50 µL of 70% EtOH and spun down at 1650 x *g* at 4°C for 15 minutes. The supernatant was discarded and the pellet left to air-dry for 10 minutes before storing the plate at -20°C. The sequencing reaction was carried out at the Sequencing Facility (Department of Zoology, University of Oxford). Results were analysed and validated using SpanGene software (GSL Biotech LLC).

Component	per rxn
5X Buffer	2.0 µL
Big Dye	0.5 µL
10µM primer	1.0 µL
Mini-prep	1.0 µL
ddH2O	5.5 µL

	Cycles	
	Temperature	Time
	95C	1 minute
x30	95C	10 seconds
	50C	5 seconds
	60C	4 minutes

Table 2.5|Conditions for sequencing

2.1.14|DNA and RNA quantification

DNA preparations were quantified using the The NanoDrop 1000 Spectrophotometer at the wavelength of 260 nm. The protein contamination was assessed by measuring the absorbance at 260 nm and 280 nm: DNA with a ratio of 260/280 ratio is considered pure. Moreover, the 230/260 ratio was used to access the purity of the nucleic acid preparation from other contaminants; this ratio is expected to be >2 for pure DNA.

2.2|Protein expression analysis

2.2.1|Protein extraction

Cells were pelleted at 2000 x *g* and 4°C for 5 minutes and then snap-frozen before being stored at -80°C. Proteins were extracted using RIPA buffer supplemented with cOmplete protease inhibitor cocktail (Sigma-Aldrich - 4693159001) and PhosSTOP™ (Sigma-Aldrich - 4906845001). Cells were resuspended and lysed before being sonicated for 10 seconds (Model 50 Sonic Dismembrator, Fisher Scientific). After 30 minutes in ice, lysates were centrifuged at 16,100 x *g* for 30 minutes and the supernatant was collected and stored at -20°C.

2.2.2|Protein quantification (BCA assay)

Protein content was quantified by Bicinchoninic acid (BCA) assay. Protein standards were prepared using serial dilutions of Bovin Serum Albumin (BSA) from 1000 to 100 ng/µL and using ddH_2O as blank. The reaction was carried out in triplicate in a 96-well plate and each sample was diluted 1:5 in ddH_2O. The reaction was carried out for 30 minutes at 37°C before measuring the absorbance at 562 nm using the Synergy HT plate reader (BioTek). After subtracting the blank value from all samples, the protein concentration of the sample was derived using the standard curve.

2.2.3|Western blotting

Samples for gel electrophoresis were prepared by adding 5X Laemmli Buffer, before being denatured at 95°C for 10 minutes. 5-10 µg of protein were separated using Mini-PROTEAN® TGX™ Precast Protein Gels (Bio-Rad - 4561086) or 13% hand-cast Tris-Glycine gels run at 200V for about 45 minutes in 1X Running Buffer. The samples were transferred onto PVDF membranes (Trans-Blot® Turbo™ Mini 0.22µm PVDF Transfer Pack, Bio-Rad - 1704156) using a Trans-Blot® Turbo™ Transfer System (Bio-Rad). Membranes were blocked with 5% skimmed milk in TTBS for an hour. Primary antibodies (see Section 2.9) were incubated overnight at 4°C at the appropriate dilution in 1% skimmed milk in TTBS. HRP-conjugated secondary antibodies (see Section 2.9) were used at the dilution of 1:5000 and incubated with the membrane for 1 hour. The Immobilon Western Chemiluminescent HRP Substrate (Millipore) was used to develop the membrane and images were acquired using a Gel Doc™ XR+ System (Bio-Rad). Densitometry analysis was performed with ImageJ (NIH, Bethesda, Maryland, USA) to quantify bands; these were then normalised for the loading control β-actin.

2.2.4|Immunocytochemistry

Cells were fixed in 4% paraformaldehyde (PFA) and stored in PBS/Ca^{2+}+Mg^{2+}. Cells were permeabilised and blocked in PBS/Ca^{2+}+Mg^{2+} containing 0.1% Triton-X100 and 10% serum for 1 hour at RT, before incubation with primary antibodies overnight at 4°C in PBS/Ca^{2+}+Mg^{2+} containing 0.1% Triton-X100 and 1% serum. AlexaFluor-conjugated secondary antibodies were incubated for 1 hour at room temperature in PBS/Ca^{2+}+Mg^{2+} containing 0.1% Triton-X100 and 1% serum. Nuclear DNA was stained with DAPI (Thermo Fisher Scientific - D1306) for 5 minutes at RT. Coverslips were mounted onto microscope slides with FluorSave (Merk Millipore - 345789). Images were captured on a EVOS FL Auto Cell Imaging System.

2.3|Cell culture and iPSC differentiation protocols

2.3.1|BE(2)M17 cells culture for routine use

Human BE(2)-M17 neuroblastoma cells were obtained from the European Collection of Cell Cultures and used within 20 passages of the original vial. Cells were cultured in Opti-MEM (Thermo Fisher Scientific - 31985070) supplemented with 10% v/v foetal bovine serum (FBS) (Thermo Fisher Scientific - 10270-106), 100 U/mL penicillin and 0.1 mg/mL streptomycin at 37°C and in 5% CO_2. Cells were passaged once confluent with TrypLE™ Express Enzyme (Thermo Fisher Scientific - 12563-011) following manufacturer's instructions.

2.3.2|HEK293T cells cultures for routine use

Human HEK293T cells were obtained from the European Collection of Cell Cultures and used within 20 passages of the original vial. Cells were cultured in DMEM (Sigma-Aldrich

- D6546) supplemented with 10% v/v foetal bovine serum (FBS), 2 mM L-glutamine (Thermo Fisher Scientific - 25030-081), 100 U/mL penicillin and 0.1 mg/mL streptomycin at 37°C and in 5% CO_2. Cells were passaged once confluent with Trypsin-EDTA (Sigma-Aldrich - T3924) following manufacturer's instructions.

2.3.3|Expansion of feeder-free human iPS cells cultures for dopaminergic neurons differentiation

All iPSC lines used in this work were generated in the laboratory of Dr Sally Cowley at the Sir William Dunn School of Pathology (University of Oxford) from fibroblasts from PD patients and healthy controls recruited through the OPDC and StemBANCC projects. Two reprogramming methods were used for the generation of iPSC lines. The NDHF-1 iPSC line was generated via the retroviral delivery of plasmids encoding for the human reprogramming factors cMyc, Klf4, Sox2, Oct3/4 and Nanog. All other iPSC lines used in this study were reprogrammed using the commercial kit Cytotune (Life Technologies catalogue) and the delivery the four human reprogramming factors Oct3/4, Sox2, Klf4, and cMyc via the non-integrating Sendai virus. Colonies displaying iPSC morphology were picked and transferred onto mouse embryonic fibroblasts (MEFs) by manual dissection. iPSC clones were screened for genome integrity via an Illumina Human CytoSNP and pluripotency via the PluriTest using the Illumina trascriptome array analysis. iPSCs were then bulked up before freezing stock vials for subsequent use. Feeder-free iPSCs were routinely cultured on Matrigel-coated plastic (BD Biosciences - 356234) and fed daily with complete mTeSR1 (StemCell Technologies - 5850) supplemented with 100 U/ml penicillin, 0.1 mg/ml streptomycin at 37°C and in 5% CO_2. Once confluent, iPSCs were passaged using TrypLE™ Express Enzyme and replated on Matrigel-coated plates in complete mTeSR1 supplemented with 100 U/ml penicillin, 0.1 mg/ml streptomycin and 10 μM

ROCK inhibitor Y27632 (Tocris - 1254).

2.3.4|Plasmid DNA or siRNA lipofection

Cells were transfected via lipofection. BE(2)-M17 were plated at the density of $3x10^5$ cell/well in 6-well plates or $1.5x10^5$ cell/well in 12-well plates and allowed to adhere overnight. For DNA transfection, a 1:2 ratio between the plasmid and Lipofectamine 2000 (Thermo Fisher Scientific - 11668-019) was used. For siRNA transfection, increasing concentrations of siRNA were used whereas the amount of Lipofectamine 2000 was kept constant to 1 µL. DNA or siRNA and Lipofectamine 2000 mixes were prepared in Opti-MEM and left to incubate at RT for 20 minutes before being added to the cells in Opti-MEM. In the case of BE(2)M17 cells, Opti-MEM supplemented with 30% FBS was added to the wells after 6 hours and the medium was replaced with fresh Opti-MEM supplemented with 10% FBS after 24 hours. For iDAn cultures, the media was replaced with the final maturation medium after 6 hours. Cells were harvested or fixed 48 hours after transfection, unless state otherwise.

2.3.5|Differentiation of iPSCs to dopaminergic neurons using the Embryoid Body (EB)-based protocol

Feeder-free iPSCs were dissociated with TrypLE™ Express Enzyme and seeded into a well of a AggreWell™800 plate (StemCell Technologies - 27865) in mTeSR1 supplemented with 100 U/ml penicillin, 0.1 mg/ml streptomycin and 10µM Rock inhibitor Y27632. EBs were kept in culture for 3 days with a 75% daily mTeSR1 medium change and then harvested on day 4. EBs were plated onto Geltrex-coated 6-well plates (~50 EBs per well) for differentiation according to the following protocol:

• Day 0-4: Complete DMEM/F12 supplemented with 200 ng/mL Noggin, 10 µM

SB431542 and 0.7 µM CHIR 99021

- Day 5-10: Complete DMEM/F12 supplemented with 200 ng/mL SHH C24II and 0.7 µM CHIR 99021
- Day 11-17: Complete DMEM/F12 supplemented with 200 ng/mL SHH C24II, 20 ng/mL BDNF, 100 ng/mL FGF8a, 50 µg/mL Heparin and 200 µM ascorbic acid

A 50% medium change with Day 0-4 medium was performed on day 3; a 50% medium change with Day 5-10 medium was performed on day 7 and 9; a 50% medium change with Day 11-17 medium was performed on day 13 and 15. Complete DMEM/F12 medium contained DMEM/F12, 2 mM L-glutamine, 1X N2 supplement, 1 mg/mL BSA, 10 µM Y27632 and 1X Antibiotic-Antimycotic.

On day 18, EBs were manually dissected with a needle and replated onto poly-D-Lysin/laminin or Geltrex coated wells or coverslips in DMEM/F12 supplemented with 2 mM L-glutamine, 1X N2 supplement, 1 mg/mL BSA, 10 µM Y27632, 1X antibiotic-antimycotic, 20 ng/mL BDNF, 20 ng/mL GDNF, 0.5 mM db-cAMP, 1 µg/mL laminin and 200 µM ascorbic acid. From day 19 onwards, cells were 50% fed every 2-3 days with DMEM/F12 supplemented with 2 mM L-glutamine, 1X N2 supplement, 1 mg/ML BSA, 1X antibiotic-antimycotic, 20 ng/mL BDNF, 20 ng/mL GDNF, 0.5 mM db-cAMP, 1 µg/mL laminin and 200 µM ascorbic acid. All the reagents used in for this protocol are listed in section 2.8.

2.3.6|Differentiation of iPSCs to dopaminergic neurons using the Floor plate (FP)-based protocol

Feeder-free iPSCs were dissociated with TrypLE™ Express Enzyme and seeded at 125,000 cells/cm^2 in Geltrex-coated 6-well plates or 25cm^2 culture flasks in Complete mTeSR1 supplemented with 100 U/ml penicillin, 0.1 mg/ml streptomycin and 10 µM Rock inhibitor Y27632.

After 2 days in culture, iPSCs were sub-confluent and ready for differentiation using the following protocol:

- Day 0: KSR KO DMEM supplemented with 100 nM LDN-193189 and 10 µM SB-431542
- Day 1: KSR KO DMEM supplemented with 100 nM LDN-193189, 10 µM SB-431542, 100 ng/mL SHH C24II, 2 µM Purmorphamine and 100 ng/mL FGF-8a
- Day 3: KSR KO DMEM supplemented with 100 nM LDN-193189, 10 µM SB-431542, 100 ng/mL SHH C24II, 2 µM Purmorphamine, 100 ng/mL FGF-8a and 3 µM CHIR-99021
- Day 5: 75% KSR KO DMEM + 25% NB supplemented with 100 nM LDN-193189, 10 µM SB-431542, 100 ng/mL SHH C24II, 2 µM Purmorphamine, 100ng/mL FGF8a and 3 µM CHIR-99021
- Day 7: 50% KSR KO DMEM + 50% NNB supplemented with 100 nM LDN-193189 and 3 µM CHIR-99021
- Day 9: 25% KSR KO DMEM + 75% NNB supplemented with 100 nM LDN-193189 and 3 µM CHIR-99021
- Day 11: NB supplemented with 20 ng/mL BDNF, 20 ng/mL GDNF, 1 ng/mL TGFβ3, 10 µM DAPT, 200 µM ascorbic acid, 0.5 mM db-cAMP and 3 µM CHIR-99021
- Day 13-15-17-19: NB supplemented with 20 ng/mL BDNF, 20 ng/mL GDNF, 1 ng/mL TGFβ3, 10 µM DAPT, 200 µM ascorbic acid and 0.5 mM db-cAMP

Full medium change was performed on day 0, 1, 3, 5, 7, 9, 11, 13, 15, 17 and 19 with the corresponding medium. On day 4, 6, 8, 10, 12, 14, 16 and 18, 50% of the medium was replaced with frsh medium of the same composition of the previous day. Normal feeding volumes were 2 mL/well of a 6-well plate or 10 mL/25cm^2 flask. KSR KO DMEM medium was prepared with KO DMEM supplemented with 15% KSR, 1X NEAA, 10 µM

2-Mercaptoethanol and 2 mM L-glutamine; NNB medium was prepared with Neurobasal medium supplemented with 2 mM L-glutamine, 0.5X N2 and 0.5X B27 supplement; NB medium was prepared with Neurobasal medium supplemented with 2 mM L-glutamine and 1X B27 supplement.

On day 20, cells were dissociated using Accutase for 10 minutes at 37°C, spun down for 5 minutes at 250 x *g* in NB medium to neutralise Accutase and resuspended in 1 mL of NB medium supplemented with 20 ng/mL BDNF, 20 ng/mL GDNF, 1 ng/mL TGFβ3, 10 µM DAPT, 200 µM ascorbic acid, 0.5 mM db-cAMP and 10 µM Y27632; cells were then counted and diluted at the appropriate density. Plates or coverslip were prepared by coating with 0.01% (w/v) poly-L-Ornithine for 30 minutes at room temperature and with a mixture of 2 mg/mL fibronectin and 1 mg/mL laminin overnight at 37°C; prior seeding the cells, the plates or coverslips were left to air-dry. Otherwise, plates and coverslips were coated with Geltrex for at least an hour at 37°C. In a 12-well plate, 300,000 cells were spotted in a 100 µL drop whereas 100,000 cells were spotted in a 30 µL drop in a 24-well plate. Cells were left to attach to the surface for 10 minutes and then the wells were topped up with the remaining medium according to the well size. On day 22, cells were incubated in NB medium supplemented with 1 µg/mL of Mitomycin C to inactivate all proliferating cells. After an hour, cells were washed with NB medium and then fed with NB medium supplemented with 20 ng/mL BDNF, 20 ng/mL GDNF, 1 ng/mL TGFβ3, 10 µM DAPT, 200 µM ascorbic acid and 0.5 mM db-cAMP. From day 24 onwards, cells are 50% fed every 2-3 days with Final Differentiation Medium (FDM): NB medium supplemented with 20 ng/mL BDNF, 20 ng/mL GDNF, 1 ng/mL TGFβ3, 10 µM DAPT, 200 µM ascorbic acid and 0.5 mM db-cAMP.

All the reagents used in for this protocol are listed in Section 2.8.

2.3.7|Lentivirus packaging and titering in HEK293T cells

On day 1, HEK293T cell were seeded at $5x10^5$ cell/cm^2 in 150 mm plates; 12 plates were used for each individual lentivirus preparation. On day 2, cells were co-transfected by mixing the 3 packaging vectors and the lentiviral plasmid diluted in ddH_2O and 140 µL of 2M $CaCl_2$. The transfection mix was prepared as follows: 10 µg of viral genome (lentiviral plasmid), 10 µg of pMDLg/pRRE (Addgene - 12251), 3.4 µg of pMD2.G (VSVG) (Addgene - 12259) and 2 µg of pRSV-REV (Addgene - 12253). All DNA preparation used in this process were purified with the CsCl gradient. 1.1mL of HBS-pH 7.05 was added and the transfection mix was left to incubate for 30 minutes at RT for 30 minutes, before adding 2.4 mL to each plate. On day 3, the medium was replaced with fresh medium supplemented with 10 mM of sodium butyrate; the medium was collected after 10 hours, stored at 4°C (first harvest) and replaced with fresh medium. On day 4, the medium was collected again (second harvest). For the purification and concentration of the lentiviruses, the first and second harvests were pulled together and spun down at 1000 x *g* for 5 minutes and filtered through a 0.45 µm filter unit. The cell-free supernatant was transferred into 500 mL polycarbonate pot and spun down overnight at 6000 x *g* at 4°C. The following day, the supernatant was discarded and the pellet was resuspended in 5 mL of ice-cold PBS. The lentivirus suspension was transferred into a 17 mL Thinwall Polyallomer tube (Beckman Coulter - 337986) and spun down at 19573 rpm in a SW 32.1Ti rotor (Beckman Coulter - 369650) for 90 minutes at 4°C. The supernatant was then discarded and the pellet left to air-dry for 5 minutes in a biosafety cabinet. Afterwards, 100 µL of TSSM buffer were added and left to stand on ice for 2 hours. Finally, the viral pellet was resuspended, the volume adjusted to 192 µL and spun at 2000 x *g* before preparing 5-10 µL aliquots and storing them at -80°C.

2.3.8|Titering of lentivirus preparations in HEK293T cells

The calculation of the lentiviral titer was performed transducing a known amount of HEK293T with serial dilution of the virus. $7.5x10^4$ cells per well were plated in a 12-well plate (one plate per virus) the day prior the titering. The following day, one well was used for counting cell number whereas the remaining were transduced with 500 µL of serial dilution of the lentivirus preparation from 10^{-3} to 10^{-6} in duplicates in DMEM medium; one well was transduced at dilution of 10^{-2} and one well was left untransduced as positive and negative controls, respectively. After 4 hours, the wells were topped up to 1 mL with DMEM medium. After 72 hours, cells were collected in 250 µL of Trypsin for 5 minutes at 37°C and pelleted at 300 x *g* for 5 minutes. The pellet was resuspended in 150 µL of PBS before adding 150 µL of 8% PFA as fixative. Fixed cells were pelleted again, washed in PBS twice and finally resuspended in 2 mL of PBS. The percentage of eGFP positive cells in each sample was assessed counting at least 10,000 cells using the FACSCALIBUR (BD Biosciences). The viral titer (defined as the number of transducing viral particles per millilitre) was then calculated according to the following mathematical expression, where *i* is the dilution factor:

$$\frac{TU}{mL} = \frac{1}{n}\sum_{i=3}^{i=6}\frac{(\%\ GFP^+\ cells)_i \times (total\ number\ of\ cells) \times 100}{0.5mL \times 10^{-i}}$$

2.4|Functional assays for cellular phenotyping

2.4.1|Cellular bioenergetics analysis (Seahorse Analyser)

Mitochondrial respiration and glycolytic activity of iDAn were measured using the Seahorse XFe96 Analyzer (Seahorse Bioscience). Cells were plated in a XF^{96} Polystyrene

Cell Culture Microplate (Seahorse Bioscience - 101085-004) at the density of 300,000 cells/cm^2 on day 20, treated with Mytomycin C on day 22 and further matured until day 35 before the analysis; MPP^+ treatment was performed 24 hours before the assay. The cartridge for the measurement of pH and O_2 consumption XFe96 FluxPak (Seahorse Bioscience - 102601-100) was rehydrated using the XF Calibrant Solution (Seahorse Bioscience - 100840-000) for at least 6 hours in a non-CO_2 incubator at 37°C. On the day of the assay, the assay medium was prepared fresh using the XF Base Medium (Seahorse Bioscience - 102353-100) supplemented with 10 mM Glucose (Sigma-Aldrich - G8644), 1 mM Sodium Pyruvate (Sigma-Aldrich - S8636) and 2 mM L-glutamine (Thermo Fisher Scientific - 25030-081); once at 37°C, the pH was adjusted at 7.4 using 1 M NaOH. One hour before the assay, the cells were washed once with the assay medium and then incubated at 37°C in a non-CO_2 incubator in 175 µL of assay medium. Working solutions of the following compounds were made up fresh and 25 µL/port were loaded:

- 8 µM oligomycin A (Sigma-Aldrich - O4876) as complex VI inhibitor (8X, final concentration 1 µM)
- 9 µM FCCP (Sigma-Aldrich - C2920) as protonophore (9X, final concentration 1µM)
- 5 µM Rotenone (Sigma-Aldrich - R8875) and antimycin A (Sigma-Aldrich - A8674) as complex I and III inhibitor respectively (10X, final concentration 0.5 µM)
- 550 µM 2-deoxy-glucose (Sigma-Aldrich - D8375) as hexokinase inhibitor (11X, final concentration 50 µM).

The following scheme for compound/cartridge port was used:

- Port A: Oligomycin A
- Port B: FCCP
- Port C: Rotenone/antimycin A
- Port D: 2-deoxy-glucose

All assays were set up using the Wave software (Seahorse Bioscience) as follows until all the compounds were injected:

• Equilibration (12 minutes)

• 3x Mix (3 minutes)/Wait (3 minutes)/Measure (3 minutes)

• Inject port

Both oxygen rate consumption (OCR) and extracellular acidification rate (ECAR) were measured simultaneously throughout the assay. At the end of the assay, the media was discarded and disposed appropriately before adding 35 µL of RIPA buffer supplemented with proteases inhibitors. After an hour at 4°C, the determination of the protein content in each well was determined by BCA assay with 25 µL of undiluted lysates. Each value from the assay was normalised to the protein content of the correspondent well.

Mitochondrial respiration and glycolysis parameters were calculated from the OCR and ECAR traces following the manufactured instructions and averaging the three measures between each injection:

- Basal respiration: baseline OCR- non-mitochondrial respiration OCR

- Proton leak: OCR after oligomycin A injection

- ATP production: basal OCR - proton leak

- Maximal respiration: OCR after FCCP injection - non-mitochondrial respiration

- Spare capacity: maximal respiration - basal respiration

- Non-mitochondrial respiration: OCR after Rotenone/antimycin A injection

- Basal glycolysis: ECAR at baseline - non-glycolytic acidification

- Glycolytic capacity: ECAR after oligomycin A injection - non-glycolytic acidification

- Glycolytic reserve: glycolytic capacity - basal glycolysis

- Non-glycolytic acidification: ECAR after 2-deoxy-glucose injection

2.4.2|Proximity Ligation Assay (PLA) for αSyn oligomers

Fluorescence immunocytochemistry and detection of αSyn oligomeric species were carried out sequentially. iDAn were permeabilised and blocked in PLA permeabilisation buffer with 10% serum for an hour before probing with the primary antibody diluted in PLA permeabilisation buffer with 1% serum overnight in 4°C. Cells were then washed three times with PLA permeabilisation buffer and then incubated with the secondary antibody diluted in PLA permeabilisation buffer with 1% serum for an hour at RT. After three washes with TBS + 0.05% Tween, cells were blocked with the PLA blocking solution for an hour at 37°C, before being probed overnight at 4°C with the PLA conjugated Syn211 antibodies (+ and - probes). The next day, cells were washed three times with TBS + 0.05% Tween before being incubated with the Ligation reaction mix (e.g. for 40 µl reaction: 8 ul 5x ligation stock, 1 µl ligase, 31 µl MQ water) for an hour at 37°C. After three washes with TBS + 0.05% Tween, the Amplification/Detection reaction mix (e.g. for 40 µl reaction: 8 µl 5x amplification stock, 0.5 µl polymerase, 31.5 µl MQ water) was added and the cells were incubated for further 2.5 hours at 37°C. Before mounting the coverslips on a glass slide with FluorSave (Merk Millipore - 345789), the cells were washed three times in Duolink Buffer B, and the nuclei stained with DAPI (Thermo Fisher Scientific - D1306) for 5 minutes during the second wash.

2.4.3|GCase activity

Cells were lysed in GBA Lysis Buffer and sonicated for 10 seconds. Following incubation on ice for 30 minutes, samples were centrifuged at 300 x *g* for 10 minutes at 4°C to remove cell debris. The supernatant was collected and protein levels determined by BCA assay in triplicates. For each measurement of GBA activity, 2 µg of protein were used in quadruplicates; one replicate was used as a negative control to provide background values

for GBA activity by pre-incubating it with 2.5 mM of the GBA inhibitor conduritol-B-epoxide (CBE, Enzo Life Sciences - BML-S104) for 30 minutes at RT. All samples were incubated with 5 mM 4-methylumbelliferyl β-D-glucopyranosidase (Sigma-Aldrich - M3633) at 37°C for 1 hour. The reaction was stopped by adding excess of glycine buffer and fluorescence detected on a Synergy HT plate reader (BioTek) at excitation 360 nm and emission 440 nm. Final GBA activity values were calculated as the average of the values from the three wells after subtraction of the CBE-treated sample. The same protein lysates were run on a SDS-PAGE to determine GBA protein levels.

2.4.4|Native western blot for the detection of αSyn in supernatants

Supernatants were concentrated using Amicon Ultra-0.5 Centrifugal Filter Unit with 3 kDa cut-off (Millipore - UFC500308). A total of 1 mL was concentrate to about 5X by spinning the column for 2 minutes at 16,100 x *g*. 20 µL of the concentrated medium were diluted with an equal volume of Native Sample Buffer for Protein Gels (Biorad - 1610738). Proteins were separated using 4–15% Mini-PROTEAN® TGX™ Precast Protein Gels (Biorad - 4561083) run at 85V for 2.5 hours in Tris-Glycine buffer. Afterwards, protein transfer and detection was carried out as described previously.

2.4.5|Detection of αSyn in supernatant

The supernatant from iDAn or iMac cultures was collected to determine the total amount of αSyn secreted from the cell during final differentiation. The medium was spun at 300 x *g* for 5 minutes to remove cells debris and stored at -80°C; on the day of the assay, the medium was thawed at 4°C. αSyn content was determined using the Meso Scale Diagnostic (MSD) Human α-Synuclein Kit (K151TGD-2) following manufacturer's instructions. Briefly, each well of the assay plate was blocked for 1 hour at RT with shaking

with Diluent 35. The plate was then washed three times with PBS 0.05%+Tween 20 before adding 25 µL of detection antibody solution (SULFO-TAG Anti-α-Synuclein Antibody) and 25µL of undiluted samples, standard or medium as negative control/background; standards were loaded in duplicates in 4-fold serial dilution steps from 200 µg/mL to 2.4 pg/mL and Diluent 35 was used as blank. The plate was sealed with an adhesive plate film and incubated at RT with shaking for 2 hours. After 3 washes with at 150 µL/well of PBS 0.05% Tween, 150 µL of 2X Read Buffer T were added to each well and the plate was read using the MSD reader. The absolute αSyn concentration was calculated with the DISCOVERY WORKBENCH® analysis software based on the standard curve. Data was normalised to the protein content of the corresponding well that the supernatant was collected from.

2.5|Statistical analysis of experimental results

Densitometric quantification of proteins via western blot was normalised for the loading control β-actin and the average of the control samples; data were then graphed as fold change compared to Control iDAn. For the quantification of the data from the Seahorse Analyzer, each value was normalised for the protein content of the correspondent well and for the average baseline OCR of control samples; data were then graphed as a percentage of the basal OCR of Control iDAn. Measurements of αSyn release in the medium were normalised for the protein content of the correspondent well. Quantification of the percentage of cells positive for specific markers via immunocytochemistry was normalised for the total number of cells using the nuclear staining DAPI.

All statistical analysis was performed using GraphPad Prism 6.0. Experimental results were analysed using Student's t test or one-way analysis of variance (ANOVA) with Dunnet's multiple comparison test and p values of less than 0.05 were considered statistically

significant. Data from at least three multiple independent differentiations for the phenotypic analysis were analysed comparing each individual A53T *SNCA* line and the average of the three clones of the *SNCA* Tripl line to the average of Control iDAn.

2.6|Buffers and formulations

Citrate-Phosphate Buffer	22.2 mM citric acid, 55.6 mM dibasic sodium phosphate, pH 5.4
Duolink Buffer B	0.2M Tris and 0.1M NaCl (pH 7.5)
GBA Lysis Buffer	Citrate-Phosphate buffer supplemented with 0.25 % (v/v) Triton-X100 and 0.25% (w/v) taurocholic acid, pH 5.4
Glycine buffer	50 mM glycine, 38.6 mM sodium hydroxide, pH 10.4
HBS (pH 7.05)	50mM HEPES, 280mM NaCl and 1.5mM Na_2HPO_4
Laemmli Buffer	0.1% 2-mercaptoethanol, 0.0005% bromophenol blue, 10% glycerol, 2% SDS, 63mM Tris-HCl, pH 6.8
Lysosyme solution	10g/L lysosyme in 10mM Tris-HCl pH8
PLA blocking buffer	TBS, 0.1% TX100 and 1M glycine
RIPA buffer	50 mM Tris (pH 7.4), 150 mM NaCl, 1% triton X-100 (v/v), 1 % sodium deoxycholate (w/v) and 0.1% SDS
Running Buffer	25mM Tris, 192mM glycine and 0.1% SDS
Native Running Buffer	25mM Tris and 192mM glycine
Solution 2	1% SDS and 0.2M NaOH
Solution 3	7.5M ammonium acetate
STET solution	8% sucrose (w/v), 5% Triton X-100, 50mM EDTA and 50mM Tris pH 8 with HCl
TBE buffer	45 mM Tris-borate and 1 mM EDTA
TE buffer	10 mM Tris-HCl pH 8.0 and 1 mM EDTA
TBS	50mM Tris-HCl pH 7.6 and 150mM NaCl
TSSM buffer	20mM tromethamine, 200mM NaCl, 10g/L sucrose and 1g/L mannitol
TTBS	0.1% Tween 20 in TBS

Table 2.6|List of buffers and their formulations

2.7|Primers

Name	Application	Sequence 5'-3'
U6_F	Cloning	GAATTGGGTACCCGCTCTAGAACTAGTGG
shSNCA1_R	Cloning	TCGCCCTCCTCGAGAAAAAAGGAAAGACAAAAGAGGGTGTGACAGGAAGCACCCTCTTTTGTCTTTCCCAAACAAGGCTTTTCTCCAAGG
EF1A_F	Cloning	TTACAAAAATTCAAAATTTTATCGATCGTGAGGCTCCGGTGCCCGTC
EF1A_R	Cloning	CTCACCATGGTGGCGACCGGTTCACGACACCTGAAATGGAAG
CPPT_F	Cloning	TTTTTTCTCGAGGAGGGCGAATTGGAGAAGTG
CPPT_R	Cloning	CGATAAAATTTTGAATTTTTGTAATTTG
SNCA-gen_F	Genotyping	GCTAATCAGCAATTTAAGGCTAG
SNCA-gen_R	Genotyping	GATATGTTCTTAGAATGCTCAG
shseq-1F	Sequencing	AAAGTAAGACCACCGCACAG
shseq-1R	Sequencing	GCTCCTATTCCCACTGCTCT
shseq-2F	Sequencing	CGAGGAGGGCGAATTGGAGA
shseq-2R	Sequencing	CCAATTCCACAAACTTGCCC
shseq-3F	Sequencing	TGAAGAATCGCAAAACCAGCA
shseq-3R	Sequencing	GTTCAATTGCCGACCCCTC
shseq-4F	Sequencing	TAGACATAATAGCAACAGAC
shseq-4R	Sequencing	GTCGCAGCAGGTCATCAAAA
shseq-5F	Sequencing	GCCTGTCTCGCTGCTTTC
shseq-5R	Sequencing	CATCGCATAAAACCCCTCCC
shseq-6F	Sequencing	GTCCAGGCACCTCGATTAGT
shseq-6R	Sequencing	TTGAAGAAGATGGTGCGCTC
MCS_F	Cloning	(P)CTAGAACTAGTGGATCCTGCAGGCGCGCCATATGATATCACGTGTTTAAACGCGTC
MCS_R	Cloning	(P)TCGAGACGCGTTTAAACACGTGATATCATATGGCGCGCCTGCAGGATCCACTAGTT
shASYN1_R	Cloning	CTCCAATTCGCCCTCCTCGAGAAAAAAAAGAGGGTGTTCTCTATGTAGAAGCACACTACATAGAGAACACCCTCTTCAAACAAGGCTTTTCTCCAAGG
shASYN2_R	Cloning	CTCCAATTCGCCCTCCTCGAGAAAAAATGACAATGAGGCTTATGAAATAAGCACAATTTCATAAGCCTCATTGTCACAAACAAGGCTTTTCTCCAAGG
shASYN3_R	Cloning	CTCCAATTCGCCCTCCTCGAGAAAAAAAAGATATGCCTGTGGATCCTGAAGCACACAGGATCCACAGGCATATCTTCAAACAAGGCTTTTCTCCAAGG
shASYN4_R	Cloning	CTCCAATTCGCCCTCCTCGAGAAAAAAAAGGACCAGTTGGGCAAGAATAAGCACAATTCTTGCCCAACTGGTCCTTCAAACAAGGCTTTTCTCCAAGG
shCTRL1_R	Cloning	CTCCAATTCGCCCTCCTCGAGAAAAAAGGTGAGAGTGATCGTCTATTAAAGCACATAATAGACGATCACTCTCACCCAAACAAGGCTTTTCTCCAAGG
shCTRL2_R	Cloning	CTCCAATTCGCCCTCCTCGAGAAAAAAGCTACAGATAAGTTGAAGTATAAGCACAATACTTCAACTTATCTGTAGCCAAACAAGGCTTTTCTCCAAGG
shCTRL3_R	Cloning	CTCCAATTCGCCCTCCTCGAGAAAAAAGGCAAGTCTACGGAGTTTACTAAGCACAAGTAAACTCCGTAGACTTGCCCAAACAAGGCTTTTCTCCAAGG

Name	Application	Sequence 5'-3'
shCTRL4_R	Cloning	CTCCAATTCGCCCTCCTCGAGAAAAAAGAGACACTAGAGCGGGATAATAAGCACAATTATCCCGCT CTAGTGTCTCCAAACAAGGCTTTTCTCCAAGG
shFABP7#1_R	Cloning	CTCCAATTCGCCCTCCTCGAGAAAAAAGGTTGCTGTTCGCCACTATGAAAGCACATCATAGTGGCG AACAGCAACCCAAACAAGGCTTTTCTCCAAGG
shFABP7#2_R	Cloning	CTCCAATTCGCCCTCCTCGAGAAAAAAGAAACTGTAAGTCTGTTGTTAAAGCACATAACAACAGAC TTACAGTTTCCAAACAAGGCTTTTCTCCAAGG
shFABP7#3_R	Cloning	CTCCAATTCGCCCTCCTCGAGAAAAAAGTGACCAAACCAACGGTAATTAAGCACAAATTACCGTTG GTTTGGTCACCAAACAAGGCTTTTCTCCAAGG
shFABP7#4_R	Cloning	CTCCAATTCGCCCTCCTCGAGAAAAAAGATGAGTACATGAAGGCTCTAAAGCACATAGAGCCTTCA TGTACTCATCCAAACAAGGCTTTTCTCCAAGG
shScramble#1_R	Cloning	CTCCAATTCGCCCTCCTCGAGAAAAAAGTCGTTAGCAATTGCGGTCTCAAGCACAGAGACCGCAAT TGCTAACGACCAAACAAGGCTTTTCTCCAAGG
shScramble#2_R	Cloning	CTCCAATTCGCCCTCCTCGAGAAAAAAATTAAGTATGCGGATCGTTATAAGCACAATAACGATCCG CATACTTAATCAAACAAGGCTTTTCTCCAAGG
shScramble#3_R	Cloning	CTCCAATTCGCCCTCCTCGAGAAAAAAAGATAACGTATACGCCACTGAAAGCACATCAGTGGCGTA TACGTTATCTCAAACAAGGCTTTTCTCCAAGG
shScramble#4_R	Cloning	CTCCAATTCGCCCTCCTCGAGAAAAAAGTAATTCTACGCGGTAAGAAGAAGCACACTTCTTACCGC GTAGAATTACCAAACAAGGCTTTTCTCCAAGG
FABP7+polyA_F	Cloning	AATTGGGTACCCGCTCTAGAACTAGTAACTTGTTTATTGCAGCTTA
FABP7+polyA_R	Cloning	GTCGTGAACCGGTCGCCACCATGGTGGAGGCTTTCTGTGC
fabp7-EF1a_F	Cloning	GCACAGAAAGCCTCCACCATGGTGGCGACCGGTTCACGAC
fabp7-EF1a_R	Cloning	CACTTCTCCAATTCGCCCTCCTCGAGCGTGAGGCTCCGGTGCCCGT

Table 2.7|List of primers and their sequences

2.8|Plasmids maps

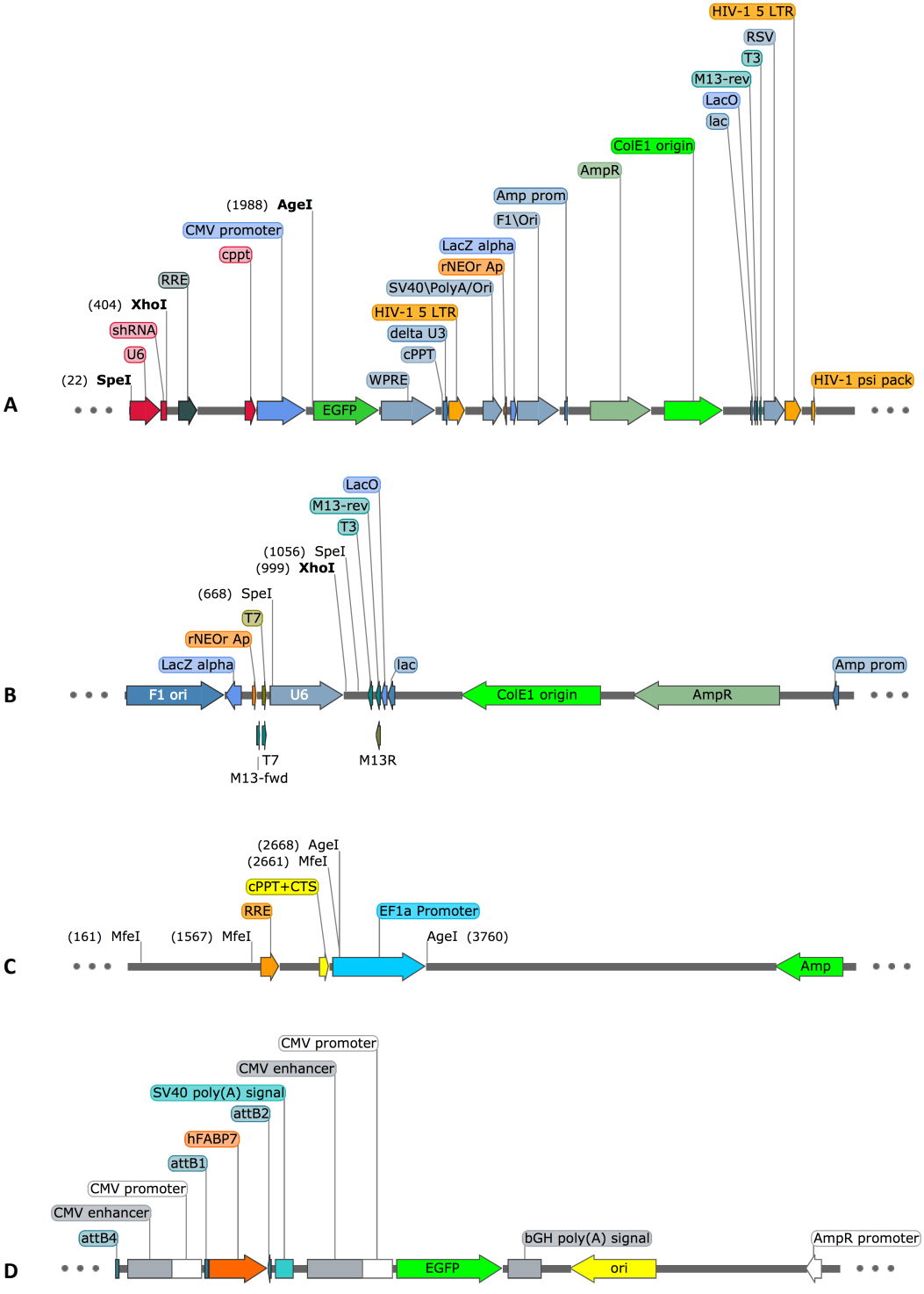

Table 2.8|Maps of plasmids used to generate lentiviral constructs
(A) pRRLsincppt-U6.ShCx43.CMV.eGFP.wpre.gb
(B) pSilencer
(C) CSii-EF-MCS
(D) CMV.hFABP7.polyA.CMV.eGFP

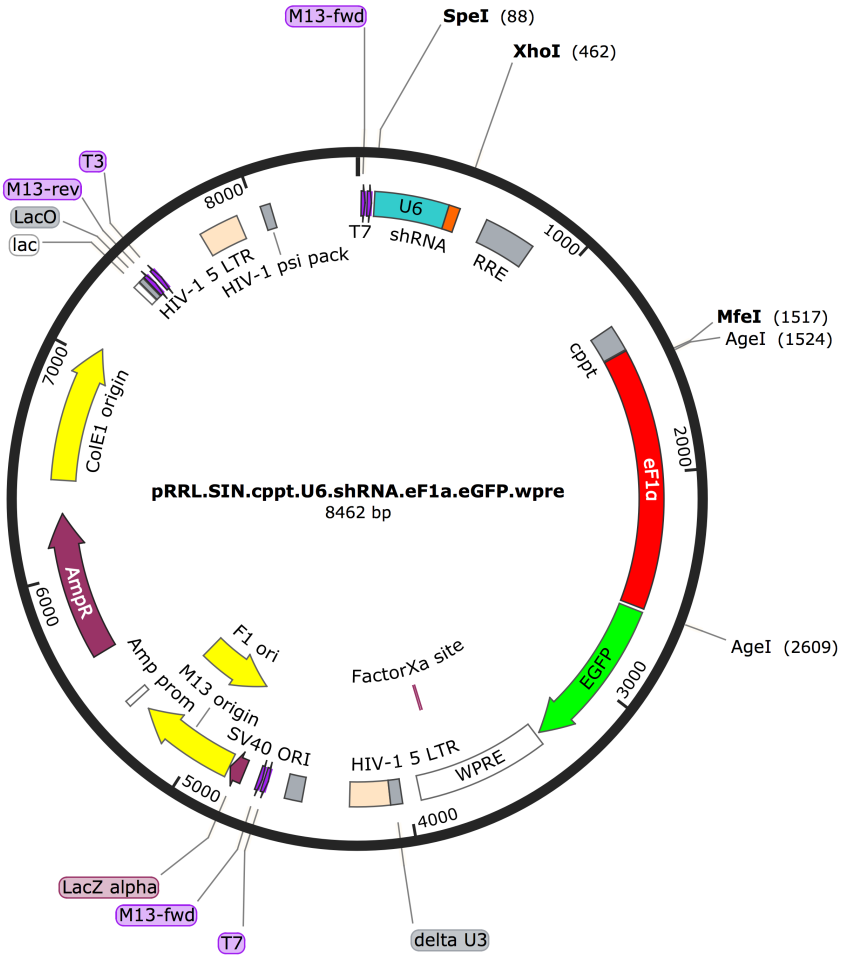

Table 2.9|Map of the lentiviral vector for the expression of shRNA(U6)

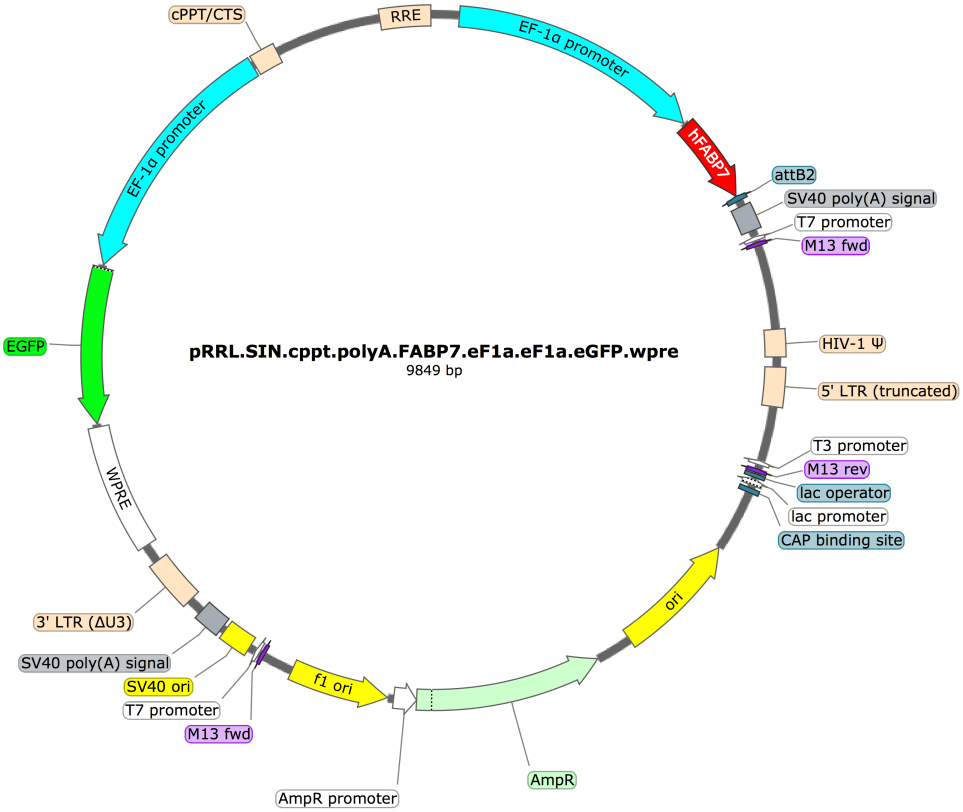

Table 2.10|Map of the lentiviral vector for the expression of FABP7$^{(eF1\alpha)}$

2.9|Antibodies

Pathway	Antigen	Supplier	Cat #	Species	WB	IF
	14-3-3	Abcam	ab9063	Rabbit	1:1000	
	BD 42/αSyn	BD	610786	Mouse	1:1000	1:500
	αSyn (4B12)	Covance	SIG-39730	Mouse	1:1000	1:500
	aSyn (MJF1)	Abcam	ab138501	Rabbit	1:1000	1:500
	aSyn (Syn211)	Abcam	ab80627	Mouse	1:2000	
	Catalase	Cell Signalling	12980	Rabbit	1:1000	
	eGFP	Invitrogen	A11122	Rabbit	1:1000	1:500
	GBA	Abcam	ab55080	Mouse	1:200	
aSyn PLA	Syn211, + and - probes	Abcam	ab80627	Mouse		1:750
Dopaminergic neuron	DAT	Alpha Diagnostic	DAT13-A	Rabbit	1:500	
	FOXA2	R&D systems	AF2400	Goat		1:250
	GIRK2	Alomone Labs	APC-006	Rabbit	1:500	
	TH	Millipore	AB152	Rabbit	1:2000	1:500
	TH	Santa Cruz	sc-25269	Mouse		1:500
	TUJ1	Covance	MMS-435P	Mouse	1:2000	
	TUJ1	Abcam	ab107216	Chicken	1:2000	1:1000
Stem cell	OCT3/4	Santa Cruz	sc-8628 X	Goat		1:3000
Fatty Acids metabolism	CYP46A1	ProteinTech	12486-1-AP	Rabbit	1:1000	
	FABP7	Cell Signalling	13347	Rabbit	1:1000	
	SIRT1	Cell Signalling	2496	Rabbit	1:1000	
ER Stress	BiP	Abcam	ab21685	Rabbit	1:1000	
	Calreticulin	Abcam	ab108395	Rabbit	1:1000	
	IRE1a	Cell Signalling	3294	Mouse	1:1000	
	C/EBP β	Santa Cruz	sc-150	Rabbit	1:250	
	PDI	Cell Signalling	3501	Rabbit	1:1000	
Autophagy	HSC70	Santa Cruz	sc-7298	Mouse	1:1000	
	LAMP2A	Abcam	ab18528	Rabbit	1:1000	
	LAMP1	Santa Cruz	sc-20011	Rabbit	1:200	
	LC3	Sigma	L7543	Rabbit	1:1000	
	p62	Abcam	ab109012	Rabbit	1:1000	

Pathway	Antigen	Supplier	Cat #	Species	WB	IF
Mitochondria	DRP1	Cell Signalling	8570	Rabbit	1:1000	
	pDRP1	Cell Signalling	4494	Rabbit	1:1000	
	Mitofusin 2	Sigma	M6319	Rabbit	1:1000	
	Opa1	BD	612606	Mouse	1:1000	
	PGC1a	Santa Cruz	sc-13067	Rabbit	1:100	
	PGC1a	Abcam	ab54481	Rabbit	1:1000	
	Prohibitin	Abcam	ab28172	Rabbit	1:1000	
	Tom20	Santa Cruz	sc-11415	Rabbit	1:1000	1:500
Secondary Antibodies	Mouse IgG (Alexa 488 conjugated)	Invitrogen	A11001	Goat		1:500
	Mouse IgG (Alexa 594 conjugated)	Invitrogen	A11005	Goat		1:500
	Rabbit IgG (Alexa 488 conjugated)	Invitrogen	A11008	Goat		1:500
	Rabbit IgG (Alexa 594 conjugated)	Invitrogen	A11012	Goat		1:500
	Rabbit IgG (Alexa 594 conjugated)	Invitrogen	A21206	Donkey		1:500
	Chicken IgY (Alexa 594 conjugated)	Abcam	ab150172	Goat		1:500
	Chicken IgY (Alexa 647 conjugated)	Abcam	ab150171	Goat		1:500
	Goat IgY (Alexa 488 conjugated)	Invitrogen		Donkey		1:500
	Mouse IgG (HRP conjugated)	Bio-Rad	170-6516	Goat	1:5000	
	Rabbit IgG (HRP conjugated)	Bio-Rad	170-6515	Goat	1:5000	

Table 2.11|List of antibodies used for western blot (WB) and immunocytochemistry (IF)

2.10|Reagents for iPSCs differentiation

Reagent	Supplier	Catalogue #	Stock	Diluent
BDNF (Brain Derived Neurotrophic Factor)	Peptrotech	450-02	100µg/µL	PBS
GDNF (Glia Derived Neurotrophic Factor)	Peptrotech	450-10	100µg/µL	PBS
Ascorbic Acid	Sigma	A4544	0.2mM	ddH_2O
cAMP (N6,2′-O-Dibutyryladenosine 3′,5′-cyclic monophosphate sodium salt)	Sigma	D0627	0.5mM	ddH_2O
TGFβ3 (recombinant human Transforming Growth Factor β3)	Peptrotech	100-36E	10µg/mL	5mM Citric acid
DAPT	Abcam	ab120633	100mM	DMSO
CHIR99021	Tocris	4423	3µM	DMSO
Noggin	Life Technologies	PHC1506	200µg/mL	PBS
SB-431542	Tocris	1614	10mM	DMSO
ROCKi (Y27632 dihydrochloride)	Tocris	1254	10mM	ddH_2O
SHH (recombinant human Sonic Hedgehog (C24II) N-Terminus)	R&D	1845-SH	100µg/µL	PBS
FGF-8a (Fibroblast Growth Factor 8 isoform a)	Stratech	16124-HNAE-SIB	500µg/mL	PBS
LDN-193189	Sigma	SML0559	1mM	DMSO
Heparin	Sigma	H3149	5mg/mL	PBS
Purmorphamine	Millipore	540220	10mM	DMSO
Neurobasal	Life Technologies	21103049		
KSR serum replacement	Life Technologies	10828010		
KO DMEM	Life Technologies	10829018		
B27 supplement	Life Technologies	12587010	50X	
N2 supplement	Life Technologies	17502048	100X	
Geltrex™	Life Technologies	A1413302	100X	
MEM NEAA	Life Technologies	11140050	100X	

Table 2.12|List of reagents used for the differentiation of iPSCs to iDAn

Chapter 3

Differentiation of iPSCs to dopaminergic neurons

3.1|Introduction and aims

Current animal and cellular model are very useful for the study of the pathological mechanisms in PD. However, there is a need for more advanced models, both in term of the genetics and cellular context. The advent of human iPSCs and the development of differentiation protocols bridged this gap: it allowed researchers to study disease specific phenotypes in cells that are affected by the disease *in vivo* and carry the genetic background that ultimately was causative to onset of the disease in the patient. Recent work demonstrated that human iDAn generated from floor plate (FP) precursors cells, but not neuronal rosettes, can be grafted into experimental animals and fully integrate in the host midbrain (Kriks et al. 2011). Moreover, a recent study reported that only FP-derived, but but not rosette-derived, iDAn carrying either Parkin or Pink1 mutations display phenotypes resembling those of typical PD (Chung et al. 2016). Nevertheless, differentiation protocols are still somewhat of a black box that might influence the eventual phenotype in the cells. The characterisation of the cell type(s) generated is therefore pivotal to study the pathological mechanisms associated with the onset of PD, that in turn affect specific cell types in the midbrain.

The aim of this chapter is to examine protocols for the differentiation of iPSCs to iDAn that are relevant for this study. The groundwork regarding the study of αSyn pathology in these cells and the analytical and statistical approach adopted will also be described.

This chapter reports the results regarding the optimisation of a protocol for the differentiation of iPSCs to iDAn, including:

- Differentiation of iPSCs to iDAn using the EB-protocol
- Differentiation and initial characterisation of iPSCs to iDAn using the FP-protocol
- Comparison of the EB- and FP-protocol
- Optimisation of αSyn detection in iDAn

3.2|Results

3.2.1|EB-protocol for the differentiation of iPSCs to iDAn

The protocol for the differentiation of iPSC to iDAn was developed in the Wade-Martins laboratory by E. Hartfield (Hartfield et al. 2014) and relies on the *in vitro* formation of Embryoid Bodies (EBs) prior to neuronal differentiation using the dual-SMAD inhibition method (Chambers et al. 2009) (hereafter referred as EB-protocol) (Figure 3.1A). EBs were manufactured by seeding iPSCs into conical shaped microwells (Aggrewell) that induce their aggregation, and harvested and plated on Geltrex-coated wells after 4 days (Figure 3.1B). After 17DIV, the EBs were manually dissected and replated on Geltrex-coated supports and further matured until 36DIV before any biochemical or functional assay. At 36DIV, an extensive neuronal network ($TUJ1^+$) develops and DAn (TH^+) are visible (Figure 3.1C). The differentiation efficiency was found to be overall ~10-20% of TH^+ cells and ~50% $TUJ1^+$ using the control iPSC line NHDF-1 (Fernandes et al. 2016; Hartfield et al. 2014).

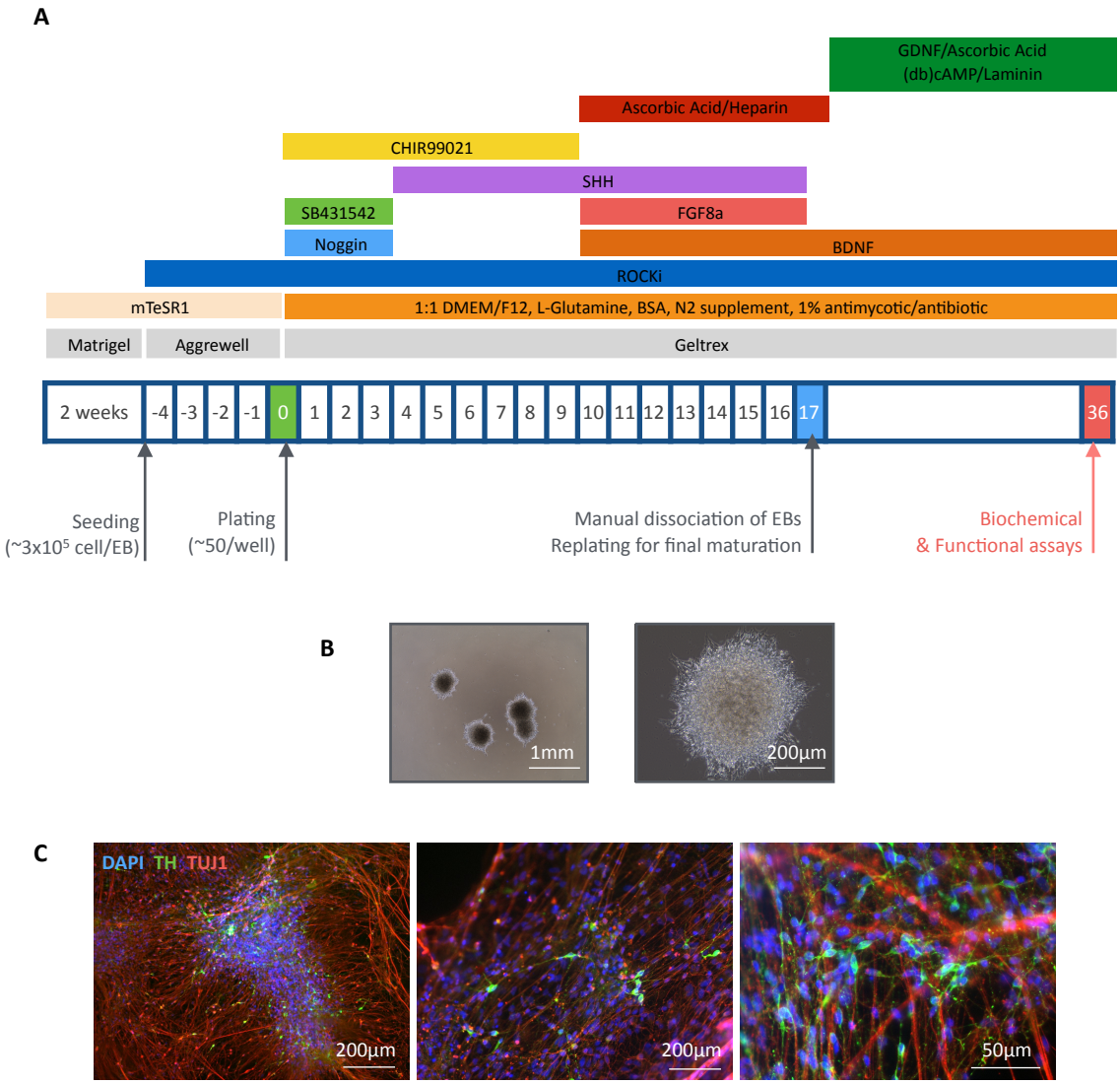

Figure 3.1|List of reagents used for the differentiation of iPSCs to iDAn
(A) Schematic of the EB-protocol for the differentiation of iPSCs to iDAn. **(B)** Representative images of Embryoid bodies (EBs) harvested from AggreWells 400® and plated onto Geltrex-coated wells. **(C)** Cells were fixed at 36DIV and immuno-stained for TH and TUJ1.

3.2.2|Low efficiency and reproducibility with the EB-protocol

The major caveats of the EB-protocol were the low efficiency and the reproducibility. In terms of low efficiency, both the neuronal (~50% TUJ1$^+$ cells) and DAn (~10-20% TH$^+$ cells) population are under-represented in the culture, especially when considering a whole cell population analysis like western blot. Reproducibility of this protocol was variable, even within multiple differentiations of the same line (Figure 3.2A). This could be explained by the nature of the replating procedure. With the EB-protocol it was not possible to count the number of cells at the replating stage since the dissected EBs are arbitrarily distributed for final differentiation to different wells. Moreover, TH$^+$ neurons tend to emerge from the dissected EB and thus cluster in very defined regions surrounded by other cells of non-neuronal nature (Figure 3.2B). Nonetheless, this protocol was extensively characterised in terms of the expression of dopaminergic and neuronal markers, such as FOXA2 or GIRK2, and the cells were shown have mature neuronal electrical properties (Hartfield et al. 2014). A comparison between the EB- and the FP-protocol is described in section 3.2.6.

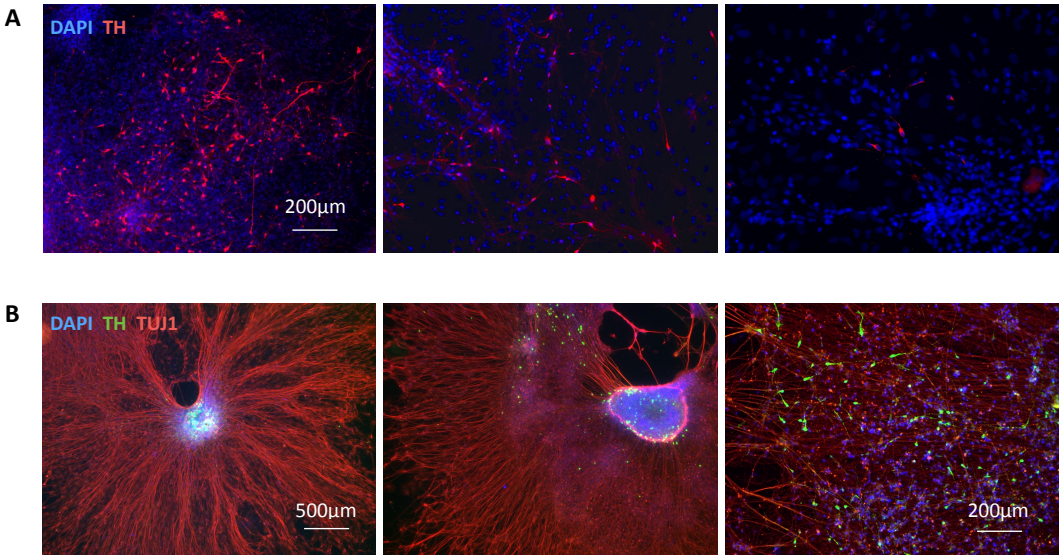

Figure 3.2|Low efficiency and reproducibility with the EB-protocol
(A) Representative images of three independent differentiations of NHDF-1 iPSCs showing variability in iDAn generation (B) Representative images showing that iDA tend to be located inside the dissected EBs or under a extensive neuronal network

3.2.3|Optimisation of the FP-protocol for the differentiation of iPSC to iDAn

Due to the low efficiency and reproducibility of the EB-protocol in producing a cell population enriched for DAn (TH^+ cells), other published protocols were taken into consideration (Table 3.1).

Reference	% TH^+ cells	Expression of vmDAN markers	ePhys validation
Hartfield et al. 2014	20%	Confirmed	Yes
Kriks et al. 2011	70%	Confirmed	Yes
Kirkeby et al. 2012	70%	Confirmed	NA
Sánchez-Danés et al. 2012	20%	Confirmed	Yes

Table 3.1|Comparison of protocols for the differentiation of iPSCs to iDAn
TH= Tyrosine hydroxylase; vmDAn= ventral midbrain dopaminergic neurons; ePhys= electrophysiology; NA= not accessible.

Notably, the protocol published by the Studer laboratory (Kriks et al. 2011) seemed to be the most advantageous in producing a high percentage of TH^+ cells (up to 70%), co-expressing important vmDAn makers such as FOXA1 and LMX1A, and was starting to be employed by other labs (Mazzulli, Zunke, Isacson, et al. 2016; Miller et al. 2013). In collaboration with H. Booth in the laboratory, this protocol was adapted and optimised to work with our iPSC cultures (hereafter referred to as FP-protocol).

One of the first challenges was that the original protocol based on the work by Kirks and colleagues had been optimised to work in human embryonic stem cells (hESCs), instead of iPSCs, cultured on mouse embryonic fibroblasts (MEFs). The original cell density of $3.5\text{-}4x10^4$ cells/cm^2 resulted in very sparse iPSC colonies after two days in culture. iPSCs density prior to the initiation of the differentiation is an important factor for the cell-fate specification, with low-density cultures acquiring preferentially a neural crest–like phenotype whereas cultures at a higher produce central nervous system-derived cells (Chambers et al. 2009). It was found that in our feeder-free iPSC cultures a seeding density

of 1.25-1.5x10^5 cells/cm^2 on Geltrex- or Matrigel-coated wells produced sub-confluent iPSCs within two days and were ready for differentiation.

The type of matrix used to support the differentiation up to 20DIV before the replating was optimised as well. Initially Matrigel (hESC-qualified Matrigel®) was used throughout but sometimes caused the cells to peel off, especially from the edges of the well or flask. The use of the Matrigel Basement Membrane Matrix (Tomishima 2012) did not solve cell peeling but it could be partially overcome using hESC-qualified Matrigel at double the recommended concentration. Finally, when iPSCs were differentiated on Geltrex, the same matrix used for the EB-protocol, this issue was almost completely solved. Moreover, since the cells tended to lift off mostly between 5 and 10DIV, which corresponds the gradual shift from KSR medium to N2-supplemented Neurobasal as basal medium (2.X.X), the use of N2- and B27-supplemented Neurobasal medium between 5 and 11DIV was introduced (Devine et al. 2011; Tomishima 2012), which further prevented cells peeling off the matrix.

Due to the very high cell density these cultures reach, especially between 3 and 13DIV, the medium tends to exhaust very quickly (over-night) and become quite acidic. The amount of medium used between 3-19DIV was increased (4mL/6-well plate well and 10mL/25cm^2 flask) and a half medium replacement with fresh medium of the same composition of the previous day was introduced between full media changes. This improved the tendency of the medium to acidify, although not completely due to the high-cell density in this type of cultures. A schematic of the optimised protocol based on the published one by Kriks and colleagues is represented in Figure 3.3A.

Neuronal cultures are generally replated for final differentiation onto poly-D-Lysine, laminin and fibronectin coated surfaces. We found this type of coating was not very reliable, with cells lifting off during both media changes and experimental procedures, like

immunocytochemistry. The replating of the cells at 20DIV onto Geltrex-coated surfaces, the same as for the EB-protocol, ensured better cell-adhesion, even for longer periods of time. On the day of the replating, we also supplemented the medium with the ROCK inhibitor Y-26732, which has been shown to promote the survival of both ESCs (Watanabe et al. 2007) and neuronal progenitors upon dissociation (Rungsiwiwut et al. 2013).

Lastly, we opted to keep the same isoforms of recombinant proteins that were used for the EB-protocol, namely human Sonic Hedgehog (C24II) N-Terminus and human FGF-8a, compared to the original protocol. After 2 weeks of maturation post-replating, TH^+ and $TUJ1^+$ cells are detectable by immunocytochemistry and formed an extensive neuronal network. Interestingly, despite being replated as single cells, the cell bodies of these neurons tend to form clumps interconnected by neuronal networks (Figure 3.3B).

Table 3.2 summarises all the changes compared to the original protocol by Kriks and colleagues.

Reference	Kriks et al. 2011	FP-protocol
Cell type	ESCs	iPSCs
iPSC density at -2DIV	3.5-4x10^4 cells/cm^2	1.25-1.5x10^5 cells/cm^2
Matrix	Matrigel Basement Membrane	Geltrex
Sonic Hedgehog (SHH)	Mouse SHH (C25II) N-Terminus	Human SHH (C24II) N-Terminus
Fibroblast growth factor 8 (FGF8)	FGF8	FGF8a
Neurobasal supplement (between 5-10 DIV)	N2 supplement	N2 and B27 supplements
Matrix at 20DIV	Poly-Ornithine, Laminin & Fibronectin	Geltrex
ROCKi at the replating	Not used	Yes

Table 3.2|Summary of the changes in the FP-protocol compared to the original work by Kriks and colleagues

FP= Floor plate; ESC= embryonic stem cells; iPSC= Induced pluripotent stem cells; DIV= Days in vitro; ROCKi= Y-27632 dihydrochloride.

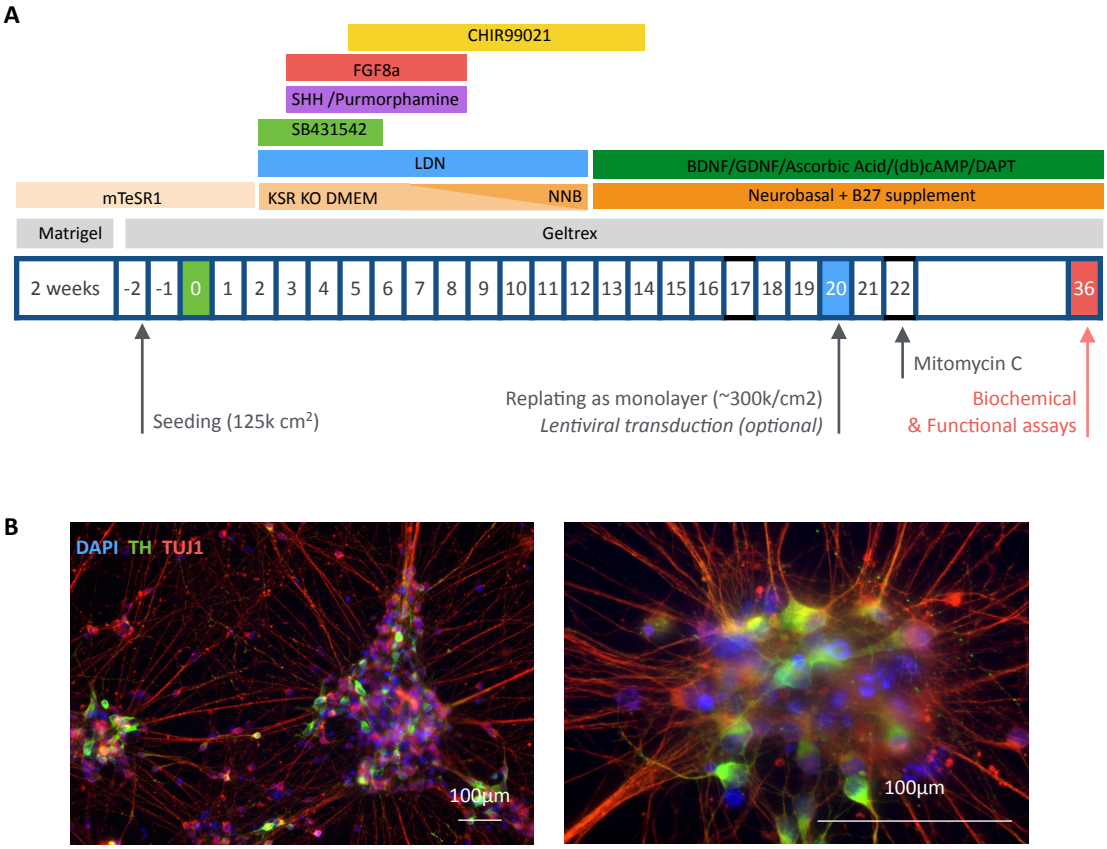

Figure 3.3|Optimisation of the FP-protocol for the differentiation of iPSC to iDAn
(A) Schematic of the FP-protocol for the differentiation of iPSCs to iDAn. **(B)** Representative images of iDAn cultures were fixed at 35DIV and immuno-stained for TH and TUJ1.

3.2.4|Characterisation of iPSC differentiated to iDAn using the FP-protocol

The initial characterisation of iDAn was carried out using the control iPSC line NHDF-1, since it had been extensively used and characterised with the EB-protocol. Overall, the main aim was to determine the efficacy of the FP-protocol in producing *bona fide* ventral midbrain A9 dopaminergic neurons (vmDAn). As described in section 1.3.3, vmDAn are characterised by the expression of midbrain specific transcription factors, like FOXA2 and LMX1A, and mature midbrain DAn markers such as TH, DAT, AADC, GIRK2 and VMAT. Moreover, it is useful to know whether these cells express proteins of interest in the context of PD, including αSyn, Parkin and GBA, that might be taken into consideration during the phenotypic analysis. Different methods were used to investigate the expression of these markers. Some A9 DAn markers were more challenging than others to be detected via immunocytochemistry, therefore their expression via western blot was used instead, although it could not inform about whether they were co-expressed in TH^+ cells. iPSC differentiated to iDAn using the FP-protocol were shown to be genuine A9 midbrain dopaminergic neurons by the co-expression of distinctive markers such as TH, TUJ1, FOXA2 and LMX1A (Figure 3.4A-B), in accordance with the work done by others (Kirkeby et al. 2012; Kriks et al. 2011). The expression of the A9-specific marker GIRK2 and the DAn-specific marker DAT could not be established by immunocytochemistry, probably due to lack of specificity of the antibody used, but was confirmed by protein expression via western blot (Figure 3.4C). Moreover, iDAn cultures were shown to express enzymes involved in the synthesis and uptake of DA, including TH, DAT, AADC and VMAT (Figure 3.4C). Lastly, iDAn expressed αSyn, Parkin and GBA as expected (Figure 3.4C).

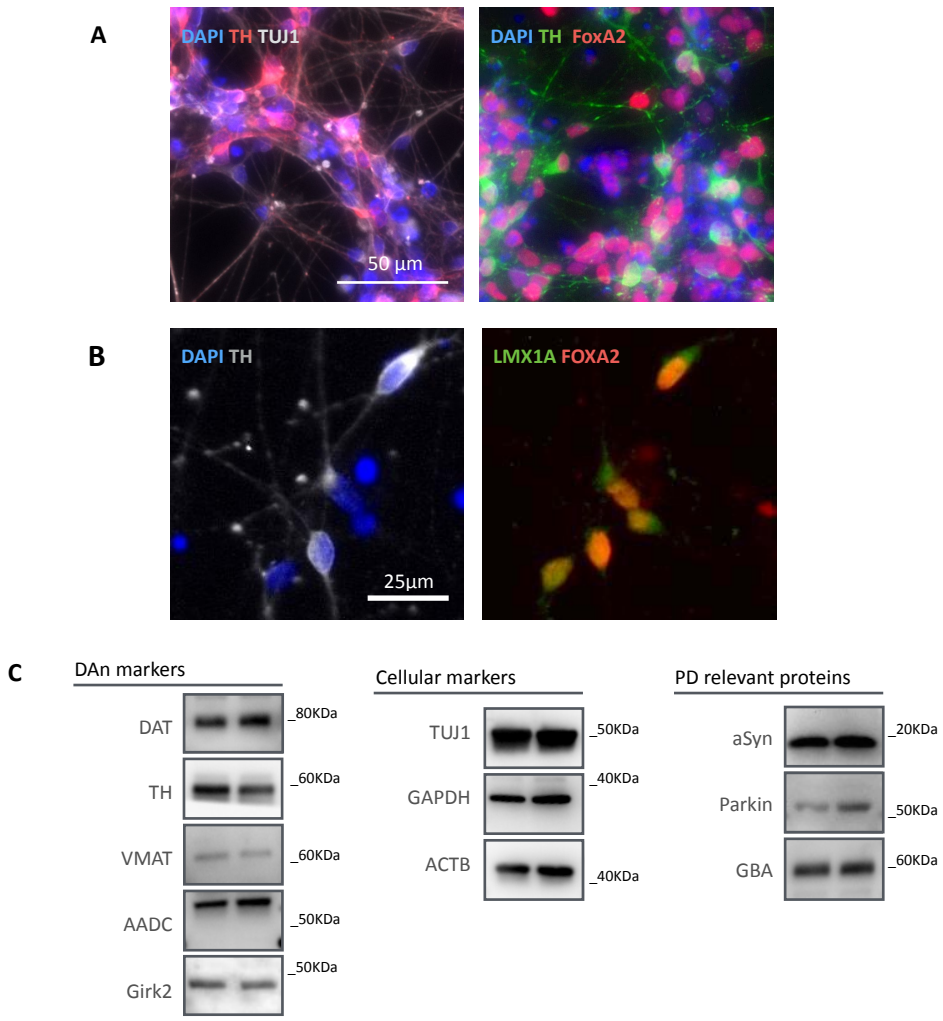

Figure 3.4|Characterisation of iDAn differentiated using the FP-protocol
(A) Representative images of NHDF-1 iDAn at 35DIV immuno-stained for TH, TUJ1 and FOXA2. **(B)** Representative images of immunocytochemistry of NHDF-1 iDAn at 35DIV for TH, FOXA2 and LMX1A to identify A9 vmDAn. **(C)** Protein expression levels of different makers in NHDF-1 iDAn at 35DIV (each band corresponds to a differentiation).

3.2.5|Comparison of the EB- and FP-protocol

Both protocols take approximately the same amount of time from the iPSC stage to the replating step (21DIV for the EB-protocol and 20DIV for the FP-protocol). Overall, three major practical differences were found between the two protocols. Firstly, the FP-protocol does not require the formation of EBs before the initiation of the differentiation. This reduces the technical variability due to the generation of EBs. Moreover, EB formation causes the generation of all three germ layers before the dual-SMAD inhibition, whereas in the FP-protocol iPSCs are directly pushed towards the ectoderm lineage upon initiation of the differentiation. Secondly, at the replating step of the FP-procotol on 20DIV it is possible to enzymatically dissociate the cells and replate a defined number for final maturation. This is definitely important for the inter-well variation in samples of the same line, but does not solve differences in differentiation efficiency, in this case how many of the replated cells are actually post-mitotic neurons, which could cause variation in the final cell density among different lines. However, this represents the inherit variability of working with iPSC lines. Lastly, the FP-protocol introduces a pharmacological treatment with Mitomycin C at 22DIV in order to remove all the proliferating cells still present in the culture and to end up with a population enriched in post-mitotic cells, in this case neurons (Tomishima 2012). Nevertheless, this is not an exclusive advantage of the FP-protocol but could be applied to the EB-protocol as well. Probably the most important advantage of the FP-protocol is the overall higher percentage of TH^+ and $TUJ1^+$. The FP-protocols yields 55±4% of TH^+ cells compared to 18±1% for the EB-protocol (mean±SEM, Student *t*-test, $^{**}p<0.01$) and 78±5% of $TUJ1^+$ cells compared to 40±3% (mean±SEM, Student *t*-test, $^{**}p<0.01$) (Figure 3.5A). The same difference can also be appreciated by analysing the difference in protein expression levels of both TH and β3-tubulin in the EB- or FP-protocol samples (Figure 3.5B). Lastly, a crucial difference between the protocols is the inter-well

variability in αSyn expression, which will be discussed later in this chapter (3.2.7).

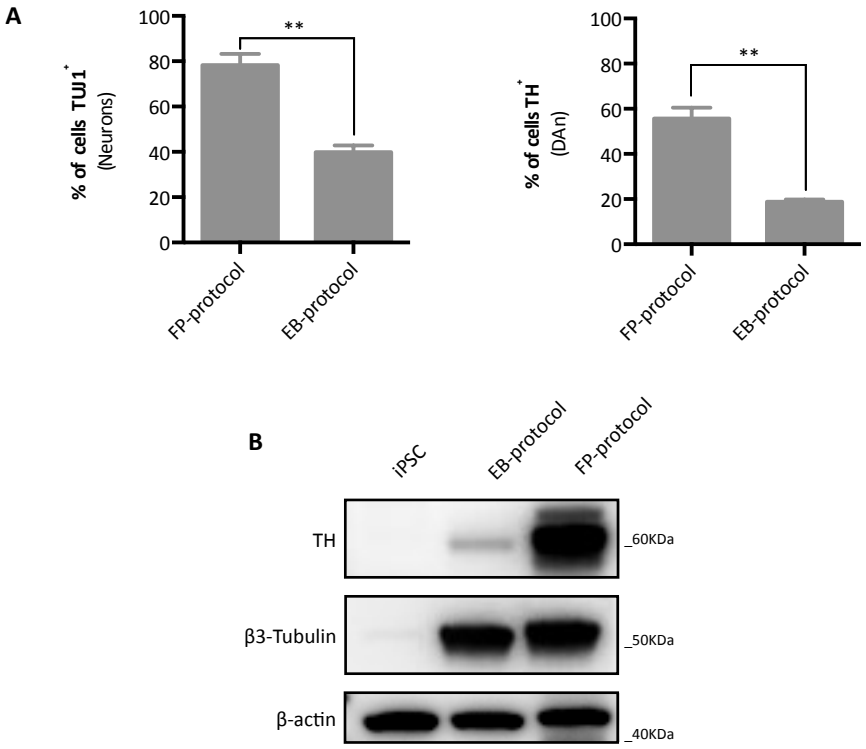

Figure 3.5|Comparison of the EB- and FP-protocols

Analysis of NHDF-1 iDA differentiated with either the EB- or FP-protocol. Data from the EB-protocol was kindly provided by Dr Hartfield (Hartfield et al. - 2014). **(A)** Comparison of the percentage of TH^+ and $TUJ1^+$ cells in the FP- and EB-protocol (N=3, mean ± SEM, Student *t*-test ** $p<0.01$) **(B)** western blot analysis of TH and β3-tubulin in undifferentiated iPSC and iDAn from the EB- or FP-protocol.

3.2.6|Optimisation of the antibodies for αSyn detection in iDAn

There are many commercially available antibodies against αSyn and it is known that some of them have a different preference for monomeric, oligomeric or fibrillar αSyn species.

All the antibodies against αSyn available in the laboratory at the time this project was set up were tested to find the most applicable for protein detection both using western blot and immunocytochemistry. Three antibodies were tested: Covance αSyn (4B12), BD 42/αSyn and Abcam MJFR1. All three seem to recognise different non-specific bands on western blots (Figure 3.6A): Covance αSyn (4B12) and Abcam MJFR1 recognises high molecular weight αSyn molecules even in iPSC; BD 42/αSyn recognises a band between 40 and 50kDa only in cells expressing αSyn instead (iDAn and BE(2)M17). The pattern of staining for these antibodies was similar using immunocytochemistry, with most of the signal coming from the cell soma of $TUJ1^{+}$ cells and extending to a lesser extent to neuronal processes (Figure 3.6B). The BD 42/αSyn antibody was chosen since it recognises only one non-specific band via western blot and had been used in previous publications regarding αSyn iDAn (Orenstein et al. 2013; Reinhardt et al. 2013; Ryan et al. 2013; Schöndorf et al. 2014; Oliveira et al. 2015; Devine et al. 2011; Dettmer et al. 2013).

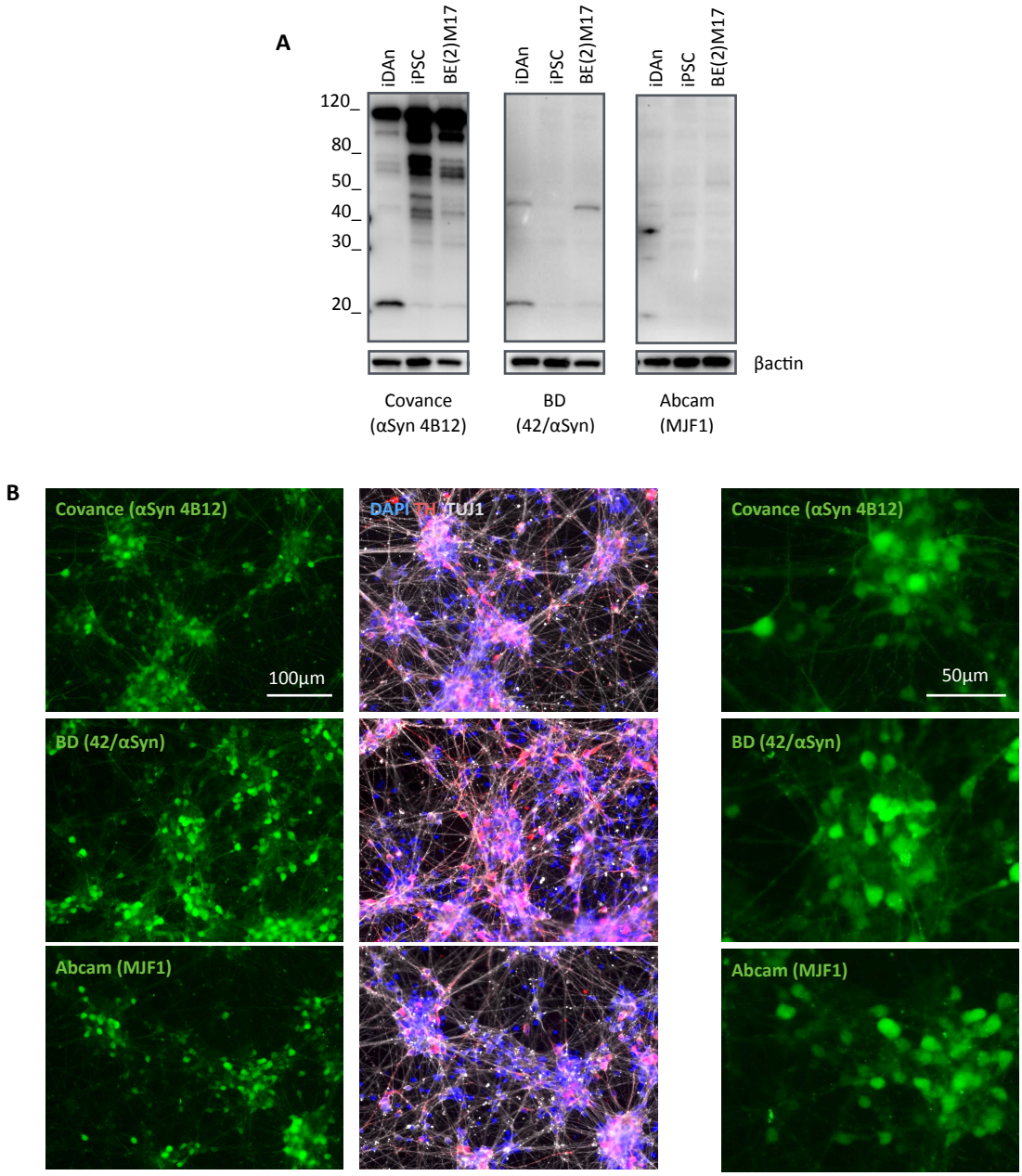

Figure 3.6|Optimisation of the antibodies for αSyn detection in iDAn
(A) Detection of αSyn via western blot using three different antibodies for αSyn (iDAn at 35DIV) **(B)** TH, TUJ1 and αSyn via immunocytochemistry using three different antibodies for αSyn in iDAn at 35DIV.

3.2.7|Differences in αSyn expression levels between the two protocols

To estimate the inter-well variability in αSyn expression levels in both protocols, protein lysates from ten different wells were analysed. The variance in αSyn levels across these samples was significantly lower in the FP-protocol (1.00 ± 0.15) compared to the EB-protocol (1.00 ± 0.49) (F-test to compare variances, $p<0.01$) (Figure 3.7). This is probably because with the FP-protocol is it possible to plate a known number of cells, which results in higher inter-well reproducibility. It is possible that this variability is present in other proteins, especially for non-ubiquitously expressed proteins, depending for example on the percentage of TUJ1$^+$ in the well.

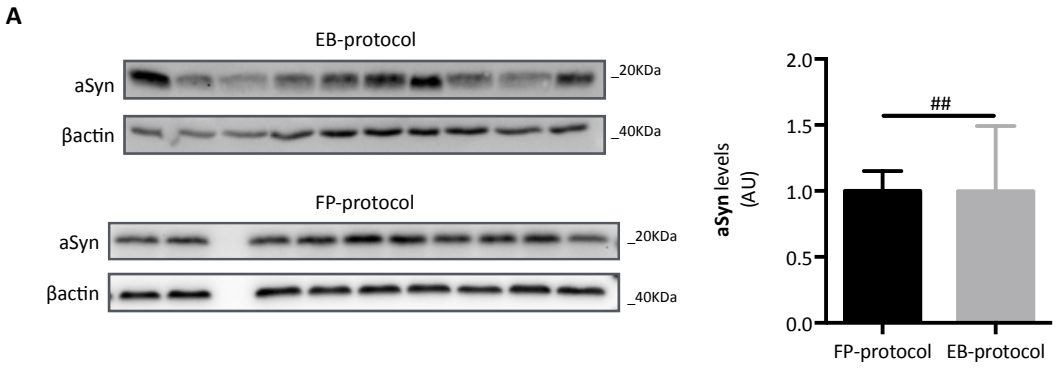

Figure 3.7|Differences in αSyn expression between the EB- and FP-protocol
Ten wells of NDHF-1 iDAn from both the EB- and FP-protocol were collected and analysed for αSyn expression levels (N=1, n=10, F-test of equality of variances, ## $p<0.01$).

3.3|Discussion

This chapter identified a differentiation protocol for the generation of vmDAn from iPSCs to study the pathological mechanisms associated with PD in a relevant *in vitro* cell model. The protocol developed by E. Hartfield in the Wade-Martins laboratory was initially used for most of the siRNA work and for the groundwork regarding the phenotypic analysis. However, low reproducibility and efficiency in generating a cell population enriched for TH^+ cells led to search for alternatives among published protocols. The method published by Kriks and colleagues seemed to be particularly favourable in generating *bona fide* A9 vmDAn (Kriks et al. 2011). This protocol is nowadays one of the most adopted in the field, despite minor changes possibly introduced to achieve a high percentage of TH^+ cells with different iPSC lines. Interestingly, the FP-protocol produced the most promising results in the field of grafting iDAn into the midbrain of PD animal models (Kirkeby et al. 2012; Kriks et al. 2011) and it is also currently used to generate commercially available iDAn precursors (Cellular Dynamics Inc.). Nonetheless, one study found that only 10-20% of the cells differentiated with this protocol were TH^+, which seemed to exaggerate the phenotypic differences between patient and control lines (Woodard et al. 2014).

In this study, iDAn were generated using an optimised and adapted version of the FP-protocol and were shown to be genuine A9 vmDAn by the co-expression of TH and specific midbrain dopaminergic neuron markers, namely FOXA2 and LMX1A. Compared to the EB-protocol, the FP-protocol generated a significantly higher percentage of TH^+ and $TUJ1^+$ cells, which is certainly useful when analysing the whole cell population, like in the case of western blot or measurement of mitochondrial respiration. However, this is less troublesome when using techniques based on the identification of a specific cell type, such as immunocytochemistry for TH. The advantage in the way the cells are replated for final maturation in the FP-protocol is also of huge importance. Single-cell dissociation allows for

greater accuracy in the number of replated cells and gives the possibility to vary the cell density. Of great advantage, a monolayer of cells is easier to transduce both in terms of accuracy of the MOI and accessibility of cell to the viruses, which is something not possible with the dissected EBs. Nevertheless, replating of the cells as a monolayer at 20DIV did not generate a monolayer of neurons by 35DIV, since iDAn formed clumps shortly after replating. No differences in clumping were noticed between the two coating methods that were used (Geltrex and poly-D-Lysine/Laminin), but it cannot be excluded that a finer titration of cell density coupled with either different coatings or astrocytes co-culture might improve this. Further characterisation also showed that these cells were functional. Synthesis and uptake of DA (H. Booth, personal communication) coupled with detection of protein expression of enzymes involved in DA synthesis, storage and uptake, including TH, DAT, AADC and VMAT, demonstrated the dopaminergic nature of these cells. Analysis of tau isoforms expression in 6-month old neurons confirmed that these neuronal cultures eventually resemble neurons in the adult brain (Beevers et al. 2017, submitted for review). Lastly, iDAn showed electrophysiological activity 8 weeks post-replating (H. Booth and E. Whiteley, personal communication).

Overall, the possibility of culturing and analysing human iDAn that carry the genetic background of a PD patient is certainly a useful achievement in itself. These cells are normally inaccessible in patients until the *post-mortem* examination, when most of the DAn have already been lost and the surviving neurons only display late pathological hallmarks of the disease. As with any other *in vitro* cell model, the use of iDAn has some disadvantages as well. One of the drawback of using iDAn is that PD onsets predominantly in the later stages of life, even despite some patients carrying genetic mutations. iDAn are generally matured for about 35-40 DIV (Ryan et al. 2013; Sánchez-Danés, Richaud-Patin, et al. 2012; Woodard et al. 2014), or at most for 6 to 12 months (Mazzulli, Zunke, Isacson,

et al. 2016) Beevers et al. 2017, submitted for review). To overcome this, researchers in the field have opted for the artificial expression of Progerin, a nuclear marker of ageing in iDAn. As a result, the up-regulation of transcriptional networks associated with ageing caused the manifestation of late-onset PD phenotypes, such as apoptotic nuclei and neurite degeneration (Miller et al. 2013). This is clearly a proof-of-principle demonstrating the high physiological relevance of using iPSC-derived neurons for modelling late-onset disorders, since this "induced-ageing" can phenocopy the disease. However, it is interesting to consider the data generated in the Wade-Martins laboratory suggesting that the transcriptome of iDAn cultures at 35DIV clusters closer to adult midbrain neurons than to iPSCs or fetal neurons (Sandor et al. 2017).

The neurodegeneration of DAn in the midbrain of PD patients is likely to be a consequence of multiple factors coupled with genetic predisposition and the contribution of many cell types. Therefore, many studies have pointed out the need to generate well defined and characterised cell types that are relevant to the disease model (Kirkeby et al. 2012; Kriks et al. 2011; Chung et al. 2016). Differentiation protocols that achieve a pure TH^+ cell population are clearly far from being physiologically relevant, since these DAn will lack supporting cells, like astrocytes, and target cells to synapse to. Worryingly, culture medium might also play a role in the physiological relevance of iPSC-derived neuronal cultures. For example, neuronal maintenance medium contains high amounts of glucose, like in the case of Neurobasal (25mM), compared to the normal glycemia in the blood (~5mM). This may as well impact on cellular bioenergetics, rendering cells much more glycolytic due to the abundance of glucose. A recent study showed that action potentials and synaptic activity were also disrupted as a consequence of the composition of classic culture media (Bardy et al. 2015).

Overall, it is naïve to think that one protocol will be applicable to every single iPSC

line ever generated. Some iPSC lines or clones may have reduced differentiation capacity due to epigenetic signatures, like DNA methylation, or other mutations, like SNPs, which might derive from the cell type of origin or the reprogramming procedure. To date, many differentiation protocols are available, with differentiation efficiencies ranging from 5 to 70% TH^+, and have already generated a considerable amount of data (see Table 1.2 in section 1.2.9). Clearly, no protocol is perfect or better than others above all. Overall, iDAn need to be considered as a highly relevant *in vitro* human cellular model that opens the possibility of studying the effect of the genetic background in a disease context.

Chapter 4

Identification and initial characterisation of A53T *SNCA* and *SNCA* triplication iPSC-derived DAn

4.1|Introduction and aims

The aim of this chapter is to identify and differentiate iPSC lines from healthy individuals and PD patients carrying either the A53T *SNCA* mutation or a triplication of the *SNCA* gene. With the scope of having at least three biological replicates, efforts are put into the identification of iPSC lines from at least three individuals per genotype; however, should this not be possible, multiple iPSC clones from the same individual will be used to account for biological variability. Moreover, characterisation of the correct cell identity and differentiation efficiency across samples is crucial when working with multiple iPSC lines. This is important when trying to compare phenotypes that could be confounded or skewed by biological variability that is more dependent on intrinsic properties of the cell line rather than its genotype.

Lastly, the use of iDAn is crucial because it not only allows work with the exact human cell type that is affected the most by PD *in vivo*, but they also carry the entire genetic background of an individual affected by the disease. Yet, the genetic reprogramming and long differentiation protocols makes their use very challenging and time consuming.

This chapter details the results regarding the generation of a PD cell model using control, A53T *SNCA* and *SNCA* Tripl iDA, including:

- Identification of iPSC cell lines
- Monitoring of differentiation efficiency
- Initial characterisation of iDAn cultures
- Statistical method used for the comparison of multiple iPSC lines

4.2|Results

4.2.1|Identification and genotyping of control, A53T *SNCA and SNCA* triplication iPSC lines

All iPSC lines were generated in the James Martin Stem Cell Facility by Dr Sally Cowley and colleagues. Fibroblasts from each individual were reprogrammed using Sendi viruses and three clones were expanded and banked using highly standardised conditions throughout. All clones were characterised for genome integrity, pluripotency and silencing of viral transgenes used for reprogramming (similar to Hartfield et al. 2014) and are reported in Figure 4.1A. With the aim of identifying a set of three healthy individuals and three A53T *SNCA* PD patients iPSC clones, all control and A53T *SNCA* iPSC lines available through the StemBANCC project were identified and subjected to genotyping to exclude or confirm the presence of the G>A (A53T) mutation in *SNCA*. Genomic DNA (gDNA) was purified from iPSCs and screened by restriction enzyme digestion following the same method used to first describe the association of this mutation with PD (Polymeropoulos et al. 1997). The G>A substitution creases a Tsp45I site that results in cleavage of the PCR product into two bands. As expected, all iPSC lines generated from PD patients carrying the A53T *SNCA* mutation were found positive by the genotyping (Figure 4.1B). Fibroblasts from a patient carrying the *SNCA* triplication were characterised elsewhere for the presence of a triplication region in chr4:89,375,425 to 90,880,891, including the genes *HERC5*, *PIGY*, *HERC3*, *NAP1L5*, *FAM13AOS*, *FAM13A*, TIGD2, *GPRIN3*, *SNCA* and *MMRN1* (Devine et al. 2011; Haenseler et al., submitted for review).

A

Reference	Clone	iPSC line	Genotype	Age	Sex
SFC841-03	01	**Control #1**	Control	36	M
	02	Control #1.2			
SFC840-03	03	Control #2.2		67	F
	05	Control #2.3			
	06	**Control #2**			
SFC856-03	04	**Control #3**		78	F
SFC180-03	01	Control #4		60	F
SBAD3-01	01	Control #5		36	F
	05	Control #5.2			
SFC828-03	04	A53T *SNCA* #1.3	A53T *SNCA*	51	F
	06	**A53T SNCA #1**			
	09	A53T SNCA #1.2			
SFC829-03	02	A53T *SNCA* #2.2		46	M
	04	A53T SNCA #2.3			
	06	**A53T SNCA #2**			
SFC830-03	01	A53T *SNCA* #3.3		51	M
	06	A53T SNCA #3.4			
SFC830-04	08	A53T SNCA #3.2			
	09	**A53T *SNCA* #3**			
SFC831-03	01	***SNCA* Tripl #1.1**	*SNCA* Tripl	55	F
	03	***SNCA* Tripl #1.2**			
	05	***SNCA* Tripl #1.1**			

B

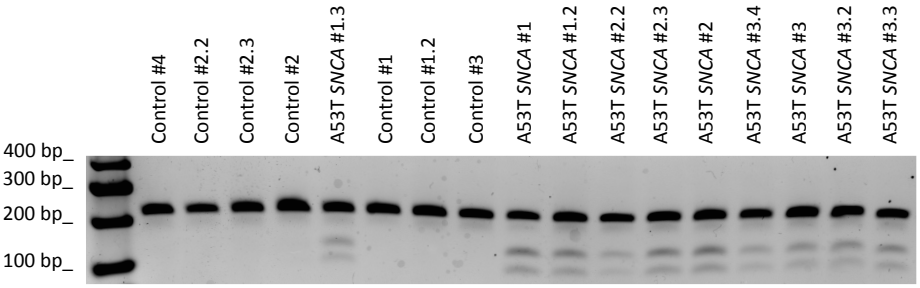

Figure 4.1|Control, A53T *SNCA* and *SNCA* Tripl iPSC lines cohort
(A) The table reports all the iPSC lines considered for this study. **(B)** Confirmation of the genotype for both the control and the A53T *SNCA* iPSC lines via Tsp45I restriction enzyme digestion

4.2.2|Testing the differentiation capacity of control, A53T *SNCA and SNCA* triplication iPSC lines

At the beginning of this work, not all iPSC lines were available due to a bottleneck caused by the sourcing of fibroblasts, the reprogramming and characterisation of all iPSC clones. All available iPSC clones of Control #1, Control #2, A53T *SNCA* #1 and A53T *SNCA* #2 iPSC in June 2014 were tested for their differentiation capacity by the presence of cells immuno-reactive for TH and TUJ1 at 35DIV (Figure 4.2A). No significant difference was found between the two genotypes (Student *t*-test, not significant) (Figure 4.2B).

Control #5 iPSC clones were available from August 2015, Control #3 and Control #4 from September 2015 and A53T *SNCA #3* from October 2015. Clones from the A53T *SNCA* #3 line were accessible from June 2014 but the reprogramming of the fibroblasts only generated two clones that were not very viable upon thawing (S. Cowley and J. Vowles, personal communication). Fibroblasts were reprogrammed again and clones were made available in late 2015 as mentioned above.

It is worth noting that not all iPSC lines could efficiently differentiate to iDAn and some did not differentiate at all. Control #5 iPSCs were differentiated multiple times but never generated any neuronal cells. At 22DIV, Control #5 cells display a non-neuronal morphology compared to Control #1 and would not survive the treatment with Mitomycin C (Figure 4.2C). Similarly, iPSCs from the first reprogramming of A53T *SNCA* #3 (clone 3.4) could differentiate once but only generated 6% TH^+ and 12% $TUJ1^+$ cells at 35DIV (Figure 4.2D).

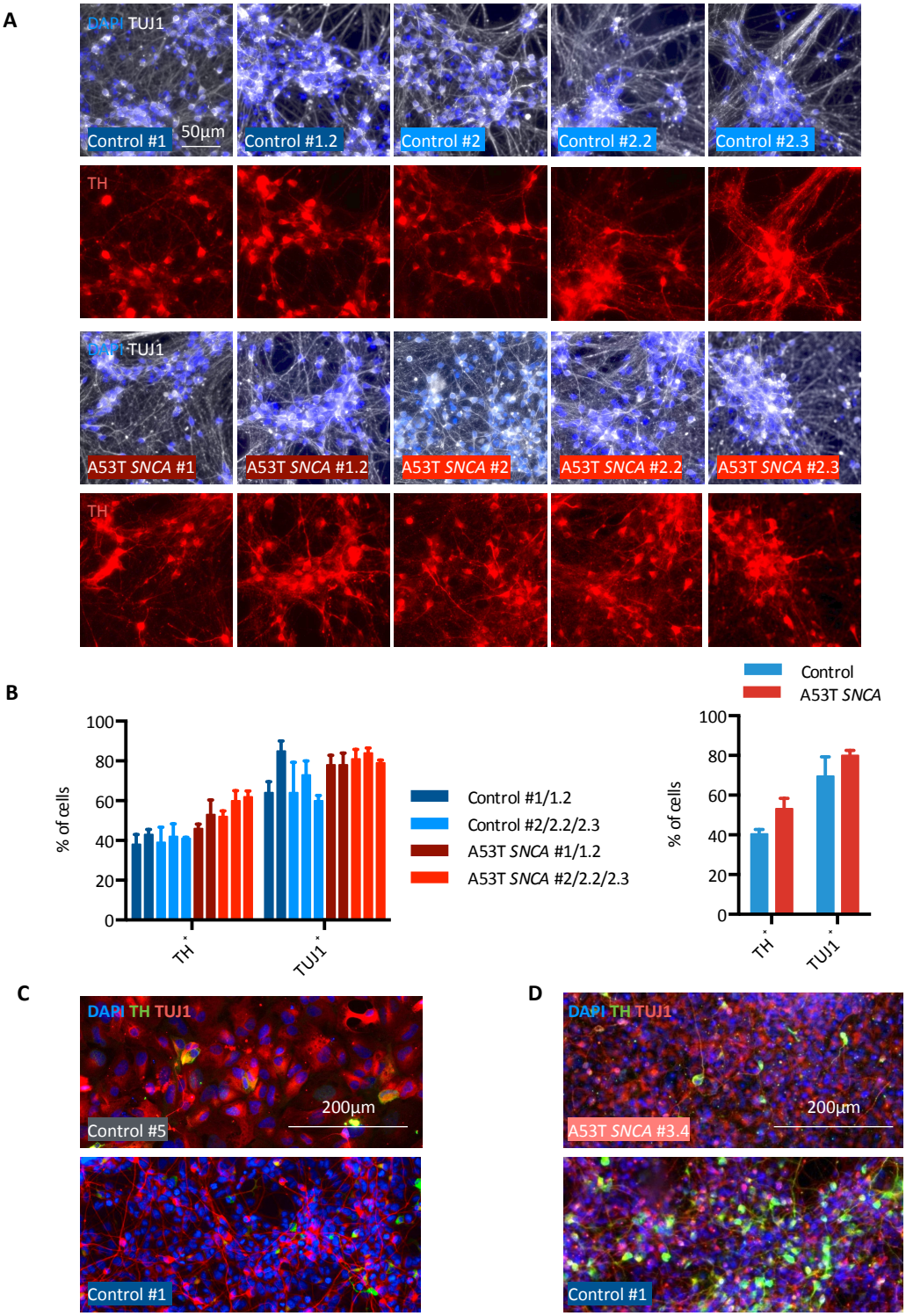

Figure 4.2|Initial testing of the differentiation capacity of Control and A53T *SNCA* iPSC lines
(A) Representative images of Control and A53T *SNCA* iPSC lines at 35DIV stained for TH and TUJ1. **(B)** Estimation of the percentage of cells positive for TH and for TUJ1 shown by lines and genotype (mean±SD, N=1). **(C)** Control #5 compared to Control #1 at D22. **(D)** A53T *SNCA* #3.4 immunocytochemistry for TH and TUJ at 35DIV.

4.2.3|Monitoring the reliability of the differentiation process

Due to inherent variability, iPSCs grow at different rates and, as shown previously, do not always efficiency differentiate to iDAn. It is then clearly important to keep track of some parameters regarding the performance of the iPSC lines. These include successful thawing and bulking up of iPSCs, successful differentiation to 22DIV, judged by the presence of cells immuno-positive for TH and TUJ1, and successful differentiation to 35DIV, assessed visually by the presence of an extensive neuronal network and experimentally with immunocytochemistry for TH and TUJ1 (Figure 4.3A). Out of all the iPSC lines, Control (n=7) and A53T *SNCA* iPSCs (n=8) differentiated successfully with a frequency of 92±5% and 90±11%, respectively. The three clones of the *SNCA* Tripl iPSC line (n=3) differentiated less successfully, on average 68±9% of the times. When considering the iPSC lines and clones used for the phenotypic analysis detailed in chapter 5, Control, A53T *SNCA* and *SNCA* Tripl iPSC clones differentiated successfully 95±3%, 91±3%, and 68% ±9% of the times respectively (one-way ANOVA, $p<0.01$) (Figure 4.3B). Another parameter that may be important to judge the outcome of a differentiation is the number of cells that get replated at 20DIV. This not only gives an idea on initial amount of iPSCs to start with and roughly how many cells are available at the replating, but can also indirectly informs on whether the differentiation was successful or not. Control, A53T *SNCA* and *SNCA* Tripl iPSCs used for the phenotyping work yielded on average 8.92±0.39 $x10^5$, 8.71±0.06 $x10^5$ and 11.19±0.11$x10^5$ cell/cm^2 respectively at the replating on 20DIV (one-way ANOVA, $p<0.001$) (Figure 4.3C).

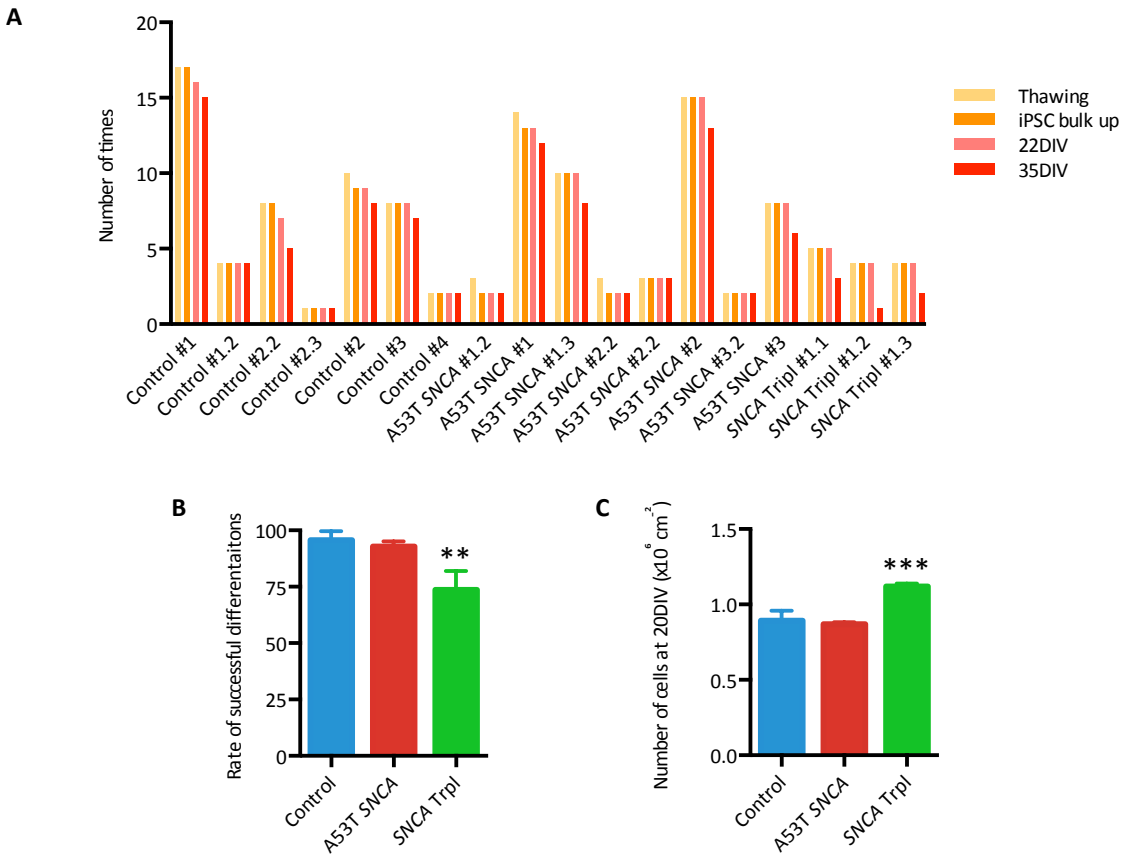

Figure 4.3|Differentiation efficiency of Control, A53T *SNCA* and *SNCA* Tripl iPSC lines
(A) Overview of all the iPSC lines in terms of thawing, bulk up, differentiation to 22 and 35DIV. **(B)** Percentage of successful differentiations (mean±SEM, N>5, one-way ANOVA, $p<0.01$). **(C)** Average cell yield per cm² at 20DIV (N>5, mean±SEM, one-way ANOVA, $p<0.001$).

4.2.4|Initial characterisation of Control, A53T *SNCA* and *SNCA* Tripl iDAn

Due to limitations in time and availability of the iPSC lines, most of the phenotypic screen was restricted to multiple differentiations of one clone per line from three different individuals per genotype. In the case of the *SNCA* Tripl iPSCs, because fibroblasts from only one patient were accessible, three clones were used as biological replicates instead.

Control #1, Control #2, Control #3, A53T *SNCA* #1, A53T *SNCA* #2, A53T *SNCA* #3, *SNCA* Tripl #1.1, *SNCA* Tripl #1.2 and *SNCA* Tripl #1.3 iPSCs were differentiated to iDAn using the FP-protocol. Upon thawing, passaging and culturing during the bulk up before the differentiation, iPSC remained positive for the pluripotency marker Oct3/4 (Figure 4.4). At 11DIV, cells expressed the ventral midbrain floor plate markers LMX1A and FOXA2 (Figure 4.4), whereas after replating at 22DIV, cells expressed the DAn markers, TH and TUJ1, and had the characteristic neuronal morphology (Figure 4.4).

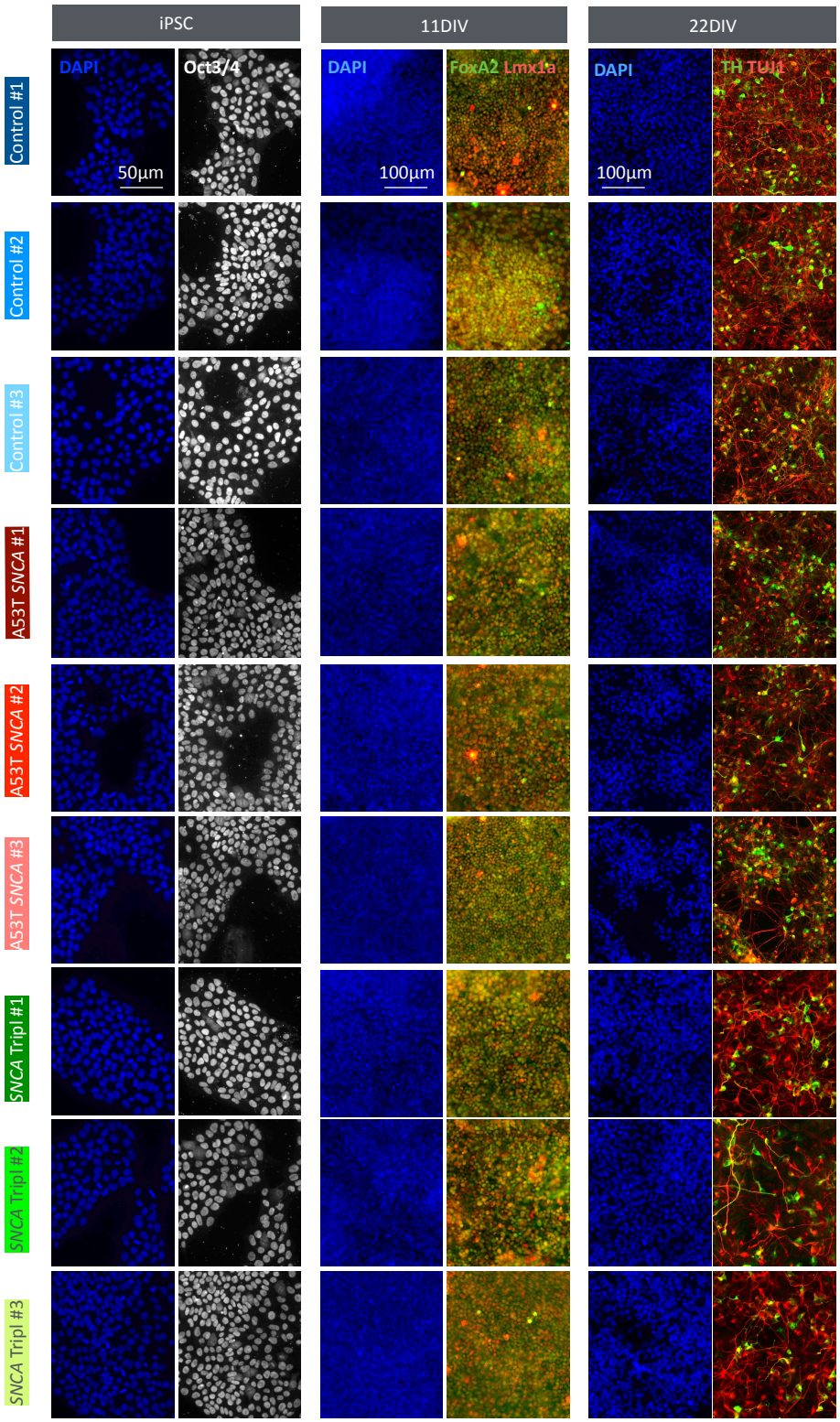

Figure 4.4|Characterisation of control, A53T *SNCA* and *SNCA* Tripl iPSCs differentiation
Cells were fixed and stained at the iPSC stage, at 11DIV and 22DIV. iPSC stained positive for the pluripotency marker Oct 3/4. At 11DIV, vmDAn precursors are positive for FoxA2 and Lmx1a. At 22DIV, DAn stain positive for TUJ1 and TH, indicating a successful differentiation.

At 35DIV, cells were immuno-stained for TH, the dopaminergic neuron marker, TUJ1, a neuronal marker, and FOXA2, the marker of A9 vmDAn (Figure 4.5A). On average, all iPSCs differentiated with similar efficiencies, with around 77% of the total cells being $TUJ1^+$ (neurons) and 44% TH^+(DAn). Of all the TH^+ cells, 70% were also $FOXA2^+$ and therefore A9 vmDAn (one-way ANOVA, not significant) (Figure 4.5B,C,D). The data was further confirmed by the quantification of fluorescence-activated cell sorting (FACS) of iPSC-derived DAn cultures at 35DIV. Upon gating for single live-cells by size and live/dead staining, Control iPSC-DAn had 68±6% TH^+ cells whereas A53T *SNCA* and *SNCA* Tripl samples had 70±10% and 69±8% TH^+ cells respectively (Figure 4.5E). Discrepancy in cell count by FACS or microscopy may arise due to the clumpiness of the cells, which probably results in the over-estimation of the number of nuclei by the latter. Lastly, different reports have shown that iPSC passage number has a considerable impact. Late-passage iPSCs were shown to have an expression profile more similar to ESCs (Chin et al. 2009) and to increase their efficiency in neuronal differentiation (Koehler et al. 2011). iPSCs passage number was similar among all the lines used, on average 23 (N=10 for controls and A53T *SNCA*, N=5 for *SNCA* Tripl), apart from Control #1 since two different batches of frozen vials were used (Figure 4.5F). Moreover, on average all iPSC lines were passaged 2-3 times before the start of the differentiation.

These results indicate that all these iPSC lines differentiate to iDAn with the same efficiency and can therefore be compared with each other for the phenotypic analysis.

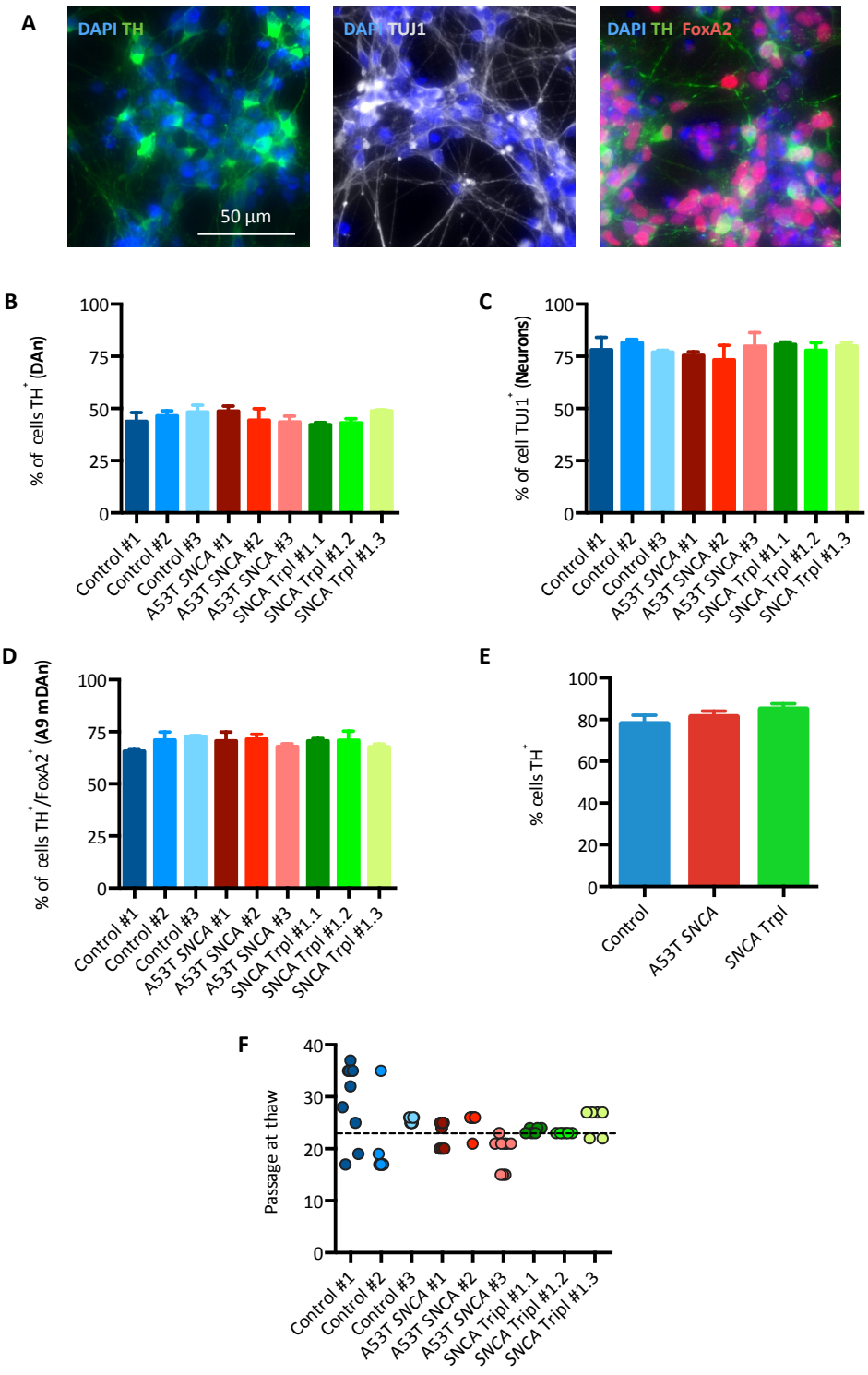

Figure 4.5|Characterisation of control, A53T *SNCA* and *SNCA* TripI iDAn at 35DIV

iDAn were immuno-stained for the neuronal marker TUJ1, the dopaminergic neurons maker TH and the vmDAn marker (FoxA2) **(A)** **(B)** The graphs show the percentage of TH+ cells per line (N=3, 3 lines per genotype, mean ± SEM). **(C)** The graphs show the percentage of TUJ1+ cells per line (N=3, 3 lines per genotype, mean ± SEM). **(D)** The graphs show the percentage of TH+/FOXA2+ cells per line (N=3, 3 lines per genotype, mean ± SEM). **(E)** The graphs show the percentage of TH+ cells per line analysed by FACS (N=1, 3 lines per genotype, mean ± SD). **(F)** Passage number in iPSC lines, the dotted line indicates the average.

4.2.5|Data normalisation and statistical analysis

Due to the inherent variability of iDAn cultures, it is generally accepted that a phenotypic analysis in iPSC-derived DAn needs to be analysed in at least three independent differentiations. Moreover, to be able to normalise the data across multiple differentiations and lines, data will be displayed as the fold change over the average of the control samples. Briefly, for every given experiment, excluding immunocytochemistry where values were normalised for the number of cells, the value of each sample was first normalised for protein content or a housekeeping gene and then for the average value of the control samples. In this way, every dataset from independent differentiations will have values displayed as the fold change compared to the controls.

Statistical analysis was carried out in two ways: Student's *t*-test was used for the comparison of the average of two groups; one-way ANOVA was used or the comparison of the average of three or more groups, as in the case of PD lines versus the controls. With regards to the A53T *SNCA* lines, statistical comparisons will be made between each line and the average of the Control lines. For *SNCA* Tripl iDAn instead, values from each differentiation will be averaged and treated as a single line. For all statistical tests, a confidence interval of 95% is used.

4.3|Discussion

This chapter reported the identification and initial characterisation of iPSC lines from PD patients carrying either the A53T *SNCA* mutation of a triplication of the *SNCA* gene differentiated to dopaminergic neurons (iDAn). Biological variability was considered by aiming to use three iPSC lines for each genotype. The use of multiple clones per line would be undoubtedly useful to highlight phenotypic differences that are clone- rather than genotype-dependent or to further confirm the causative role of the genetic background associated with a PD patient. However, time and affordability restricted the use to only one clone per line for the Control and A53T *SNCA* genotypes. Due to the availability of fibroblasts from only one patient carrying the *SNCA* triplication, three clones of this iPSC line were used instead. The A53T *SNCA* iPSC genotype was confirmed by the presence of a Tsp45I restriction site in the mutated allele (Polymeropoulos et al. 1997), whereas *SNCA* triplication was confirmed in another study by SNP array (Haenseler et al., submitted). All the available iPSC lines were tested for their differentiation capacity using the FP-protocol. Most of the lines differentiated to iDAn with similar efficiencies and generated an extended neuronal network enriched in TH^+ cells by 35DIV. However, some iPSC lines did not differentiate as efficiently, or not at all, and this was not linked to any genotype. It is interesting to discuss two control iPSC lines at the two opposites of their differentiation capacity. The NHDF-1 iPSC line was used in the work of E. Hartfield in the laboratory for the development of the EB-protocol and iDAn from these cells were shown to be electrophysiologically active upon becoming neurons (Hartfield et al. 2014). Despite this, iPSC-derived cortical neurons from the same line did not display any synaptic activity despite differentiating accordingly (E. Whiteley, personal communication). At the other end of the spectrum, Control #5 iPSCs are routinely used to generate electrophysiologically active cortical neurons (E. Whiteley, personal communication) but the same cell line cannot

differentiate to iDAn at all (Figure 4.2C). What is surprising is that both the cortical (Shi et al. 2012) and dopaminergic neuron (Kriks et al. 2011) differentiation protocols rely on the induction of neuronal differentiation by the addition the TGFβ-signalling inhibitor SB431542 and the BMP-signalling blockers LDN-193189 or Dorsomorphin, before differing in the treatment of the cells with lineage-specific growth factors. If anything, this best describes once again the effect of the heterogeneity amongst iPSC that may carry epigenetic signatures or SNPs that can reduce their differentiation potential towards a specific cell type. Clearly, both iPSCs came from fibroblasts of individuals with fully developed brain cortices and midbrains. Yet, it cannot be demonstrated that reprogramming methods do not affect the differentiation capacity of a specific line. In this context, NDHF-1 iPSCs were reprogrammed using integrating retroviruses, whereas Control #5 were generated using non-integrating Sendai viruses.

It was also discussed how it is important to monitor the reliability of the differentiation protocol, especially when using multiple iPSC lines. The nine iPSC lines used for the phenotypic analysis in chapter 5 were chosen for their reliability in successfully going through the entire differentiation protocol. For example, Control #2.2 was initially included in the study but subsequently found to have a variable outcome in generating $TH^+/TUJ1^+$ cells at 20DIV of the protocol (Figure 4.3A).

The statistical method adopted for the phenotypic analysis that will be employed in chapter 5 was described as well. Overall, it is arguable that there is a right way to statistically compare results from multiple iPSC lines. Each line may be considered on its own but at the same time they may be grouped by genotype; anyhow, comparison of multiple lines per genotype will require a higher statistical power to observe a phenotype. For example, the possibility that one PD iPSC line does not show a phenotype consistent with the other lines of the same genotype makes the comparison of control and PD iDAn

less powerful. To date, only the study by Fernandes and colleagues in the field used multiple lines for controls and N370S GBA iDAn and relied on the statistical comparison of the average of the two phenotypes (Fernandes et al. 2016).

Overall, all iDAn cultures used for the phenotypic analysis were found to differentiate with the same efficiency to 77% TUJ1$^+$ cells (neurons) and 44% TH$^+$ cells (DAn). Importantly, 70% of the TH$^+$ cells were also found to co-express FOXA2$^+$. This is in line with most of published studies in this field using the same protocol. Specifically, the percentage of TH$^+$ cells is similar to ~50% reported by Chung and colleagues (Chung et al. 2016), ~60% by Ryan and colleagues (Ryan et al. 2013) and ~50% by Chang and colleagues (Chang et al. 2016). The percentage of TH$^+$/FOXA2$^+$ cells was also comparable to other reports (Mazzulli, Zunke, Isacson, et al. 2016).

Chapter 5

Phenotypic analysis of A53T *SNCA* and *SNCA* triplication iPSC-derived DAn

5.1|Introduction and aims

This chapter focuses on the phenotypic analysis of induced pluripotent stem cell (iPSC) derived dopaminergic neurons (iDAn) carrying mutations or copy number variants in the *SNCA* gene. α-Synuclein (αSyn) pathology is cardinal in PD, and therefore the study of pathological mechanisms in A53T *SNCA* and *SNCA* Tripl cells may reveal pathways and dysfunctions that are widely involved in idiopathic PD.

It is expected that phenotypes which characterise these cells will be small in magnitude, since this *in vitro* cell model does not involve any genetic manipulation for over-expression or knock out and only relies on physiological expression and cellular pathways. Moreover, variability across samples is expected, not only because of the intrinsic variability of iPSCs and differentiation protocols, but also because they will reflect the variability among different PD patients. The A53T *SNCA* mutation was estimated to have a penetrance of about 85% (Klein and Westenberger 2012), which could introduce further variability at the cellular level in the case of A53T *SNCA* iDAn. Compared to animal and immortalised cell models, iDAn are clearly more physiologically relevant for disease research *in vitro*. However, compared to those models, the genetic reprogramming and long differentiation protocols make their use very challenging and slow paced.

This chapter discusses the results regarding the phenotypic analysis in A53T *SNCA* and *SNCA* Tripl iDAn based on the current understanding of PD pathology, including:

- Analysis of αSyn expression, oligomerization and secretion
- Assessment of autophagy function (see introduction in section 1.2.6)
- Characterisation of ER stress (see introduction in section 1.2.7)
- Investigation of mitochondrial function (see introduction in section 1.2.5)
- Study of lipids and energy metabolism (see introduction in section 1.2.8)

5.2|Results

5.2.1|A53T *SNCA* and *SNCA* Tripl iDAn have increased intracellular αSyn staining

The differentiation of iPSC lines from healthy individuals and PD patients carrying either the A53T *SNCA* mutation or a triplication of *SNCA* to iDAn was described in chapter 4. All iPSC lines were shown to differentiate with the same efficiency to mixed neuronal cultures enriched in FOXA2$^+$ DAn (section 4.2.4). It was interesting to analyse whether PD iDAn carrying mutations in *SNCA* display αSyn accumulation. αSyn expression was analysed by two means in iDAn at 35DIV. Whole cell population protein levels analysed via western blot were variable but not significantly different in PD samples compared to control (one-way ANOVA, not significant) (Figure 5.1A). Similarly, the percentage of cells immuno-reactive for αSyn was not different among genotypes (one-way ANOVA, not significant) (Figure 5.2B,C). Nevertheless, when looking specifically at the TH$^+$ population by immunocytochemistry, PD iDAn showed a higher percentage of DAn with cytoplasmic αSyn staining compared to control (one-way ANOVA, $p<0.001$) (Figure 5.2A,B). This phenotype is in line with previous reports in iDAn models carrying mutations in GBA (Woodard et al. 2014), LRRK2 (Sánchez-Danés, Richaud-Patin, et al. 2012), Pink1 and Parkin (Chung et al. 2016), sporadic PD (Sánchez-Danés, Richaud-Patin, et al. 2012; Mazzulli, Zunke, Isacson, et al. 2016), A53T *SNCA*, *SNCA* triplication and *ATP13A2* mutants (Mazzulli, Zunke, Isacson, et al. 2016) and therefore seems a to be recurrent phenotype across laboratories and genetic PD backgrounds. Interestingly, TH$^-$ but TUJ1$^+$ cells strongly staining for αSyn were detected (Figure 5.2A).

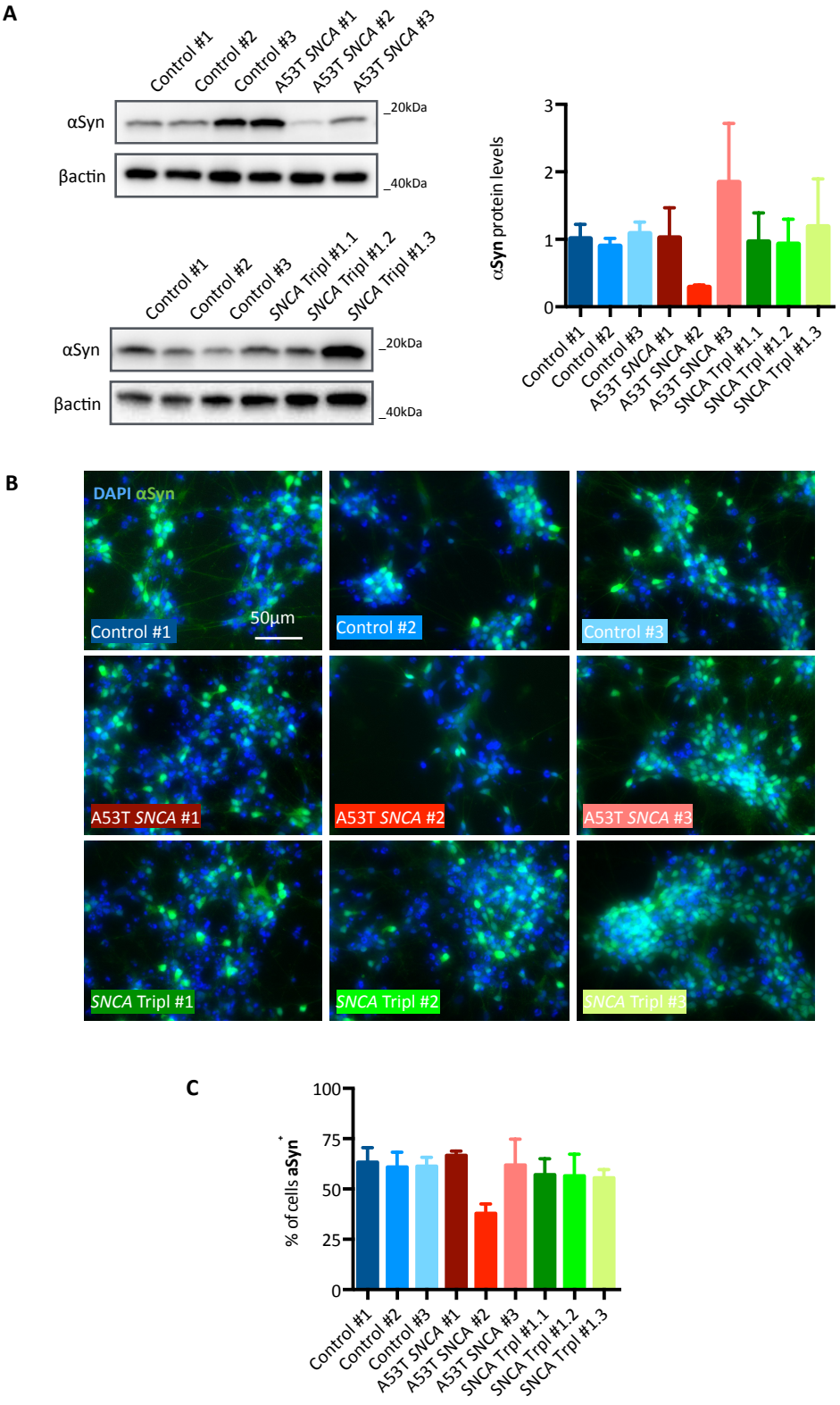

Figure 5.1|Unchanged αSyn expression levels in PD iDAn

(A) αSyn protein levels in Control, A53T *SNCA* and *SNCA* Tripl iDAn at 35DIV (N=3, mean±SEM, one-way ANOVA, not significant). **(B)** Representative images of αSyn immune-staining of iDAn at 35DIV. **(C)** Quantification of the percentage of αSyn⁺ cells in Control, A53T *SNCA* and *SNCA* Tripl iDAn at 35DIV (N=3, mean±SEM, one-way ANOVA, not significant).

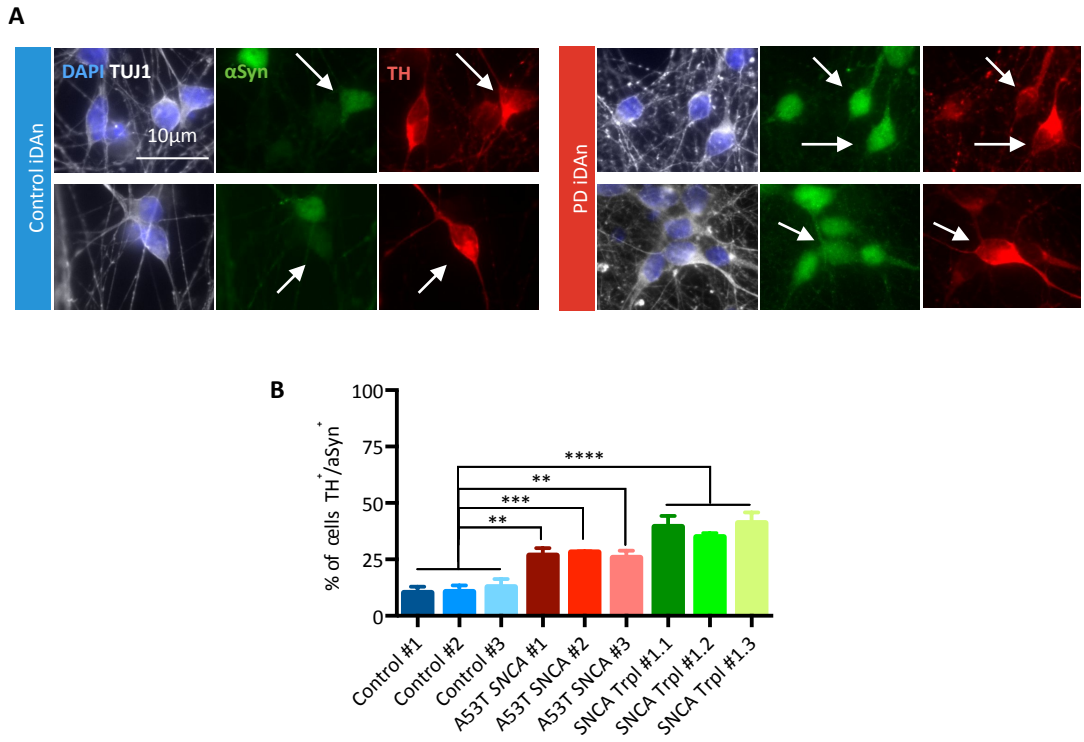

Figure 5.2|αSyn cytoplasmic staining in control, A53T *SNCA* and *SNCA* Tripl iDAn at 35DIV
(A) Representative images of αSyn/TH double immunocytochemistry. White arrows indicate TH+ neurons with cytoplasmic αSyn staining **(B)** Quantification of the percentage of αSyn+ cells in Control, A53T *SNCA* and *SNCA* Tripl iDAn at 35DIV (N=3, mean±SEM, one-way ANOVA, ***p*<0.01, ****p*<0.001, *****p*<0.0001).

5.2.2|αSyn PLA detects increased oligomerization in A53T *SNCA* and *SNCA* Tripl iDAn

αSyn oligomeric species are thought to be either off-pathway aggregates or precursors of fibrils. Either way, it is generally accepted that these αSyn species are ultimately the cause of cytotoxicity, possibly via their interaction with intracellular organelles (Luth et al. 2014; Colla et al. 2012). The Proximity Ligation Assay was previously developed in the laboratory in order to detect αSyn oligomers (αSyn PLA) (Roberts, Wade-Martins, and Alegre-Abarrategui 2015). The assay works by the detection of the monomeric protein by an antibody against αSyn with blocking activity and labelled with either a plus or minus oligonucleotide. If two or more αSyn molecules are in close proximity, as in the case of oligomers, it is possible to enzymatically ligate the two oligonucleotides and, after a rolling circle amplification, detect them using a fluorescent probe. Ultimately, αSyn oligomers are revealed as punctate fluorescent staining (schematic in Figure 5.3A).

Although the technique was well optimised for immortalised cell lines and human brains, further optimisation was required for this technique to work in iDAn. For example, TH immunocytochemistry would give the chance to specifically discriminate the signal in dopaminergic cells. A standard immunocytochemistry protocol was merged with the PLA method and consisted of immuno-labelling TH with a green fluorophore (Alexa-488) in order to not interfere with the PLA signal in the red channel (Alexa-594). In accordance with previous work, αSyn PLA signal is characterised by a punctate staining and a diffused halo co-localising with the nucleus (Figure 5.3B). When a secondary antibody for the detection of the αSyn antibody employed for PLA was used, the co-localisation of αSyn immunocytochemistry and αSyn-PLA signal confirmed the specificity (Figure 5.3C). Conversely, upon omitting the polymerase in the final step of the PLA protocol, no punctate signal is detected, further suggesting specificity. Yet, the nuclear staining remains,

suggesting a non-specific binding of the oligonucleotide probe (Figure 5.3D). With the aim of further characterising the previous results reporting increased αSyn cytoplasmic staining in PD TH$^+$ cells (see section 5.2.1), αSyn PLA was coupled with immunocytochemistry using the BD 42/αSyn antibody. In this case, some cells displayed PLA signal despite being poorly positive for αSyn, or not staining at all (white arrows, Figure 5.3E). This discrepancy might arise because the epitopes recognised by the αSyn antibodies used for PLA (Syn211) and immunocytochemistry (BD 42/αSyn) are at the opposite ends of the protein and therefore might detect different αSyn pools. Lastly, in immortalised cell lines the PLA signal is generally quantified as number of PLA *puncta* divided by the number of nuclei. Because iDAn in cultures tend to clump, the amount of cell bodies in different fields of view is not homogeneous and not all PLA *puncta* from one cell sit in the same focal plane, making the determination of the PLA signal dependent on the number of nuclei in the field of view. To overcome this, the study was carried out by quantifying the PLA signal as the average number of *puncta* in the soma of TH$^+$ cell in 60X z-stacks images, using TH immunocytochemistry as a cell marker.

Preliminary data showed a small but significant increase in the average number of PLA *puncta* per TH$^+$ cell in two A53T *SNCA* lines and all *SNCA* Tripl iDAn compared to Control (N=1, one-way ANOVA, $p<0.01$) (Figure 5.3F). These data concur with the increased percentage of TH$^+$ cells with cytoplasmic αSyn staining in PD iDAn, apart from A53T *SNCA* #1. Taken together, these preliminary data indicate αSyn is not only localising in the soma of A53T *SNCA* and *SNCA* Tripl iDAn, but is also oligomerizing more compared to control cells.

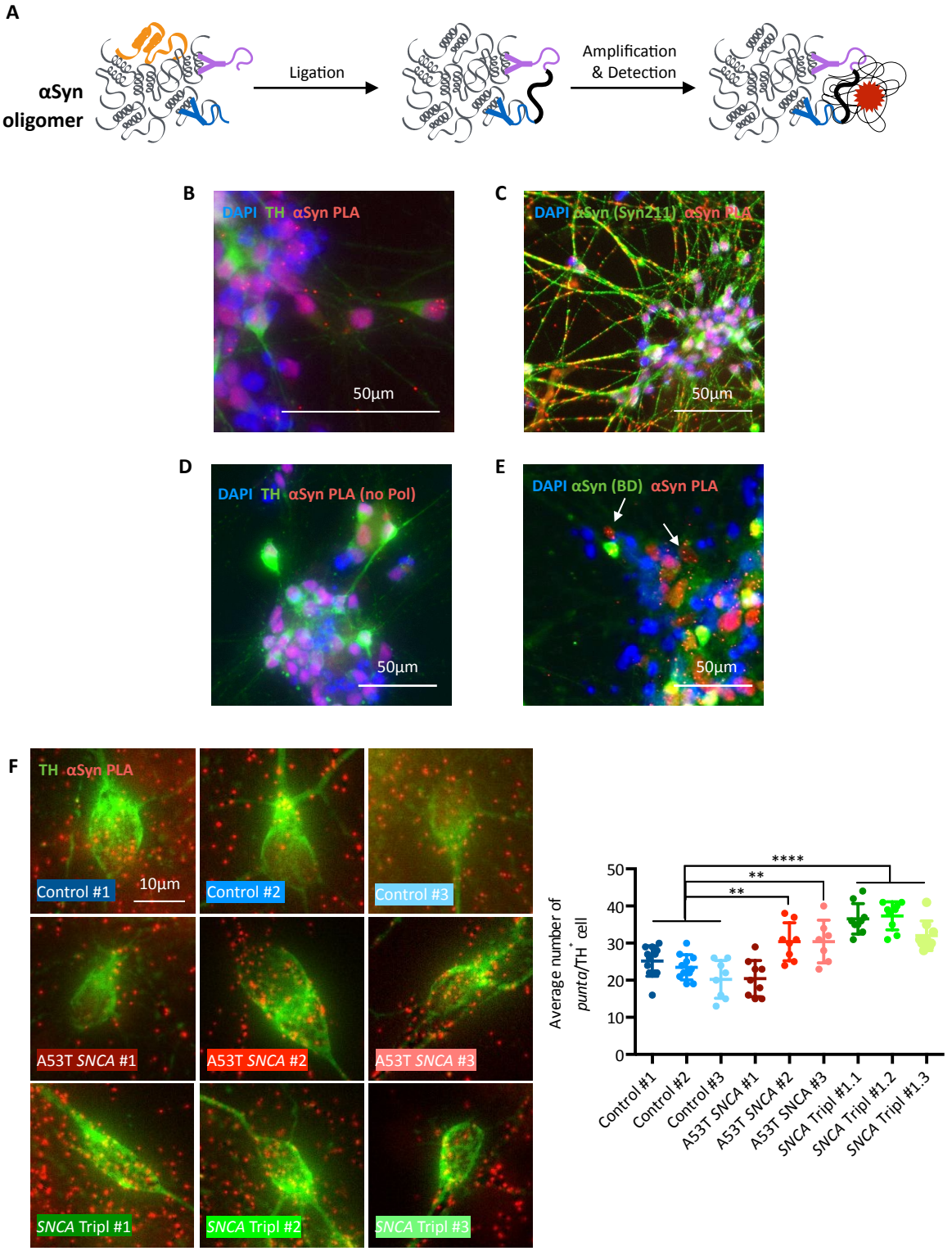

Figure 5.3|A53T *SNCA* and *SNCA* Tripl iDAn have increased PLA signal
αSyn oligomers are detected using αSyn PLA. **(A)** Schematic of the PLA assay (modified from Roberts, Wade-Martins, and Alegre-Abarrategui 2015) **(B)** Representative image of TH immuno-labelling and αSyn PLA. **(C)** Representative image of αSyn PLA and immuno-labelling of the αSyn PLA antibody Syn211 **(D)** Representative image of TH immune-labelling and αSyn PLA with the omission of the polymerase from PLA **(E)** Representative image of αSyn immuno-labelling using the BD 42/αSyn antibody and αSyn PLA **(F)** Representative images and quantification of the average number of PLA *punta* in Control, A53T *SNCA* and *SNCA* Tripl iDAn at 35DIV (N=1, mean ± SEM, one-way ANOVA, $^{**}p<0.01$, $^{***}p<0.0001$)

5.2.3|No differences in αSyn secretion between Control and A53T *SNCA* iDAn

Previous work done in the laboratory using iDAn carrying the heterozygous N370S GBA mutation reported secretion of αSyn in the culture medium during the final maturation (Fernandes et al. 2016). αSyn in the media was previously quantified using an in-house ELISA performed by collaborators. A more accurate and highly sensitive method to determine αSyn concentration in biological samples was adopted taking advantage of the commercially available Meso Scale Discovery (MSD) human αSyn kit. Samples collected at 27, 29, 34 and 36DIV were analysed undiluted based on the previous data in GBA iDAn, whereas Neurobasal medium was used as a blank. To account for differences in the number of cells in each sample, raw values were normalised for total protein content in lysates from the same samples. iDAn secreted αSyn in the supernatant during final differentiation and maturation, whereas the amount of non-specific signal in Neurobasal was negligible (Figure 5.4A). A53T *SNCA* iDAn secreted similar amounts of αSyn in the medium compared to control at all time points analysed (two-way ANOVA, not significant) (Figure 5.4A). In collaboration with W. Haenseler (Dunn School of Pathology, University of Oxford), the same experiment was performed with supernatant from Control, A53T *SNCA* and *SNCA* Tripl iPSC-derived macrophages (iMac) (van Wilgenburg et al. 2013). *SNCA* Tripl iMac secreted 7.1±1.2 fold more αSyn in the medium compared to Control, whereas A53T *SNCA* iMac displayed only a non-significant trend towards increased secretion (Haenseler et al., submitted for review) (N=3, mean± SEM, one-way ANOVA, $p<0.001$) (Figure 5.4B). Overall, this assay only quantifies the total amount of αSyn in the supernatant but does not discriminate or inform about which type of αSyn species are detected. To investigate this, supernatants were concentrated and resolved under native western blot conditions. A53T *SNCA* iDAn showed the same species of high molecular weight (HMW) αSyn compared to

Control iDAn, whereas *SNCA* Tripl iMac had more abundant HMW αSyn species compared to Control iMac, further confirming the data from the quantification of secreted αSyn (Figure 5.4C).

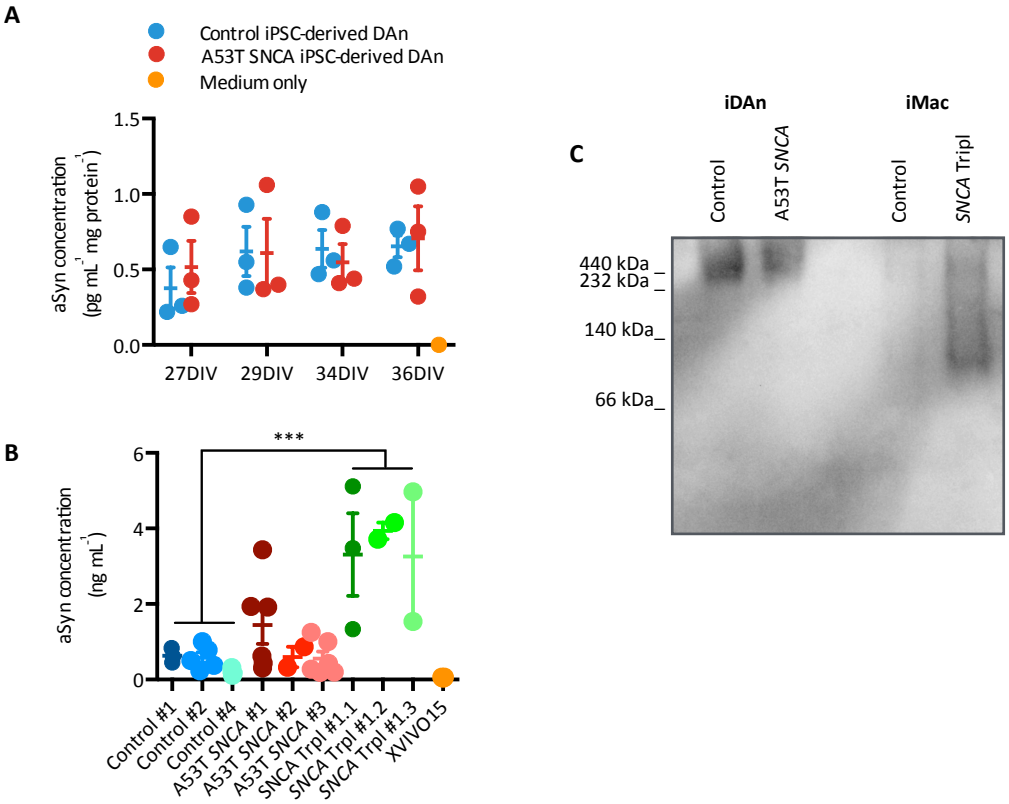

Figure 5.4|A53T iDAn and iMac do not secrete more αSyn in the supernatant compared to controls
αSyn concentration in the supernatant of both iDAn and iMac cultures was analysed using the MSD platform. **(A)** αSyn concentration at 27, 29, 34 and 36DIV in in Control and A53T *SNCA* iDAn at 35DIV normalised for protein content of cell lysate (N=1, mean±SD, two-way ANOVA). **(B)** αSyn concentration in Control, A53T *SNCA* and *SNCA* Tripl iMac (N=3, n>2 clones per line, mean± SEM, one-way ANOVA, ***p<0.001). **(C)** Detection of αSyn in native western blot of concentrated supernatant from both iDAn and iMac.

5.2.4|A53T *SNCA* and *SNCA* Tripl iDAn show dysregulation of autophagy induction

Autophagy has been long implicated in PD (Webb et al. 2003; Ebrahimi-Fakhari et al. 2011) and its dysregulation is thought to underlie the accumulation of dysfunctional mitochondria (Ryan et al. 2015) and lysosomes (Fernandes et al. 2016). To evaluate the state of autophagic machinery, protein levels of different molecules involved in key aspects of this process were analysed.

Sequestosome-1 p62/SQSTM1 is a protein important for the recognition of ubiquitinated proteins and their degradation; via its binding to the lipidated form of microtubule-associated protein 1A/1B-light chain 3 (LC3-II), p62 induces the formation of autophagosomes containing molecules or organelles destined to be degraded (Kabeya et al. 2000). Despite being variable and small in magnitude, results showed an overall increase in p62 and a decrease in LC3-II in A53T *SNCA* and *SNCA* Tripl iDAn lines compared to Control. Specifically, A53T *SNCA* #2 and #3 had a significant up-regulation of p62 (one-way ANOVA, $p<0.01$), whereas A53T *SNCA* #2 and *SNCA* Tripl iDAn had decreased processing of LC3 to its lipidated form LC3-II (one-way ANOVA, $p<0.05$) (Figure 5.5A,B). Analysis of the transmembrane lysosomal glycoprotein LAMP1, widely used as a lysosome marker (Fernandes et al. 2016), did not reveal any significant difference in PD samples compared to Control (one-way ANOVA, not significant) (Figure 5.5C). Similarly, levels of Lysosome-associated membrane protein 2 (LAMP2A), a receptor for chaperon-mediated autophagy (CMA) in the lysosomes, and Heat shock 70 kDa protein 8 (HSC70), a chaperone that shuttles CMA substrates to the lysosome via the interaction with LAMP2A (Cuervo et al. 2004), were unchanged among lines (one-way ANOVA, not significant) (Figure 5.5D,E).

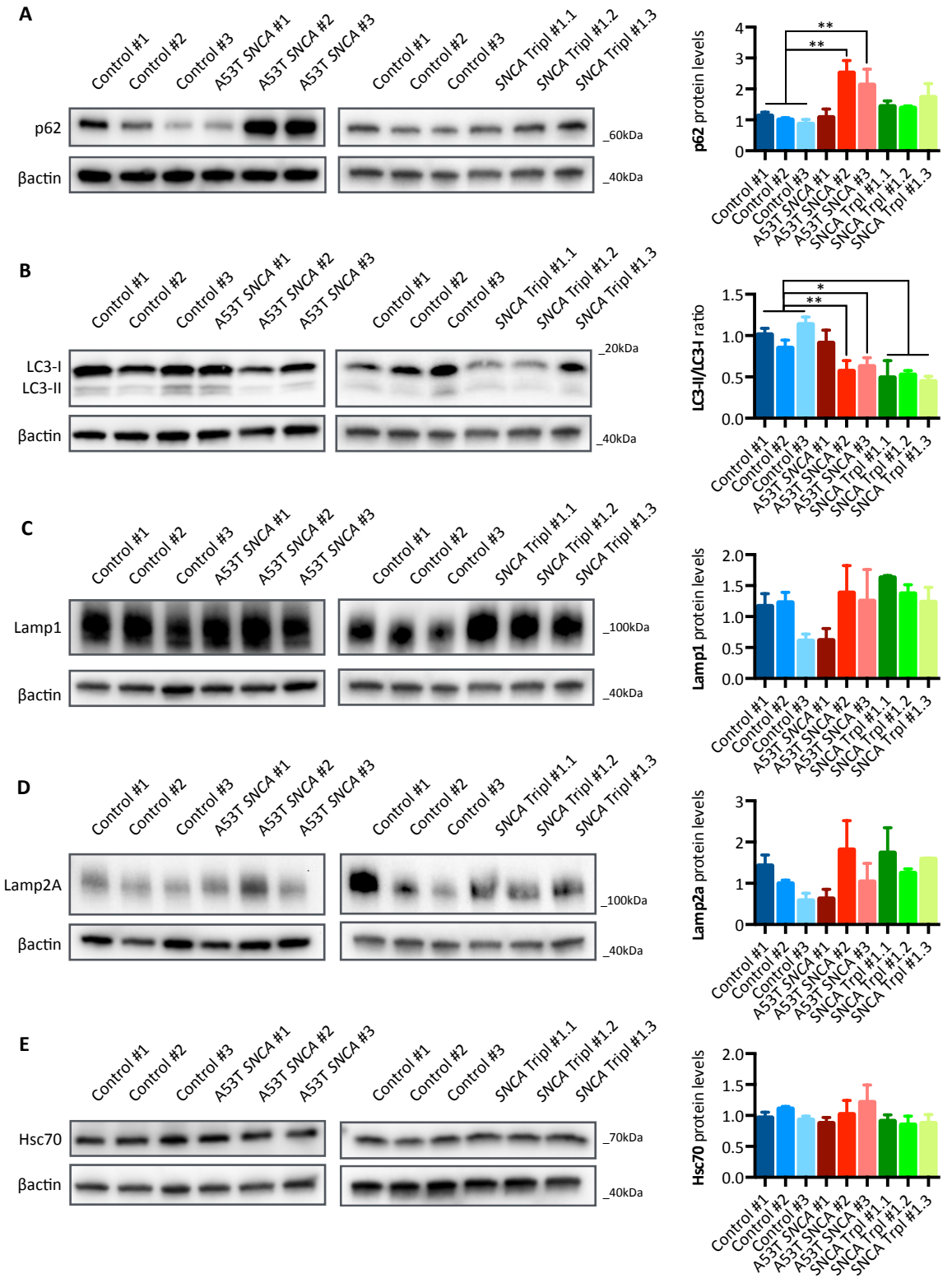

Figure 5.5|Autophagy dysregulation in A53T *SNCA* and *SNCA* Tripl iDAn

(A) p62 protein levels in Control, A53T *SNCA* and *SNCA* Tripl iDAn at 35DIV (N=3, mean±SEM, one-way ANOVA, *p<0.05, **p<0.01). **(B)** LC3-I and LC3-II protein levels in Control, A53T *SNCA* and *SNCA* Tripl iDAn at 35DIV (N=3, mean±SEM, one-way ANOVA, **p<0.01). **(C)** LAMP1 protein levels in Control, A53T *SNCA* and *SNCA* Tripl iDAn at 35DIV (N=3, mean±SEM, one-way ANOVA, not significant). **(D)** LAMP2A protein levels in Control, A53T *SNCA* and *SNCA* Tripl iDAn at 35DIV (N=3, mean±SEM, one-way ANOVA, not significant). **(E)** HSC70 protein levels in Control, A53T *SNCA* and *SNCA* Tripl iDAn at 35DIV (N=3, mean±SEM, one-way ANOVA,not significant).

5.2.5|Different impact of A53T *SNCA* and *SNCA* Tripl on ER stress in iDAn

ER stress is a cellular coping mechanism by which effectors of the unfolded protein response (UPR) are activated upon binding of BiP to misfolded proteins in the ER (Hendershot 2004). A53T *SNCA* iPSC-derived cortical neurons have been previously reported to accumulate the ER stress markers BiP and PDI alongside with ERAD substrates, including GBA (Chung et al. 2013). Levels of the ER chaperone Grp78/BiP were increased in two A53T *SNCA* iDAn lines but not in *SNCA* Tripl samples (one-way ANOVA, $p<0.01$) (Fig 5.6A). This suggests that ER stress has been triggered in these cells, possibly in response to harmful stimuli, including protein misfolding. Expression levels of PDI, a chaperone involved in disulphide bonds (Hatahet and Ruddock 2009), were no different across genotypes (one-way ANOVA, not significant) (Fig 5.6B). Measurements of calreticulin levels, another ER chaperone with Ca^{2+} buffer activity (Michalak et al. 2009), did not show any differences across the three genotypes suggesting no ER Ca^{2+} dysfunction in PD iDAn at this stage (one-way ANOVA, not significant) (Figure 5.6C). Analysis of IRE1α expression levels, one of the effectors of the UPR pathway (Hetz 2012), showed an increase in two A53T *SNCA* and *SNCA* Tripl lines indicating that at least one of the UPR pathways has been switched on (one-way ANOVA, $p<0.01$) (Figure 5.6D). Lastly, protein levels of C/EBPβ, another transcription factor supposedly activated upon ER stress and linked to apoptotic cell death (Meir et al. 2010), were increased in A53T *SNCA* #2 and #3 and in *SNCA* Tripl iDAn (one-way ANOVA, $p<0.01$) (Figure 5.6E), further suggesting that there is an overall up-regulation or activation of effectors of ER stress.

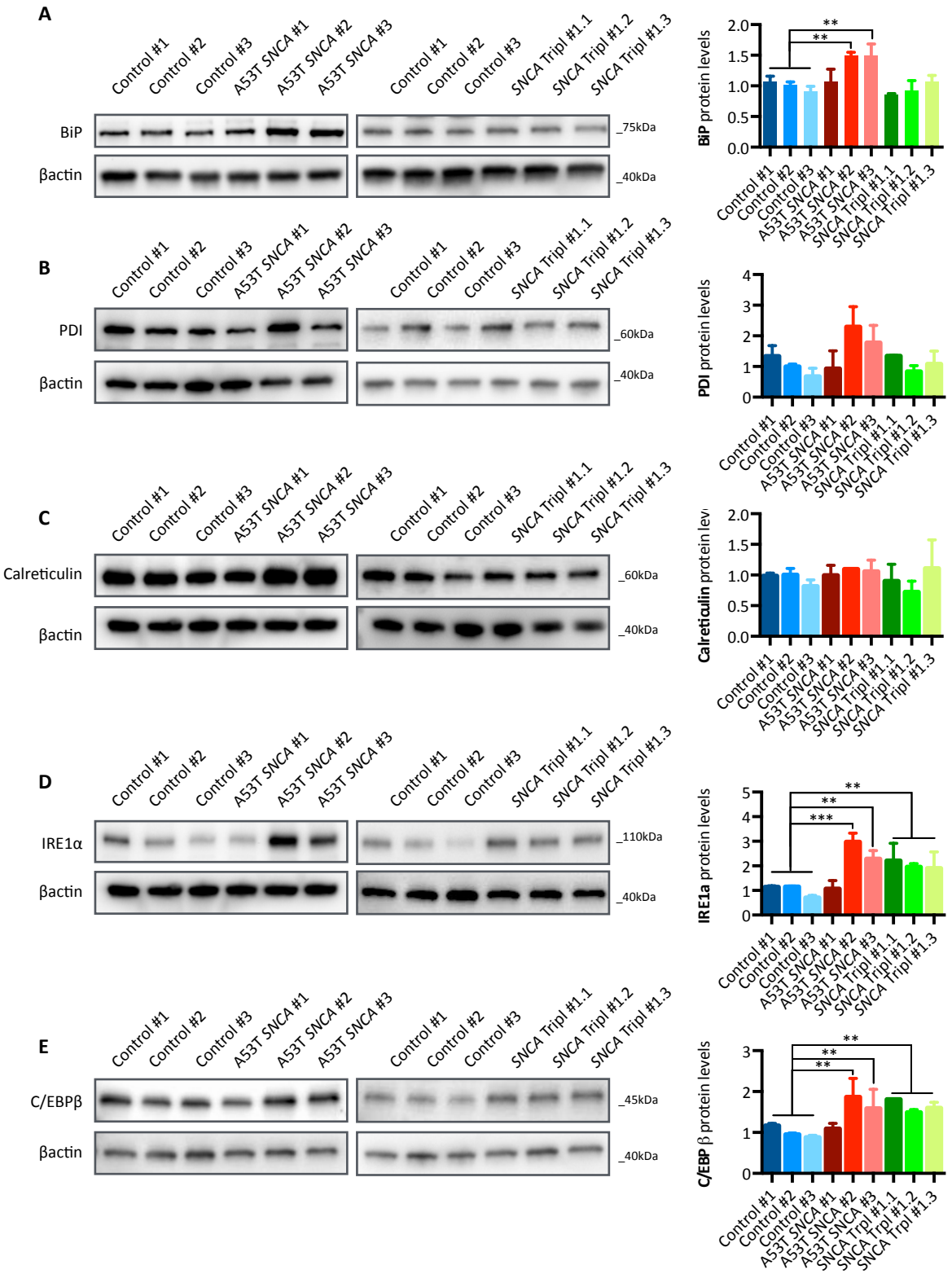

Figure 5.6|Upregulation of ER stress markers in A53T *SNCA* and *SNCA* Tripl iDAn
(A) BiP protein levels in Control, A53T *SNCA* and *SNCA* Tripl iDAn at 35DIV (N=3, mean±SEM, one-way ANOVA, $^{**}p<0.01$). **(B)** PDI protein levels in Control, A53T *SNCA* and *SNCA* Tripl iDAn at 35DIV (N=3, mean±SEM, one-way ANOVA, not significant). **(C)** Calreticulin protein levels in Control, A53T *SNCA* and *SNCA* Tripl iDAn at 35DIV (N=3, mean±SEM, one-way ANOVA, $^{**}p<0.01$, $^{***}p<0.01$). **(D)** IRE1α protein levels in Control, A53T *SNCA* and *SNCA* Tripl iDAn at 35DIV (N=3, mean±SEM, one-way ANOVA, not significant). **(E)** C/EBPβ protein levels in Control, A53T *SNCA* and *SNCA* Tripl iDAn at 35DIV (N=3, mean±SEM, one-way ANOVA, $^{**}p<0.01$).

5.2.6|A53T *SNCA* and *SNCA* Tripl iDAn have increased GBA activity

The glucosylceramidase activity of the lysosomal enzyme GBA has been associated with the pathogenesis of PD (Fernandes et al. 2016) and linked to αSyn pathology (Mazzulli et al. 2011; Mazzulli, Zunke, Tsunemi, et al. 2016; Mazzulli, Zunke, Isacson, et al. 2016). GBA and αSyn are thought to form a bidirectional pathogenic loop where an increase in αSyn levels (sporadic and monogenic PD cases) can reduce GBA activity and a reduction in GBA activity (heterozygous GBA mutations) can result in increased intracellular αSyn levels. It is still not clear yet whether αSyn and GBA physically interact (Mazzulli, Zunke, Tsunemi, et al. 2016; Dermentzaki et al. 2013) but clearly both influence each others' normal or pathological function. Total GBA activity was measured using an in-house assay (Fernandes et al. 2016). A53T *SNCA* and *SNCA* Tripl iDAn displayed a small but significant increase in GBA activity compared to Control (one-way ANOVA, $p<0.05$) (Figure 5.7A), opposite to what has been previously shown in the literature (Mazzulli et al. 2011; Mazzulli, Zunke, Tsunemi, et al. 2016).

GBA protein levels were variable in PD iDAn and not significantly different (one-way ANOVA, not significant) (Figure 5.7B).

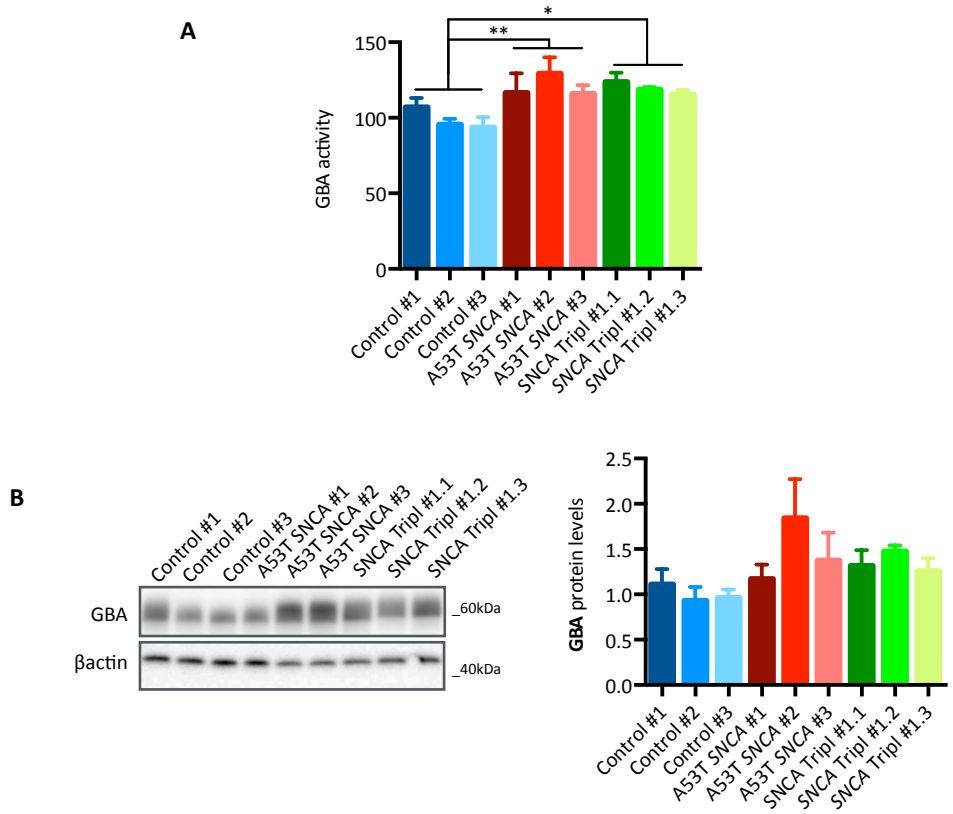

Figure 5.7|A53T *SNCA* and *SNCA* Tripl iDAn have increased GBA activity

GBA activity and protein were analysed at 35DIV. **(A)** Measurement of GBA activity in Control, A53T *SNCA* and *SNCA* Tripl iDAn at 35DIV (N=5 for controls and A53T *SNCA*, N=3 for *SNCA* Tripl, mean ± SEM, one-way ANOVA, *p<0.05, **p<0.01). **(B)** Quantification of GBA protein levels in Control, A53T *SNCA* and *SNCA* Tripl iDAn at 35DIV (N=5 for controls and A53T *SNCA*, N=3 for *SNCA* Tripl, mean ± SEM, one-way ANOVA, not significant).

5.2.7|A53T *SNCA* iDAn are characterised by dysfunctions in mitochondrial respiration

Many studies have reported mitochondrial dysfunction in animal and cell models of PD based on either mutant or over-expressed αSyn (Ryan et al. 2013; Smith et al. 2005). Most mitochondria-based assays rely on purifying these organelles but require a large number of cells as a starting material, something that is not easily achievable with iDAn cultures. Mitochondrial respiration can be determined using the Seahorse Analyzer that measures Oxygen Consumption Rate (OCR) and can be applied to cells cultured in a 96-well plate format. The injection of different compounds and the simultaneous measurement of OCR allows for the determination of informative parameters regarding mitochondrial function. Concurrently, it is possible to measure the Extracellular Acidification rate (ECAR), which is an indirect measure of glycolytic activity. A schematic of the assay and the parameters that can be derived from the OCR and ECAR readings is reported in Figure 5.8A. To date, only the study by Ryan and colleagues addressed mitochondrial dysfunction in A53T *SNCA* iDAn and reported decreased maximal respiration in one line compared to its isogenic control (Ryan et al. 2013). Taking advantage of the number of iPSC lines available to this study, all parameters relative to mitochondrial respiration were measured in Control and A53T *SNCA* iDAn. The low success in replating iDAn cultures at any point beyond 20DIV, due to the formation of clumps and an extensive neuronal network, was overcome by replating and differentiating the cells in the Seahorse 96-well microplate until 35DIV. To account for differences in the number of cells in each well across lines, raw values were normalised for total protein content in lysates from the same wells. A53T *SNCA* iDAn showed dysfunction in mitochondrial respiration, with a decrease in basal (38.9±7.8%) and maximal respiration (35.7±9.8%), ATP production (37.6±9.6%) and spare capacity (33.7±13.4%) compare to Control (Student *t*-test, $p<0.05$) (Figure 5.8B). No difference was

observed in glycolytic activity, despite a remarked reduction in glycolytic reserve (Student *t*-test, not significant) (Figure 5.8C). Western blot analysis of the mitochondrial marker TOM20 showed no difference in total mitochondrial mass between the two genotypes (one-way ANOVA, not significant) (Figure 5.8D), implying that the differences in OCR are not due to reduction in total mitochondrial content.

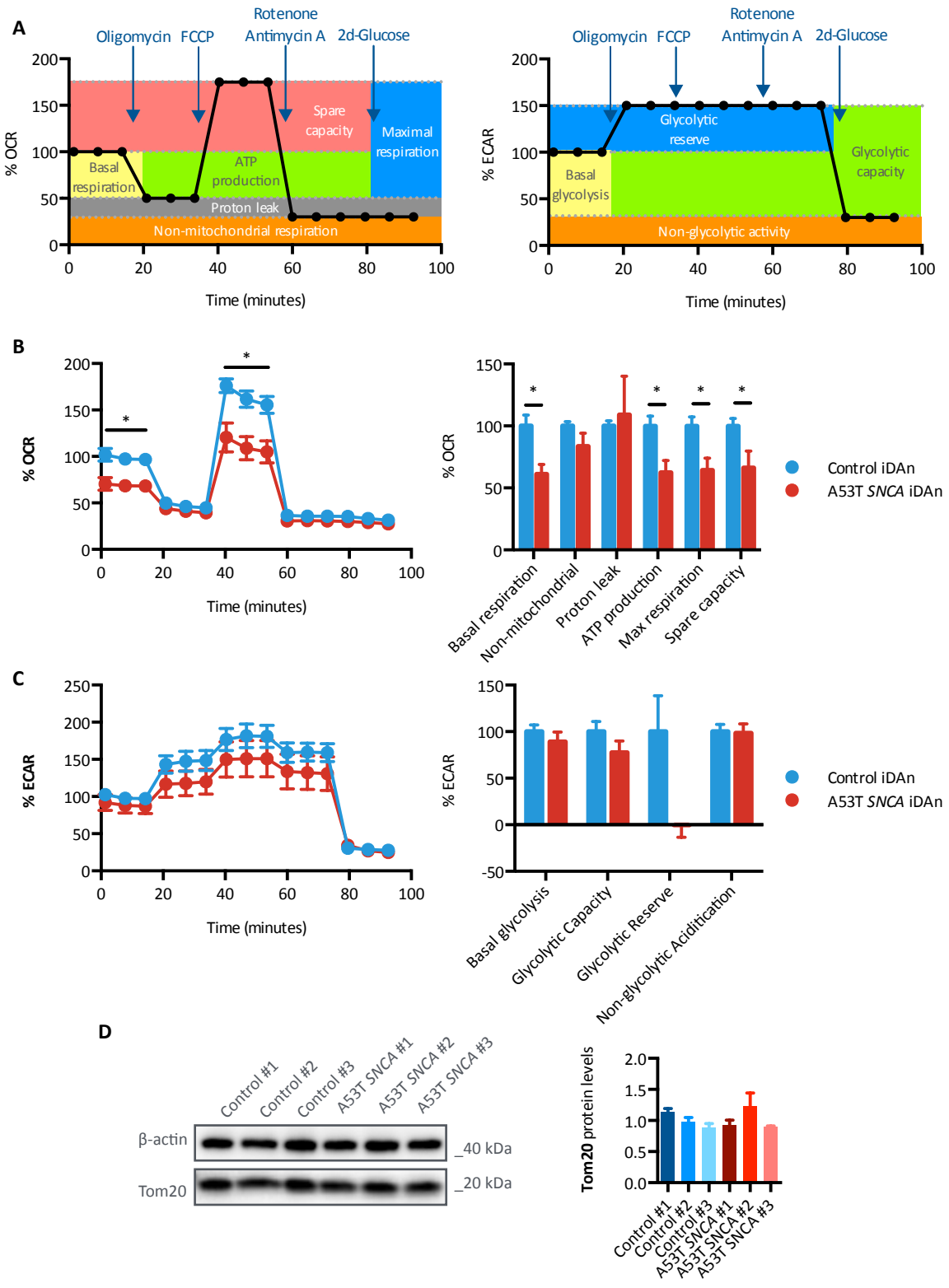

Figure 5.8|A53T *SNCA* iDAn have dysfunctional mitochondrial respiration

(A) Schematic of the Seahorse Analyser assay for mitochondrial respiration (OCR) and glycolytic activity (ECAR). **(B)** OCR traces and mitochondria respiration parameters of Control and A53T *SNCA* iDAn at 35DIV (N=3, n=3 iPSC lines per genotype, mean ± SEM, Student *t*-test, **p*<0.05) **(C)** ECAR traces and glycolysis parameters of Control and A53T *SNCA* iDAn at 35DIV (N=3, n=3 iPSC lines per genotype, mean ± SEM, Student *t*-test, **p*<0.05) **(D)** Analysis of Tom20 protein in Control and A53T SNCA iDAn at 35DIV (N=3, mean ± SEM, one-way ANOVA, not significant).

Since iPSC lines are derived from the reprogramming of a single fibroblast that could carry somatic abnormalities in mitochondrial function, undifferentiated iPSCs were analysed using the same method. In contrast to iDAn, A53T *SNCA* iPSCs did not differ in the mitochondrial respiration compared to Control (Figure 5.9A). This could be explained by the fact that only at the iDAn stage cells express considerable amounts αSyn compared to undifferentiated iPSCs (Figure 5.9C). The same cell lines were also differentiated to iMac (van Wilgenburg et al. 2013; Haenseler et al., submitted for review) by W. Haenseler (Dunn School of Pathology, University of Oxford) and were provided for the analysis of mitochondrial respiration. A53T *SNCA* iMac did not differ to Control for their OCR, further confirming that the respiration dysfunction is specific to iDAn. Lastly, preliminary data showed that *SNCA* Tripl iDAn have a similar respiration phenotype to A53T *SNCA* (Figure 5.9D).

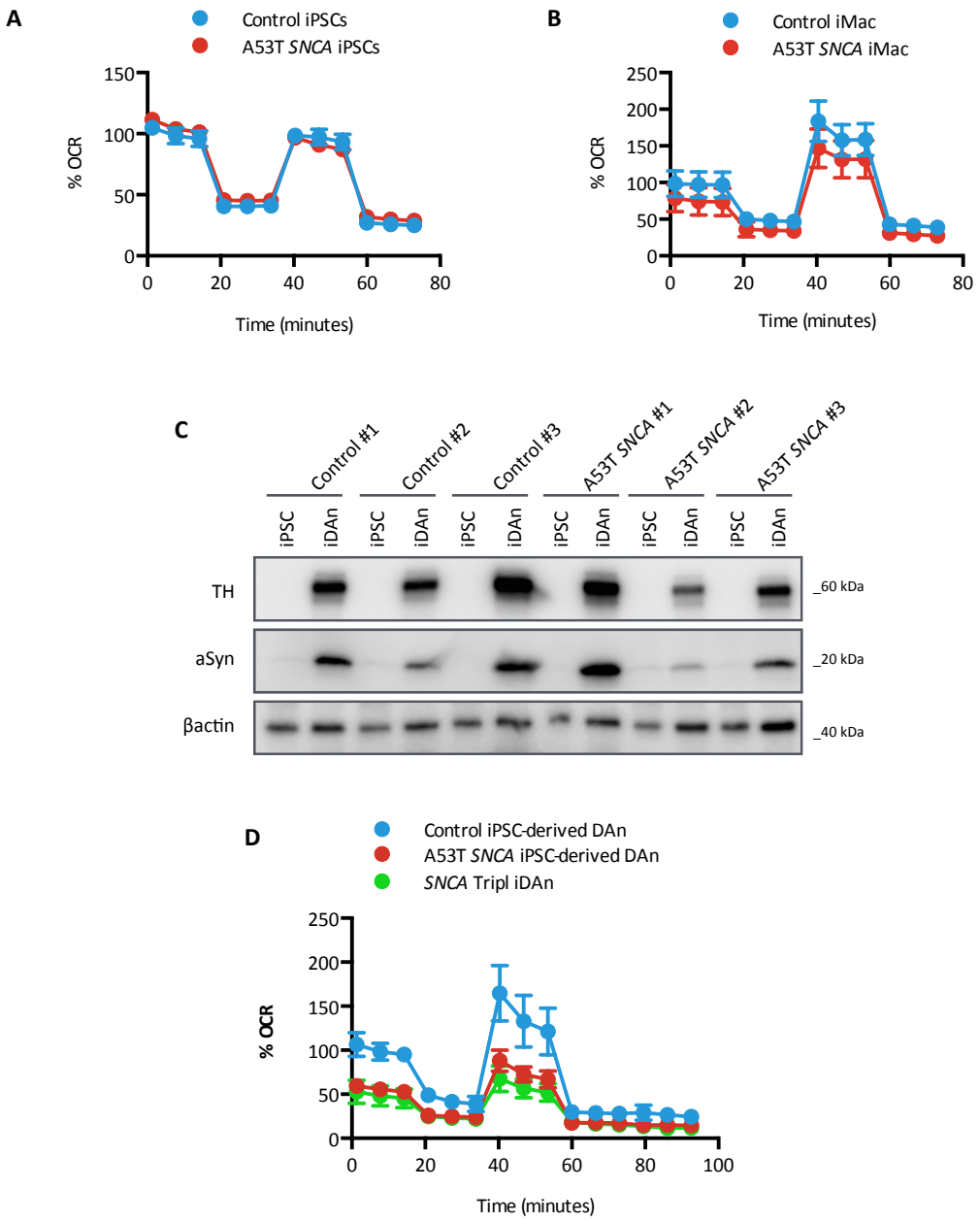

Figure 5.9|Mitochondrial respiration dysfunction is specific for iDAn
(A) OCR traces of Control and A53T *SNCA* undifferentiated iPSCs (N=3, n=3 iPSC lines per genotype, mean ± SEM, Student *t*-test, not significant). **(B)** OCR traces of Control and A53T *SNCA* iMac (N=3, n=3 iPSC lines per genotype, mean ± SEM, Student *t*-test, not significant). **(C)** TH and αSyn expression in undifferentiated iPSCs and iDAn at 35DIV. **(D)** OCR traces of Control, A53T *SNCA* and *SNCA* Tripl iDAn at 35DIV (N=1, n=3 iPSC lines for Control and A53T *SNCA*, three clones for *SNCA* Tripl, mean ± SD).

Because mitochondria function is tightly regulated by fission and fusion, proteins involved in these processes were analysed. Both the long and short isoform of the protein Dynamin-like 120 kDa protein (L-OPA1 and S-OPA1 respectively), known to regulate mitochondrial fusion (Song et al. 2007), were detected but neither was changed between genotypes (one-way ANOVA, not significant) (Figure 5.10A). Levels of Mitofusin 2 (MFN2), another protein involved in mitochondrial fusion (Westermann 2010), were also unchanged (one-way ANOVA, not significant) (Figure 5.10B). Levels of the mitochondrial fission Dynamin-1-like protein (DRP1) (Westermann 2010) were similar between genotypes; however, DRP1 phosphorylation of Ser616 was decreased in two of the A53T *SNCA* iDAn lines (one-way ANOVA, $p<0.05$) (Figure 5.10C), possibly indicating an inhibition of the fission process (Taguchi et al. 2007). Expression of Prohibitin (PHB), a mitochondrial protein in the inner membrane with multiple described roles in *cristae* morphology maintenance, functional integrity of mitochondria and control of ROS production by CoxI (Merkwirth and Langer 2009; Zhou et al. 2012), was increased in A53T *SNCA* iDAn (one-way ANOVA, $p<0.01$) (Figure 5.10D). Linked to ROS production, protein levels of catalase, a peroxisome enzyme involve in scavenging these harmful molecules (Schrader and Fahimi 2006), were up-regulated in A53T *SNCA* #2 and #3, but not #1, compared to Control (one-way ANOVA, $p<0.05$) (Figure 5.10E). Last, expression levels of the master regulation of mitochondrial biogenesis, peroxisome proliferator-activated receptor gamma coactivator 1-α (PGC-1α) (Liang and Ward 2006), were increased in A53T *SNCA* #2 and #3 iDAn compared to Control (one-way ANOVA, $p<0.001$) (Figure 5.10F), contrary to what was previously shown by Ryan and colleagues in A53T *SNCA* iDAn compared to an isogenic control (Ryan et al. 2013).

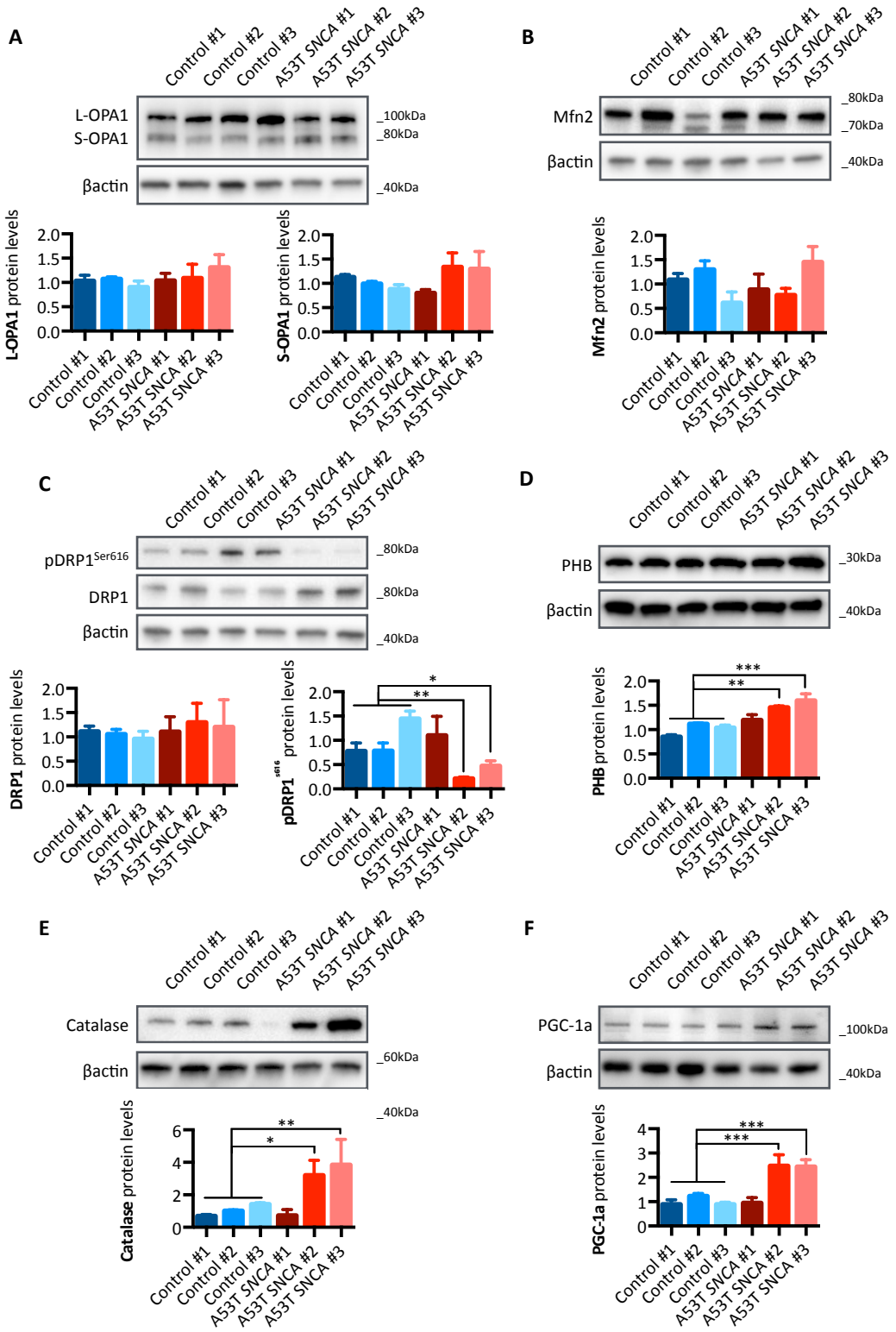

Figure 5.10|Analysis of markers involved in mitochondrial fission/fusion and function in iDAn
(A) L- and S-OPA1 protein levels in Control and A53T SNCA iDAn at 35DIV (N=3, mean±SEM, one-way ANOVA, not significant). **(B)** Mfn2 protein levels in Control and A53T SNCA iDAn at 35DIV (N=3, mean±SEM, one-way ANOVA, not significant).**(C)** DRP1 and phosphorylated DRP1^{Ser616} protein levels in Control and A53T SNCA iDAn at 35DIV (N=3, mean±SEM, one-way ANOVA, *p<0.05, **p<0.01). **(D)** PHB protein levels in Control and A53T SNCA iDAn at 35DIV (N=3, mean±SEM, one-way ANOVA, **p<0.01, ***p<0.001). **(E)** Catalase protein levels in Control and A53T SNCA iDAn at 35DIV (N=3, mean±SEM, one-way ANOVA, *p<0.05, **p<0.01). **(F)** PGC-1α protein levels in Control and A53T SNCA iDAn at 35DIV (N=3, mean±SEM, one-way ANOVA, ***p<0.001).

5.2.8|Inhibition of CoxI by MPP^+ affects basal but not maximal respiration in Control iDAn

MPP^+ is a mitochondrial toxin that acts via the reversible inhibition of Complex I (CoxI) (Richardson et al. 2005; Giordano et al. 2012) and is widely used to model PD (Ryan et al. 2013; Ryan et al. 2014; Cooper et al. 2012; Hartfield et al. 2014). Moreover, αSyn has been shown to impair CoxI function (Chinta et al. 2010; Devi et al. 2008). It is therefore interesting to investigate whether inhibition of CoxI via MPP^+ can recapitulate the A53T *SNCA* iDAn mitochondrial phenotype in Control cells. The concentration of the MPP^+ treatment was optimised based on published data using Control #1 iDAn treated for 24 hours before the assay (Cooper et al. 2012; Watmuff et al. 2015; Hartfield et al. 2014). All treatments were performed in NB medium since it has been proposed that GDNF, a component of the medium used for iDAn culture maintenance, could be protective towards MPP^+ toxicity (Peng et al. 2013). Control #1 iDAn cultured in either NB medium or NB medium supplemented with 10 μM MPP^+ did not show any difference in their basal respiration compared to cells cultured in final differentiation medium. Cells treated with increasing concentrations of MPP^+ showed a negatively correlated decrease in basal respiration to drug concentration (Figure 5.11A). Based on this data, iDAn were treated for 24 hours with 100 μM MPP^+ to achieve a considerable reduction in basal respiration. Cytotoxicity was monitored using ECAR measurements; in case of cytotoxicity, both OCR and ECAR would be expected to decrease. As a positive control for CoxI inhibition, cells were also treated with the irreversible inhibitor Rotenone (200 nM) (Ryan et al. 2013; Cooper et al. 2012). Compared to untreated samples, 100 μM MPP^+ treatment caused a reduction in basal respiration (61.7±14.5%) and ATP production (56.7±16.1%) due to CoxI inhibition (one-way ANOVA, $p<0.05$) (Figure 5.11C,D). Maximal respiration was unaffected, probably because of the reversibility of MPP^+, whereas the spare capacity was

increased due to the lower basal OCR. Overall, CoxI inhibition by MPP^+ in Control iDAn caused a similar phenotype to A53T *SNCA* iDAn but did not affect maximal respiration. This suggests that the deficit in OCR in A53T *SNCA* iDAn cannot be fully recapitulated by MPP^+ inhibition of CoxI but is probably the result of a more complex pathological mechanism affecting mitochondrial function.

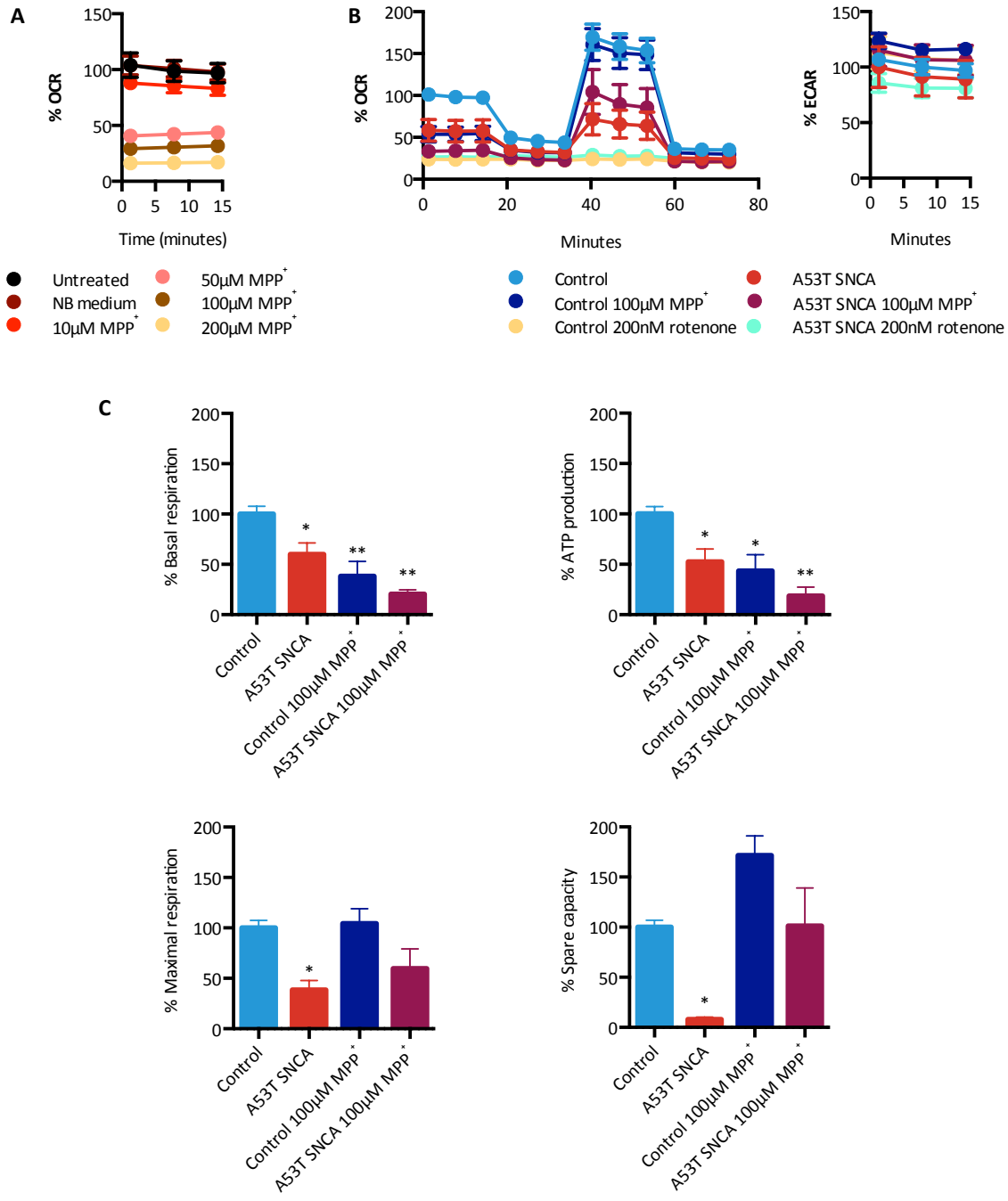

Figure 5.11|CoxI inhibition by MPP⁺ affects basal but not maximal respiration in iDAn
Analysis of mitochondria respiration using the Seahorse Analyzer. **(A)** OCR trace showing the effects of MPP⁺ treatment on basal respiration (N=1, mean ± SD) **(B)** OCR and ECAR traces of Control and A53T *SNCA* iDAn treated with MPP⁺ or Rotenone (N=3 for MPP⁺, N=1 for Rotenone, n=3 iPSC lines per genotype, mean ± SEM). **(C)** Mitochondrial respiration parameter of control and A53T *SNCA* iDAn treated with MPP⁺ (N=3, n=3 iPSC lines per genotype, mean ± SEM, one-way ANOVA, **p*<0.05, ***p*<0.01).

5.2.9|A53T *SNCA* iDAn show perturbations in lipid and energy metabolism

It has been proposed that dysregulation of lipid metabolism may contribute to pathology in neurodegenerative diseases, like PD. Schöndorf and colleagues reported that iDAn do recapitulate the type of lipids present in the human brain and that those carrying GBA mutations are characterised by abnormal lipid profiles, especially with accumulation of glucoceramide (Schöndorf et al. 2014). Similarly, work by H. Fernandes in the laboratory reported that, despite no difference in total glucoceramide levels, N370S GBA iDAn displayed differences in the distribution of glucoceramide species (Fernandes et al. 2016).

Following up on this and previous other reports regarding αSyn interaction with lipids, markers of lipid metabolism and homeostasis or regulators of cellular bioenergetics were analysed in iDAn at 35DIV. This work was prompted by H. Fernandes in the laboratory, who analysed publicly available transcriptomics datasets comparing results from A53T *SNCA* iDAn (Ryan et al. 2013), G2019S LRRK2 iDAn (Fernández-Santiago et al. 2015) and data generated in the Wade-Martins laboratory from αSyn over-expressing mice (Janezic et al. 2013); B. Ryan, personal communication) and G2019S LRRK2 iDAn (Sandor et al. 2017). Interestingly, mRNA expression data from the work of Ryan and colleagues (Gene Expression Omnibus database - GSE46798) showed changes in transcript levels for genes involved in FA metabolism. Strikingly, fatty acid binding proteins (FABPs) expression levels were increased upon gene correction of the A53T *SNCA* mutation (Ryan et al. 2013). Accordingly, both A53T *SNCA* and *SNCA* Tripl iDAn were found to have significantly reduced levels of FABP7 compared to Control (one-way ANOVA, $p<0.05$) (Figure 5.12A). Double immunocytochemistry for TH and FABP7 revealed that the protein is expressed in iDAn, revealing a punctate staining and a more diffuse halo, and the intensity of the immunocytochemistry followed the same trend as the expression levels reported via western blot (Figure 5.12B). Moreover, FABP7 protein levels increased, at least

in control iDAn, upon αSyn KD (see Section 6.2.12). The expression of FABP3, another isoform expressed in neurons, could not be detected at 35DIV in iDAn.

After this positive pilot data, the investigation was extended to other markers related to lipids and energy metabolism, specifically those expressed in the brain and relevant for αSyn and PD pathologies. Cholesterol 24-hydroxylase (CYP46A1) is an ER protein expressed in the brain, where it converts cholesterol to 24S-hydroxycholesterol, regulating the rate of cholesterol degradation in the neurons (Lund, Guileyardo, and Russell 1999). This enzyme was decreased in two A53T *SNCA* iDAn lines and in *SNCA* Tripl iDAn (one-way ANOVA, $p<0.05$) (Figure 5.12C), further indicating a dysregulation in lipid handling in these cells and suggesting a potential correlation with ER stress. Lastly, Sirtuin 1 (SIRT1) is considered the master regulator of metabolism and its activity is tightly regulated by NAD^+/NADH level (Haigis and Sinclair 2010); in turn, SIRT1 regulates the activation of transcription factors involved in cellular metabolism, including PGC-1α, and metabolic pathways like glucose and lipids metabolism (Li 2013). SIRT1 levels were found to be significantly increased in A53T *SNCA* #2, #3 and *SNCA* Tripl iDAn compared to Control (one-way ANOVA, $p<0.05$) (Figure 5.12D).

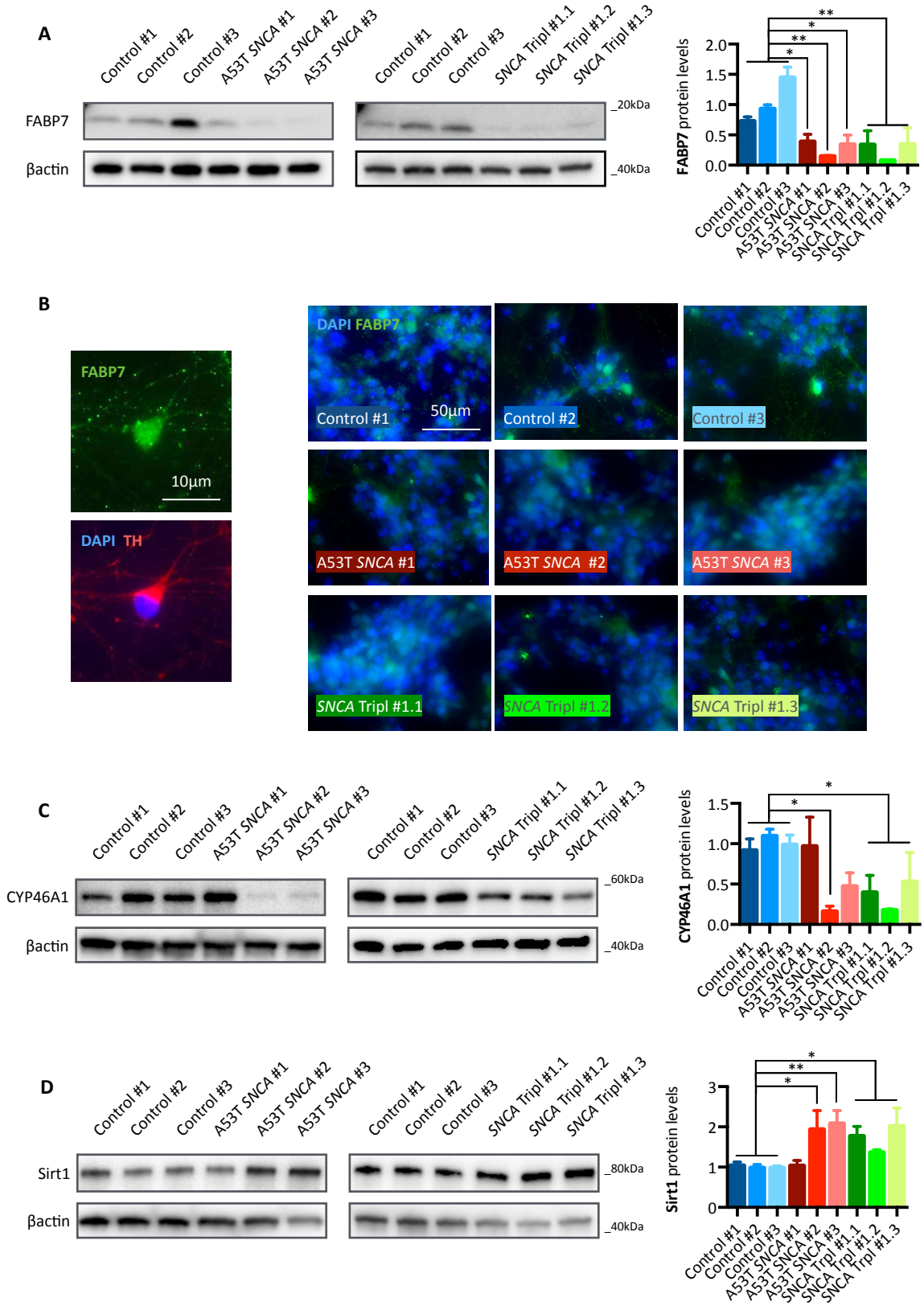

Figure 5.12|Dysregulation of lipids homeostasis in A53T *SNCA* and *SNCA* Tripl iDAn
(A) FABP7 protein levels in Control, A53T *SNCA* and *SNCA* Tripl iDAn at 35DIV (N=3, mean±SEM, one-way ANOVA, *p<0.05, **p<0.01). **(B)** iDAn immuno-stained for FABP7 and TH at 35DIV **(C)** CYP46A1 protein levels in Control, A53T *SNCA* and *SNCA* Tripl iDAn at 35DIV (N=3, mean±SEM, one-way ANOVA, *p<0.05). **(D)** Sirt1 protein levels in Control, A53T *SNCA* and *SNCA* Tripl iDAn at 35DIV (N=3, mean±SEM, one-way ANOVA, *p<0.05, **p<0.01).

5.3|Discussion

The results from the phenotypic analysis of A53T *SNCA* and *SNCA* Tripl iDAn were detailed in this chapter. The phenotypic analysis was carried out at 35DIV, that is two weeks of maturation after the replating of the cells, in line with many other studies in the field (Chung et al. 2016; Fernandes et al. 2016; Ryan et al. 2013; Sánchez-Danés, Richaud-Patin, et al. 2012; Devine et al. 2011). It would be certainly useful to interrogate the same phenotypes at later stages of the maturation, especially when the cells also become electrophysiologically active (>80DIV).

αSyn protein levels were found to be variable among lines and no difference was detected in PD iDAn compared to Control. Despite this, double immunocytochemistry for TH and αSyn revealed a significantly higher percentage of TH^+ cells with αSyn intracellular staining in both A53T *SNCA* and *SNCA* Trip iDAn compared to Control. This is in line with other reports in iDAn carrying PD-associated mutations and shows the same magnitude of fold-change of ~1.5-2 (Chung et al. 2016; Imaizumi et al. 2012; Mazzulli, Zunke, Tsunemi, et al. 2016; Sánchez-Danés, Richaud-Patin, et al. 2012; Shaltouki et al. 2015; Woodard et al. 2014). This phenotype could be explained either as a pathological mechanism of αSyn accumulation or its re-localisation from the pre-synaptic terminals, where it is normally present (Iwai et al. 1995), to the soma of TH^+ neurons. The discrepancy between the data from the western blot analysis and immunocytochemistry could arise because the latter is specific for TH^+ cells. Likewise, western blot quantification only accounts for the whole cell population and is biased by the absolute expression levels among cells. Moreover, the contribution of $TH^+/αSyn^+$ cells to the percentage of total $αSyn^+$ cells or expression levels in the PD lines might not be detectable or be lost within the variability of the data, since it only accounts for an overall 5-10% increase compared to Control lines.

αSyn oligomerization was investigated using PLA. The increase in the average number of PLA *puntca* in TH^+ cells in two A53T *SNCA* and all *SNCA* Trip lines suggests that not only αSyn is localising in the soma of TH^+ cell but it is also forming more oligomers. However, it was not possible to directly correlate the increase in intracellular αSyn staining with the increase in PLA signal in TH^+ cell because some cells displayed PLA signal despite not being immuno-reactive for αSyn using the same antibody employed for immunocytochemistry. There is clearly a difference in the staining pattern between the antibodies against αSyn used for PLA and immunocytochemistry: Syn211 (αSyn PLA), gives a punctate staining mostly localised in neuronal processes compared to BD 42/αSyn (immunocytochemistry), which instead gives a cytoplasmic and to a lesser extent neuronal processes staining. Yet, the epitopes recognised by these two antibodies map at the opposite extremities of the αSyn molecule, with the BD 42/αSyn the N-terminus and the Syn211 at the C-terminus, and can therefore label different pools of αSyn. Eventually, PLA is also much more sensitive than immunocytochemistry, being able to detect as little as a αSyn dimer. Altogether, the PLA preliminary results suggest that more optimisation is needed, especially to understand the significance of the abundant PLA signal even in control iDAn, before investigating the relevance of the increased PLA signal in PD iDAn. Lastly, αSyn secretion in the culture medium during the later stages of neuronal maturation was found to be a feature of iDAn cultures, according to previous work in the laboratory (Fernandes et al. 2016). However, no difference was detected between Control and A53T *SNCA* iDAn. Native western blot analysis of the supernatant suggested that αSyn secreted from iDAn is characterised by a high molecular weight, suggesting that further investigation is needed to characterise the αSyn species secreted in the medium by iDAn.

In future, it would be interesting to assess αSyn aggregation by either Thioflavin S staining (Lázaro et al. 2014; Ryan et al. 2013) or analysis of the Triton-insoluble fraction of lysates

from iDAn cultures (Mazzulli, Zunke, Isacson, et al. 2016), and investigate the phosphorylation status of αSyn^{Ser129} (Ryan et al. 2013; Fujiwara et al. 2002).

Analysis of autophagy function and machinery revealed variable results. The increase in p62 levels in A53T *SNCA* iDAn could indicate an incremented demand for cargo to be selectively degraded via the lysosomes, which is comparable with other reports describing the effects of αSyn aggregation on macroautophagy (Watanabe et al. 2012); the PLA data indeed correlates with the up-regulation of p62 in the A53T *SNCA* iDAn lines. Furthermore, the decrease in LC3-II levels is in line with both a cellular and animal models of αSyn over-expression (Winslow et al. 2010). Conversely, lysosomal and CMA markers were unchanged in PD iDAn samples, despite A53T αSyn being previously shown to affect the CMA markers LAMP2A and HSC70 (Cuervo et al. 2004). Overall, this may indicate that autophagic dysfunction is not a prominent phenotype of A53T *SNCA* and *SNCA* Trip iDAn, at least at this stage of the neuronal maturation (35DIV). A recent study demonstrated that, upon maturation for more than 300DIV, αSyn accumulation causes a reduction in the lysosomal degradation capacity (Mazzulli, Zunke, Isacson, et al. 2016), possibly implicating that autophagy failure is downstream of PD pathology, at least in iDAn carrying a *SNCA* triplication.

GBA activity was increased in iDAn but the variability in GBA and LAMP1 protein levels were not be informative towards understanding whether the increase in GBA activity is the result of changes in lysosomal homeostasis. This increase in GBA activity could be a consequence of αSyn accumulation, possibly in the form of oligomers, that requires an increase in cellular degradative capacity. In accordance to this, A53T *SNCA* iPSC-derived cortical neurons display accumulation of GBA (Chung et al. 2013), whereas pharmacological activation or over-expression of GBA were beneficial towards lowering αSyn levels in iDAn (Woodard et al. 2014; Mazzulli, Zunke, Tsunemi, et al. 2016).

The increased expression of the ER chaperone BiP in two A53T *SNCA* suggests that the UPR has been triggered, whereas the increase in IRE1α in A53T *SNCA* #2 and #3 and all *SNCA* Tripl iDAn indicates that downstream events linked to ER stress have been switched on. Lastly, levels of C/EBPβ were increased in the same lines. This transcription factor has been linked to ER stress-induced apoptosis (Meir et al. 2010) and contains a responsive element that binds XBP-1, of which transcription and processing are controlled by IRE1α (Chen et al. 2004). Overall, these findings are in line with a previous report in A53T *SNCA* iPSC-derived cortical neurons showing accumulation of ER stress markers (Chung et al. 2013). In general terms, accumulation of BiP in αSyn over-expressing and toxin-based PD models, iDAn and PD brains seems to be a possible pathological mechanism, likely due to αSyn misfolding in the form of oligomers and their interaction with the ER (Colla et al. 2012; Credle et al. 2015; Egawa et al. 2011; Fernandes et al. 2016). Further characterisation of XBP1 splicing, expression or phosphorylation levels of other UPR enzymes and analysis of late makers associated with ER stress-induced apoptosis, namely C/EBP homologous protein (CHOP) (Oyadomari and Mori 2004) and activated Caspase 12 (Nakagawa et al. 2000), will better inform on the pathological mechanism associated with αSyn and the ER stress.

As expected from the previous literature (Ryan et al. 2013), A53T *SNCA* iDAn had deficits in mitochondrial respiration. However, this phenotype could not be fully recapitulated in Control iDAn by MPP^+-mediated inhibition of CoxI. Preliminary results showed that *SNCA* Tripl iDAn followed the same trend but this requires further investigation. Undifferentiated iPSCs and iMac from the same iPSC lines did not show any difference in these parameters, indicating that the phenotype is not an intrinsic property of these cells and is specific for iDAn. This was also corroborated by the fact that substantial expression of αSyn was only present in the differentiated neurons compared to iPSCs,

indicating that it might be essential for the onset of the phenotype. The decrease in phosphorylation of Drp1^{S616} would suggest an inhibition of mitochondrial fission (Taguchi et al. 2007). However, cyclin-dependent kinase 5 (CDK5) was discovered to phosphorylate Drp1^{S616} and consequently cause a counterintuitive increase in Drp1-dependent mitochondrial fission in post-mitotic neurons (Cho et al. 2014). By the same logic, a decrease in phosphorylation of Drp1^{S616} in iDAn may underlie mitochondrial fragmentation that could in turn explain the respiration deficit seen in A53T *SNCA* iDAn. Levels of Prohibitin were also increased, potentially linking mitochondria dysfunction with ROS production (Zhou et al. 2012). Concurrently, levels of catalase were markedly increased in two A53T *SNCA* lines as well. Lastly, PGC-1α protein levels, the master regulator of mitochondrial biogenesis, were increased in two A53T *SNCA* lines, contrary to what was previously shown in iDAn carrying the same mutation (Ryan et al. 2013) but in line with data from mutant Pink1 iDAn (Seibler et al. 2011). Overall, because PGC-1α is involved in many other bioenergetics processes (Liang and Ward 2006), it cannot be excluded that its up-regulation arises as part of a wider bioenergetics stress.

Future directions may include the analysis of the possible causes of mitochondria dysfunction. ROS production by mitochondria can be detected using selective probes like MitoSOX®. Loss of mitochondrial membrane potential (MMP) is generally measured by either fluorescence intensity of tetramethylrhodamine methyl ester (TMRM) or a ratiometric measure of the JC-10 dye; both molecules change their emission properties depending on the MMP. Mitochondrial morphology and size using electron microscopy (Chung et al. 2016) or confocal microscopy can be employed to describe the mitochondrial network. Lastly, whether mitochondria dysfunction ultimately causes apoptosis can be investigated by analysing the activation of Caspase-3 and -9, the two downstream effectors in the mitochondrial pathway of apoptosis (Kroemer and Reed 2000).

Preliminary analysis of markers associated with lipids homeostasis and energy metabolism provided novel insights on PD cellular pathology. A marked decrease in FABP7 expression in A53T *SNCA* and *SNCA* Tripl iDAn was described. However, little is known about the functional interaction between αSyn and FABPs (Sharon et al. 2001; Shioda et al. 2014). Interestingly, knockdown of αSyn iDAn increased FABP7 expression, at least in Control iDAn (see section 6.2.12). Similarly, cholesterol 24-hydroxylase (CYP46A1) was found to be significantly down-regulated in PD iDAn. Both proteins also offer a link between ER stress and FA homeostasis with CYP46A1 being an ER enzyme and FABP7 having a C/EBPβ-binding motif in its promoter (Takaoka et al. 2011). The FABP7 phenotype in PD iDAn also recapitulates changes associated with ageing and neurodegeneration, since this protein was found to be decreased in brains of aged mice (Pu et al. 1999). Moreover, FABP7 levels were also decreased in serum of patients affected by neurodegenerative disease, including PD (Teunissen et al. 2011). In the context of αSyn oligomerization and interaction with lipids, this phenotype is consistent with previous studies describing αSyn oligomerization and interaction with intracellular lipids droplets (Cole et al. 2002), presence of lipids within αSyn aggregates (Hellstrand et al. 2013) and that the physiological interaction between αSyn and lipids at the membrane might underlie its aggregation (Galvagnion et al. 2015). Lastly, up-regulation of SIRT1, a deacetylase involved in controlling energy metabolism, further supports the data and points towards a wider bioenergetics imbalance in PD iDAn. It is also possible to draw a link between PGC-1α and SIRT1 and mitochondria dysfunction since both proteins are involved in governing intracellular energy production and metabolism (Cantó and Auwerx 2009).

Overall, further characterisation of FA metabolism in iDAn will provide useful insights on PD pathology. Omics approaches, metabolomics and lipidomics, may reveal dysregulation in pathways that might not be detectable by the analysis of the individual enzymes.

Physical interaction between αSyn and FABP7 can be analysed using immuno-precipitation, whereas functional synergy can be examined by analysing the effects of FABP7 knockdown on αSyn levels, and potentially oligomerization (αSyn PLA), in iDAn. PLA could also be used to detect the direct interaction between FABP7 and αSyn, as previously described for TOM20 (Di Maio et al. 2016).

From the results detailed in this chapter, a model describing the pathological mechanisms associated with αSyn and PD in iDAn is proposed (Figure 5.13). The increase in cytoplasmic αSyn staining in TH^+ cells (5.2.1) could underlie its oligomerization (5.2.3) and eventually aggregation. Because αSyn precise cellular function in poorly understood, it can only be speculated that the phenotypes here described are part of pathological gain-of-function mechanisms triggered by an increased burden in either monomeric or oligomeric αSyn. Up-regulation of p62, decreased levels of LC3-II (5.2.4) and increased GBA activity (5.2.6) may hint at a process by which αSyn accumulation causes autophagic failure that is a typical feature of PD. Should this happen, it could as well impact on the cellular degradative capacity of dysfunctional mitochondria via mitophagy or intracellular αSyn aggregates. On the other hand, mitochondrial dysfunction (5.2.7) can result in bioenergetics deficit, perturbation of fission/fusion processes and loss of membrane potential. The decrease in phosphorylation of $Drp1^{Ser616}$ (5.2.7) proposes a pathological mechanism involving altered mitochondrial fission. Consequently, mitochondrial dysfunction and oxidative stress can trigger mitochondria-dependent apoptosis (Winklhofer and Haass 2010; Perier et al. 2005). Similarly, ER stress (5.2.5) could be caused by αSyn misfolding and oligomerization that eventually causes ER stress-induced apoptosis via a pathway involving mitochondria (Szegezdi et al. 2006). The concomitance of ER stress and mitochondria dysfunction is also in line with previous findings in a A53T αSyn cell model (Smith et al. 2005). Due to αSyn localisation at the mitochondria-associated membranes

(MAM), it can be speculated that its pathological mechanism may happen at these intracellular micro domains (Guardia-Laguarta et al. 2015). Lipid metabolism and homeostasis dysfunction (5.2.9) could be either a direct effect of αSyn on FABP7 and other enzymes or again linked to its localisation to MAM and ER, which are the main sites of lipid synthesis (Colgan, Hashimi, and Austin 2011; Vance 2014).

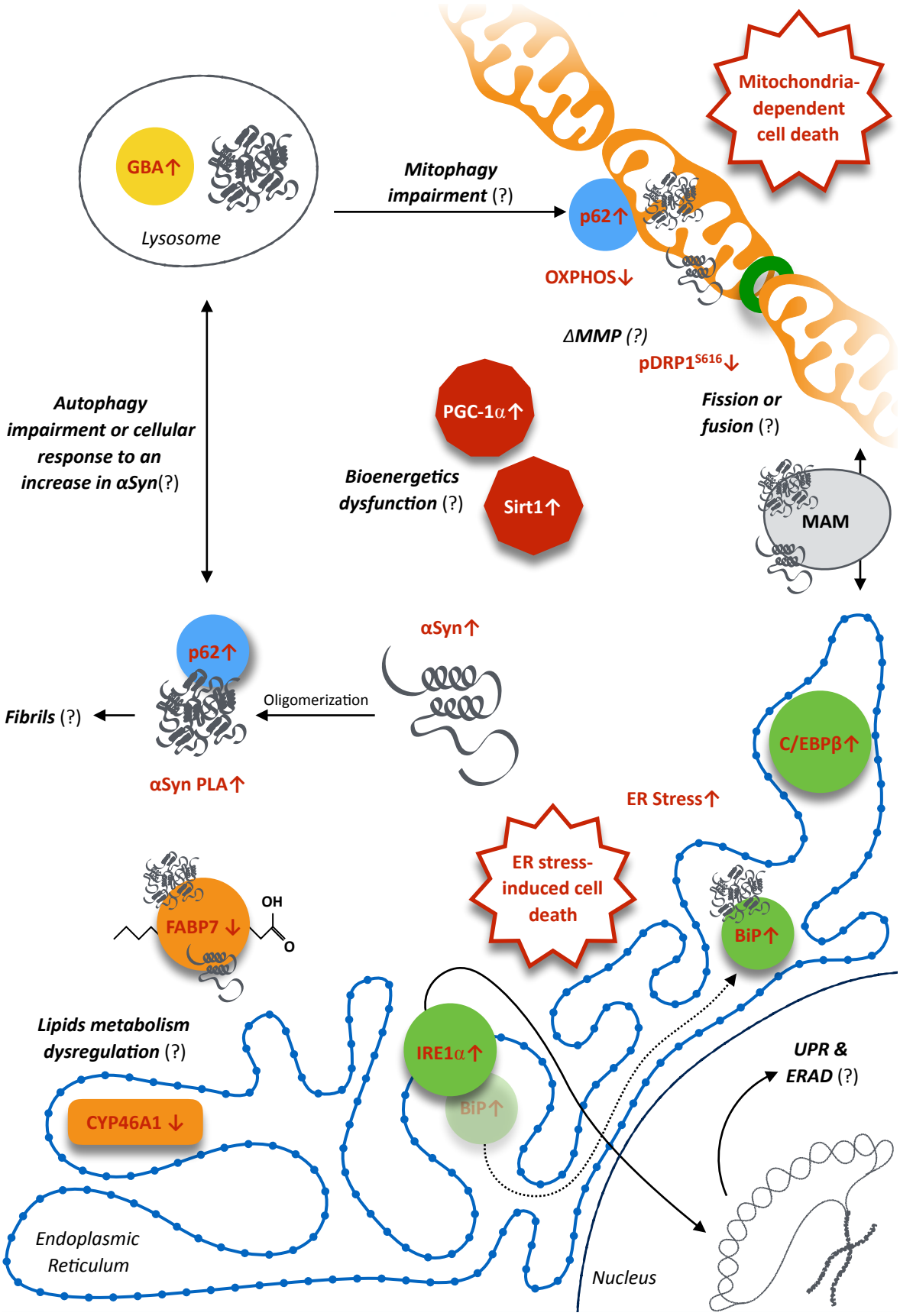

Figure 5.13|Summary of phenotypic analysis of A53T *SNCA* and *SNCA* Tripl iDAn

URP: Unfolded Protein Response; OXPHOS: OXidative PHOSphorylation; ERAD: ER Associated Degradation: ER: Endoplasmic Reticulum; MAM: Mitochondria Associated Membrane; MMP: Mitochondrial Membrane Potential; PLA: Proximity Ligation Assay; αSyn: α-Synuclein;

To conclude, this chapter points towards a plethora of phenotypes in A53T *SNCA* iDAn that can be further investigated. To a lesser extent, similar perturbations were found in *SNCA* Tripl iDAn as well, but these were not analysed as thoroughly. Because all iPSC lines where characterised for their similar differentiation efficiency, it is likely that these phenotypes are a consequence of pathological mechanisms rather than, for example, a different nature or maturation stage of the TH^+ cells among lines or genotypes. Using iDAn lines from three patients carrying the A53T *SNCA* mutation was also pivotal to unveil pathological phenotypes. Had the analysis be restricted for example only to A53T *SNCA* #1, few of the phenotypes could have been detected. The effort of using a 9 iPSC lines revealed the profound variability of iPSCs, especially upon differentiation.

Interestingly, A53T *SNCA* #1 displayed only a few phenotypes compared to the other A53T *SNCA* iPSC lines, including increased cytoplasmic αSyn staining and mitochondrial dysfunction. It can be speculated that the lack of αSyn oligomerization (αSyn PLA) might underlie the phenotypic differences between this line and the other PD lines. Since A53T *SNCA* #1 differentiated with the same efficiency as the other iPSC lines, it can be excluded that the lack of phenotypes is not due to variability in the differentiation efficiency or neuronal maturation. Unfortunately, no clinical data is available for any of the PD iPSC lines, which could have been useful to explain the differences observed for A53T *SNCA* #1.

iDAn proved to be a highly relevant cell model for PD research because they provided a unique link to the pathology *in vivo*: they carry the genetic background that underlined the onset the disease in the patient and provide the possibility of interrogating the exact cell type that is affected by the pathology in the brain.

Knockdown of α-Synuclein in iPSC-derived DAn

6.1|Introduction and aims

The down-regulation of the expression of a protein of interest can be achieved *in vitro* by different means, including halting of gene transcription, disruption of mRNA translation or targeting the protein for degradation. RNAi is a process by which the expression of non-coding RNAs results in the silencing of the expression of a target gene. Two methods are generally used to down-regulate the expression of a protein of interest and they rely on the ability to deliver genetic material to the cell and target the mRNA of the protein of interest. The small interfering RNA (siRNA) approach relies on transfection of 20 bp antisense oligonucleotides, whereas short hairpin RNAs (shRNAs) are transfected as DNA plasmids or transduced with viral particles and transcribe an RNA that will be then processed into an antisense oligonucleotide by the cellular machinery.

Given the relative poor efficiency in gene editing to date, the lack of a αSyn knockout or isogenic control A53T *SNCA* and *SNCA* triplication iPSC lines, αSyn knockdown is the method of choice to study the causative role of this protein. Knockdown in control lines aims to study the physiological role of αSyn, whereas down-regulation of the protein in PD lines will allow the investigation of αSyn involvement or contribution to the phenotypes that were described in chapter 5.

This chapter discusses the results regarding the knockdown αSyn in iDAn and the study of its effects on the phenotypes described in A53T *SNCA* iDAn, including:

- Transfection of siRNA targeting αSyn
- Generation of shRNA targeting αSyn and their delivery to iDAn via lentiviral infection
- Analysis of the effect of αSyn knockdown on mitochondrial function and FABP7 expression in Control and A53T *SNCA* iDAn

6.2|Results

6.2.1|Delivery of fluorescently labelled siRNA to iDAn by lipofection

Because post-mitotic cells, like neurons, are notoriously difficult to transfect (Karra and Dahm 2010), testing and optimisation of siRNAs transfection in iDAn was required. Control NHDF-1 iDAn differentiated using the EB-protocol were used for most for the screening and testing process, since this iPSC lines was the most used and characterised control iPSC line at the time these experiments were carried out. Detection of siRNA transfection *in vitro* was achieved using a fluorescently labelled non-targeting siRNA (BLOCK-iT™ Alexa Fluor® Red Fluorescent Control). In BE(2)M17 cells, transfection of BLOCK-iT with Lipofectamine 2000 following manufacturer guidelines resulted in both punctate and diffuse red fluorescence as previously reported in the literature (Figure 6.1A) (Tönges et al. 2006; Ostlund et al. 2009), indicating that this probe could be used as a read out of transfection efficiency. To test whether iDAn could be effectively transfected with siRNAs via lipofection, five reagents were selected: Lipofectamine 2000 (Dalby et al. 2004), Lipofectamine RNAiMAX (Zhao et al. 2008), HiPerFect (Landry et al. 2012), X-tremeGENE and Lullaby (Ruepp et al. 2010). iDAn were transfected with 50 μM Block-iT using these reagents and imaged 48 hours post-transfection. Live-cell imaging showed that only Lipofectamine 2000 could efficiently transfect iDAn (Figure 6.1B). Moreover, serial dilutions of Block-iT showed a positive correlation with the percentage of transfected cells (Figure 6.1C).

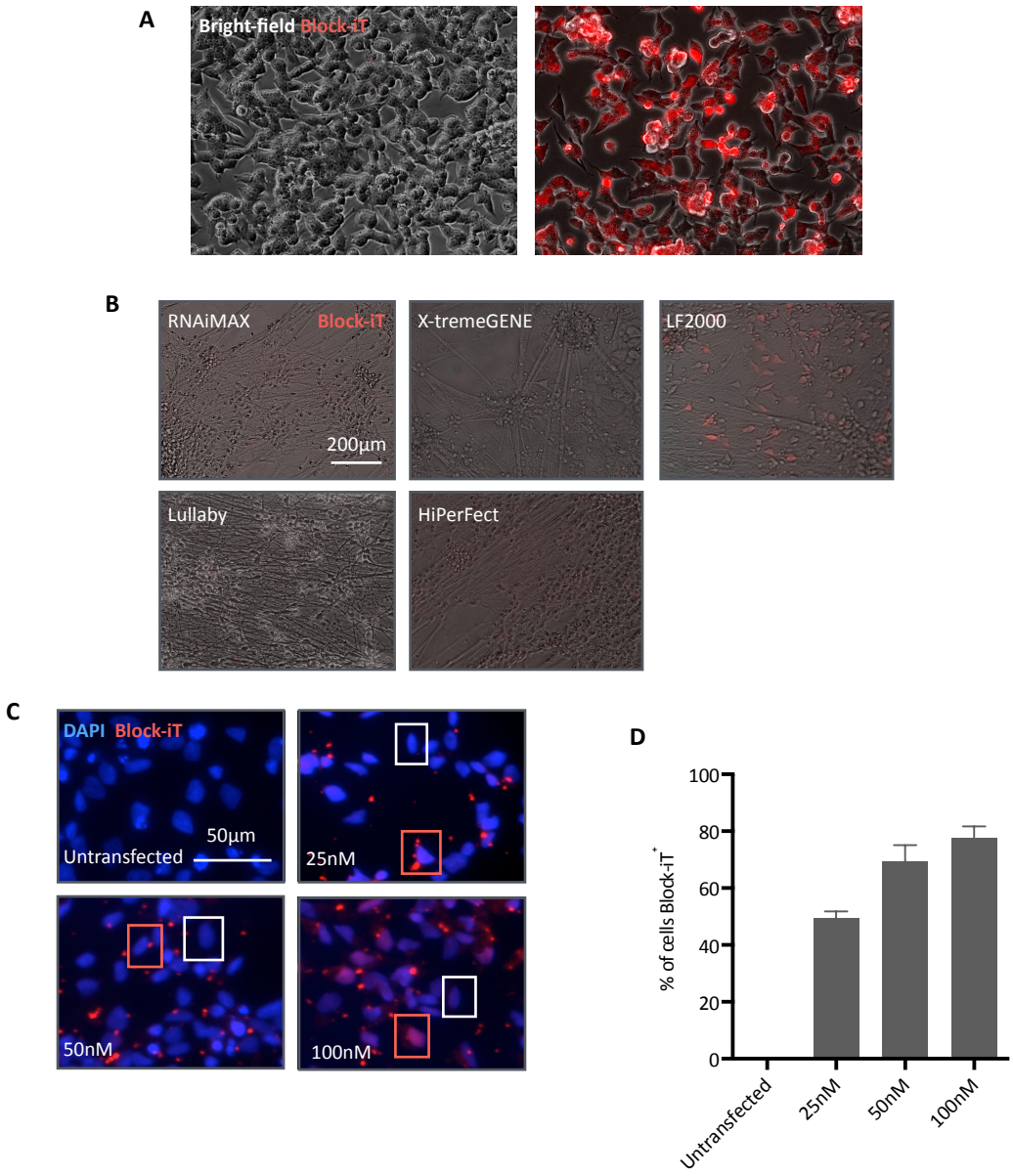

Figure 6.1|Lipofection of a fluorescent siRNA in iDAn

(A) BE(2)M17 cells transfected with Lipofectamine 2000 and Block-iT**(B)** Five different lipofection reagents were tested in NHDF-1 iDAn. **(C)** Transfection of Block-iT into iDAn using Lipofectamine 2000. White box indicates untransfected cells. Red boxes indicated transfected cells. **(D)** Quantification of Block-iT transfection efficiency with Lipofectamine 2000 in iDAn (N=3, mean ± SEM).

6.2.2|Lipofection of siSNCA1 is not a reliable method for knocking down αSyn in iDAn

The initial RNAi experiments carried out using the siRNA approach took advantage of the work previously done in the laboratory in immortalised cell lines with SNCA1, a specific siRNA against αSyn (hereafter referred as siSNCA1) and its mutated and ineffective version mut12 (Fountaine and Wade-Martins 2007). In BE(2)M17 cells, siSNCA1 significantly knocked down αSyn compared to mut12 (one-way ANOVA, $p<0.05$) (Figure 6.2A). iDAn were then transfected with Lipofectamine 2000 and siSNCA1 or mut12 and αSyn protein levels were analysed 48 hours later; Silencer® Negative Control No. 1 siRNA was also used as negative controls. Serial dilution of siSNCA1 (100, 50 and 25nM) could decrease αSyn protein levels in NHDF-1 iDAn compared to the untransfected sample. However, negative control samples showed a reduction in αSyn as well (one-way ANOVA, $p<0.01$) (Figure 6.2B). It was not possible to replicate the initial promising results with siSNCA1 in the following experiments or in other iPSC lines (Figure 6.2B). siSNCA1 failed to knockdown αSyn protein levels whereas the negative controls gave variable results, ranging from increased to decreased protein levels (Figure 6.2C). Interestingly, the analysis of 6 replicates of untransfected cells or cells transfected with 25 nM siSNCA1, resulted in a significant reduction of αSyn protein levels (Student t-test-way, $p<0.05$) (Figure 6.2D), indicating that a higher number of technical replicates might counterbalance the variability of the knockdown effect or αSyn expression levels.

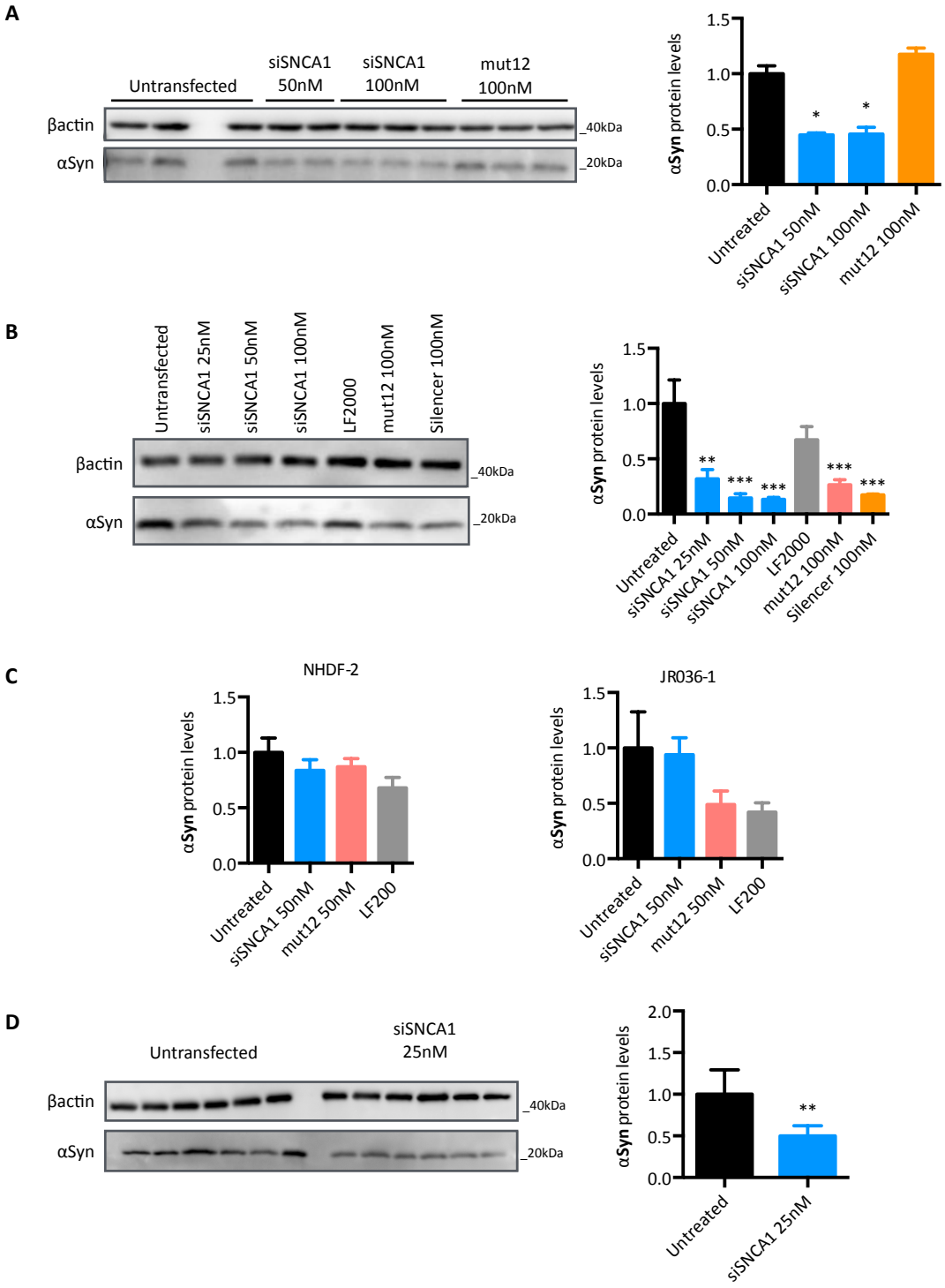

Figure 6.2|Knockdown of αSyn by siSNCA1 is not reproducible in iDAn

The delivery of siRNAs to iDAn was achieved via lipofection. **(A)** siSNCA1 was validated in BE(2)M17 cells (N=3, mean ± SEM, one-way ANOVA, *p<0.05) **(B)** NHDF-1 iDAn were transfected with Lipofectamine and either siSNCA1 or scambled controls at different concentrations (N=2, mean ± SEM, one-way ANOVA, **p<0.01, **p<0.001) **(C)** In order to exclude an iPSC line or clone specify effect, NHDF-2 and JR036-1 iDAn were lipofected with siSNCA1 (N=1, n=3 replicates, mean ± SD) **(D)** The efficacy of siSNCA1 is confirmed analysis six replicates (N=1, n=6 replicates, mean ± SD, Student t-test, *p<0.05).

6.2.3|Generation of a plasmid-based RNAi (shRNA) for the suppression of αSyn expression

The inconclusive results obtained with siRNAs led to approach an alternative method to knockdown αSyn in iDAn that would benefit from higher efficiency. Lentiviruses were chosen for their ability to transduce post-mitotic neurons and deliver genetic material, in this case shRNAs, to knockdown proteins of interest (see section 1.4.4). The lentiviral backbone used for this work is based on the third-generation lentivirus vector with conditional packaging system developed in the Trono laboratory (Dull et al. 1998). A modified version containing all the required lentiviral elements and expressing a shRNA under the control of the mouse U6 promoter and the enhanced green fluorescent protein (eGFP) under the control of the CMV promoter was kindly provided by O. Cordero Llana (map in Table 2.8A) (Hartfield et al. 2011).

First of all, the design of the new construct involved swapping the shRNA sequence for the one targeting αSyn. Secondly, the substitution the Cytomegalovirus (CMV) promoter for the human elongation factor 1-α (eF1α) promoter was introduced to have a constitutive expression without viral elements that could be silenced in iPSC-derived cells (Norrman et al. 2010). Because the cloning involved the ligation of three fragments and the backbone together, the Gibson Assembly method seemed to better fit the purpose than normal cloning techniques (Gibson et al. 2009). A schematic of the cloning design is reported in Figure 6.3A. The three fragments were inserted between the SpeI site upstream of the U6 promoter and the AgeI upstream of eGFP. The new shRNA cassette was cloned following the PCR method (Harper and Davidson 2005) using the pSilencer plasmid (kindly provided by O. Cordero Llana, University of Oxford) containing the entire U6 sequence as a template (map in Table 2.8B) and accounting for the homology arms required for the Gibson Assembly. Briefly, two primers were used: a forward primer

containing 20 bp of homology arms upstream the SpeI site in the lentiviral backbone and binding to the 5'-end of U6 in the pSilencer; a reverse primer binding to the 3'-end of the U6 promoter in the pSilencer with a long non-binding tail containing the shRNA sequence, a string of four thymidines and the 20bp homology arm downstream the XhoI site in the lentiviral backbone. Because αSyn mRNA can be targeted by the SNCA1 sequence, at least as an siRNA, the shRNA was designed based on siSNCA1. For the loop in the shRNA hairpin, two sequences were chosen: the loop from the original plasmid (5'-CTTCCTGTCA-3') and a so-described "universal" sequence (5'-TGTGCTT-3') (Jensen et al. 2012). All primer pairs were tested for the optimal annealing temperature and the correct bands were extracted from the agarose gel. The shRNA cassette always resulted in the presence of two bands, the correct 412bp fragment and a lower one probably corresponding to DNA with a different secondary structure due to the presence of the complementary sequence in the shRNA hairpin; both bands were extracted together before the cloning (Figure 6.3B). The genetic material encoding for the RRE and cPPT elements between the shRNA cassette and the CMV:eGFP sequence was amplified via PCR with primers with homology arms at their 5'-end to the two flanking fragments. Last, the human eF1α promoter was amplified from the CSii-EF-MCS plasmid (map in Table 2.8C) (kindly provided by M. Lufino, University of Oxford), with a forward primer containing a homology arm at the 5'-end to the RRE/cPPT fragment and a reverse primer with a 20 bp homology arm downstream the AgeI site in the lentiviral backbone upstream of eGFP (Figure 6.3B). The lentiviral backbone was linearised using SpeI and AgeI and the corresponding band (5879 bp) extracted from the agarose gel.

The three fragments and the linearised lentiviral backbone were ligated together using the Gibson Assembly method and transformed into Top10 *E.coli*. Colonies were screened for the presence of two additional bands of 1438 and 1085 bp after enzymatic

digestion with SpeI and AgeI (Figure 6.3C). The DNA from positive colonies was sequenced using primers on both strands spanning the entire sequence from upstream of the U6 promoter to downstream of eGFP (Figure 6.3D). The correct plasmid was finally transformed into Stbl3 *E.coli* before screening the colonies for the presence of the right insert between the SpeI and AgeI restriction sites. Hereafter, these plasmids will be referred to as shSNCA1 (containing the original loop) and shSNCA1-uLoop (containing the universal loop sequence). All primers are reported in Table 2.7.

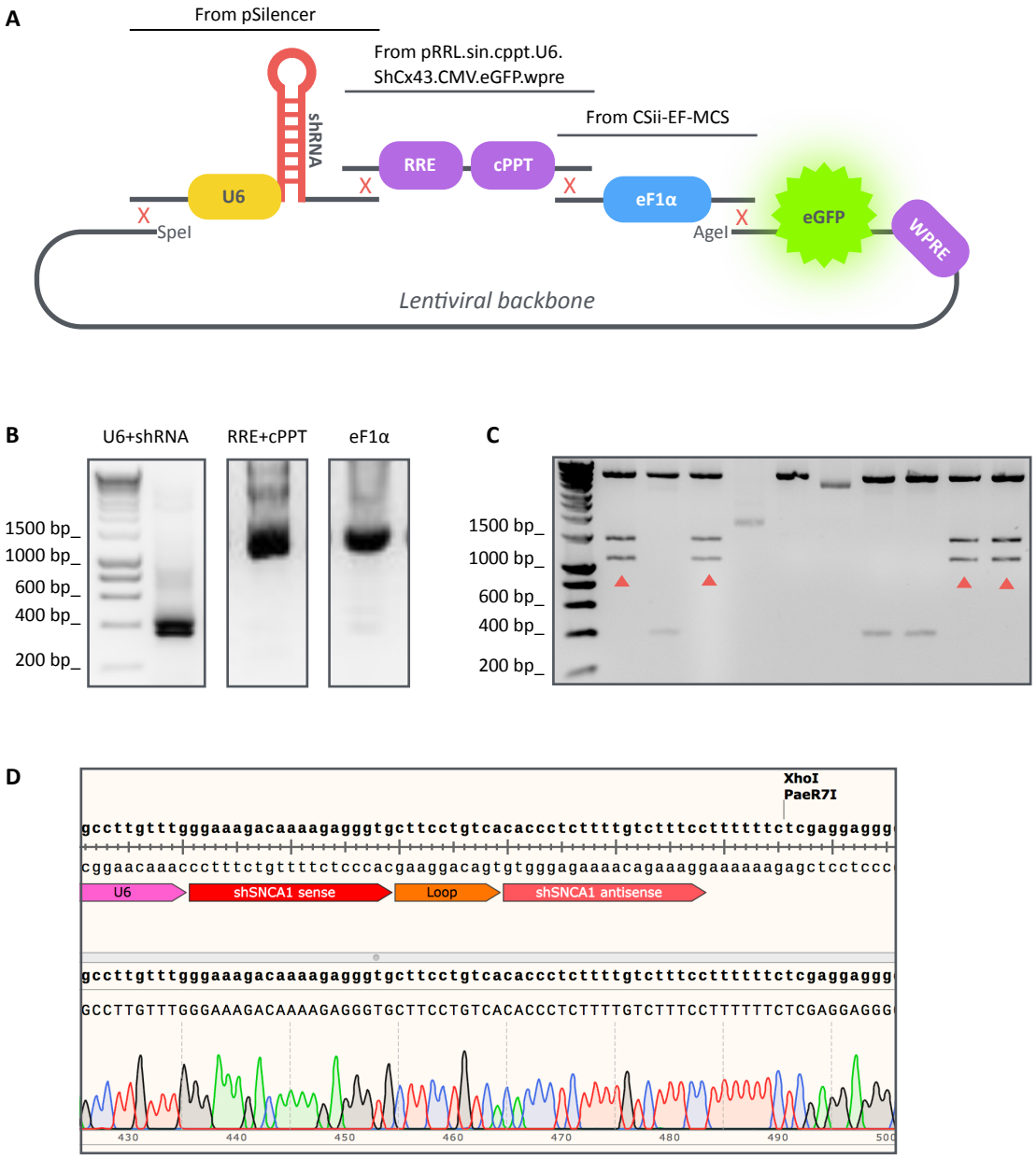

Figure 6.3|Design and cloning of the lentiviral vector for the expression of an shRNA
PCR, restriction enzyme digestion and Gibson Assembly were used to clone a lentiviral vector for the expression of an shRNA. **(A)** Schematic of the cloning. **(B)** Agarose gels show PCR amplificates of each of the three fragments for the Gibson Assembly. **(C)** Screening of Top10 E.*coli* colonies with SpeI and AgeI for the presence of the insert (two bands, 1440 and 1085bp, due to the presnce of a Age1 site in heF1α); positive colonies are marked with a red triangle. **(D)** Confirmation of the sequence by sequencing.

6.2.4|shSNCA1 does not knockdown αSyn in BE(2)M17 cells

The knockdown efficiency of shSNCA1 and shSNCA1-uLoop was tested via transfection in BE(2)M17 cells. After 48 hours, immunocytochemistry for eGFP showed that both plasmids were successfully transfected (Figure 6.4A). However, αSyn protein levels analysis by western blot did not show any differences between both shRNAs compared to untransfected cells (Figure 6.4B), suggesting that not all siRNA sequences can be converted into functional shRNAs expressed from plasmids.

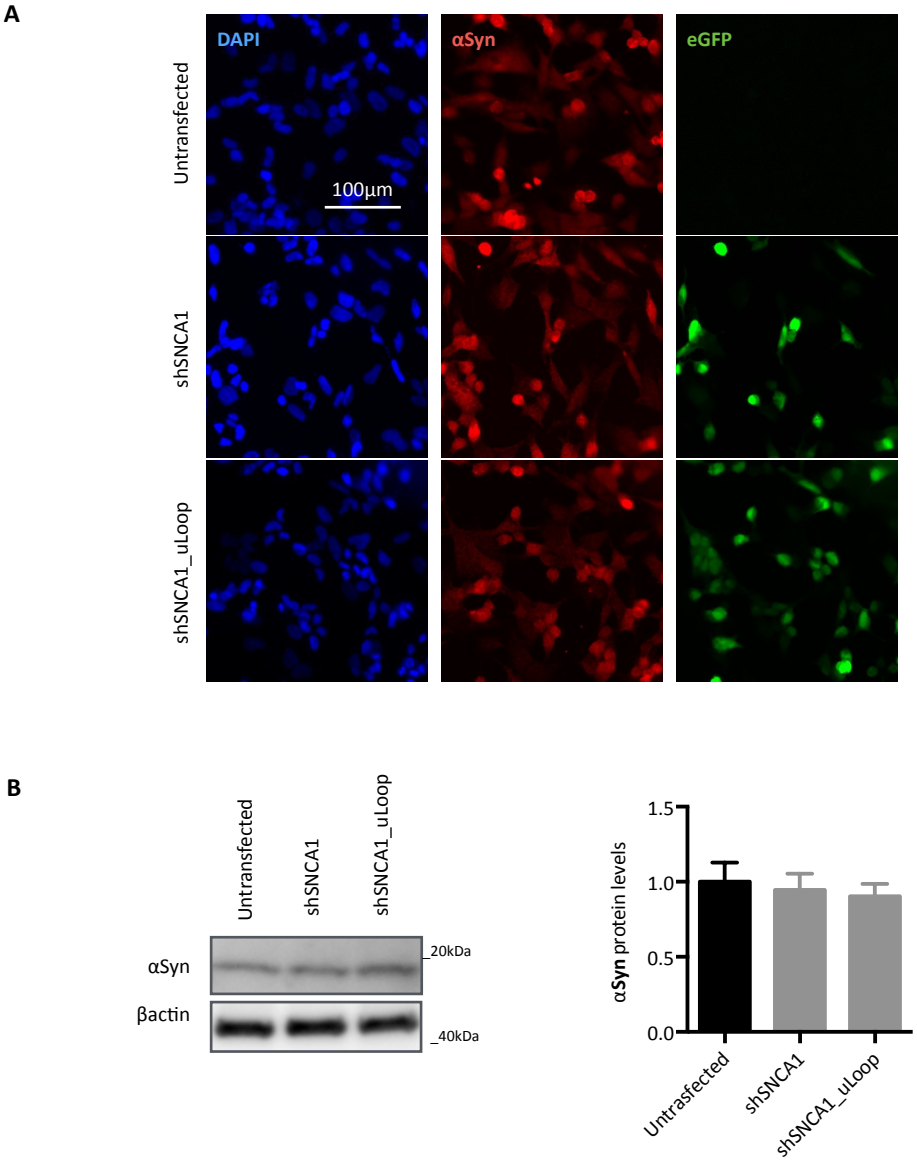

Figure 6.4|Both versions of shSNCA1 do not knockdown αSyn in BE(2)M17 cells
shSNCA1, the shRNA version of siSNCA1, was validated in BE(2)M17 cells. **(A)** Cells were fixed 48 hours post-transfection and stained for αSyn and eGFP. Transfected cells still express αSyn. **(B)** Western blot analysis of αSyn protein levels in BE(2)M17 cells transfected with either shSNCA1 or shSNCA_uLoop does not show any knockdown (N=3, mean ± SEM).

6.2.5|Design of new shRNA constructs targeting αSyn mRNA, their relative scramble controls and an empty control vector

Despite the negative results obtained with shSNCA1, four new shRNA sequences were designed to target αSyn mRNA (NM_000345.3), with the aim of selecting the one producing the best knockdown in BE(2)M17 cells, before validating it in iDAn. shASYN1 and shASYN3 were designed following RNAi design guidelines, shASYN4 is a published and validated shRNA against αSyn (Sapru et al. 2006) and shASYN2 was obtained from the RNAi Consortium database (http://portals.broadinstitute). *In silico* analysis (http://projects.insilico.us/SpliceCenter/siRNACheck.jsp) showed that all four shRNAs did not target any other mRNA even allowing up to two mismatches. The four scrambled versions (shCTRL1-4) were designed using an online tool (hwww.invivogen.com/sirnawizard/scrambled.php) and again showed no off-targets even with two mismatches allowed (Figure 6.5A). The vector expressing shSNCA1 was used as a starting point since it already contained the eGFP$^{(eF1\alpha)}$ cassette, whereas the shSNCA1 cassette was replaced with the new ones as described previously by Gibson Assembly (see section 6.2.3) (Figure 6.5B-C).

At the same time, a plasmid lacking the shRNA cassette and containing a multiple cloning site (MCS) was designed. This plasmid will be useful as a lentiviral backbone for future cloning and as a mock transfection control and for the optimisation of lentivirus infection. Analysing the list of all non-cutting enzymes in the shSNCA1 plasmid, nine were chosen for being already available in the laboratory. The length of the MCS sequence was optimised to a 62 bp sequence, with overlapping restriction site sequences. The sense and antisense oligonucleotides where annealed *in vitro* and ligated between the SpeI and XhoI sites in the lentiviral backbone creating a MCS of twelve restriction enzymes (Figure 6.5D); this construct will be hereafter referred as MCS.eGFP. The correct constructs were identified from positive colonies as previously described (Figure 6.5E).

A

Construct	shRNA sequence	Reference	Off targets
shASYN1	AAGAGGGTGTTCTCTATGTAG	Newly designed	None with up to 2 mismatches allowed
shASYN2	TGACAATGAGGCTTATGAAAT	RNAi Consortium	None with up to 2 mismatches allowed
shASYN3	AAGATATGCCTGTGGATCCTG	Newly designed	None with up to 2 mismatches allowed
shASYN4	AAGGACCAGTTGGGCAAGAAT	Sapru et al. 2009	None with up to 1 mismatches allowed
shCTRL1	GGTGAGAGTGATCGTCTATTA	Scramble of shASYN1	None with up to 2 mismatches allowed
shCTRL2	GCTACAGATAAGTTGAAGTAT	Scramble of shASYN2	None with up to 2 mismatches allowed
shCTRL3	GGCAAGTCTACGGAGTTTACT	Scramble of shASYN3	None with up to 2 mismatches allowed
shCTRL4	GAGACACTAGAGCGGGATAAT	Scramble of shASYN4	None with up to 2 mismatches allowed
MCS.eGFP	None		
shRNA loop	TGTGCTT	Jensen et al. 2012	Universal loop

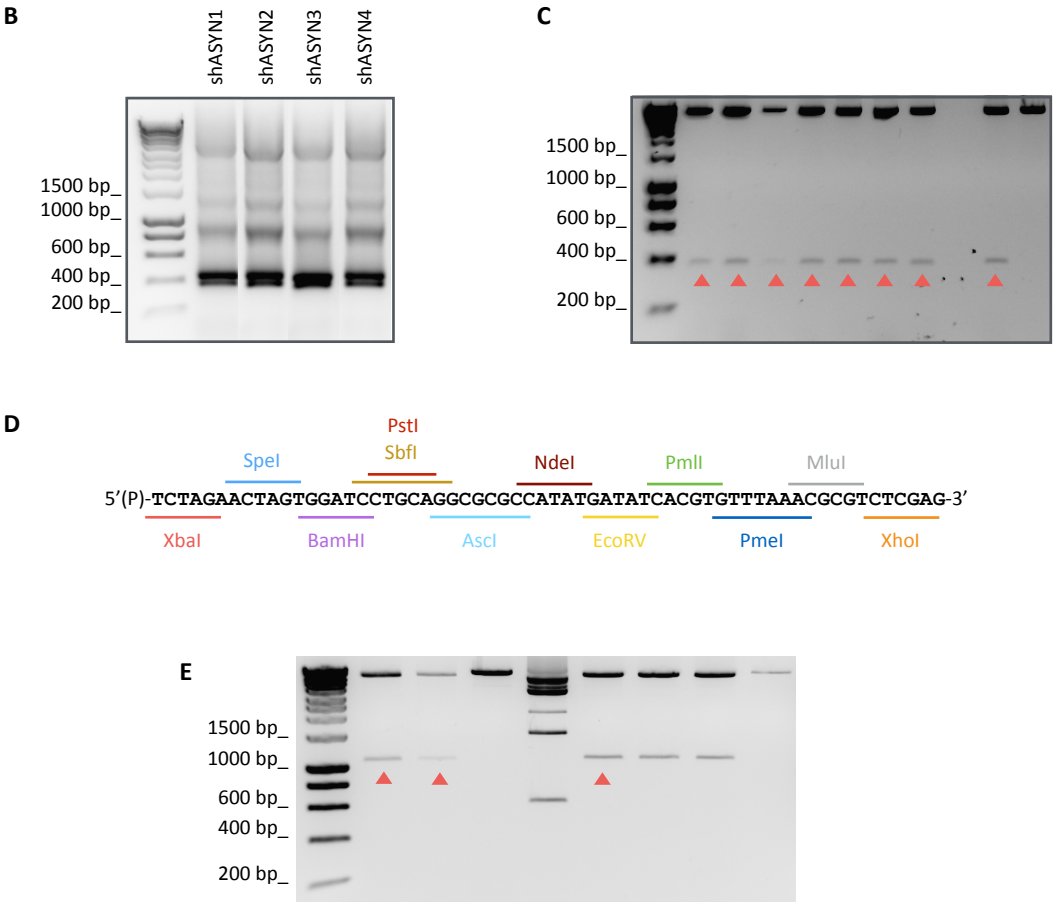

Figure 6.5|Design of new shRNAs targeting αSyn, their scrambles and an empty vector
Four new shRNAs targeting αSyn and their scramble versions were designed; TGTGCTT was used a the loop sequence. **(A)** List of the newly designed shRNAs. **(B)** Agarose gel for the PCR amplificates of the shRNAs. **(C)** Screening of Top10 E.*coli* colonies with SpeI and XhoI for the presence of the shRNA cassette (387bp); positive colonies are marked with a red triangle. **(D)** Schematic of the design of the empty vector containing a multiple cloning site instead of the shRNA cassette. **(E)** Screening of Top10 E.*coli* colonies with NdeI and MfeI for the presence of the shRNA cassette (387bp); positive colonies are marked with a red triangle.

6.2.6|Screening of shASYN and shCTRL constructs in BE(2)M17 cells

The four new shRNA targeting αSyn (shASYN1-4) were transfected into BE(2)M17 cells; MCS.eGFP was used as a positive transfection control. All constructs were expressed as shown by live-cell imaging for eGFP (Figure 6.6A). After 48 hours, shASYN2 and shSYN4 showed a significant reduction in αSyn levels compared to cell transfected with MCS.eGFP (one-way ANOVA, $p<0.05$) (Figure 6.6B). Their scrambled version shCTRL2 and shCTRL4 did not cause any reduction in αSyn expression when compared to cells transfected with MCS.eGFP (one-way ANOVA, not significant) (6.2.6C).

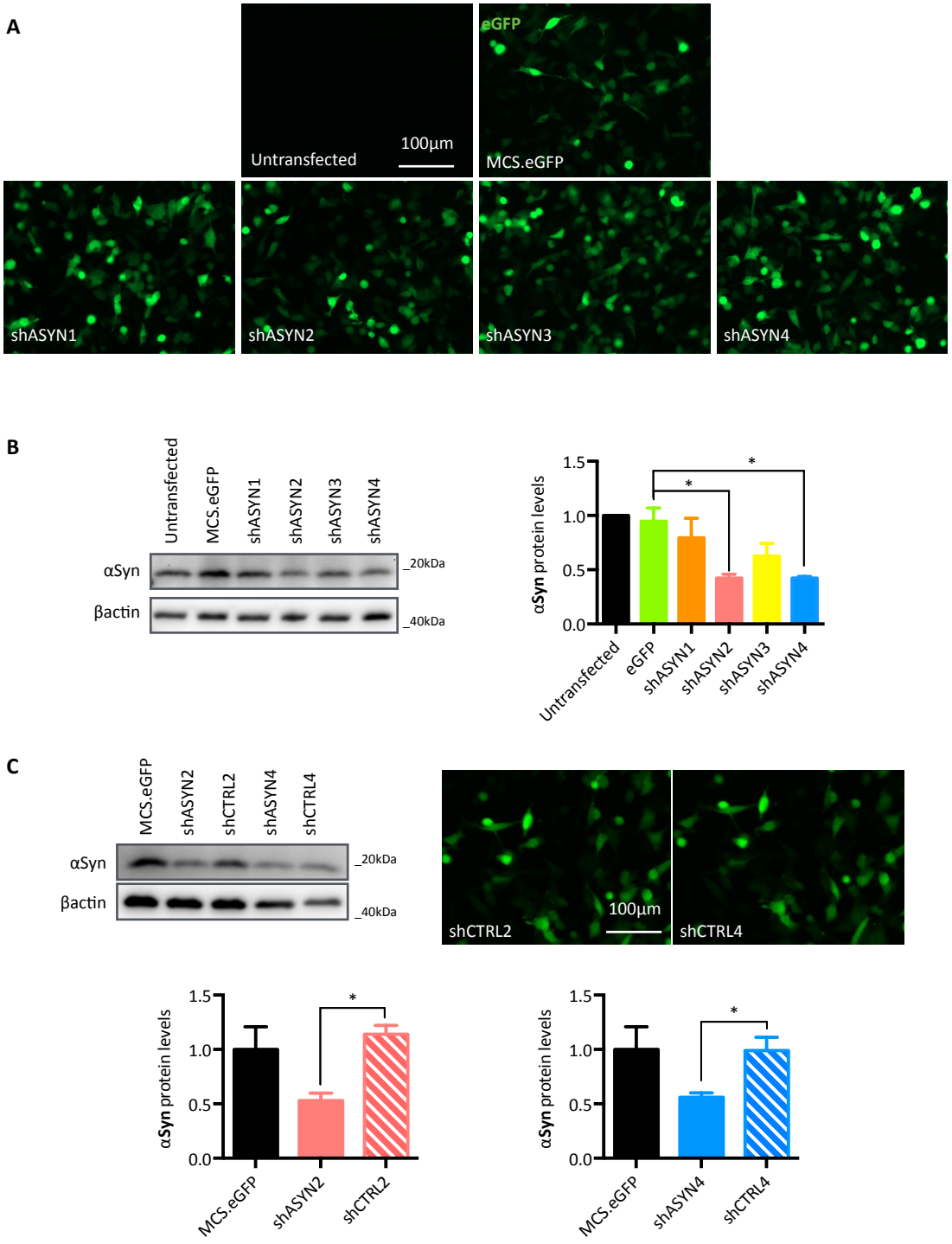

Figure 6.6|Screening of shRNAs targeting αSyn and their scramble versions
The new shRNA constructs were tested and validated in BE(2)M17 cells **(A)** Live-cell imagining shows that the all shASYN constructs get expressed **(B)** Analysis of αSyn protein levels 48 hours post-transfection shows (N=3, mean ± SEM, One-way ANOVA compared to eGFP, * $p<0.05$) **(C)** The scamble version of the two most promising shASYN were validated in BE(2)M17 (N=3, mean ± SEM, Student *t*-test, * $p<0.05$).

6.2.7|Optimisation of lentiviral transduction in iDAn

Two potential issues were considered for lentiviral transduction in iDAn cultures. First, these neuronal cultures tend to clump despite being replated as single cells, leaving exposed only axons and dendrites and making the cell bodies inside these clumps more difficult to transduce. A lentivirus particle infecting a neuron at the level of an axon or dendrite would not be retrogradely transported to the nucleus where it can integrate its genetic material with the host genome. The second issue is the unknown number of cells remaining in the dish after Mitomycin C treatment, which makes the infection based on MOI (multiplicity of infection) less accurate. For the optimisation of lentiviral transduction, viral particles were packaged with the MCS.eGFP construct so that transduced cells could be screened for the presence of eGFP fluorescence. Control #1 iDAn were transduced at 30DIV with an MOI of 5 based on the initial seeding density at 20DIV and analysed for eGFP fluorescence 5 days after. Transduction efficiency of TH^+ cells was very limited and seemed to be preferential for other non-neuronal cells still present in the culture (Figure 6.7A).

A new strategy was tested and involved transducing neurons at the day of the replating (20DIV). The main advantage is that the number of cells is known and they are still as a monolayer, making their somas more accessible to viral particles. Analysis of whether the volume of the medium containing the lentiviruses would influence the transduction efficiency was considered as well. In one set of samples, cells were spotted in a small volume, allowed to adhere to the support and then the well was topped up with medium containing lentiviral particles at the MOI of 5. Alongside, cells were spotted in a small volume of medium containing the viruses at the same MOI, allowed to attach and incubate for 2 hours before topping up with fresh medium. Live-cell imaging 48 hours post-transduction reported that both sets of samples achieved a very good transduction efficiency and that volume does not seem to play a crucial role (Figure 6.7B). At 35DIV, two

weeks post-transduction, transgene expression is retained (eGFP) and most of TH+ cells are transduced (Figure 6.7C).

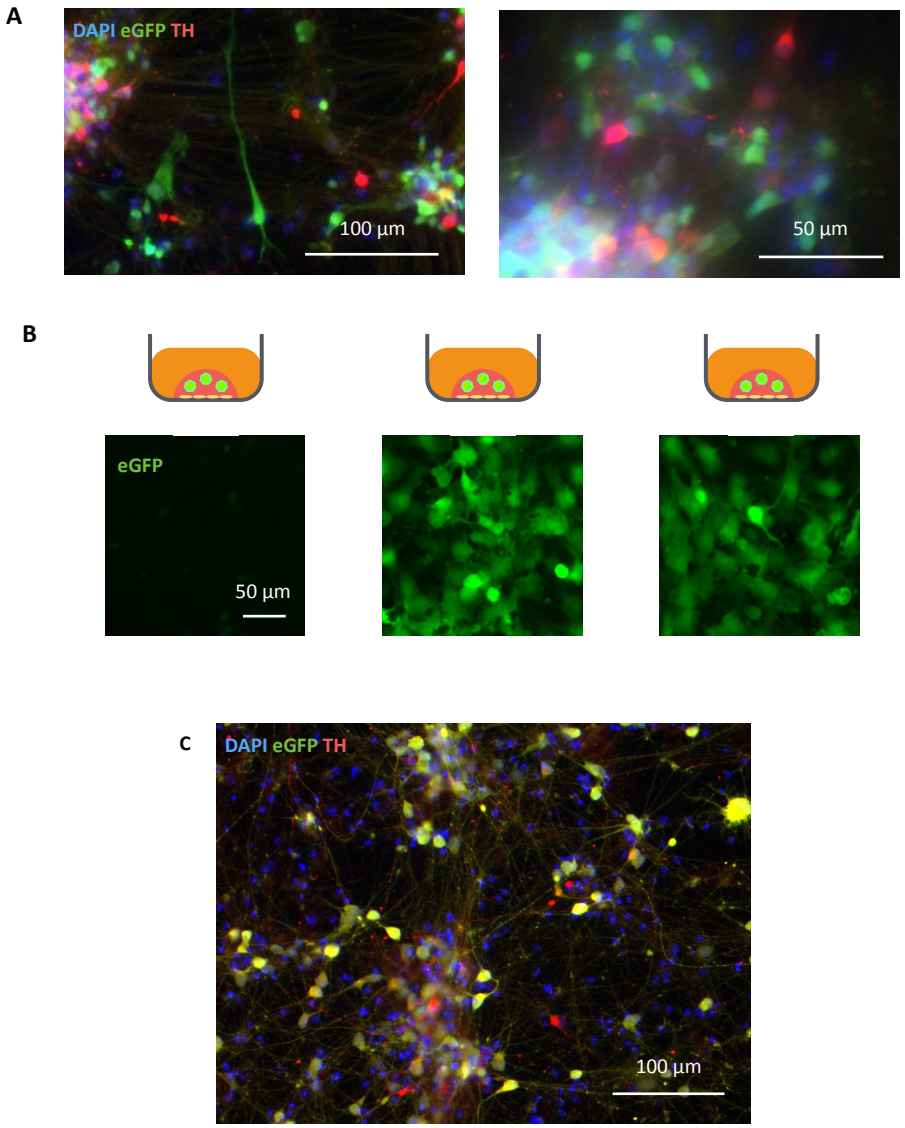

Figure 6.7|Lentiviral transduction at 20DIV achieves better efficiency than at any other time-point
(A) Representative images of control 1 iDAn fixed at 35DIV and immuno-stained for TH and eGFP; cells were previously transduced with MCS.eGFP at 30DIV. **(B)** Representative images of live-cell imaging of control 1 iDAn at 22DIV transduced with MCS.eGFP lentiviruses at 20DIV **(C)** Representative images of control 1 iDAn fixed at 35DIV and immuno-stained for TH and eGFP; cells were previously transduced with MCS.eGFP at 20DIV.

6.2.8|shASYN2 can efficiently and reproducibly knockdown αSyn in iDAn

Control #1 and A53T *SNCA* #1 iDAn were transduced at 20DIV with either shASYN2, shASYN4, shCTRL2 or shCTRL4 lentiviral particles at the MOI of 5. shCTRL4 resulted in cytotoxicity whereas all the other lentiviruses efficiently infected the cells as shown by live-cell imaging for eGFP fluorescence (Figure 6.8A). Cell were harvested 15 days post-transduction at 35DIV and αSyn protein expression was analysed. Because of the cytotoxicity of shCTRL4, shASYN4 was not included in the analysis. Compared to shCTRL2, shASYN2 produced a 92.6 ± 2.4% and 86.6 ± 0.8% decrease in αSyn in Control #1 and A53T *SNCA* #1 iDAn, respectively (N=3, Student *t*-test with, $p<0.001$) (Figure 6.8B). Immunocytochemistry for TH and eGFP was carried out to determine whether TH^+ cells were being transduced and αSyn knocked down. The analysis focused on A53T *SNCA* #1 due to the higher percentage of $TH^+/αSyn^+$ cells. In the untransduced sample, some TH^+ cells express αSyn without eGFP staining. In the shASYN2 sample, the representative image shows one transduced ($eGFP^+$) TH^+ cell that has no αSyn staining whereas an untransduced ($eGFP^-$) TH^+ cell displays αSyn staining. The opposite is true for the sample transduced with shCTRL2, where both a transduced ($eGFP^+$) and untransduced ($eGFP^-$) TH^+ cells show αSyn staining (Figure 6.8C).

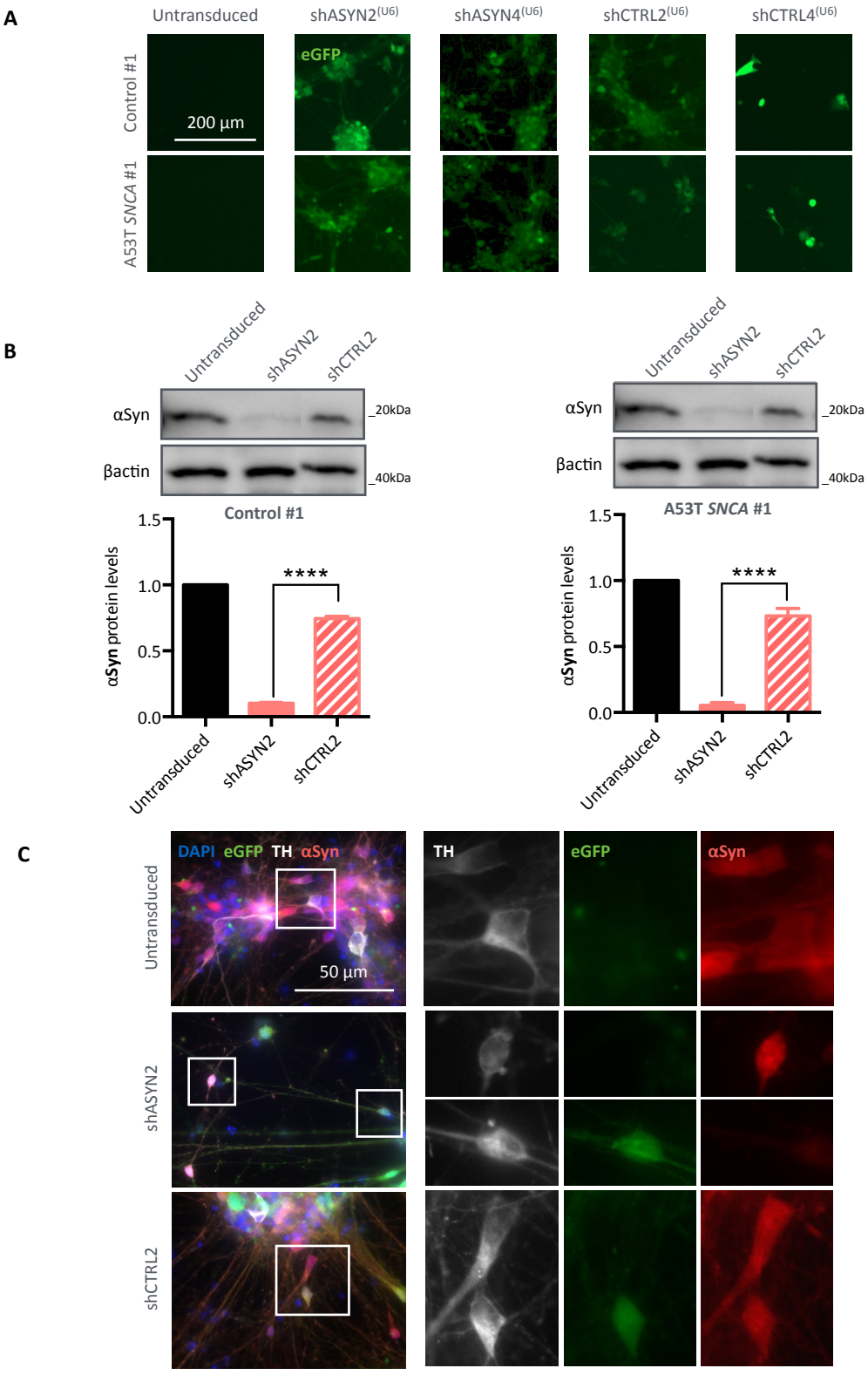

Figure 6.8|shRNA-mediated αSyn knockdown in control and A53T *SNCA* iDAn
iPSC-derived hDAn were transduced at 22DIV and then analysed at 35DIV. **(A)** Live-cell imaging of Control #1 iDAn transduced with lentiviral constructs. **(B)** αSyn protein levels in both Control #1 and A53T *SNCA* #1 iDAn transduced with shASYN2 or shCTRL2 (N=3, mean ± SEM, Student *t*-test, **** $p<0.0001$) **(C)** Representative images A53T *SNCA* #1 iDAn transfected with shASYN2 or shCTRL2. Cells were immuno-stained for αSyn, eGFP (lentivirus reporter) and TH.

To optimise the amount of virus and eventually reduce any stress on the cells, Control #1 iDAn were transduced with MOI of 1, 2, 3, 4 and 5 and expression levels of αSyn and eGFP were analysed. All MOIs but 1 achieved αSyn knockdown to some extent (Figure 6.9A). Lastly, shASYN2-transduced iDAn were kept for further 2 weeks until 55DIV (5 weeks post-transduction), and protein analysis reported that the knockdown of αSyn persists even during prolonged times of maturation in culture, apart from A53T *SNCA* #1 where transduction seems to have failed (Figure 6.9B).

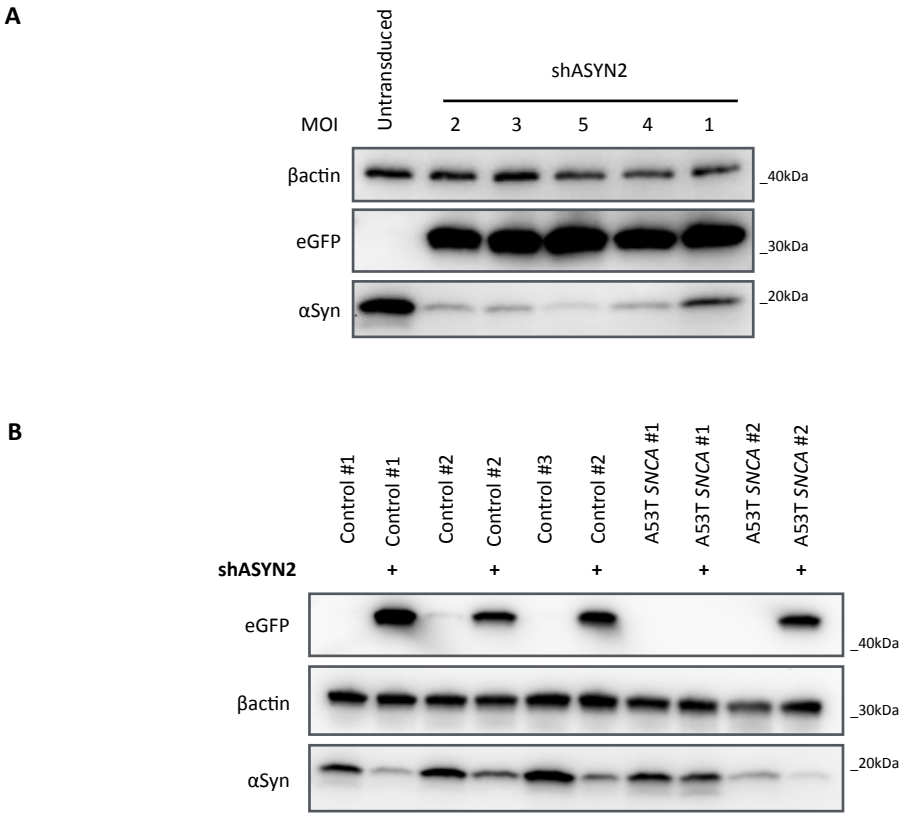

Figure 6.9|Optimisation and long term follow-up of αSyn knockdown in iDAn
(A) αSyn expression levels in Control #1 iDAn transduced with shASYN2 at different MOIs **(B)** αSyn protein levels at 55DIV after transduction at 20DIV (35 days post-transduction).

6.2.9|Transduction of undifferentiated iPSCs with shASYN2 does not evoke αSyn knockdown after differentiation to iDAn

Transduction at the day of the replating was proven to be an efficient way to deliver shRNAs to the cells and to achieve a consistent and long term knockdown of αSyn. However, due to the enormous quantity of lentiviral particles needed, especially when transfecting iDAn in 12-well plate format at the MOI of 5 (~6M viral particles/well), it was sought to determine whether iPSCs could be transduced before the start of the differentiation and still achieve αSyn knockdown by 35DIV. Some recent papers do suggest that in stem cells or during differentiation viral vectors integrated in the genome may be recognised as exogenous sequences and therefore silenced (Rival-Gervier et al. 2013; Hong et al. 2007). Control #1 iPSCs were transduced with shASYN2 viral particles at the MOI of 5 two days before the start of neuronal induction and then differentiated and matured until 35DIV. eGFP fluorescence was used as a read-out of whether the transgene was still expressed; iDAn remained positive for eGFP up until the later stages of the maturation (Figure 6.10A). At 35DIV, αSyn protein levels and eGFP expression were analysed via western blot and immunocytochemistry respectively. Despite eGFP still being expressed (Figure 6.10B), αSyn protein levels were not decreased (Figure 6.10C).

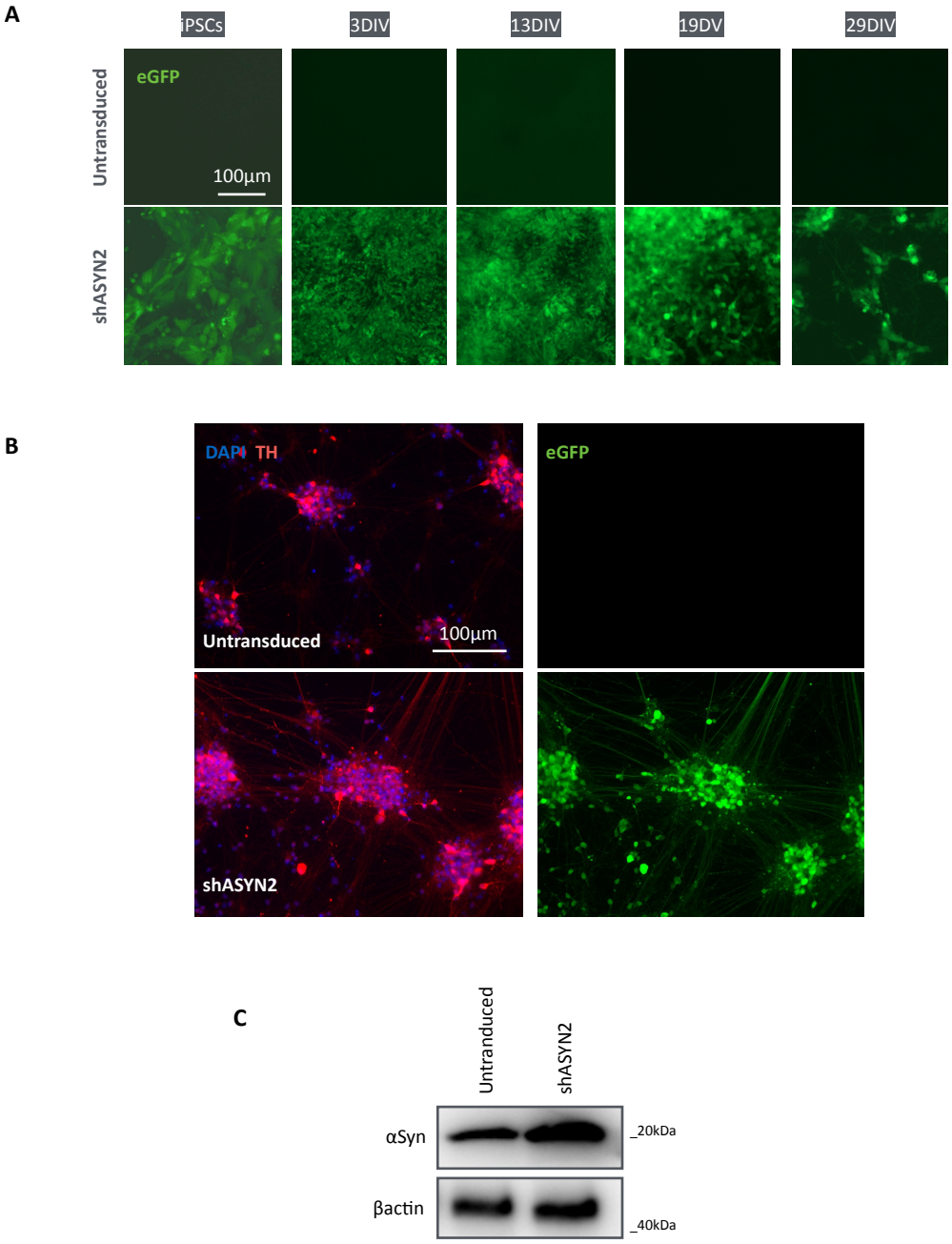

Figure 6.10|Transduction at the iPSC stage with shASYN2 does not elicit αSyn knockdown in iDAn
iPSC were transduced with shASYN2 and then differentiated to iDAn. **(A)** Live-cell imaging of cells at the iPSC stage and at 3, 13, 19 and 29DIV. **(B)** Cells were fixed at 35DIV and immuno-stained for eGFP (lentivirus reporter) and TH. **(C)** αSyn protein levels were analysed at 35DIV.

6.2.10|Peptide-based knockdown of αSyn in iDAn

The laboratory of Professor Wang at the University of British Columbia developed a peptide that can induce a rapid and reversible knockdown of a specific protein in both human and rat cellular culture systems (section 1.4.5) (Fan et al. 2014). Through a collaborative effort with the group of Professor Wang, the efficacy of this peptide (hereafter referred as tat-βSyn-degron) in knocking down αSyn in iDAn was assessed, as an alternative method to RNAi. Following the provided protocol, the lyophilised peptide was first reconstituted in PBS and then diluted in final differentiation medium. A range of concentrations and number of treatments were tested in Control iDAn at 35DIV and cells were harvested the following day for the analysis of αSyn expression. Cells were treated with either 5 and 10 μM twice for three hours before replacing the supernatant with fresh medium or 10 and 25 μM for 24 hours. Treatment with 25 μM TAT-βSyn-degron for 24 hours reduced αSyn expression by ~50%; however, a second band of lower molecular weight appears in all treated samples at all concentration, making the interpretation of the knockdown ambiguous (Figure 6.11A).

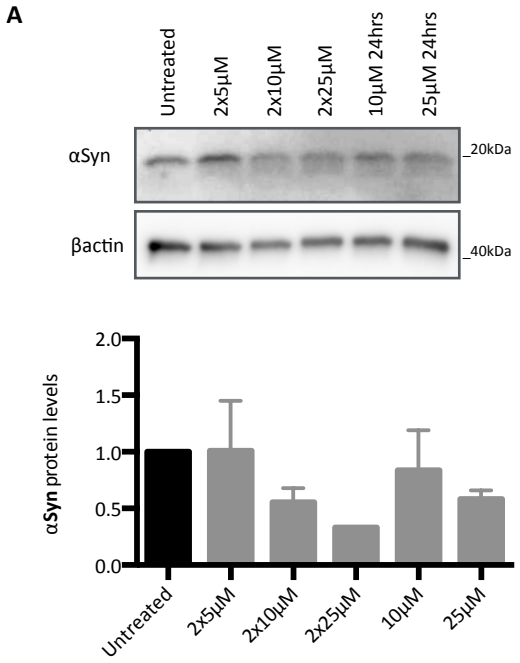

Figure 6.11| αSyn knockdown in iDAn using tat-βSyn-degron
Control #1 iDAn at 34DIV were treated with tat-βSyn-degron and then αSyn protein levels were analysed 24h later **(A)** Quantification of αSyn protein levels (N=2, mean ± SE)

6.2.11|Effects of αSyn knockdown on mitochondrial respiration in iDAn

The knockdown of αSyn using lentiviral particles was used to determine the causative role of the protein in the mitochondrial phenotypes described in A53T *SNCA* iDAn. On day 20 of the protocol, the cells were replated into the Seahorse microplates and transduced at the MOI of 5 with either shASYN2 or shCTRL2 lentiviral particles. To reduce the level of variability due to multiple lines and treatments, the analysis focused on the comparison of Control #1 and A53T *SNCA* #3 iDAn. Mitochondrial respiration was assessed at 35DIV as described previously. Inconclusive results were obtained in three separate experiments and the comparison of the basal OCR best describes these results. In one case, compared to untransduced or shCTRL2 transduced cells, knockdown of αSyn unexpectedly caused a remarkable reduction in OCR, and to a lesser extent of ECAR (Figure 6.12.A). Similarly, in one instance lentiviral transduction caused a reduction of both OCR and ECAR (Figure 6.12.B). The effect of αSyn knockdown on mitochondrial respiration of Control and A53T *SNCA* iDAn was further investigated using the tat-βSyn-degron peptide (see Section 6.2.10). iDAn treated with 25μM tat-βSyn-degron and assayed 24 hours showed variable and conflicting results for the measurements of both OCR and ECAR. (Figure 6.12.C).

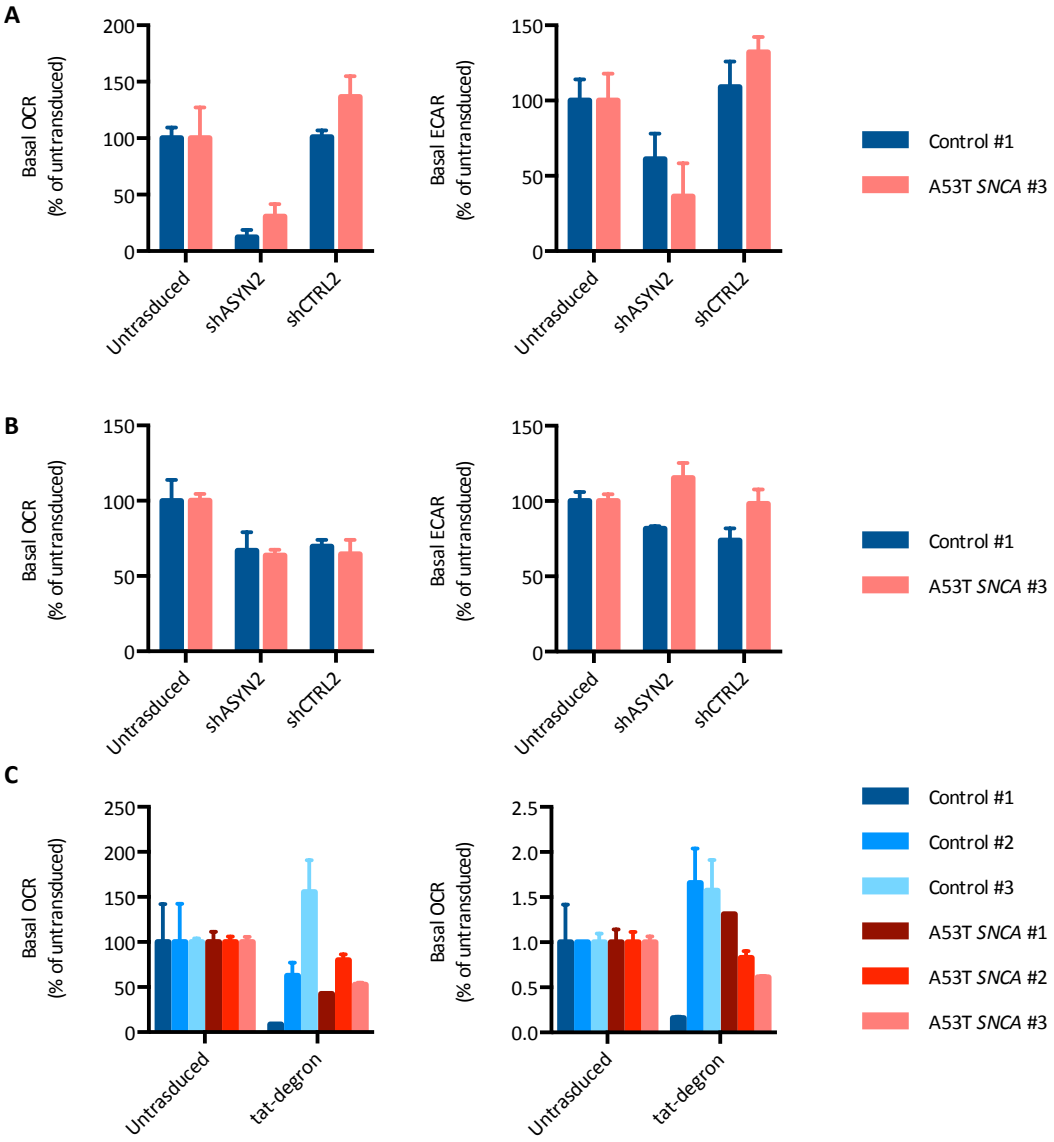

Figure 6.12|Mitochondrial respiration in Control and A53T *SNCA* iDAn with αSyn KD at 35DIV
(A) Measurement of mitochondrial respiration in Control #1 and A53T *SNCA* #3 iDAn with αSyn RNAi (N=1, n=4, mean±SD). **(B)** Measurement of mitochondrial respiration in Control #1 and A53T *SNCA* #3 iDAn with αSyn RNAi (N=1, n=4, mean±SD). **(C)** Measurement of mitochondrial respiration in Control and A53T *SNCA* iDAn with αSyn knockdown using tat-βSyn-degron (N=1, n=4, mean±SD).

6.2.12|Investigation of the functional interaction between αSyn and FABP7 in iDAn

The expression levels of the FABP7 were found to be reduced in both A53T *SNCA* and *SNCA* Tripl iDA at 35DIV (section 5.2.9). Little is known about the functional or physical interaction between FABP7 and αSyn (Sharon et al. 2003)(Shioda et al. 2014).

The functional interaction between αSyn and FABP7 in iDAn was investigated via knockdown of αSyn and analysis of FABP7 expression levels at 35DIV. Control iDAn transduced with shASYN2 showed increased FABP7 levels compared to shCTRL samples (Student *t*-test, $p<0.05$) (Figure 6.13A). A similar trend was detected for A53T *SNCA* iDAn (Student *t*-test, $p=0.06$). To confirm these results, αSyn was knocked down using the tat-βSyn-degron peptide (section 6.2.10). In this case, no changes in FABP7 levels were detected 24 hours after treatment, despite the decrease in αSyn levels (Figure 6.13B).

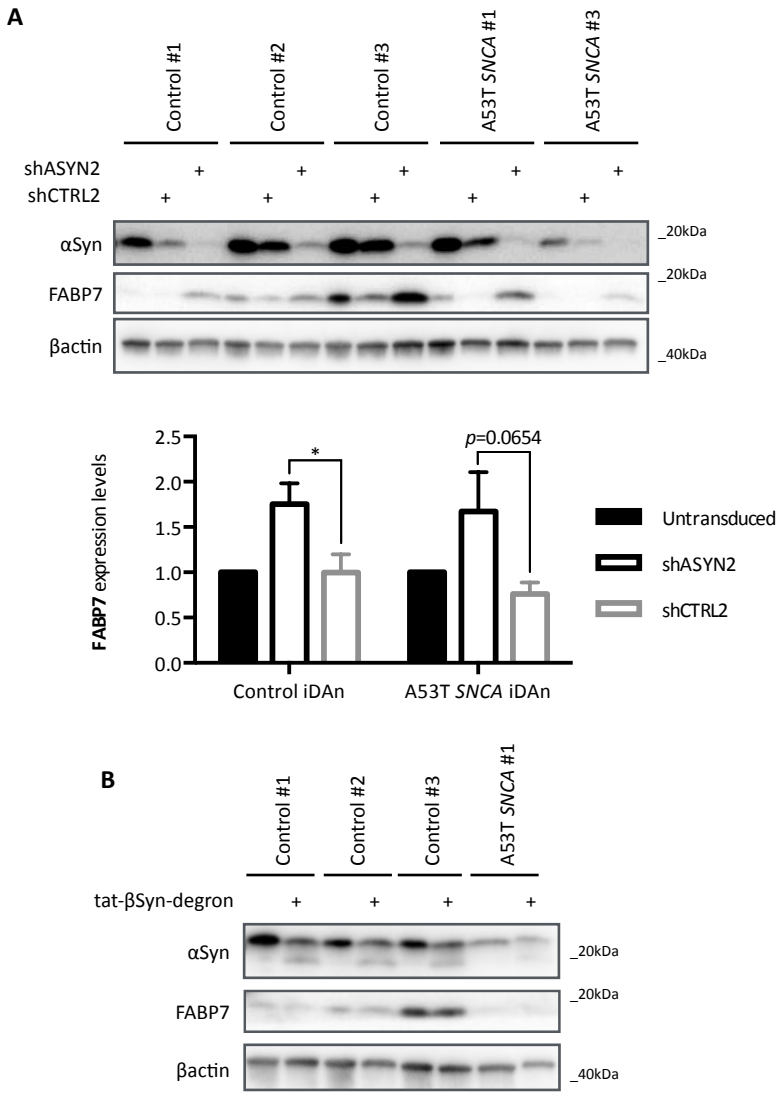

Figure 6.13|αSyn knockdown via RNAi increases FABP7 expression in iDAn
(A) Quantification of αSyn and FABP7 expression in Control and A53T *SNCA* iDAn at 35DIV with αSyn knockdown via RNAi (N=3, mean±SEM, Student's *t*-test, *p<0.05). **(B)** Expression of αSyn and FABP7 in Control and A53T *SNCA* iDAn at 35DIV with αSyn knockdown using tat-βSyn-degron.

To generate genetic tools to study the functional relationship between FABP7 and αSyn, lentiviral vectors for the knockdown or over-expression of FABP7 in iDAn were generated. Over-expression can be used to investigate whether increased FAPB7 levels could revert the phenotypes seen in A53T *SNCA* iDAn. Conversely, down-regulation of FABP7 could be used to examine its function in Control iDAn and examine whether it would induce a phenotype similar to those of A53T *SNCA* iDAn, including mitochondrial dysfunction and ER stress. Likewise, preliminary work by H. Fernandes in the laboratory showing increased expression of FABP7 in N370S GBA and sporadic iDAn would benefit from the possibility of knocking down this protein.

The design of a dual RNApolIII promoter lentiviral vector expressing both FABP7 and eGFP carries some limitations that needed to be considered. The human cDNA sequence of FABP7 was obtained from the construct CMV.hFABP7.polyA.CMV.eGFP (map in Table 2.8D) (kindly provided by B. Ryan, University of Oxford) that contains FABP7 cDNA under the control of the CMV promoter and a downstream polyadenylation site (polyA). First, the CMV promoter driving FABP7 expression might be silenced in iPSC and iDAn; the eF1α was shown previously to be a valid substitute (see section 6.2.8). Secondly, the presence of a polyA signal downstream of FABP7 could produce a reduced lentiviral titer, probably caused by a reduction in full-length viral genome due to the recognition of the polyA signal as a termination sequence by the RNApol III during viral genome transcription (Hager et al. 2008; Blø et al. 2007). To overcome this, the two expression cassette could be inserted in opposite directions, which also avoids possible interactions between the two promoters (Tolmachov 2011). Therefore, the reading frame of FABP7$^{(eF1\alpha)}$ can be placed in the minus strand in a 3' to 5' orientation, while maintaining eGFP$^{(eF1\alpha)}$ in the vector, and still achieve expression.

For the generation of this vector, the two fragments containing the promoter and

cDNA+polyA were inserted between the SpeI and XhoI in the MCS.eGFP. The new FABP7$^{(eF1\alpha)}$ cassette was designed accounting for the homology arms required for the Gibson Assembly and its insertion in a 3' to 5' orientation in the lentiviral backbone (Figure 6.14A). Briefly, two primers were used to amplify the FABP7+polyA cDNA: a forward primer containing a 20 bp homology arm upstream of the transcription start site of eF1α; a reverse primer containing a 20 bp homology arm to the minus strand upstream of the SpeI sequence in the MCS.eGFP construct. The eF1α promoter was amplified from MCS.eGFP using a forward primer containing a 20 bp homology arm downstream of the XhoI sequence in the MCS.eGFP construct, and a reverse primer containing 20 bp of homology arm with the of FABP7+polyA.

For the generation of FABP7 shRNAs, four sequences were accessed as described previously (section 6.2.5) and inserted between the SpeI and XhoI sites in MCS.eGFP (Figure 6.14A,B). Briefly, shFABP7#1 and #4 were obtained from the RNAi Consortium database whereas shFABP7#2 and #3 are published and validated sequences (Lock et al. 2014). Scrambled version of these shRNAs (ShScramble1-4) were generated accordingly and verified not to target any transcript even allowing up to 2 mismatches. Sequencing of the constructed confirmed the correct sequence.

The shFABP7$^{(U6)}$ constructs were screened for their efficacy in BE(2)M17 cells; the expression of the FABP7$^{(eF1\alpha)}$ construct was assessed alongside, whereas the MCS.eGFP was used as negative control. Cells were also transfected with shASYN2 and shCTRL2 to analyse whether the same effect of αSyn knockdown on FABP7 could be reproduced in other cell models. Despite all constructs being expressed, BE(2)M17 do not express any FABP7 and therefore the knockdown could not be quantified (Figure 6.14C). Nonetheless, FABP7$^{(eF1\alpha)}$ was expressed as shown by the appearance of a band of the right molecular weight (Figure 6.14C). The testing of the shFABP7 construct was not carried out any

further since none of the other cell lines available in the laboratory had suitable FABP7 expression (H. Fernandes and B. Ryan, personal communication).

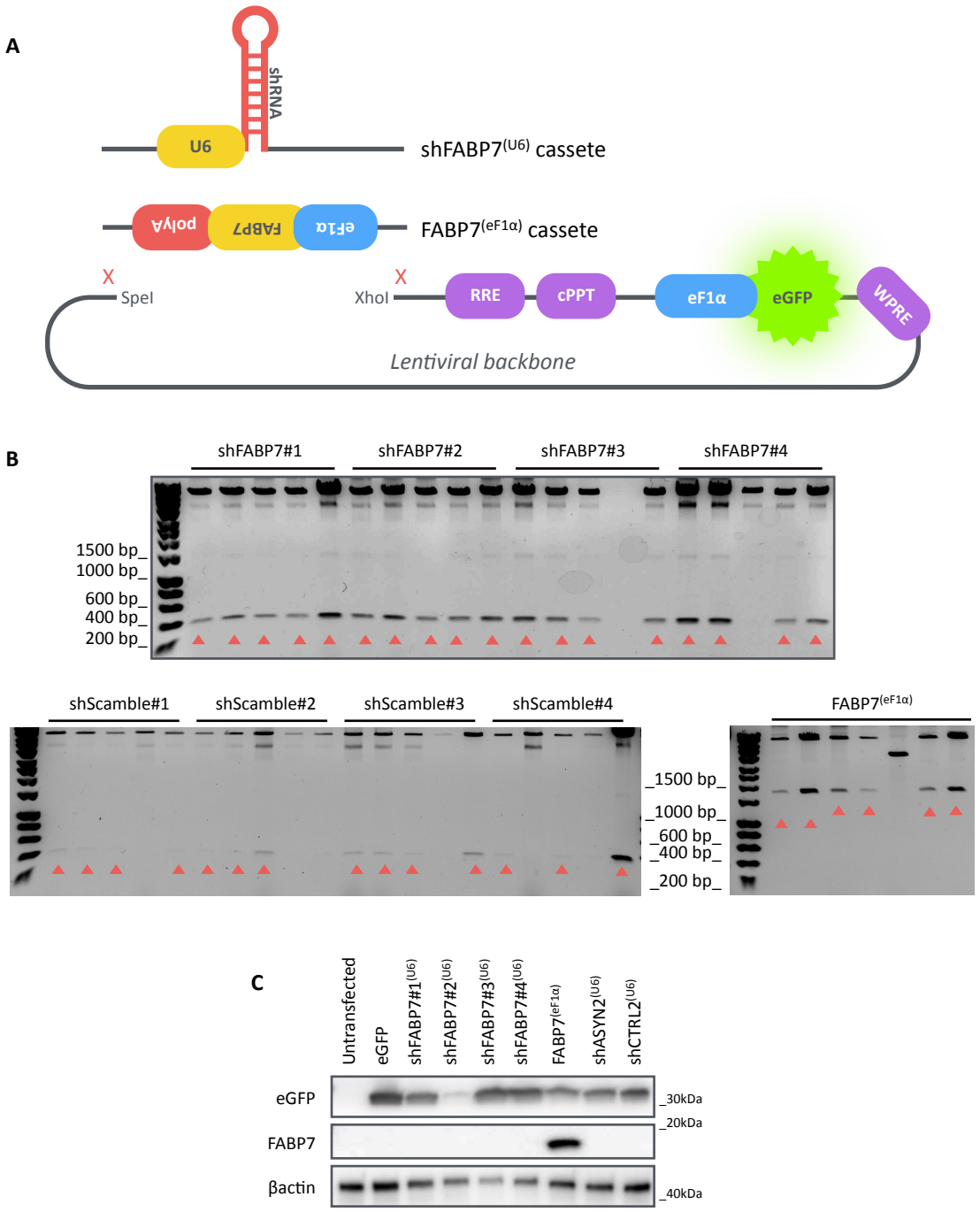

Figure 6.14|Lentiviral vectors for the over-expression or knockdown of FABP7 in iDAn
(A) Schematic of the cloning of FABP7$^{(eF1\alpha)}$, shFABP7$^{(U6)}$ and shScramble$^{(U6)}$. **(B)** Screening of Top10 E.*coli* colonies with SpeI and AgeI for the presence of the insert (for shFABP7: two bands at 8088 and 378bp; for FABP7$^{(eF1\alpha)}$: two bands at 8088 and 1761bp); positive colonies are marked with a red triangle. **(C)** Analysis of FABP7 and eGFP protein levels 48 hours post-transfection.

6.3|Discussion

The work involving the knockdown of αSyn in iDAn was presented in this chapter. It aimed to study αSyn cellular function in Control iDAn and investigate the pathological contribution of this protein to the phenotypes described in A53T *SNCA* iDAn; eventually it could be extended to other phenotypes in iDAn bearing different mutations, like *SNCA* triplication.

The initial approach involved the use of siRNAs because of their affordability and accessibility of well-established transfection techniques. Upon optimisation of iDAn transfection, knockdown using the validated siSNCA1 against αSyn (Fountaine and Wade-Martins 2007) produced variable results. The interpretation was also made more challenging since even non-targeting siRNAs, namely mut12 and Silencer® Negative Control, induced αSyn knockdown to a certain extent. Another source of variability certainly came from the substantial inter-well variability in cell number and αSyn expression in iDAn differentiated with the EB-protocol (see section 3.2.7). Some papers have recently reported efficient transfection of genetic material into iDAn (Ryan et al. 2013) (Miller et al. 2013), suggesting that further optimisation of the transfection technique may resolve the reproducibility issues encountered with siRNA transfection in this work.

A new approach involving lentiviral delivery of shRNAs was chosen to overcome difficulties in achieving siRNA-mediated knockdown in iDAn. Since the region of the αSyn mRNA targeted by siSNCA1 is accessible to RNAi, SNCA1 sequence was embedded in the shRNA cassette and a new lentiviral construct was generated. Nevertheless, shSNCA1 did not achieve αSyn knockdown in BE(2)M17 cells. At a closer look, the siSNCA1 sequence reveals a string of four adenines that determines the presence of four thymidine in the sense strand of shSNCA1. This could be recognised as an early termination signal by RNApolIII, resulting in the generation of short shRNAs (Nielsen, Yuzenkova, and Zenkin

2013) and therefore could underlie the lack of knockdown by shSNCA1.

To overcome this, four new shRNA targeting αSyn mRNA (shASYN1-4) and their scrambled sequences (shCTRL1-4) were generated based on the previous vector and tested in BE(2)M17 cells; shASYN2 and 4 induced a significant knockdown of αSyn compared to eGFP alone. Prior to further validation in iDAn, transduction of lentivirus particles in iDAn was tested and optimised. Infection at 30DIV and analysis of eGFP expression 5 days later showed poor transduction efficiency, mostly localised to non-neuronal cells. Conversely, cells transduced with MCS.eGFP lentiviruses at D20 showed abundant eGFP expression by 35DIV in most of cells. Analysis of αSyn knockdown in iDAn showed that shASYN2 significantly decreased αSyn expression at 35DIV compared to shCTRL2.

Because the packaging of lentiviral particles is time consuming and transduction of many iDAn lines requires a considerable volume of viral preparations even at the MOI of 5, the possibility of transducing undifferentiated iPSCs prior differentiation was considered. Despite the cells expressing eGFP throughout the differentiation and up to 35DIV, αSyn knockdown could not be detected. It is unlikely that the shRNA cassette gets silenced since it includes a mammalian promoter that should not be recognised as an exogenous sequence by the host cell. Otherwise, the same silencing would apply to eGFP as well, since it is only 1 kb downstream. Anyway, despite representing an interesting biological question, this was not investigated any further.

In parallel and complementary to the knockdown of αSyn using RNAi, an alternative method based on the tat-βSyn-degron peptide was tested in collaboration with the laboratory of Prof Wang (Fan et al. 2014). However, contrary to previous results by Wang and colleagues using HEK293 cells and rat primary neurons, tat-βSyn-degron treatment in iDAn caused the appearance of a second lower MW αSyn band that made the actual knockdown difficult to interpret. It can be speculated that this band might represent

a degradative product of αSyn and therefore the treatment does not evoke an actual knockdown, at least in the time-frame analysed. Because of time restrictions, the lack of a control peptide and the achievement of αSyn using RNAi, no further experiments were set up to optimise the peptide-based method.

Of interest was the possibility of studying αSyn mitochondrial function in Control iDAn and its pathological contribution to dysfunction in A53T *SNCA* iDAn taking advantage of the shRNA constructs generated. Unfortunately, the effect of αSyn knockdown on mitochondrial function was difficult to interpret, mostly due to the discordant results generated measuring the oxygen consumption rate.

Because of the decrease in FABP7 expression levels in both A53T *SNCA* and *SNCA* Tripl iDAn (section 5.2.9), the effect of αSyn knockdown on FABP7 was investigated in Control and A53T *SNCA* cells. Interestingly, αSyn knockdown drove a significant increase in FABP7 expression, at least in Control iDAn. It was beyond the timeframe/scope of this study to take this finding further, however, genetic tools for the study of the functional interaction between FABP7 and αSyn were generated, namely shRNAs targeting FABP7 and a FABP7 over-expression lentiviral vector. Preliminary analysis was interrupted by the lack of FABP7 expression in the cell lines available in the laboratory. Future work should include validation of the new constructs in iDAn, alongside with the analysis of the effect of both αSyn and FABP7 knockdown on other markers that were shown to be dysregulated in A53T *SNCA*, including CYP46A1, p62, LC3-II, SIRT1, PGC-1α, pDRP1, BiP, IRE1α, C/EBPβ.

Overall, the generation of lentiviral vectors for the knockdown of αSyn was a lengthy process compared to the siRNA approach. The cloning of shRNAs is a very laborious process, especially when coupled with the validation in iDAn. Unfortunately, it was not possible to investigate the effect on αSyn knockdown on mitochondrial function.

Nonetheless, the results generated with shRNAs in the context of FABP7 expression are a novel and important finding in the context of PD and possibility neuronal biology. Importantly, the effect of αSyn knockdown on FABP7 would not have been appreciated in immortalised non-neuronal cell lines, often used as PD models, that might not express this protein, further highlighting the relevance of using iDAn as an *in vitro* cell model to study protein biology in human neurons. The detection of the effects of αSyn knockdown would probably benefit from the use of fewer lines, for example one Control and one A53T *SNCA*, to limit the source of variability. However, this approach would raise the question of which line would best represent a phenotype or genotype; likewise, some lines may respond to αSyn knockdown differently, in a similar way to A53T *SNCA* #1 iDAn being phenotypically different from the other lines of the same genotype (chapter 5). Last, the fact that lentiviral infection was shown to work best at 20DIV may raise the question of whether prolonged expression of the transgene may introduce further variability. It would be interesting to explore the possibility of using drug-inducible constructs to temporally define the expression of the transgene (Szulc et al. 2006).

To conclude, the RNAi described in this chapter led the generation of genetic tools for the investigation of αSyn function and dysfunction in iDAn and the discovery of a novel functional interaction between FABP7 and αSyn. To date, most of the genetic manipulation of iPSC and iDAn has focused on the generation of isogenic control lines to study PD pathology in iDAn (Ryan et al. 2013; Reinhardt et al. 2013; Schöndorf et al. 2014) or the generation of reporter lines, namely PITX3-eGFP (Watmuff et al. 2015) and LRRK2-mCherry (S. Cowley, personal communication). However, the creation of isogenic or reporter iPSC lines is generally restricted to a small number of lines, mostly because of the low efficiency of this technique. Conversely, transfection or transduction of shRNAs and proteins could be applied to a virtually unlimited number of iPSC lines. Overall, more

work is required for the generation of these important genetic tools to study disease biology in iDAn and the optimisation of their efficient delivery.

Chapter 7

Final discussion

This work aimed to understand the pathological mechanisms associated with αSyn in the context of PD. Firstly, the optimisation of a protocol for dopaminergic neuron differentiation of iPSCs and the initial characterisation of iDAn was necessary to validate the relevance of this cell model to the study of PD *in vitro*. Secondly, multiple iPSC lines or clones from healthy individuals and PD patients carrying the A53T *SNCA* mutation or a triplication of the *SNCA* gene were identified to account for biological variability. Additionally, iDAn cultures were characterised for their differentiation efficiency to be able to compare them to each other. Afterwards, a phenotypic analysis was carried out to determine whether A53T *SNCA* or *SNCA* triplication iDAn cultures could recapitulate phenotypes already reported for PD or to uncover novel and early pathological mechanisms associated with the disease. Last, a method for the knockdown of αSyn in iDAn was developed and validated to understand the function of this protein and its contribution to the phenotypes present in PD iDAn.

7.1|Generation of a highly relevant *in vitro* PD cell model

The generation of highly relevant *in vitro* cell models is crucial to understanding αSyn pathology. Most current animal or cell models rely on genetic manipulation to over-express wild-type or mutant αSyn and study the downstream pathological mechanisms but cannot fully recapitulate the disease pathophysiology.

The Nobel Prize-winning discovery of cellular reprogramming led to the generation of iPSCs from PD patients carrying genetic mutations or sporadic cases. In turn, iPSCs can be differentiated to any cell type that is most relevant the disease pathology, including iDAn. For the first time, patient-derived iPSCs carrying the genetic background that was causative to the onset of the disease in patients could be used to generate a relevant *in vitro* PD cell model. This model holds many expectations since it bridges the gap between classic animal and cell models, especially in neurodegenerative disorders like PD. Nonetheless, the hurdle of "ageing" is still difficult to overcome and, without understanding environmental risk factors associated with a disease, only the genetic factors can be studied *in vitro*. Despite iPSC-derived neuronal cultures being shown to be viable for up to one year in culture, it is unimaginable to routinely set up a number of lengthy and costly cultures in parallel that require months to generate.

The experiments described in chapter 3 aimed to establish a protocol for the differentiation of iPSCs to iDAn. At the time this work was set out, a few differentiation protocols were available, including the one generated in the Wade-Martins laboratory. The EB-protocol developed generates a mixed cell population with ~20% TH^+ (Hartfield et al. 2014). The main issues associated with this protocol were the under-representation of the cell population of interest (TH^+ cells) and the low reproducibility. The protocol from the Studer laboratory based on the generation of floor plate (FP) precursors (Kriks et al. 2011) was tested and optimised and eventually compared to the EB-protocol. Cell cultures differentiated with the FP-protocol were shown to be enriched in TH^+ cells (44%) that co-expressed the ventral midbrain dopaminergic neurons specific markers FOXA2 and LMX1A, confirming the correct cell identity. This groundwork was essential to validate this *in vitro* cell model, since previous reports have highlighted the importance of generating a specific subtype of TH^+ to study PD pathology *in vitro* (Kriks et al. 2011; Chung et al.

2016). Compared to the EB-protocol, the FP-protocol generated a significantly higher percentage of both TH^+ and $TUJ1^+$ cells. Importantly for this work, there was also a significantly lower inter-well variability in αSyn protein levels in the FP-protocol compared to the EB-protocol.

Taken all together, the work described in chapter 3 corroborates the relevancy of using iDAn cultures as a PD *in vitro* cell model since they recapitulate many of the molecular properties of the A9 ventral midbrain DAn, which are the most affected by the disease *in vivo*.

7.2|Control, A53T SNCA and SNCA triplications iPSC lines as an *in vitro* cell model

Although iPSCs are pluripotent, not all lines differentiate with the same efficiency, and not necessarily to all lineages. Moreover, phenotypic heterogeneity between different iPSC lines and reduced reproducibility from multiple differentiations is certainly expected as compared to more established animal or existing cell models.

The first level of variability comes from the genetic background of the cells that reflects the genetic heterogeneity that distinguishes every human being from another. Secondly, iPSC clones from the same line will possess a certain degree of variability introduced by the reprogramming process itself and by the fact that each clone is derived from a single fibroblast, which in turn could carry heterogeneous somatic genetic polymorphisms. Last, variability could arise within the culture over time possibly because of the generation of mixed cell populations that inevitably are derived using current differentiation protocols.

To date, variability among iPSC lines can be addressed in two ways. The first

approach was used in this work and consists of using multiple iPSC lines from different donors to account for biological variability. However, these cells need to be thoroughly characterised both as iPSCs and upon differentiation to iDAn to be able to compare them to each other. The second method consists in the generation of isogenic control lines, but this is only possible if the cells carry a causative genetic mutation. This approach reduces the heterogeneity arising from using multiple disease and control lines. Yet, because gene editing is a long and inefficient process, the analysis is generally restricted to the study of one iPSC line and its isogenic control. It should be noted that, whilst this approach is certainly valid to study the effect of single gene mutation on cell biology, it fails to compare the disease line to one derived from a healthy individual. Ideally, the analysis of multiple iPSC lines and clones from both control and patients, isogenic lines and the genetic engineering of the mutation in control lines would allow to compensate for the biological variably and generate very robust data. However, iPSCs availability is also limited by the fact that specific genetic mutations may be very rare.

Chapter 4 described the identification and initial characterisation of iPSC lines from healthy individuals and PD patients carrying either A53T *SNCA* or a triplication of the *SNCA* region. All iPSC lines were generated using non-integrating Sendai viruses and thoroughly characterised. Three lines from healthy individuals and three from A53T *SNCA* PD patients were identified and their genotype confirmed. Because only one donor bearing a triplication of *SNCA* was available, all three clones available for this line were included in this study to account for clonal variability. All iPSC lines that were selected to be included in the phenotypic analysis differentiated with similar efficiency, on average to 77% neurons ($TUJ1^+$) and 44% DAn (TH^+), of which 70% were also co-expressing the ventral midbrain marker FOXA2. This represents a gold standard in the field and aims to exclude the possibility of phenotypic differences arising from variations in differentiation efficiency or

neuronal maturity.

Altogether these results showed that all iPSC lines identified for this study differentiated with the same efficiency and could therefore be used for the phenotypic analysis and compared to each other. This represents one of the main advantages of this study, since previous work with iPSC carrying these same mutations was restricted to the comparison of one A53T *SNCA* line to its isogenic control (Ryan et al. 2013; Chung et al. 2016) or one *SNCA* triplication line to iPSC from an unaffected sibling (Byers et al. 2011; Devine et al. 2011).

7.3|Phenotypic analysis in A53T *SNCA* and *SNCA* triplication iDAn

Cells from sporadic PD patients are without doubt relevant to study PD pathology since they represent more than 90% of the cases. Yet, because of the cardinal role of αSyn in PD pathology, A53T *SNCA* and *SNCA* Tripl iPSCs used in this study were expected to be informative on the pathological mechanisms associated with the disease that may go beyond these very rare genetic cases.

Chapter 5 aimed to determine whether iDAn cultures from PD patients carrying the A53T *SNCA* mutation or a triplication of *SNCA* could recapitulate phenotypes previously reported in the field using animal and cell PD models and to uncover novel pathological mechanisms associated to αSyn. An increase in total protein levels of αSyn was expected, especially in *SNCA* Tripl iDAn, but could not be detected, probably due to the heterogeneity and variability in αSyn expression in the neuronal cultures. Nonetheless, an increase in the percentage of TH^+ cells with intracellular αSyn staining was detected in all PD iDAn samples. This phenotype is probably the most common among studies involving iDAn from PD patients with different genetic backgrounds. In mutant Pink1 and

Parkin iDAn, ~20-40% of TH+ cells had intracellular αSyn staining, compared to only ~10% in control cells (Chung et al. 2016). Similarly, ~75% of TH+ cells in G2019S LRRK2 iDAn had cytoplasmic αSyn staining compared to ~20% in control and idiopathic PD neurons (Sánchez-Danés, Richaud-Patin, et al. 2012). Heterozygous N370S GBA iDAn were also shown to have 1.5 fold increase in αSyn expression in the soma of TH+ cells (Woodard et al. 2014). This further reassures the relevance of this *in vitro* cell model to study PD and αSyn pathology. Novel in the field was the use of αSyn-PLA in iDAn to detect increased oligomerization of αSyn in TH+ cells in PD iDAn samples, giving an important insight on αSyn aggregation that is normally only detected using native western blot. It is still debated whether oligomers or fibrils are the most toxic species that cause neurodegeneration. This methodology is well placed to study αSyn aggregation in a relevant *in vitro* cell model and as a screening platform for therapies aiming to reduce αSyn oligomerization, since it could be used in a high-throughput format with automated detection using software for image analysis.

Mitochondria dysfunction has been broadly associated with PD (Ryan et al. 2015) and A53T *SNCA* iDAn were previously shown to be characterised by nitrosative stress linked to impaired mitochondria function (Ryan et al. 2013). As expected, A53T *SNCA* this iDAn were found to have decreased basal oxygen consumption rate and ATP production. Yet, a complete analysis of mitochondria function further described a decrease in maximal respiration and spare capacity, which was not previously addressed by Ryan and colleagues (Ryan et al. 2013), and the use of three iPSC lines per genotype further supports this phenotype. Importantly, experimental evidence suggests that this phenotype is not an intrinsic property of these iPSC lines but is specific to iDAn, which is something that is not currently considered in the literature. It cannot be excluded that there is a specific role for αSyn in mitochondria in different cell types. Other neuronal and non-neuronal cell types

do express αSyn, including macrophages (Haenseler et al., submitted) and fibroblasts (Mak et al. 2011), but might not be directly affected or might relay more on glycolytic activity than oxidative phosphorylation to meet their energy demands. A novel finding regarding decreased phosphorylation of DRP1^{Ser616} was detected and points towards a mechanism involving altered mitochondrial fission/fusion that could be either upstream or downstream of the decreased oxygen consumption rate. Little is known about mitochondrial fission/fusion in post-mitotic neurons but the work by Cho and colleagues points towards a more complex mechanisms governing mitochondria homeostasis compared to those of proliferating cells (Cho et al. 2014). Interestingly, increased levels of PGC-1α were detected in A53T *SNCA* iDAn. This is again in contrast with previous work published by the Lipton laboratory; it is worth mentioning that in this case only one A53T *SNCA* line was compared to its isogenic control and only showed a decreased expression of PGC-1α at the mRNA level (Ryan et al. 2013). The PGC-1α phenotype described in this thesis is more robust due to the analysis of multiple A53T *SNCA* and Control iDAn lines over multiple independent differentiations.

Induction of ER stress was detected in A53T *SNCA* and *SNCA* Tripl iDAn, consistent with previous reports in both iPSC-derived cortical neurons (Chung et al. 2013), animal and immortalised cell line models (Colla et al. 2012; Smith et al. 2005) and post-mortem PD brains (Credle et al. 2015). Increased BiP levels were detected only in A53T *SNCA* cultures, whereas both A53T *SNCA* and *SNCA* Tripl iDAn showed up-regulation of IRE1α. This phenotype also recapitulates previous work done in the laboratory by H. Fernandes using heterozygous N370S GBA iDAn (Fernandes et al. 2016), suggesting that ER stress might be a cardinal feature of PD pathology. Intracellular degradative pathways were also shown to be dysregulated. The increase in p62 and decrease in processing of LC3 are in line with previous studies in immortalised cell lines and can be linked with αSyn

oligomerization (Winslow et al. 2010), but whether this is upstream or downstream of αSyn is yet to be determined. Interestingly, the presence of the A53T mutation in αSyn did not evoke any CMA dysfunction, contrary to what was reported previously (Cuervo et al. 2004). GBA activity was found to be increased in PD iDAn, which is in contrast to previous reports suggesting GBA inhibition as a consequence of of αSyn accumulation (Mazzulli, Zunke, Isacson, et al. 2016). In this study, the small but significant increase in GBA activity might be a compensatory cellular mechanism to increased αSyn levels and oligomerization, as opposed to the late-stage phenotype reported by Mazzulli and colleagues in >300 days old iDAn cultures.

Lastly, preliminary results regarding dysregulation of FA homeostasis and metabolism were detected, which represent novel and interesting findings, not only in iDAn, but also in PD. A marked decrease in FABP7, a brain-specific FA binding protein, and a decrease in CYP46A1, the neuron-specific enzyme involved in cholesterol degradation, suggest an imbalance in FA handling and metabolism in PD iDAn. These results point towards a wide bioenergetic impairment, at least in terms of mitochondria function and lipid metabolism, which is a relevant contribution to the understanding of PD pathology. Supporting this is the finding that levels of the master regulator of cellular bioenergetics SIRT1 were increased in PD iDAn. Furthermore, increased levels of PGC-1α fit with this model since this transcription factor is involved not only in regulating mitochondria biogenesis but also in intracellular metabolism regulation.

It is perhaps surprising that these cells display phenotypes after only a few weeks in culture, whereas PD generally presents clinically in late adulthood in sporadic cases or between 30 and 60 years of age for monogenic PD cases. However, little is known about the timeframe of the onset of the cellular pathology in patients. Various external factors can play a role in this, especially when comparing the *in vivo* pathology with the *in vitro*

phenotypes. In the *SNpc*, DAn are not on their own but are surrounded by supporting cells like astrocytes and an immune system. It is known that PD symptoms develop only upon a significant cell loss, suggesting the presence of copy mechanisms and perhaps redundancy in function that allow the system to be able to deal with the initial cell loss. In iDAn cultures *in vitro*, cells need to promptly face any physiological or molecular changes and this can result in cellular dysfunction or higher vulnerability detectable at early time points. It can be speculated that a phenotypic analysis would benefit from the follow-up of relevant phenotypes at later stages of neuronal maturation. In the case of this thesis, time limitations and the use of a total of 9 iPSC lines restricted the analysis to 35DIV, that is 2 weeks of final maturation. For example, the fact that no CMA perturbation was detected at this time-point does not preclude that this phenotype might arise in more mature iDAn cultures. It should also be noted that neurons do not become electrophysiologically active until around 80DIV, which precludes the possibility of detecting phenotypes involved in synaptic activity and generation of action potentials at 35DIV.

Altogether, the results described in chapter 5 suggest a multitude of dysregulated pathways in PD iDAn carrying the A53T *SNCA* mutation of a triplication of *SNCA*. At the same time, biological variability was described for the A53T *SNCA* #1 line, which did not manifest any phenotype apart from the increase in αSyn intracellular staining in TH^+ cells, the reduction in mitochondrial respiration and the decrease in FABP7 protein levels. At the same time, the initial characterisation of both iPSCs and iDAn described in chapter 4 allowed to exclude the possibility that these phenotypes are the result of intrinsic variability among iPSC lines or the generation of different cell populations upon differentiation. Once again, this variability points at the importance of using more than one disease iPSC line where possible. Overall, iDAn cultures were essential for the detection of the FABP7 phenotype that might have not been detectable using immortalised cell lines due to their

non-neuronal nature or lack of FABP7 expression. Because of the variety of pathways and processes that seem to be dysregulated in A53T *SNCA* and *SNCA* triplication iDAn, -omics approaches, especially transcriptomics and proteomics, will be well suited to inform on dysfunctions in cellular processes that might be difficult to detect or interpret when specifically looking at single proteins or enzymes.

7.4|Effect of αSyn knockdown in iDAn

Knocking down αSyn in iDAn enables to study its cellular function in cells from healthy individuals and also allows to investigate the contribution of αSyn to phenotypes present in PD iDAn.

The initial work described in chapter 6 relied on the use of siRNAs transfected into iDAn to knockdown αSyn. Despite successful transfection, the potency of the knockdown was very variable and probably affected by the variability in αSyn levels among wells. To increase both delivery efficiency and knockdown potency, lentiviral vectors were developed to deliver shRNAs targeting αSyn mRNA via viral transduction. Upon optimisation of lentiviral transduction, shASYN2 achieved substantial knockdown of αSyn in iDAn. The initial attempt to study the effect of αSyn knockdown on mitochondrial phenotypes in A53T *SNCA* iDAn was affected by the variable results obtained with the measurement of oxygen consumption rate, probably in response to lentiviral infection and the sensitivity of the Seahorse Analyzer. Nonetheless, αSyn knockdown was used successfully to study the functional relationship between αSyn and FABP7, which found an increase in FABP7 levels upon down-regulation of αSyn expression. This phenotype is a unique finding in the field and is supported by the fact that αSyn and FABP7 share sequence homology for a domain that can bind FA and that *Fabp3*$^{-/-}$ mice are more resistant to the toxic effect of MPP^{+},

similar to *Snca*$^{-/-}$ animals (Sharon et al. 2001; Shioda et al. 2014). New lentiviral vectors aimed at better understanding the relationship between αSyn and FABP7, namely shRNAs targeting FABP7 and a construct for FABP7 over-expression, were generated and will be available for continuing the analysis of this novel finding.

Altogether, chapter 6 showed that genetic manipulation is necessary to further investigate or interrogate pathological mechanisms in iDAn. The use of lentiviruses proved to be cardinal to the efficient delivery of shRNAs to down-regulate proteins of interested. Nonetheless, further development of lentiviral constructs and their delivery will allow to explore the full potential of genetic manipulation as in the case of immortalised cell models.

7.5|Future directions

Despite PD being described by J. Parkinson 200 years ago and αSyn being first linked to PD by Polymeropoulos and colleagues two decades ago, there is still no cure for this disease and the pathological mechanisms associated with neurodegeneration are still elusive.

Altogether, the work reported in this thesis demonstrates the relevance of iDAn cultures for the study of PD pathology *in vitro* and some future directions may be outlined from it. Differentiation protocols generated and optimised during the last decade since the generation of the first iPSC line in 2007 by K. Takahashi are now routinely used worldwide to generate *bona fide* ventral midbrain DAn. Yet the issue of maturation or "ageing" is only just now starting to be appreciated and addressed. Future optimisation of differentiation protocols will need to include the possibility of studying fully mature neurons, especially from an electrophysiological point of view, and/or to include supporting cells, like astrocytes, to better model the human brain *in vitro*.

In the context of using iPSCs for phenotypic analysis in PD, the StemBANCC initiative has been fundamental for the generation of many lines from patients carrying monogenic mutations or from sporadic cases. Differentiation of iPSCs to iDAn is expensive and time-consuming. In an ideal experiment, iPSC lines and their clones from multiple individuals would be considered for any phenotypic analysis. Yet, in some cases the number of lines that are available is limited by the rarity of specific mutations or by the differentiation efficiency that characterises each line or clone. In future, priority should be given to the use of multiple lines, considering costs and time, and to a thorough characterisation of the differentiated cells to validate the cell model and exclude any intrinsic differences that may cofound a phenotype. At the same time, the generation of isogenic control or gene edited lines should be included to further validate the findings. Nonetheless, the comparison between multiple disease and control lines should still be the gold-standard to account for biological variability, when possible.

Because iDAn cultures are a relatively new *in vitro* cell model, little is known about their physiology and intracellular mechanisms. It would be useful to consider the use of pharmacological treatment as a positive control when interrogating a specific pathway, given the novelty of this cell model. A good example is the decrease in phosphorylated DRP1^{Ser616} levels. Most of the literature regarding mitochondrial fission/fusion points towards network fragmentation upon increased phosphorylation of DRP1^{Ser616} in dividing cells (Taguchi et al. 2007). However, Cyclin-dependent kinase 5 (CDK5) was found to phosphorylate DRP1^{Ser616} specifically in post-mitotic neurons and to reduce its fission-promoting activity (Cho et al. 2014). Consequently, the decrease in phosphorylation of DRP1^{Ser616} in PD iDAn may underlie mitochondria fragmentation. In other cases, like the analysis of ER stress, drug treatment with specific compounds known to trigger ER stress, such as tunicamycin, may inform on whether molecular changes detected in PD iDAn can

be recapitulated in control cells or to further dissect the molecular pathways involved. It is perhaps not surprising that the molecular pathways governing cellular homeostasis in iPSC-derived cells are somewhat more complex than in immortalised cells lines or animal-derived primary cultures and their study would benefit from using molecules that aim to evoke specific perturbations.

As shown in this work, iPSC can reveal pathological mechanisms, but genetic manipulation is then necessary to follow through in a targeted manner on those observations, and this approach would benefit from the development of robust and efficient ways to deliver genetic material to these cells (Miller et al. 2013; Ryan et al. 2013). Genetic engineering using CRISPRs would be essential for the generation of useful iPSC lines like *SNCA*-eGFP or *SNCA*$^{-/-}$. At the same time, the possibility to deliver reporter gene constructs is crucial. Some of the most interesting genetic tools that could be applied to the work described in this thesis include: MitoTimer to analyse mitochondria turnover (Hernandez et al. 2013); luciferase reporter genes for the activation of XBP1 and ATF6 involved in ER stress (Samali et al. 2010); a LC3-eGFP-mCherry reporter to monitor autophagy flux (Pankiv et al. 2007).

The study of αSyn in iDAn is certainly promising because it offers the possibility to analyse disease relevant phenotypes in a highly relevant model without relying on the over-expression of the protein. Discrepancies among phenotypes in iDAn are probably the results of differences in differentiation protocols, iPSC lines used and the time-point chosen for the analysis. Because of the complexity and variability of iPSCs and iDAn, -omics approaches are well placed to detect changes that may be not be approachable when focusing on single targets via quantification of mRNA or protein levels. These datasets will provide valuable insight into changes in gene networks, proteome, metabolome and lipidome that have an impact on human iDAn and are relevant to the onset of PD.

References

Abeliovich, A., Y. Schmitz, I. Fariñas, D. Choi-Lundberg, W. H. Ho, P. E. Castillo, N. Shinsky, J. M. Verdugo, M. Armanini, A. Ryan, M. Hynes, H. Phillips, D. Sulzer, and A. Rosenthal. 2000. 'Mice lacking alpha-synuclein display functional deficits in the nigrostriatal dopamine system', *Neuron*, 25: 239-52.

Abeywardana, Tharindumala, Yu H. Lin, Ruth Rott, Simone Engelender, and Matthew R. Pratt. 2013. 'Site-Specific Differences in Proteasome-Dependent Degradation of Monoubiquitinated α-Synuclein', *Chemistry & biology*, 20: 1207-13.

Alegre-Abarrategui, Javier, Helen Christian, Michele M. Lufino, Ruxandra Mutihac, Lara L. Venda, Olaf Ansorge, and Richard Wade-Martins. 2009. 'LRRK2 regulates autophagic activity and localizes to specific membrane microdomains in a novel human genomic reporter cellular model', *Human molecular genetics*, 18: 4022-34.

Alves, G., M. Kurz, S. A. Lie, and J. P. Larsen. 2004. 'Cigarette smoking in Parkinson's disease: influence on disease progression', *Mov Disord*, 19: 1087-92.

Anderson, John P., Donald E. Walker, Jason M. Goldstein, Rian de Laat, Kelly Banducci, Russell J. Caccavello, Robin Barbour, Jiping Huang, Kristin Kling, Michael Lee, Linnea Diep, Pamela S. Keim, Xiaofeng Shen, Tim Chataway, Michael G. Schlossmacher, Peter Seubert, Dale Schenk, Sukanto Sinha, Wei P. Gai, and Tamie J. Chilcote. 2006. 'Phosphorylation of Ser-129 is the dominant pathological modification of alpha-synuclein in familial and sporadic Lewy body disease', *The Journal of biological chemistry*, 281: 29739-52.

Anwar, Sabina, Owen Peters, Steven Millership, Natalia Ninkina, Natalie Doig, Natalie Connor-Robson, Sarah Threlfell, Gurdeep Kooner, Robert M. Deacon, David M. Bannerman, J. P. Bolam, Sreeganga S. Chandra, Stephanie J. Cragg, Richard Wade-Martins, and Vladimir L. Buchman. 2011. 'Functional alterations to the nigrostriatal system in mice lacking all three members of the synuclein family', *The Journal of neuroscience*, 31: 7264-74.

Appel-Cresswell, Silke, Carles Vilarino-Guell, Mary Encarnacion, Holly Sherman, Irene Yu, Brinda Shah, David Weir, Christina Thompson, Chelsea Szu-Tu, Joanne Trinh, Jan O. Aasly, Alex Rajput, Ali H. Rajput, A. Jon Stoessl, and Matthew J. Farrer. 2013. 'Alpha-synuclein p.H50Q, a novel pathogenic mutation for Parkinson's disease', *Movement disorders*, 28: 811-13.

Arima, K., S. Hirai, N. Sunohara, K. Aoto, Y. Izumiyama, K. Uéda, K. Ikeda, and M. Kawai. 1999. 'Cellular co-localization of phosphorylated tau- and NACP/alpha-synuclein-epitopes in lewy bodies in sporadic Parkinson's disease and in dementia with Lewy bodies', *Brain research*, 843: 53-61.

Aschner, M., K. M. Erikson, E. Herrero Hernández, E. H. Hernández, and R. Tjalkens. 2009. 'Manganese and its role in Parkinson's disease: from transport to neuropathology', *Neuromolecular Med*, 11: 252-66.

Assayag, K., E. Yakunin, V. Loeb, D. J. Selkoe, and R. Sharon. 2007. 'Polyunsaturated fatty

acids induce alpha-synuclein-related pathogenic changes in neuronal cells', *Am J Pathol*, 171: 2000-11.

Bar-Nur, O., H. A. Russ, S. Efrat, and N. Benvenisty. 2011. 'Epigenetic memory and preferential lineage-specific differentiation in induced pluripotent stem cells derived from human pancreatic islet beta cells', *Cell Stem Cell*, 9: 17-23.

Barbeau, A. 1969. 'L-dopa therapy in Parkinson's disease: a critical review of nine years' experience', *Canadian Medical Association journal*, 101: 59-68.

Barceló-Coblijn, G., M. Y. Golovko, I. Weinhofer, J. Berger, and E. J. Murphy. 2007. 'Brain neutral lipids mass is increased in alpha-synuclein gene-ablated mice', *J Neurochem*, 101: 132-41.

Bardy, C., M. van den Hurk, T. Eames, C. Marchand, R. V. Hernandez, M. Kellogg, M. Gorris, B. Galet, V. Palomares, J. Brown, A. G. Bang, J. Mertens, L. Böhnke, L. Boyer, S. Simon, and F. H. Gage. 2015. 'Neuronal medium that supports basic synaptic functions and activity of human neurons in vitro', *Proceedings of the National Academy of Sciences of the United States of America*, 112: E2725-34.

Barker, R. A., J. Barrett, S. L. Mason, and A. Björklund. 2013. 'Fetal dopaminergic transplantation trials and the future of neural grafting in Parkinson's disease', *Lancet Neurol*, 12: 84-91.

Bartels, Tim, Joanna G. Choi, and Dennis J. Selkoe. 2011. 'α-Synuclein occurs physiologically as a helically folded tetramer that resists aggregation', *Nature*, 477: 107-10.

Bates, T. E., S. J. Heales, S. E. Davies, P. Boakye, and J. B. Clark. 1994. 'Effects of 1-methyl-4-phenylpyridinium on isolated rat brain mitochondria: evidence for a primary involvement of energy depletion', *J Neurochem*, 63: 640-8.

Ben-David, U., and N. Benvenisty. 2011. 'The tumorigenicity of human embryonic and induced pluripotent stem cells', *Nat Rev Cancer*, 11: 268-77.

Bernstein, E., A. A. Caudy, S. M. Hammond, and G. J. Hannon. 2001. 'Role for a bidentate ribonuclease in the initiation step of RNA interference', *Nature*, 409: 363-6.

Bertolotti, A., Y. Zhang, L. M. Hendershot, H. P. Harding, and D. Ron. 2000. 'Dynamic interaction of BiP and ER stress transducers in the unfolded-protein response', *Nat Cell Biol*, 2: 326-32.

Betarbet, R., T. B. Sherer, G. MacKenzie, M. Garcia-Osuna, A. V. Panov, and J. T. Greenamyre. 2000. 'Chronic systemic pesticide exposure reproduces features of Parkinson's disease', *Nature neuroscience*, 3: 1301-06.

Beyer, Katrin, Montserrat Domingo-Sábat, José I. Lao, Cristina Carrato, Isidro Ferrer, and Aurelio Ariza. 2008. 'Identification and characterization of a new alpha-synuclein isoform and its role in Lewy body diseases', *Neurogenetics*, 9: 15-23.

Bibbiani, F., L. C. Costantini, R. Patel, and T. N. Chase. 2005. 'Continuous dopaminergic stimulation reduces risk of motor complications in parkinsonian primates', *Exp Neurol*, 192: 73-8.

Björklund, Anders, and Stephen B. Dunnett. 2007. 'Dopamine neuron systems in the brain: an update', *Trends in neurosciences*, 30: 194-202.

Blø, M., J. M. Bogenberger, S. E. Swift, D. R. Micklem, and J. B. Lorens. 2007. 'Expanding the spectrum of genetic elements transferable by retroviral vectors', *DNA Cell Biol*, 26: 773-9.

Braak, H., D. Sandmann-Keil, W. Gai, and E. Braak. 1999. 'Extensive axonal Lewy neurites in Parkinson's disease: a novel pathological feature revealed by alpha-synuclein immunocytochemistry', *Neuroscience letters*, 265: 67-69.

Braak, Heiko, Kelly Del Tredici, Udo Rüb, Rob A. de Vos, Ernst N. Jansen Steur, and Eva

Braak. 2003. 'Staging of brain pathology related to sporadic Parkinson's disease', *Neurobiology of aging*, 24: 197-211.

Breit, S., J. B. Schulz, and A. L. Benabid. 2004. 'Deep brain stimulation', *Cell Tissue Res*, 318: 275-88.

Brummelkamp, T. R., R. Bernards, and R. Agami. 2002. 'A system for stable expression of short interfering RNAs in mammalian cells', *Science*, 296: 550-3.

Burré, Jacqueline, Manu Sharma, and Thomas C. Südhof. 2014. 'α-Synuclein assembles into higher-order multimers upon membrane binding to promote SNARE complex formation', *Proceedings of the National Academy of Sciences of the United States of America*, 111: 83.

Burré, Jacqueline, Manu Sharma, Theodoros Tsetsenis, Vladimir Buchman, Mark R. Etherton, and Thomas C. Südhof. 2010. 'Alpha-synuclein promotes SNARE-complex assembly in vivo and in vitro', *Science (New York, N.Y.)*, 329: 1663-67.

Burré, Jacqueline, Sandro Vivona, Jiajie Diao, Manu Sharma, Axel T. Brunger, and Thomas C. Südhof. 2013. 'Properties of native brain α-synuclein', *Nature*, 498.

Byers, Blake, Branden Cord, Ha N. Nguyen, Birgitt Schüle, Lief Fenno, Patrick C. Lee, Karl Deisseroth, J. W. Langston, Renee R. Pera, and Theo D. Palmer. 2011. 'SNCA triplication Parkinson's patient's iPSC-derived DA neurons accumulate α-synuclein and are susceptible to oxidative stress', *PloS one*, 6.

Cabin, Deborah E., Kazuhiro Shimazu, Diane Murphy, Nelson B. Cole, Wolfram Gottschalk, Kellie L. McIlwain, Bonnie Orrison, Amy Chen, Christopher E. Ellis, Richard Paylor, Bai Lu, and Robert L. Nussbaum. 2002. 'Synaptic vesicle depletion correlates with attenuated synaptic responses to prolonged repetitive stimulation in mice lacking alpha-synuclein', *The Journal of neuroscience*, 22: 8797-807.

Cai, J., A. Donaldson, M. Yang, M. S. German, G. Enikolopov, and L. Iacovitti. 2009. 'The role of Lmx1a in the differentiation of human embryonic stem cells into midbrain dopamine neurons in culture and after transplantation into a Parkinson's disease model', *Stem Cells*, 27: 220-9.

Calfon, M., H. Zeng, F. Urano, J. H. Till, S. R. Hubbard, H. P. Harding, S. G. Clark, and D. Ron. 2002. 'IRE1 couples endoplasmic reticulum load to secretory capacity by processing the XBP-1 mRNA', *Nature*, 415: 92-6.

Cantó, C., and J. Auwerx. 2009. 'PGC-1alpha, SIRT1 and AMPK, an energy sensing network that controls energy expenditure', *Curr Opin Lipidol*, 20: 98-105.

Chambers, Stuart M., Christopher A. Fasano, Eirini P. Papapetrou, Mark Tomishima, Michel Sadelain, and Lorenz Studer. 2009. 'Highly efficient neural conversion of human ES and iPS cells by dual inhibition of SMAD signaling', *Nature biotechnology*, 27: 275-80.

Chan, C. S., T. S. Gertler, and D. J. Surmeier. 2010. 'A molecular basis for the increased vulnerability of substantia nigra dopamine neurons in aging and Parkinson's disease', *Mov Disord*, 25 Suppl 1: S63-70.

Chandra, S., F. Fornai, H. B. Kwon, U. Yazdani, D. Atasoy, X. Liu, R. E. Hammer, G. Battaglia, D. C. German, P. E. Castillo, and T. C. Südhof. 2004. 'Double-knockout mice for alpha- and beta-synucleins: effect on synaptic functions', *Proceedings of the National Academy of Sciences of the United States of America*, 101: 14966-71.

Chandra, S., G. Gallardo, R. Fernández-Chacón, O. M. Schlüter, and T. C. Südhof. 2005. 'Alpha-synuclein cooperates with CSPalpha in preventing neurodegeneration', *Cell*, 123: 383-96.

Chang, Kuo-Hsuan H., Guey-Jen J. Lee-Chen, Yih-Ru R. Wu, Yi-Jing J. Chen, Jia-Li L. Lin, Meng Li, I. Cheng C. Chen, Yen-Shi S. Lo, Hsiu-Chuan C. Wu, and Chiung-Mei M. Chen. 2016. 'Impairment of proteasome and anti-oxidative pathways in the

induced pluripotent stem cell model for sporadic Parkinson's disease', *Parkinsonism & related disorders*.

Chartier-Harlin, Marie-Christine C., Jennifer Kachergus, Christophe Roumier, Vincent Mouroux, Xavier Douay, Sarah Lincoln, Clotilde Levecque, Lydie Larvor, Joris Andrieux, Mary Hulihan, Nawal Waucquier, Luc Defebvre, Philippe Amouyel, Matthew Farrer, and Alain Destée. 2004. 'Alpha-synuclein locus duplication as a cause of familial Parkinson's disease', *Lancet*, 364: 1167-69.

Checkoway, Harvey, Karen Powers, Terri Smith-Weller, Gary M. Franklin, W. T. Longstreth, and Phillip D. Swanson. 2002. 'Parkinson's disease risks associated with cigarette smoking, alcohol consumption, and caffeine intake', *American journal of epidemiology*, 155: 732-38.

Chen, C., E. E. Dudenhausen, Y. X. Pan, C. Zhong, and M. S. Kilberg. 2004. 'Human CCAAT/enhancer-binding protein beta gene expression is activated by endoplasmic reticulum stress through an unfolded protein response element downstream of the protein coding sequence', *J Biol Chem*, 279: 27948-56.

Chin, M. H., M. J. Mason, W. Xie, S. Volinia, M. Singer, C. Peterson, G. Ambartsumyan, O. Aimiuwu, L. Richter, J. Zhang, I. Khvorostov, V. Ott, M. Grunstein, N. Lavon, N. Benvenisty, C. M. Croce, A. T. Clark, T. Baxter, A. D. Pyle, M. A. Teitell, M. Pelegrini, K. Plath, and W. E. Lowry. 2009. 'Induced pluripotent stem cells and embryonic stem cells are distinguished by gene expression signatures', *Cell Stem Cell*, 5: 111-23.

Chinta, S. J., J. K. Mallajosyula, A. Rane, and J. K. Andersen. 2010. 'Mitochondrial α-synuclein accumulation impairs complex I function in dopaminergic neurons and results in increased mitophagy in vivo', *Neurosci Lett*, 486: 235-9.

Cho, B., H. M. Cho, H. J. Kim, J. Jeong, S. K. Park, E. M. Hwang, J. Y. Park, W. R. Kim, H. Kim, and W. Sun. 2014. 'CDK5-dependent inhibitory phosphorylation of Drp1 during neuronal maturation', *Exp Mol Med*, 46: e105.

Choubey, Vinay, Dzhamilja Safiulina, Annika Vaarmann, Michal Cagalinec, Przemyslaw Wareski, Malle Kuum, Alexander Zharkovsky, and Allen Kaasik. 2011. 'Mutant A53T alpha-synuclein induces neuronal death by increasing mitochondrial autophagy', *The Journal of biological chemistry*, 286: 10814-24.

Chung, Chee Y., Vikram Khurana, Pavan K. Auluck, Daniel F. Tardiff, Joseph R. Mazzulli, Frank Soldner, Valeriya Baru, Yali Lou, Yelena Freyzon, Sukhee Cho, Alison E. Mungenast, Julien Muffat, Maisam Mitalipova, Michael D. Pluth, Nathan T. Jui, Birgitt Schüle, Stephen J. Lippard, Li-Huei H. Tsai, Dimitri Krainc, Stephen L. Buchwald, Rudolf Jaenisch, and Susan Lindquist. 2013. 'Identification and rescue of α-synuclein toxicity in Parkinson patient-derived neurons', *Science (New York, N.Y.)*, 342: 983-87.

Chung, S. Y., S. Kishinevsky, J. R. Mazzulli, J. Graziotto, A. Mrejeru, E. V. Mosharov, L. Puspita, P. Valiulahi, D. Sulzer, T. A. Milner, T. Taldone, D. Krainc, L. Studer, and J. W. Shim. 2016. 'Parkin and PINK1 Patient iPSC-Derived Midbrain Dopamine Neurons Exhibit Mitochondrial Dysfunction and α-Synuclein Accumulation', *Stem Cell Reports*, 7: 664-77.

Ciron, Carine, Lu Zheng, Wojciech Bobela, Graham W. Knott, Teresa C. Leone, Daniel P. Kelly, and Bernard L. Schneider. 2015. 'PGC-1α activity in nigral dopamine neurons determines vulnerability to α-synuclein', *Acta neuropathologica communications*, 3: 16.

Cole, N. B., D. D. Murphy, T. Grider, S. Rueter, D. Brasaemle, and R. L. Nussbaum. 2002. 'Lipid droplet binding and oligomerization properties of the Parkinson's disease protein alpha-synuclein', *J Biol Chem*, 277: 6344-52.

Colgan, S. M., A. A. Hashimi, and R. C. Austin. 2011. 'Endoplasmic reticulum stress and lipid dysregulation', *Expert Rev Mol Med*, 13: e4.

Colla, E., P. H. Jensen, O. Pletnikova, J. C. Troncoso, C. Glabe, and M. K. Lee. 2012. 'Accumulation of toxic α-synuclein oligomer within endoplasmic reticulum occurs in α-synucleinopathy in vivo', *J Neurosci*, 32: 3301-5.

Cooper, Oliver, Gunnar Hargus, Michela Deleidi, Alexandra Blak, Teresia Osborn, Elizabeth Marlow, Kristen Lee, Adam Levy, Eduardo Perez-Torres, Alyssa Yow, and Ole Isacson. 2010. 'Differentiation of human ES and Parkinson's disease iPS cells into ventral midbrain dopaminergic neurons requires a high activity form of SHH, FGF8a and specific regionalization by retinoic acid', *Molecular and cellular neurosciences*, 45: 258-66.

Cooper, Oliver, Hyemyung Seo, Shaida Andrabi, Cristina Guardia-Laguarta, John Graziotto, Maria Sundberg, Jesse R. McLean, Luis Carrillo-Reid, Zhong Xie, Teresia Osborn, Gunnar Hargus, Michela Deleidi, Tristan Lawson, Helle Bogetofte, Eduardo Perez-Torres, Lorraine Clark, Carol Moskowitz, Joseph Mazzulli, Li Chen, Laura Volpicelli-Daley, Norma Romero, Houbo Jiang, Ryan J. Uitti, Zhigao Huang, Grzegorz Opala, Leslie A. Scarffe, Valina L. Dawson, Christine Klein, Jian Feng, Owen A. Ross, John Q. Trojanowski, Virginia M. Lee, Karen Marder, D. J. Surmeier, Zbigniew K. Wszolek, Serge Przedborski, Dimitri Krainc, Ted M. Dawson, and Ole Isacson. 2012. 'Pharmacological rescue of mitochondrial deficits in iPSC-derived neural cells from patients with familial Parkinson's disease', *Science translational medicine*, 4.

Corti, S., M. Nizzardo, C. Simone, M. Falcone, C. Donadoni, S. Salani, F. Rizzo, M. Nardini, G. Riboldi, F. Magri, C. Zanetta, I. Faravelli, N. Bresolin, and G. P. Comi. 2012. 'Direct reprogramming of human astrocytes into neural stem cells and neurons', *Exp Cell Res*, 318: 1528-41.

Crawford, T. Q., and H. Roelink. 2007. 'The notch response inhibitor DAPT enhances neuronal differentiation in embryonic stem cell-derived embryoid bodies independently of sonic hedgehog signaling', *Dev Dyn*, 236: 886-92.

Credle, J. J., P. A. Forcelli, M. Delannoy, A. W. Oaks, E. Permaul, D. L. Berry, V. Duka, J. Wills, and A. Sidhu. 2015. 'α-Synuclein-mediated inhibition of ATF6 processing into COPII vesicles disrupts UPR signaling in Parkinson's disease', *Neurobiol Dis*, 76: 112-25.

Cuervo, Ana M., Leonidas Stefanis, Ross Fredenburg, Peter T. Lansbury, and David Sulzer. 2004. 'Impaired degradation of mutant alpha-synuclein by chaperone-mediated autophagy', *Science (New York, N.Y.)*, 305: 1292-95.

Dahm, R., M. Zeitelhofer, B. Götze, M. A. Kiebler, and P. Macchi. 2008. 'Visualizing mRNA localization and local protein translation in neurons', *Methods Cell Biol*, 85: 293-327.

Dalby, B., S. Cates, A. Harris, E. C. Ohki, M. L. Tilkins, P. J. Price, and V. C. Ciccarone. 2004. 'Advanced transfection with Lipofectamine 2000 reagent: primary neurons, siRNA, and high-throughput applications', *Methods*, 33: 95-103.

Dauer, W., N. Kholodilov, M. Vila, A. C. Trillat, R. Goodchild, K. E. Larsen, R. Staal, K. Tieu, Y. Schmitz, C. A. Yuan, M. Rocha, V. Jackson-Lewis, S. Hersch, D. Sulzer, S. Przedborski, R. Burke, and R. Hen. 2002. 'Resistance of alpha -synuclein null mice to the parkinsonian neurotoxin MPTP', *Proceedings of the National Academy of Sciences of the United States of America*, 99: 14524-9.

Dauer, William, and Serge Przedborski. 2003. 'Parkinson's disease: mechanisms and models', *Neuron*, 39: 889-909.

Davidson, W. S., A. Jonas, D. F. Clayton, and J. M. George. 1998. 'Stabilization of alpha-

synuclein secondary structure upon binding to synthetic membranes', *The Journal of biological chemistry*, 273: 9443-49.

Davis, G. C., A. C. Williams, S. P. Markey, M. H. Ebert, E. D. Caine, C. M. Reichert, and I. J. Kopin. 1979. 'Chronic Parkinsonism secondary to intravenous injection of meperidine analogues', *Psychiatry research*, 1: 249-54.

Davis, R. L., H. Weintraub, and A. B. Lassar. 1987. 'Expression of a single transfected cDNA converts fibroblasts to myoblasts', *Cell*, 51: 987-1000.

de Lau, Lonneke M., and Monique M. Breteler. 2006. 'Epidemiology of Parkinson's disease', *The Lancet. Neurology*, 5: 525-35.

Denham, M., C. Bye, J. Leung, B. J. Conley, L. H. Thompson, and M. Dottori. 2012. 'Glycogen synthase kinase 3β and activin/nodal inhibition in human embryonic stem cells induces a pre-neuroepithelial state that is required for specification to a floor plate cell lineage', *Stem Cells*, 30: 2400-11.

Dermentzaki, Georgia, Evangelia Dimitriou, Maria Xilouri, Helen Michelakakis, and Leonidas Stefanis. 2013. 'Loss of β-Glucocerebrosidase Activity Does Not Affect Alpha-Synuclein Levels or Lysosomal Function in Neuronal Cells', *PloS one*, 8.

Desplats, P., H. J. Lee, E. J. Bae, C. Patrick, E. Rockenstein, L. Crews, B. Spencer, E. Masliah, and S. J. Lee. 2009. 'Inclusion formation and neuronal cell death through neuron-to-neuron transmission of alpha-synuclein', *Proceedings of the National Academy of Sciences of the United States of America*, 106: 13010-5.

Dettmer, Ulf, Andrew J. Newman, Eric S. Luth, Tim Bartels, and Dennis Selkoe. 2013. 'In vivo cross-linking reveals principally oligomeric forms of α-synuclein and β-synuclein in neurons and non-neural cells', *The Journal of biological chemistry*, 288: 6371-85.

Dettmer, Ulf, Andrew J. Newman, Frank Soldner, Eric S. Luth, Nora C. Kim, Victoria E. von Saucken, John B. Sanderson, Rudolf Jaenisch, Tim Bartels, and Dennis Selkoe. 2015. 'Parkinson-causing α-synuclein missense mutations shift native tetramers to monomers as a mechanism for disease initiation', *Nature communications*, 6: 7314.

Devi, Latha, Vijayendran Raghavendran, Badanavalu M. Prabhu, Narayan G. Avadhani, and Hindupur K. Anandatheerthavarada. 2008b. 'Mitochondrial import and accumulation of alpha-synuclein impair complex I in human dopaminergic neuronal cultures and Parkinson disease brain', *The Journal of biological chemistry*, 283: 9089-100.

Devine, Michael J., Mina Ryten, Petr Vodicka, Alison J. Thomson, Tom Burdon, Henry Houlden, Fatima Cavaleri, Masumi Nagano, Nicola J. Drummond, Jan-Willem W. Taanman, Anthony H. Schapira, Katrina Gwinn, John Hardy, Patrick A. Lewis, and Tilo Kunath. 2011. 'Parkinson's disease induced pluripotent stem cells with triplication of the α-synuclein locus', *Nature communications*, 2: 440.

Dhillon, A. S., G. L. Tarbutton, J. L. Levin, G. M. Plotkin, L. K. Lowry, J. T. Nalbone, and S. Shepherd. 2008. 'Pesticide/environmental exposures and Parkinson's disease in East Texas', *J Agromedicine*, 13: 37-48.

Di Fonzo, A., M. C. Dekker, P. Montagna, A. Baruzzi, E. H. Yonova, L. Correia Guedes, A. Szczerbinska, T. Zhao, L. O. Dubbel-Hulsman, C. H. Wouters, E. de Graaff, W. J. Oyen, E. J. Simons, G. J. Breedveld, B. A. Oostra, M. W. Horstink, and V. Bonifati. 2009. 'FBXO7 mutations cause autosomal recessive, early-onset parkinsonian-pyramidal syndrome', *Neurology*, 72: 240-5.

Di Maio, Roberto, Paul J. Barrett, Eric K. Hoffman, Caitlyn W. Barrett, Alevtina Zharikov, Anupom Borah, Xiaoping Hu, Jennifer McCoy, Charleen T. Chu, Edward A. Burton, Teresa G. Hastings, and J. T. Greenamyre. 2016. 'α-Synuclein binds to TOM20 and inhibits mitochondrial protein import in Parkinson's disease', *Science*

translational medicine, 8.

Dickson, Dennis W., Hiroshige Fujishiro, Carolyn Orr, Anthony DelleDonne, Keith A. Josephs, Roberta Frigerio, Melinda Burnett, Joseph E. Parisi, Kevin J. Klos, and J. E. Ahlskog. 2009. 'Neuropathology of non-motor features of Parkinson disease', *Parkinsonism & related disorders*, 15 Suppl 3: 5.

Dodel, R. C., M. Singer, R. Köhne-Volland, T. Szucs, B. Rathay, E. Scholz, and W. H. Oertel. 1998. 'The economic impact of Parkinson's disease. An estimation based on a 3-month prospective analysis', *Pharmacoeconomics*, 14: 299-312.

Doench, J. G., and P. A. Sharp. 2004. 'Specificity of microRNA target selection in translational repression', *Genes Dev*, 18: 504-11.

Doi, Daisuke, Bumpei Samata, Mitsuko Katsukawa, Tetsuhiro Kikuchi, Asuka Morizane, Yuichi Ono, Kiyotoshi Sekiguchi, Masato Nakagawa, Malin Parmar, and Jun Takahashi. 2014. 'Isolation of human induced pluripotent stem cell-derived dopaminergic progenitors by cell sorting for successful transplantation', *Stem cell reports*, 2: 337-50.

Donzé, O., and D. Picard. 2002. 'RNA interference in mammalian cells using siRNAs synthesized with T7 RNA polymerase', *Nucleic Acids Res*, 30: e46.

Dorsey, E. R., R. Constantinescu, J. P. Thompson, K. M. Biglan, R. G. Holloway, K. Kieburtz, F. J. Marshall, B. M. Ravina, G. Schifitto, A. Siderowf, and C. M. Tanner. 2007. 'Projected number of people with Parkinson disease in the most populous nations, 2005 through 2030', *Neurology*, 68: 384-86.

Dos Santos, A. B., G. E. Barreto, and K. A. Kohlmeier. 2014. 'Treatment of sleeping disorders should be considered in clinical management of Parkinson's disease', *Front Aging Neurosci*, 6: 273.

Doxakis, Epaminondas. 2010. 'Post-transcriptional regulation of alpha-synuclein expression by mir-7 and mir-153', *The Journal of biological chemistry*, 285: 12726-34.

Drolet, R. E., B. Behrouz, K. J. Lookingland, and J. L. Goudreau. 2004. 'Mice lacking alpha-synuclein have an attenuated loss of striatal dopamine following prolonged chronic MPTP administration', *Neurotoxicology*, 25: 761-9.

Dull, T., R. Zufferey, M. Kelly, R. J. Mandel, M. Nguyen, D. Trono, and L. Naldini. 1998. 'A third-generation lentivirus vector with a conditional packaging system', *Journal of virology*, 72: 8463-71.

Ebrahimi-Fakhari, Darius, Ippolita Cantuti-Castelvetri, Zhanyun Fan, Edward Rockenstein, Eliezer Masliah, Bradley T. Hyman, Pamela J. McLean, and Vivek K. Unni. 2011. 'Distinct roles in vivo for the ubiquitin-proteasome system and the autophagy-lysosomal pathway in the degradation of α-synuclein', *The Journal of neuroscience*, 31: 14508-20.

Egawa, N., K. Yamamoto, H. Inoue, R. Hikawa, K. Nishi, K. Mori, and R. Takahashi. 2011. 'The endoplasmic reticulum stress sensor, ATF6α, protects against neurotoxin-induced dopaminergic neuronal death', *J Biol Chem*, 286: 7947-57.

Elbashir, S. M., J. Harborth, W. Lendeckel, A. Yalcin, K. Weber, and T. Tuschl. 2001. 'Duplexes of 21-nucleotide RNAs mediate RNA interference in cultured mammalian cells', *Nature*, 411: 494-8.

Ellis, C. E., E. J. Murphy, D. C. Mitchell, M. Y. Golovko, F. Scaglia, G. C. Barceló-Coblijn, and R. L. Nussbaum. 2005. 'Mitochondrial lipid abnormality and electron transport chain impairment in mice lacking alpha-synuclein', *Mol Cell Biol*, 25: 10190-201.

Erickson, J. T., T. A. Brosenitsch, and D. M. Katz. 2001. 'Brain-derived neurotrophic factor and glial cell line-derived neurotrophic factor are required simultaneously for survival of dopaminergic primary sensory neurons in vivo', *J Neurosci*, 21: 581-9.

Eschbach, Judith, Björn von Einem, Kathrin Müller, Hanna Bayer, Annika Scheffold, Bradley E. Morrison, K. L. Rudolph, Dietmar R. Thal, Anke Witting, Patrick Weydt, Markus Otto, Michael Fauler, Birgit Liss, Pamela J. McLean, Albert R. Spada, Albert C. Ludolph, Jochen H. Weishaupt, and Karin M. Danzer. 2015. 'Mutual exacerbation of peroxisome proliferator-activated receptor γ coactivator 1α deregulation and α-synuclein oligomerization', *Annals of neurology*, 77: 15-32.

Etlinger, J. D., and A. L. Goldberg. 1977. 'A soluble ATP-dependent proteolytic system responsible for the degradation of abnormal proteins in reticulocytes', *Proceedings of the National Academy of Sciences of the United States of America*, 74: 54-8.

Fan, Xuelai, Wu Y. Jin, Jie Lu, Jin Wang, and Yu T. Wang. 2014. 'Rapid and reversible knockdown of endogenous proteins by peptide-directed lysosomal degradation', *Nature neuroscience*, 17: 471-80.

Fantini, J., D. Carlus, and N. Yahi. 2011. 'The fusogenic tilted peptide (67-78) of α-synuclein is a cholesterol binding domain', *Biochim Biophys Acta*, 1808: 2343-51.

Fares, M. B., N. Ait-Bouziad, I. Dikiy, M. K. Mbefo, A. Jovičić, A. Kiely, J. L. Holton, S. J. Lee, A. D. Gitler, D. Eliezer, and H. A. Lashuel. 2014. 'The novel Parkinson's disease linked mutation G51D attenuates in vitro aggregation and membrane binding of α-synuclein, and enhances its secretion and nuclear localization in cells', *Hum Mol Genet*, 23: 4491-509.

Farrer, M., D. M. Maraganore, and P. Lockhart. 2001. 'α-Synuclein gene haplotypes are associated with Parkinson's disease', *Human molecular ….*

Fasano, Christopher A., Stuart M. Chambers, Gabsang Lee, Mark J. Tomishima, and Lorenz Studer. 2010. 'Efficient derivation of functional floor plate tissue from human embryonic stem cells', *Cell stem cell*, 6: 336-47.

Fauvet, Bruno, Martial K. Mbefo, Mohamed-Bilal B. Fares, Carole Desobry, Sarah Michael, Mustafa T. Ardah, Elpida Tsika, Philippe Coune, Michel Prudent, Niels Lion, David Eliezer, Darren J. Moore, Bernard Schneider, Patrick Aebischer, Omar M. El-Agnaf, Eliezer Masliah, and Hilal A. Lashuel. 2012. 'α-Synuclein in central nervous system and from erythrocytes, mammalian cells, and Escherichia coli exists predominantly as disordered monomer', *The Journal of biological chemistry*, 287: 15345-64.

Fearnley, J. M., and A. J. Lees. 1991. 'Ageing and Parkinson's disease: substantia nigra regional selectivity', *Brain : a journal of neurology*, 114 (Pt 5): 2283-301.

Fernandes, Hugo J., Elizabeth M. Hartfield, Helen C. Christian, Evangelia Emmanoulidou, Ying Zheng, Heather Booth, Helle Bogetofte, Charmaine Lang, Brent J. Ryan, S. P. Sardi, Jennifer Badger, Jane Vowles, Samuel Evetts, George K. Tofaris, Kostas Vekrellis, Kevin Talbot, Michele T. Hu, William James, Sally A. Cowley, and Richard Wade-Martins. 2016. 'ER Stress and Autophagic Perturbations Lead to Elevated Extracellular α-Synuclein in GBA-N370S Parkinson's iPSC-Derived Dopamine Neurons', *Stem cell reports*.

Fernandez, H. H., and J. J. Chen. 2007. 'Monamine oxidase inhibitors: current and emerging agents for Parkinson disease', *Clin Neuropharmacol*, 30: 150-68.

Fernández-Santiago, Rubén, Iria Carballo-Carbajal, Giancarlo Castellano, Roger Torrent, Yvonne Richaud, Adriana Sánchez-Danés, Roser Vilarrasa-Blasi, Alex Sánchez-Pla, José L. L. Mosquera, Jordi Soriano, José López-Barneo, Josep M. Canals, Jordi Alberch, Ángel Raya, Miquel Vila, Antonella Consiglio, José I. I. Martín-Subero, Mario Ezquerra, and Eduardo Tolosa. 2015. 'Aberrant epigenome in iPSC-derived dopaminergic neurons from Parkinson's disease patients', *EMBO molecular medicine*, 7: 1529-46.

Ferrari, D., R. Sanchez-Pernaute, H. Lee, L. Studer, and O. Isacson. 2006. 'Transplanted

dopamine neurons derived from primate ES cells preferentially innervate DARPP-32 striatal progenitors within the graft', *Eur J Neurosci*, 24: 1885-96.

Ferri, A. L., W. Lin, Y. E. Mavromatakis, J. C. Wang, H. Sasaki, J. A. Whitsett, and S. L. Ang. 2007. 'Foxa1 and Foxa2 regulate multiple phases of midbrain dopaminergic neuron development in a dosage-dependent manner', *Development*, 134: 2761-9.

Firbank, M. J., A. J. Yarnall, R. A. Lawson, G. W. Duncan, T. K. Khoo, G. S. Petrides, J. T. O' Brien, R. A. Barker, R. J. Maxwell, D. J. Brooks, and D. J. Burn. 2016. 'Cerebral glucose metabolism and cognition in newly diagnosed Parkinson's disease: ICICLE-PD study', *Journal of Neurology, Neurosurgery & Psychiatry*.

Flierl, Adrian, Luís M. Oliveira, Lisandro J. Falomir-Lockhart, Sally K. Mak, Jayne Hesley, Frank Soldner, Donna J. Arndt-Jovin, Rudolf Jaenisch, J. W. Langston, Thomas M. Jovin, and Birgitt Schüle. 2014. 'Higher vulnerability and stress sensitivity of neuronal precursor cells carrying an alpha-synuclein gene triplication', *PloS one*, 9.

Fountaine, Timothy M., Lara L. Venda, Nicholas Warrick, Helen C. Christian, Patrik Brundin, Keith M. Channon, and Richard Wade-Martins. 2008. 'The effect of alpha-synuclein knockdown on MPP+ toxicity in models of human neurons', *The European journal of neuroscience*, 28: 2459-73.

Fountaine, Timothy M., and Richard Wade-Martins. 2007. 'RNA interference-mediated knockdown of alpha-synuclein protects human dopaminergic neuroblastoma cells from MPP(+) toxicity and reduces dopamine transport', *Journal of neuroscience research*, 85: 351-63.

Fragkouli, Apostolia, and Epaminondas Doxakis. 2014. 'miR-7 and miR-153 protect neurons against MPP(+)-induced cell death via upregulation of mTOR pathway', *Frontiers in cellular neuroscience*, 8: 182.

Friling, S., E. Andersson, L. H. Thompson, M. E. Jönsson, J. B. Hebsgaard, E. Nanou, Z. Alekseenko, U. Marklund, S. Kjellander, N. Volakakis, O. Hovatta, A. El Manira, A. Björklund, T. Perlmann, and J. Ericson. 2009. 'Efficient production of mesencephalic dopamine neurons by Lmx1a expression in embryonic stem cells', *Proceedings of the National Academy of Sciences of the United States of America*, 106: 7613-8.

Fujiwara, Hideo, Masato Hasegawa, Naoshi Dohmae, Akiko Kawashima, Eliezer Masliah, Matthew S. Goldberg, Jie Shen, Koji Takio, and Takeshi Iwatsubo. 2002. 'alpha-Synuclein is phosphorylated in synucleinopathy lesions', *Nature cell biology*, 4: 160-64.

Funayama, Manabu, Kazuko Hasegawa, Hisayuki Kowa, Masaaki Saito, Shoji Tsuji, and Fumiya Obata. 2002. 'A new locus for Parkinson's disease (PARK8) maps to chromosome 12p11.2-q13.1', *Annals of neurology*, 51: 296-301.

Fusaki, Noemi, Hiroshi Ban, Akiyo Nishiyama, Koichi Saeki, and Mamoru Hasegawa. 2009. 'Efficient induction of transgene-free human pluripotent stem cells using a vector based on Sendai virus, an RNA virus that does not integrate into the host genome', *Proceedings of the Japan Academy. Series B, Physical and biological sciences*, 85: 348-62.

Galvagnion, C., A. K. Buell, G. Meisl, T. C. Michaels, M. Vendruscolo, T. P. Knowles, and C. M. Dobson. 2015. 'Lipid vesicles trigger α-synuclein aggregation by stimulating primary nucleation', *Nat Chem Biol*, 11: 229-34.

Geisler, S., K. M. Holmström, D. Skujat, F. C. Fiesel, O. C. Rothfuss, P. J. Kahle, and W. Springer. 2010. 'PINK1/Parkin-mediated mitophagy is dependent on VDAC1 and p62/SQSTM1', *Nat Cell Biol*, 12: 119-31.

George, J. M., H. Jin, W. S. Woods, and D. F. Clayton. 1995. 'Characterization of a novel protein regulated during the critical period for song learning in the zebra finch', *Neuron*, 15: 361-72.

George, Julia M. 2002. 'The synucleins', *Genome biology*, 3.

German, D. C., K. Manaye, W. K. Smith, D. J. Woodward, and C. B. Saper. 1989. 'Midbrain dopaminergic cell loss in Parkinson's disease: computer visualization', *Annals of neurology*, 26: 507-14.

Ghosh, D., M. Mondal, G. M. Mohite, P. K. Singh, P. Ranjan, A. Anoop, S. Ghosh, N. N. Jha, A. Kumar, and S. K. Maji. 2013. 'The Parkinson's disease-associated H50Q mutation accelerates α-Synuclein aggregation in vitro', *Biochemistry*, 52: 6925-7.

Giasson, B. I., J. E. Duda, I. V. J. Murray, and Q. Chen. 2000. 'Oxidative damage linked to neurodegeneration by selective α-synuclein nitration in synucleinopathy lesions', ….

Giasson, B. I., J. E. Duda, S. M. Quinn, B. Zhang, J. Q. Trojanowski, and V. M. Lee. 2002. 'Neuronal alpha-synucleinopathy with severe movement disorder in mice expressing A53T human alpha-synuclein', *Neuron*, 34: 521-33.

Giasson, B. I., I. V. Murray, J. Q. Trojanowski, and V. M. Lee. 2001. 'A hydrophobic stretch of 12 amino acid residues in the middle of alpha-synuclein is essential for filament assembly', *The Journal of biological chemistry*, 276: 2380-86.

Gibson, D. G., L. Young, R. Y. Chuang, J. C. Venter, C. A. Hutchison, and H. O. Smith. 2009. 'Enzymatic assembly of DNA molecules up to several hundred kilobases', *Nat Methods*, 6: 343-5.

Gilbert, Luke A., Matthew H. Larson, Leonardo Morsut, Zairan Liu, Gloria A. Brar, Sandra E. Torres, Noam Stern-Ginossar, Onn Brandman, Evan H. Whitehead, Jennifer A. Doudna, Wendell A. Lim, Jonathan S. Weissman, and Lei S. Qi. 2013. 'CRISPR-mediated modular RNA-guided regulation of transcription in eukaryotes', *Cell*, 154: 442-51.

Gilks, W. P., P. M. Abou-Sleiman, S. Gandhi, S. Jain, A. Singleton, A. J. Lees, K. Shaw, K. P. Bhatia, V. Bonifati, N. P. Quinn, J. Lynch, D. G. Healy, J. L. Holton, T. Revesz, and N. W. Wood. 2005. 'A common LRRK2 mutation in idiopathic Parkinson's disease', *Lancet*, 365: 415-6.

Giordano, S., J. Lee, V. M. Darley-Usmar, and J. Zhang. 2012. 'Distinct effects of Rotenone, 1-methyl-4-phenylpyridinium and 6-hydroxydopamine on cellular bioenergetics and cell death', *PLoS One*, 7: e44610.

Goker-Alpan, O., B. K. Stubblefield, B. I. Giasson, and E. Sidransky. 2010. 'Glucocerebrosidase is present in α-synuclein inclusions in Lewy body disorders', *Acta Neuropathol*, 120: 641-9.

Golovko, M. Y., N. J. Faergeman, N. B. Cole, P. I. Castagnet, R. L. Nussbaum, and E. J. Murphy. 2005. 'Alpha-synuclein gene deletion decreases brain palmitate uptake and alters the palmitate metabolism in the absence of alpha-synuclein palmitate binding', *Biochemistry*, 44: 8251-9.

Gorbatyuk, M. S., A. Shabashvili, W. Chen, C. Meyers, L. F. Sullivan, M. Salganik, J. H. Lin, A. S. Lewin, N. Muzyczka, and O. S. Gorbatyuk. 2012. 'Glucose regulated protein 78 diminishes α-synuclein neurotoxicity in a rat model of Parkinson disease', *Mol Ther*, 20: 1327-37.

Gorell, J. M., C. C. Johnson, B. A. Rybicki, E. L. Peterson, G. X. Kortsha, G. G. Brown, and R. J. Richardson. 1997. 'Occupational exposures to metals as risk factors for Parkinson's disease', *Neurology*, 48: 650-58.

Greggio, Elisa. 2012. 'Role of LRRK2 kinase activity in the pathogenesis of Parkinson's disease', *Biochemical Society transactions*, 40: 1058-62.

Greten-Harrison, Becket, Manuela Polydoro, Megumi Morimoto-Tomita, Ling Diao, Andrew M. Williams, Esther H. Nie, Sachin Makani, Ning Tian, Pablo E. Castillo, Vladimir L. Buchman, and Sreeganga S. Chandra. 2010. 'αβγ-Synuclein triple knockout mice reveal age-dependent neuronal dysfunction', *Proceedings of the National Academy of Sciences of the United States of America*, 107: 19573-78.

Guardia-Laguarta, Cristina, Estela Area-Gomez, Cornelia Rüb, Yuhui Liu, Jordi Magrané, Dorothea Becker, Wolfgang Voos, Eric A. Schon, and Serge Przedborski. 2014. 'α-Synuclein is localized to mitochondria-associated ER membranes', *The Journal of neuroscience*, 34: 249-59.

Guardia-Laguarta, Cristina, Estela Area-Gomez, Eric A. Schon, and Serge Przedborski. 2015. 'A new role for α-Synuclein in Parkinson's disease: Alteration of ER-Mitochondrial communication', *Movement disorders*.

Guerreiro, Patrícia S., Yue Huang, Amanda Gysbers, Danni Cheng, Wei P. Gai, Tiago F. Outeiro, and Glenda M. Halliday. 2013. 'LRRK2 interactions with α-synuclein in Parkinson's disease brains and in cell models', *Journal of molecular medicine (Berlin, Germany)*, 91: 513-22.

Guerreiro, Patrícia S. S., Joana E. Coelho, Inês Sousa-Lima, Paula Macedo, Luísa V. V. Lopes, Tiago F. Outeiro, and Teresa F. Pais. 2016. 'Mutant A53T α-Synuclein Improves Rotarod Performance Before Motor Deficits and Affects Metabolic Pathways', *Neuromolecular medicine*.

Gurdon, J. B. 1962. 'The developmental capacity of nuclei taken from intestinal epithelium cells of feeding tadpoles', *Journal of embryology and experimental morphology*, 10: 622-40.

Hager, S., F. M. Frame, A. T. Collins, J. E. Burns, and N. J. Maitland. 2008. 'An internal polyadenylation signal substantially increases expression levels of lentivirus-delivered transgenes but has the potential to reduce viral titer in a promoter-dependent manner', *Hum Gene Ther*, 19: 840-50.

Haigis, M. C., and D. A. Sinclair. 2010. 'Mammalian sirtuins: biological insights and disease relevance', *Annu Rev Pathol*, 5: 253-95.

Hallett, P. J., M. Deleidi, A. Astradsson, G. A. Smith, O. Cooper, T. M. Osborn, M. Sundberg, M. A. Moore, E. Perez-Torres, A. L. Brownell, J. M. Schumacher, R. D. Spealman, and O. Isacson. 2015. 'Successful function of autologous iPSC-derived dopamine neurons following transplantation in a non-human primate model of Parkinson's disease', *Cell Stem Cell*, 16: 269-74.

Hamilton, Bruce A. 2004. 'alpha-Synuclein A53T substitution associated with Parkinson disease also marks the divergence of Old World and New World primates', *Genomics*, 83: 739-42.

Harper, S. Q., and B. L. Davidson. 2005. 'Plasmid-based RNA interference: construction of small-hairpin RNA expression vectors', *Methods Mol Biol*, 309: 219-35.

Hartfield, E. M., F. Rinaldi, C. P. Glover, L. F. Wong, M. A. Caldwell, and J. B. Uney. 2011. 'Connexin 36 expression regulates neuronal differentiation from neural progenitor cells', *PLoS One*, 6: e14746.

Hartfield, Elizabeth M., Michiko Yamasaki-Mann, Hugo J. Ribeiro Fernandes, Jane Vowles, William S. James, Sally A. Cowley, and Richard Wade-Martins. 2014. 'Physiological characterisation of human iPS-derived dopaminergic neurons', *PloS one*, 9.

Hasegawa, M., H. Fujiwara, T. Nonaka, K. Wakabayashi, H. Takahashi, V. M. Lee, J. Q. Trojanowski, D. Mann, and T. Iwatsubo. 2002. 'Phosphorylated alpha-synuclein is ubiquitinated in alpha-synucleinopathy lesions', *J Biol Chem*, 277: 49071-6.

Hasson, Samuel A., Lesley A. Kane, Koji Yamano, Chiu-Hui H. Huang, Danielle A. Sliter, Eugen Buehler, Chunxin Wang, Sabrina M. Heman-Ackah, Tara Hessa, Rajarshi Guha, Scott E. Martin, and Richard J. Youle. 2013. 'High-content genome-wide RNAi screens identify regulators of parkin upstream of mitophagy', *Nature*, 504: 291-95.

Hatahet, F., and L. W. Ruddock. 2009. 'Protein disulfide isomerase: a critical evaluation of its function in disulfide bond formation', *Antioxid Redox Signal*, 11: 2807-50.

Hatano, T., S. Kubo, S. Imai, M. Maeda, K. Ishikawa, Y. Mizuno, and N. Hattori. 2007. 'Leucine-rich repeat kinase 2 associates with lipid rafts', *Hum Mol Genet*, 16: 678-90.

Hellstrand, E., A. Nowacka, D. Topgaard, S. Linse, and E. Sparr. 2013. 'Membrane lipid co-aggregation with α-synuclein fibrils', *PLoS One*, 8: e77235.

Hendershot, L. M. 2004. 'The ER function BiP is a master regulator of ER function', *Mt Sinai J Med*, 71: 289-97.

Hernandez, G., C. Thornton, A. Stotland, D. Lui, J. Sin, J. Ramil, N. Magee, A. Andres, G. Quarato, R. S. Carreira, M. R. Sayen, R. Wolkowicz, and R. A. Gottlieb. 2013. 'MitoTimer: a novel tool for monitoring mitochondrial turnover', *Autophagy*, 9: 1852-61.

Hetz, C. 2012. 'The unfolded protein response: controlling cell fate decisions under ER stress and beyond', *Nat Rev Mol Cell Biol*, 13: 89-102.

Hong, S., D. Y. Hwang, S. Yoon, O. Isacson, A. Ramezani, R. G. Hawley, and K. S. Kim. 2007. 'Functional analysis of various promoters in lentiviral vectors at different stages of in vitro differentiation of mouse embryonic stem cells', *Mol Ther*, 15: 1630-9.

Hoozemans, J. J., E. S. van Haastert, P. Eikelenboom, R. A. de Vos, J. M. Rozemuller, and W. Scheper. 2007. 'Activation of the unfolded protein response in Parkinson's disease', *Biochem Biophys Res Commun*, 354: 707-11.

Hu, B. Y., J. P. Weick, J. Yu, L. X. Ma, X. Q. Zhang, J. A. Thomson, and S. C. Zhang. 2010. 'Neural differentiation of human induced pluripotent stem cells follows developmental principles but with variable potency', *Proceedings of the National Academy of Sciences of the United States of America*, 107: 4335-40.

Ibáñez, P., A. M. M. Bonnet, B. Débarges, E. Lohmann, F. Tison, P. Pollak, Y. Agid, A. Dürr, and A. Brice. 2004. 'Causal relation between alpha-synuclein gene duplication and familial Parkinson's disease', *Lancet*, 364: 1169-71.

Imaizumi, Yoichi, Yohei Okada, Wado Akamatsu, Masato Koike, Naoko Kuzumaki, Hideki Hayakawa, Tomoko Nihira, Tetsuro Kobayashi, Manabu Ohyama, Shigeto Sato, Masashi Takanashi, Manabu Funayama, Akiyoshi Hirayama, Tomoyoshi Soga, Takako Hishiki, Makoto Suematsu, Takuya Yagi, Daisuke Ito, Arifumi Kosakai, Kozo Hayashi, Masanobu Shouji, Atsushi Nakanishi, Norihiro Suzuki, Yoshikuni Mizuno, Noboru Mizushima, Masayuki Amagai, Yasuo Uchiyama, Hideki Mochizuki, Nobutaka Hattori, and Hideyuki Okano. 2012. 'Mitochondrial dysfunction associated with increased oxidative stress and α-synuclein accumulation in PARK2 iPSC-derived neurons and postmortem brain tissue', *Molecular brain*, 5: 35.

Iranzo, A., H. Stockner, M. Serradell, K. Seppi, F. Valldeoriola, B. Frauscher, J. L. Molinuevo, I. Vilaseca, T. Mitterling, C. Gaig, D. Vilas, J. Santamaria, B. Högl, E. Tolosa, and W. Poewe. 2014. 'Five-year follow-up of substantia nigra echogenicity in idiopathic REM sleep behavior disorder', *Mov Disord*, 29: 1774-80.

Isacson, O., L. M. Bjorklund, and J. M. Schumacher. 2003. 'Toward full restoration of synaptic and terminal function of the dopaminergic system in Parkinson's disease by stem cells', *Ann Neurol*, 53 Suppl 3: S135-46; discussion S46-8.

Ishizawa, Takashi, Petri Mattila, Peter Davies, Dengshun Wang, and Dennis W. Dickson. 2003. 'Colocalization of tau and alpha-synuclein epitopes in Lewy bodies', *Journal of neuropathology and experimental neurology*, 62: 389-97.

Iwai, A., E. Masliah, M. Yoshimoto, N. Ge, L. Flanagan, H. A. de Silva, A. Kittel, and T. Saitoh. 1995. 'The precursor protein of non-A beta component of Alzheimer's disease amyloid is a presynaptic protein of the central nervous system', *Neuron*, 14: 467-75.

Iwatsubo, Takeshi. 2007. 'Pathological biochemistry of alpha-synucleinopathy', *Neuropathology*, 27: 474-78.

Jacobs, K., F. Zambelli, A. Mertzanidou, I. Smolders, M. Geens, H. T. Nguyen, L. Barbé, K. Sermon, and C. Spits. 2016. 'Higher-Density Culture in Human Embryonic Stem Cells Results in DNA Damage and Genome Instability', *Stem Cell Reports*, 6: 330-41.

Jana, Vandrovcova, M. Pittman Alan, Malzer Elke, M. Abou-Sleiman Patrick, J. Lees Andrew, W. Wood Nicholas, and Silva Rohan de. 2009. 'Association of MAPT haplotype-tagging SNPs with sporadic Parkinson's disease', *Neurobiology of Aging*, 30: 1477-82.

Janetzky, B., S. Hauck, M. B. Youdim, P. Riederer, K. Jellinger, F. Pantucek, R. Zöchling, K. W. Boissl, and H. Reichmann. 1994. 'Unaltered aconitase activity, but decreased complex I activity in substantia nigra pars compacta of patients with Parkinson's disease', *Neurosci Lett*, 169: 126-8.

Janezic, Stephanie, Sarah Threlfell, Paul D. Dodson, Megan J. Dowie, Tonya N. Taylor, Dawid Potgieter, Laura Parkkinen, Steven L. Senior, Sabina Anwar, Brent Ryan, Thierry Deltheil, Polina Kosillo, Milena Cioroch, Katharina Wagner, Olaf Ansorge, David M. Bannerman, J. P. Bolam, Peter J. Magill, Stephanie J. Cragg, and Richard Wade-Martins. 2013. 'Deficits in dopaminergic transmission precede neuron loss and dysfunction in a new Parkinson model', *Proceedings of the National Academy of Sciences of the United States of America*, 110: 25.

Jankovic, J. 2008. 'Parkinson's disease: clinical features and diagnosis', *Journal of neurology, neurosurgery, and psychiatry*, 79: 368-76.

Jensen, Stig M., Alexander Schmitz, Finn S. Pedersen, Jørgen Kjems, and Jesper B. Bramsen. 2012. 'Functional selection of shRNA loops from randomized retroviral libraries', *PloS one*, 7.

Jiang, Houbo, Yong Ren, Eunice Y. Yuen, Ping Zhong, Mahboobe Ghaedi, Zhixing Hu, Gissou Azabdaftari, Kazuhiro Nakaso, Zhen Yan, and Jian Feng. 2012. 'Parkin controls dopamine utilization in human midbrain dopaminergic neurons derived from induced pluripotent stem cells', *Nature communications*, 3: 668.

Jo, E., J. McLaurin, C. M. Yip, P. St George-Hyslop, and P. E. Fraser. 2000. 'alpha-Synuclein membrane interactions and lipid specificity', *The Journal of biological chemistry*, 275: 34328-34.

Junn, Eunsung, Kang-Woo W. Lee, Byeong S. Jeong, Teresa W. Chan, Joo-Young Y. Im, and M. M. Mouradian. 2009. 'Repression of alpha-synuclein expression and toxicity by microRNA-7', *Proceedings of the National Academy of Sciences of the United States of America*, 106: 13052-57.

Kabeya, Y., N. Mizushima, T. Ueno, A. Yamamoto, T. Kirisako, T. Noda, E. Kominami, Y. Ohsumi, and T. Yoshimori. 2000. 'LC3, a mammalian homologue of yeast Apg8p, is localized in autophagosome membranes after processing', *EMBO J*, 19: 5720-8.

Kahle, Philipp J. 2008. 'alpha-Synucleinopathy models and human neuropathology: similarities and differences', *Acta neuropathologica*, 115: 87-95.

Karra, Daniela, and Ralf Dahm. 2010. 'Transfection techniques for neuronal cells', *The Journal of neuroscience*, 30: 6171-77.

Kawamoto, Yasuhiro, Ichiro Akiguchi, Shinichi Nakamura, Yasuyuki Honjyo, Hiroshi Shibasaki, and Herbert Budka. 2002. '14-3-3 proteins in Lewy bodies in Parkinson disease and diffuse Lewy body disease brains', *Journal of neuropathology and experimental neurology*, 61: 245-53.

Kawasaki, Hiroshi, Hirofumi Suemori, Kenji Mizuseki, Kiichi Watanabe, Fumi Urano, Hiroshi Ichinose, Masatoshi Haruta, Masayo Takahashi, Kanako Yoshikawa, Shin-

Ichi Nishikawa, Norio Nakatsuji, and Yoshiki Sasai. 2002. 'Generation of dopaminergic neurons and pigmented epithelia from primate ES cells by stromal cell-derived inducing activity', *Proceedings of the National Academy of Sciences of the United States of America*, 99: 1580-85.

Kim, D. S., J. S. Lee, J. W. Leem, Y. J. Huh, J. Y. Kim, H. S. Kim, I. H. Park, G. Q. Daley, D. Y. Hwang, and D. W. Kim. 2010. 'Robust enhancement of neural differentiation from human ES and iPS cells regardless of their innate difference in differentiation propensity', *Stem Cell Rev*, 6: 270-81.

Kim, Dohoon, Chun-Hyung H. Kim, Jung-Il I. Moon, Young-Gie G. Chung, Mi-Yoon Y. Chang, Baek-Soo S. Han, Sanghyeok Ko, Eungi Yang, Kwang Y. Cha, Robert Lanza, and Kwang-Soo S. Kim. 2009. 'Generation of human induced pluripotent stem cells by direct delivery of reprogramming proteins', *Cell stem cell*, 4: 472-76.

Kim, K., A. Doi, B. Wen, K. Ng, R. Zhao, P. Cahan, J. Kim, M. J. Aryee, H. Ji, L. I. Ehrlich, A. Yabuuchi, A. Takeuchi, K. C. Cunniff, H. Hongguang, S. McKinney-Freeman, O. Naveiras, T. J. Yoon, R. A. Irizarry, N. Jung, J. Seita, J. Hanna, P. Murakami, R. Jaenisch, R. Weissleder, S. H. Orkin, I. L. Weissman, A. P. Feinberg, and G. Q. Daley. 2010. 'Epigenetic memory in induced pluripotent stem cells', *Nature*, 467: 285-90.

Kirkeby, Agnete, Shane Grealish, Daniel A. Wolf, Jenny Nelander, James Wood, Martin Lundblad, Olle Lindvall, and Malin Parmar. 2012. 'Generation of regionally specified neural progenitors and functional neurons from human embryonic stem cells under defined conditions', *Cell reports*, 1: 703-14.

Kish, S. J., K. Shannak, and O. Hornykiewicz. 1988. 'Uneven pattern of dopamine loss in the striatum of patients with idiopathic Parkinson's disease. Pathophysiologic and clinical implications', *The New England journal of medicine*, 318: 876-80.

Kitada, T., S. Asakawa, N. Hattori, H. Matsumine, Y. Yamamura, S. Minoshima, M. Yokochi, Y. Mizuno, and N. Shimizu. 1998. 'Mutations in the parkin gene cause autosomal recessive juvenile parkinsonism', *Nature*, 392: 605-08.

Klein, C., and A. Westenberger. 2012. 'Genetics of Parkinson's disease', *Cold Spring Harb Perspect Med*, 2: a008888.

Klivenyi, P., D. Siwek, G. Gardian, L. Yang, A. Starkov, C. Cleren, R. J. Ferrante, N. W. Kowall, A. Abeliovich, and M. F. Beal. 2006. 'Mice lacking alpha-synuclein are resistant to mitochondrial toxins', *Neurobiol Dis*, 21: 541-8.

Koehler, K. R., P. Tropel, J. W. Theile, T. Kondo, T. R. Cummins, S. Viville, and E. Hashino. 2011. 'Extended passaging increases the efficiency of neural differentiation from induced pluripotent stem cells', *BMC Neurosci*, 12: 82.

Kordower, Jeffrey H., Yaping Chu, Robert A. Hauser, Thomas B. Freeman, and C. W. Olanow. 2008. 'Lewy body-like pathology in long-term embryonic nigral transplants in Parkinson's disease', *Nature medicine*, 14: 504-06.

Kriks, Sonja, Jae-Won W. Shim, Jinghua Piao, Yosif M. Ganat, Dustin R. Wakeman, Zhong Xie, Luis Carrillo-Reid, Gordon Auyeung, Chris Antonacci, Amanda Buch, Lichuan Yang, M. F. Beal, D. J. Surmeier, Jeffrey H. Kordower, Viviane Tabar, and Lorenz Studer. 2011. 'Dopamine neurons derived from human ES cells efficiently engraft in animal models of Parkinson's disease', *Nature*, 480: 547-51.

Kroemer, G., and J. C. Reed. 2000. 'Mitochondrial control of cell death', *Nat Med*, 6: 513-9.

Krüger, R., W. Kuhn, T. Müller, D. Woitalla, M. Graeber, S. Kösel, H. Przuntek, J. T. Epplen, L. Schöls, and O. Riess. 1998. 'Ala30Pro mutation in the gene encoding alpha-synuclein in Parkinson's disease', *Nature genetics*, 18: 106-08.

Krüger, R., and Menezes A. M. Vieira-Saecker. 1999. 'Increased susceptibility to sporadic Parkinson's disease by a certain combined α-synuclein/apolipoprotein E genotype',

Annals of ….

Kyttälä, A., R. Moraghebi, C. Valensisi, J. Kettunen, C. Andrus, K. K. Pasumarthy, M. Nakanishi, K. Nishimura, M. Ohtaka, J. Weltner, B. Van Handel, O. Parkkonen, J. Sinisalo, A. Jalanko, R. D. Hawkins, N. B. Woods, T. Otonkoski, and R. Trokovic. 2016. 'Genetic Variability Overrides the Impact of Parental Cell Type and Determines iPSC Differentiation Potential', *Stem Cell Reports*, 6: 200-12.

Lagos-Quintana, M., R. Rauhut, W. Lendeckel, and T. Tuschl. 2001. 'Identification of novel genes coding for small expressed RNAs', *Science*, 294: 853-8.

Lagos-Quintana, M., R. Rauhut, J. Meyer, A. Borkhardt, and T. Tuschl. 2003. 'New microRNAs from mouse and human', *RNA*, 9: 175-9.

Landry, B., H. M. Aliabadi, A. Samuel, H. Gül-Uludağ, X. Jiang, O. Kutsch, and H. Uludağ. 2012. 'Effective non-viral delivery of siRNA to acute myeloid leukemia cells with lipid-substituted polyethylenimines', *PLoS One*, 7: e44197.

Langston, J. W., P. Ballard, J. W. Tetrud, and I. Irwin. 1983. 'Chronic Parkinsonism in humans due to a product of meperidine-analog synthesis', *Science (New York, N.Y.)*, 219: 979-80.

Lars, Bertram, and E. Tanzi Rudolph. 2005. 'The genetic epidemiology of neurodegenerative disease', *Journal of Clinical Investigation*, 115: 1449-57.

Lashuel, Hilal A., Cassia R. Overk, Abid Oueslati, and Eliezer Masliah. 2013. 'The many faces of α-synuclein: from structure and toxicity to therapeutic target', *Nature reviews. Neuroscience*, 14: 38-48.

Lashuel, Hilal A., Benjamin M. Petre, Joseph Wall, Martha Simon, Richard J. Nowak, Thomas Walz, and Peter T. Lansbury. 2002. 'Alpha-synuclein, especially the Parkinson's disease-associated mutants, forms pore-like annular and tubular protofibrils', *Journal of molecular biology*, 322: 1089-102.

Lau, N. C., L. P. Lim, E. G. Weinstein, and D. P. Bartel. 2001. 'An abundant class of tiny RNAs with probable regulatory roles in Caenorhabditis elegans', *Science*, 294: 858-62.

Lee, A. H., N. N. Iwakoshi, and L. H. Glimcher. 2003. 'XBP-1 regulates a subset of endoplasmic reticulum resident chaperone genes in the unfolded protein response', *Mol Cell Biol*, 23: 7448-59.

Lee, H., G. A. Shamy, Y. Elkabetz, C. M. Schofield, N. L. Harrsion, G. Panagiotakos, N. D. Socci, V. Tabar, and L. Studer. 2007. 'Directed differentiation and transplantation of human embryonic stem cell-derived motoneurons', *Stem Cells*, 25: 1931-9.

Lee, R. C., R. L. Feinbaum, and V. Ambros. 1993. 'The C. elegans heterochronic gene lin-4 encodes small RNAs with antisense complementarity to lin-14', *Cell*, 75: 843-54.

Lee, Y., C. Ahn, J. Han, H. Choi, J. Kim, J. Yim, J. Lee, P. Provost, O. Rådmark, S. Kim, and V. N. Kim. 2003. 'The nuclear RNase III Drosha initiates microRNA processing', *Nature*, 425: 415-9.

Lees, Andrew J., John Hardy, and Tamas Revesz. 2009. 'Parkinson's disease', *Lancet*, 373: 2055-66.

Leoni, V., and C. Caccia. 2013. '24S-hydroxycholesterol in plasma: a marker of cholesterol turnover in neurodegenerative diseases', *Biochimie*, 95: 595-612.

Lesage, S., M. Anheim, F. Letournel, L. Bousset, A. Honoré, N. Rozas, L. Pieri, K. Madiona, A. Dürr, R. Melki, C. Verny, A. Brice, and French Parkinson's Disease Genetics Study Group. 2013. 'G51D α-synuclein mutation causes a novel parkinsonian-pyramidal syndrome', *Ann Neurol*, 73: 459-71.

Lesage, Suzanne, and Alexis Brice. 2009. 'Parkinson's disease: from monogenic forms to genetic susceptibility factors', *Human molecular genetics*, 18: 59.

Leverenz, J. B., I. Umar, Q. Wang, T. J. Montine, P. J. McMillan, D. W. Tsuang, J. Jin, C. Pan, J. Shin, D. Zhu, and J. Zhang. 2007. 'Proteomic identification of novel proteins in cortical lewy bodies', *Brain Pathol*, 17: 139-45.

Li, J. Y., E. Englund, J. L. Holton, D. Soulet, P. Hagell, A. J. Lees, T. Lashley, N. P. Quinn, S. Rehncrona, A. Björklund, H. Widner, T. Revesz, O. Lindvall, and P. Brundin. 2008. 'Lewy bodies in grafted neurons in subjects with Parkinson's disease suggest host-to-graft disease propagation', *Nat Med*, 14: 501-3.

Li, Wenxue, Neva West, Emanuela Colla, Olga Pletnikova, Juan C. Troncoso, Laura Marsh, Ted M. Dawson, Pekka Jäkälä, Tobias Hartmann, Donald L. Price, and Michael K. Lee. 2005. 'Aggregation promoting C-terminal truncation of alpha-synuclein is a normal cellular process and is enhanced by the familial Parkinson's disease-linked mutations', *Proceedings of the National Academy of Sciences of the United States of America*, 102: 2162-67.

Li, X. 2013. 'SIRT1 and energy metabolism', *Acta Biochim Biophys Sin (Shanghai)*, 45: 51-60.

Liang, H., and W. F. Ward. 2006. 'PGC-1alpha: a key regulator of energy metabolism', *Adv Physiol Educ*, 30: 145-51.

Lin, Xian, Loukia Parisiadou, Xing-Long L. Gu, Lizhen Wang, Hoon Shim, Lixin Sun, Chengsong Xie, Cai-Xia X. Long, Wan-Jou J. Yang, Jinhui Ding, Zsu Z. Chen, Paul E. Gallant, Jung-Hwa H. Tao-Cheng, Gay Rudow, Juan C. Troncoso, Zhihua Liu, Zheng Li, and Huaibin Cai. 2009. 'Leucine-rich repeat kinase 2 regulates the progression of neuropathology induced by Parkinson's-disease-related mutant alpha-synuclein', *Neuron*, 64: 807-27.

Lindersson, E., R. Beedholm, P. Højrup, T. Moos, W. Gai, K. B. Hendil, and P. H. Jensen. 2004. 'Proteasomal inhibition by alpha-synuclein filaments and oligomers', *J Biol Chem*, 279: 12924-34.

Lindvall, O., S. Rehncrona, P. Brundin, B. Gustavii, B. Astedt, H. Widner, T. Lindholm, A. Björklund, K. L. Leenders, J. C. Rothwell, R. Frackowiak, D. Marsden, B. Johnels, G. Steg, R. Freedman, B. J. Hoffer, A. Seiger, M. Bygdeman, I. Strömberg, and L. Olson. 1989. 'Human fetal dopamine neurons grafted into the striatum in two patients with severe Parkinson's disease. A detailed account of methodology and a 6-month follow-up', *Arch Neurol*, 46: 615-31.

Lindvall, O., H. Widner, S. Rehncrona, P. Brundin, P. Odin, B. Gustavii, R. Frackowiak, K. L. Leenders, G. Sawle, and J. C. Rothwell. 1992. 'Transplantation of fetal dopamine neurons in Parkinson's disease: one-year clinical and neurophysiological observations in two patients with putaminal implants', *Ann Neurol*, 31: 155-65.

Liou, H. H., M. C. Tsai, C. J. Chen, J. S. Jeng, Y. C. Chang, S. Y. Chen, and R. C. Chen. 1997. 'Environmental risk factors and Parkinson's disease: a case-control study in Taiwan', *Neurology*, 48: 1583-88.

Liu, R. Z., R. Mita, M. Beaulieu, Z. Gao, and R. Godbout. 2010. 'Fatty acid binding proteins in brain development and disease', *Int J Dev Biol*, 54: 1229-39.

Lo Bianco, C., J. L. L. Ridet, B. L. Schneider, N. Deglon, and P. Aebischer. 2002. 'alpha -Synucleinopathy and selective dopaminergic neuron loss in a rat lentiviral-based model of Parkinson's disease', *Proceedings of the National Academy of Sciences of the United States of America*, 99: 10813-18.

Lock, F. E., R. Rebollo, K. Miceli-Royer, L. Gagnier, S. Kuah, A. Babaian, M. Sistiaga-Poveda, C. B. Lai, O. Nemirovsky, I. Serrano, C. Steidl, M. M. Karimi, and D. L. Mager. 2014. 'Distinct isoform of FABP7 revealed by screening for retroelement-activated genes in diffuse large B-cell lymphoma', *Proceedings of the National Academy of Sciences of the United States of America*, 111: E3534-43.

Loh, Yuin-Han H., Suneet Agarwal, In-Hyun H. Park, Achia Urbach, Hongguang Huo,

Garrett C. Heffner, Kitai Kim, Justine D. Miller, Kitwa Ng, and George Q. Daley. 2009. 'Generation of induced pluripotent stem cells from human blood', *Blood*, 113: 5476-79.

Luk, Kelvin C., Cheng Song, Patrick O'Brien, Anna Stieber, Jonathan R. Branch, Kurt R. Brunden, John Q. Trojanowski, and Virginia M. Lee. 2009. 'Exogenous alpha-synuclein fibrils seed the formation of Lewy body-like intracellular inclusions in cultured cells', *Proceedings of the National Academy of Sciences of the United States of America*, 106: 20051-56.

Lund, E. G., J. M. Guileyardo, and D. W. Russell. 1999. 'cDNA cloning of cholesterol 24-hydroxylase, a mediator of cholesterol homeostasis in the brain', *Proceedings of the National Academy of Sciences of the United States of America*, 96: 7238-43.

Luth, Eric S., Tim Bartels, Ulf Dettmer, Nora C. Kim, and Dennis J. Selkoe. 2015. 'Purification of α-synuclein from human brain reveals an instability of endogenous multimers as the protein approaches purity', *Biochemistry*, 54: 279-92.

Luth, Eric S., Irina G. Stavrovskaya, Tim Bartels, Bruce S. Kristal, and Dennis J. Selkoe. 2014. 'Soluble, prefibrillar α-synuclein oligomers promote complex I-dependent, Ca2+-induced mitochondrial dysfunction', *The Journal of biological chemistry*, 289: 21490-507.

Lázaro, Diana F., Eva F. Rodrigues, Ramona Langohr, Hedieh Shahpasandzadeh, Thales Ribeiro, Patrícia Guerreiro, Ellen Gerhardt, Katharina Kröhnert, Jochen Klucken, Marcos D. Pereira, Blagovesta Popova, Niels Kruse, Brit Mollenhauer, Silvio O. Rizzoli, Gerhard H. Braus, Karin M. Danzer, and Tiago F. Outeiro. 2014. 'Systematic comparison of the effects of alpha-synuclein mutations on its oligomerization and aggregation', *PLoS genetics*, 10.

Löhle, M., A. Hermann, H. Glass, A. Kempe, S. C. Schwarz, J. B. Kim, C. Poulet, U. Ravens, J. Schwarz, H. R. Schöler, and A. Storch. 2012. 'Differentiation efficiency of induced pluripotent stem cells depends on the number of reprogramming factors', *Stem Cells*, 30: 570-9.

Mak, S. K., D. Tewari, J. W. Tetrud, J. W. Langston, and B. Schüle. 2011. 'Mitochondrial dysfunction in skin fibroblasts from a Parkinson's disease patient with an alpha-synuclein triplication', *J Parkinsons Dis*, 1: 175-83.

Mali, P., L. Yang, K. M. Esvelt, J. Aach, M. Guell, J. E. DiCarlo, J. E. Norville, and G. M. Church. 2013. 'RNA-guided human genome engineering via Cas9', *Science*, 339: 823-6.

Manning-Bog, Amy B., Alison L. McCormack, Maya G. Purisai, Laurel M. Bolin, and Donato A. Di Monte. 2003. 'Alpha-synuclein overexpression protects against Paraquat-induced neurodegeneration', *The Journal of neuroscience*, 23: 3095-99.

Manning-Boğ, A. B., B. Schüle, and J. W. Langston. 2009. 'Alpha-synuclein-glucocerebrosidase interactions in pharmacological Gaucher models: a biological link between Gaucher disease and parkinsonism', *Neurotoxicology*, 30: 1127-32.

Maraganore, D. M., De M. Andrade, and A. Elbaz. 2006. 'Collaborative analysis of α-synuclein gene promoter variability and Parkinson disease', *Jama*.

Maroteaux, L., J. T. Campanelli, and R. H. Scheller. 1988. 'Synuclein: a neuron-specific protein localized to the nucleus and presynaptic nerve terminal', *The Journal of neuroscience*, 8: 2804-15.

Marwarha, G., T. Rhen, T. Schommer, and O. Ghribi. 2011. 'The oxysterol 27-hydroxycholesterol regulates α-synuclein and tyrosine hydroxylase expression levels in human neuroblastoma cells through modulation of liver X receptors and estrogen receptors--relevance to Parkinson's disease', *J Neurochem*, 119: 1119-36.

Masuda-Suzukake, M., T. Nonaka, M. Hosokawa, T. Oikawa, T. Arai, H. Akiyama, D. M.

Mann, and M. Hasegawa. 2013. 'Prion-like spreading of pathological α-synuclein in brain', *Brain*, 136: 1128-38.

Mazzulli, J. R., F. Zunke, T. Tsunemi, N. J. Toker, S. Jeon, L. F. Burbulla, S. Patnaik, E. Sidransky, J. J. Marugan, C. M. Sue, and D. Krainc. 2016. 'Activation of β-Glucocerebrosidase Reduces Pathological α-Synuclein and Restores Lysosomal Function in Parkinson's Patient Midbrain Neurons', *J Neurosci*, 36: 7693-706.

Mazzulli, Joseph R., You-Hai H. Xu, Ying Sun, Adam L. Knight, Pamela J. McLean, Guy A. Caldwell, Ellen Sidransky, Gregory A. Grabowski, and Dimitri Krainc. 2011. 'Gaucher disease glucocerebrosidase and α-synuclein form a bidirectional pathogenic loop in synucleinopathies', *Cell*, 146: 37-52.

Mazzulli, Joseph R., Friederike Zunke, Ole Isacson, Lorenz Studer, and Dimitri Krainc. 2016. 'α-Synuclein-induced lysosomal dysfunction occurs through disruptions in protein trafficking in human midbrain synucleinopathy models', *Proceedings of the National Academy of Sciences of the United States of America*, 113: 1931-36.

McCarthy, Jeanette J., Colton Linnertz, Laura Saucier, James R. Burke, Christine M. Hulette, Kathleen A. Welsh-Bohmer, and Ornit Chiba-Falek. 2011. 'The effect of SNCA 3' region on the levels of SNCA-112 splicing variant', *Neurogenetics*, 12: 59-64.

McRitchie, D. A., H. R. Cartwright, and G. M. Halliday. 1997. 'Specific A10 dopaminergic nuclei in the midbrain degenerate in Parkinson's disease', *Exp Neurol*, 144: 202-13.

Meir, O., E. Dvash, A. Werman, and M. Rubinstein. 2010. 'C/EBP-beta regulates endoplasmic reticulum stress-triggered cell death in mouse and human models', *PLoS One*, 5: e9516.

Meissner, W. G. 2012. 'When does Parkinson's disease begin? From prodromal disease to motor signs', *Rev Neurol (Paris)*, 168: 809-14.

Mena, M. A., M. J. Casarejos, A. Bonin, J. A. Ramos, and J. García Yébenes. 1995. 'Effects of dibutyryl cyclic AMP and retinoic acid on the differentiation of dopamine neurons: prevention of cell death by dibutyryl cyclic AMP', *J Neurochem*, 65: 2612-20.

Merkwirth, C., and T. Langer. 2009. 'Prohibitin function within mitochondria: essential roles for cell proliferation and cristae morphogenesis', *Biochim Biophys Acta*, 1793: 27-32.

Michalak, M., J. Groenendyk, E. Szabo, L. I. Gold, and M. Opas. 2009. 'Calreticulin, a multi-process calcium-buffering chaperone of the endoplasmic reticulum', *Biochem J*, 417: 651-66.

Miller, D. W., S. M. Hague, J. Clarimon, M. Baptista, K. Gwinn-Hardy, M. R. Cookson, and A. B. Singleton. 2004. 'Alpha-synuclein in blood and brain from familial Parkinson disease with SNCA locus triplication', *Neurology*, 62: 1835-38.

Miller, Justine D., Yosif M. Ganat, Sarah Kishinevsky, Robert L. Bowman, Becky Liu, Edmund Y. Tu, Pankaj K. Mandal, Elsa Vera, Jae-won W. Shim, Sonja Kriks, Tony Taldone, Noemi Fusaki, Mark J. Tomishima, Dimitri Krainc, Teresa A. Milner, Derrick J. Rossi, and Lorenz Studer. 2013. 'Human iPSC-based modeling of late-onset disease via progerin-induced aging', *Cell stem cell*, 13: 691-705.

Mudò, G., J. Mäkelä, V. Di Liberto, T. V. Tselykh, M. Olivieri, P. Piepponen, O. Eriksson, A. Mälkiä, A. Bonomo, M. Kairisalo, J. A. Aguirre, L. Korhonen, N. Belluardo, and D. Lindholm. 2012. 'Transgenic expression and activation of PGC-1α protect dopaminergic neurons in the MPTP mouse model of Parkinson's disease', *Cell Mol Life Sci*, 69: 1153-65.

Mueller, J. C., J. Fuchs, A. Hofer, A. Zimprich, P. Lichtner, T. Illig, D. Berg, U. Wüllner, T. Meitinger, and T. Gasser. 2005. 'Multiple regions of alpha-synuclein are associated with Parkinson's disease', *Ann Neurol*, 57: 535-41.

Murray, Ian V., Benoit I. Giasson, Shawn M. Quinn, Vishwanath Koppaka, Paul H. Axelsen, Harry Ischiropoulos, John Q. Trojanowski, and Virginia M. Lee. 2003. 'Role of alpha-synuclein carboxy-terminus on fibril formation in vitro', *Biochemistry*, 42: 8530-40.

Musgrove, R.E., J. Horne, R. Wilson, A.E. King, L. M. Edwards, and T. C. Dickson. 2014. 'The metabolomics of alpha-synuclein (SNCA) gene deletion and mutation in mouse brain', *Metabolomics*, 10.

Muñoz-Sanjuán, I., and A. H. Brivanlou. 2002. 'Neural induction, the default model and embryonic stem cells', *Nat Rev Neurosci*, 3: 271-80.

Nakagawa, T., H. Zhu, N. Morishima, E. Li, J. Xu, B. A. Yankner, and J. Yuan. 2000. 'Caspase-12 mediates endoplasmic-reticulum-specific apoptosis and cytotoxicity by amyloid-beta', *Nature*, 403: 98-103.

Nakamura, Ken, Venu M. Nemani, Farnaz Azarbal, Gaia Skibinski, Jon M. Levy, Kiyoshi Egami, Larissa Munishkina, Jue Zhang, Brooke Gardner, and Junko Wakabayashi. 2011. 'Direct membrane association drives mitochondrial fission by the Parkinson disease-associated protein -synuclein', *Journal of Biological Chemistry*, 286: 20710-26.

Nalls, Mike A., Nathan Pankratz, Christina M. Lill, Chuong B. Do, Dena G. Hernandez, Mohamad Saad, Anita L. DeStefano, Eleanna Kara, Jose Bras, Manu Sharma, Claudia Schulte, Margaux F. Keller, Sampath Arepalli, Christopher Letson, Connor Edsall, Hreinn Stefansson, Xinmin Liu, Hannah Pliner, Joseph H. Lee, Rong Cheng, Consortium International Parkinson's Disease Genomics, GENetics Initiative Parkinson's Study Group Parkinson's Research: The Organized, andMe, GenePd, Consortium NeuroGenetics Research, Genomics Hussman Institute of Human, Investigator Ashkenazi Jewish Dataset, Epidemiology Cohorts for Health and Aging Research in Genetic, Consortium North American Brain Expression, Consortium United Kingdom Brain Expression, Consortium Greek Parkinson's Disease, Group Alzheimer Genetic Analysis, M. A. Ikram, John P. Ioannidis, Georgios M. Hadjigeorgiou, Joshua C. Bis, Maria Martinez, Joel S. Perlmutter, Alison Goate, Karen Marder, Brian Fiske, Margaret Sutherland, Georgia Xiromerisiou, Richard H. Myers, Lorraine N. Clark, Kari Stefansson, John A. Hardy, Peter Heutink, Honglei Chen, Nicholas W. Wood, Henry Houlden, Haydeh Payami, Alexis Brice, William K. Scott, Thomas Gasser, Lars Bertram, Nicholas Eriksson, Tatiana Foroud, and Andrew B. Singleton. 2014. 'Large-scale meta-analysis of genome-wide association data identifies six new risk loci for Parkinson's disease', *Nature genetics*, 46: 989-93.

Napoli, C., C. Lemieux, and R. Jorgensen. 1990. 'Introduction of a Chimeric Chalcone Synthase Gene into Petunia Results in Reversible Co-Suppression of Homologous Genes in trans', *Plant Cell*, 2: 279-89.

Nemani, V. M., W. Lu, V. Berge, K. Nakamura, B. Onoa, M. K. Lee, F. A. Chaudhry, R. A. Nicoll, and R. H. Edwards. 2010. 'Increased expression of alpha-synuclein reduces neurotransmitter release by inhibiting synaptic vesicle reclustering after endocytosis', *Neuron*, 65: 66-79.

Neumann, J., J. Bras, E. Deas, S. S. O'Sullivan, L. Parkkinen, R. H. Lachmann, A. Li, J. Holton, R. Guerreiro, R. Paudel, B. Segarane, A. Singleton, A. Lees, J. Hardy, H. Houlden, T. Revesz, and N. W. Wood. 2009. 'Glucocerebrosidase mutations in clinical and pathologically proven Parkinson's disease', *Brain*, 132: 1783-94.

Nguyen, Ha N., Blake Byers, Branden Cord, Aleksandr Shcheglovitov, James Byrne, Prachi Gujar, Kehkooi Kee, Birgitt Schüle, Ricardo E. Dolmetsch, William Langston, Theo D. Palmer, and Renee R. Pera. 2011. 'LRRK2 mutant iPSC-derived DA neurons demonstrate increased susceptibility to oxidative stress', *Cell stem cell*, 8:

267-80.

Nichols, R. J., Nicolas Dzamko, Nicholas A. Morrice, David G. Campbell, Maria Deak, Alban Ordureau, Thomas Macartney, Youren Tong, Jie Shen, Alan R. Prescott, and Dario R. Alessi. 2010. '14-3-3 binding to LRRK2 is disrupted by multiple Parkinson's disease-associated mutations and regulates cytoplasmic localization', *The Biochemical journal*, 430: 393-404.

Nielsen, S., Y. Yuzenkova, and N. Zenkin. 2013. 'Mechanism of eukaryotic RNA polymerase III transcription termination', *Science*, 340: 1577-80.

Norrman, K., Y. Fischer, B. Bonnamy, F. Wolfhagen Sand, P. Ravassard, and H. Semb. 2010. 'Quantitative comparison of constitutive promoters in human ES cells', *PLoS One*, 5: e12413.

Nuytemans, Karen, Jessie Theuns, Marc Cruts, and Christine Van Broeckhoven. 2010. 'Genetic etiology of Parkinson disease associated with mutations in the SNCA, PARK2, PINK1, PARK7, and LRRK2 genes: a mutation update', *Human mutation*, 31: 763-80.

Oaks, A. W., N. Marsh-Armstrong, J. M. Jones, J. J. Credle, and A. Sidhu. 2013. 'Synucleins antagonize endoplasmic reticulum function to modulate dopamine transporter trafficking', *PLoS One*, 8: e70872.

Okita, Keisuke, Yasuko Matsumura, Yoshiko Sato, Aki Okada, Asuka Morizane, Satoshi Okamoto, Hyenjong Hong, Masato Nakagawa, Koji Tanabe, Ken-ichi Tezuka, Toshiyuki Shibata, Takahiro Kunisada, Masayo Takahashi, Jun Takahashi, Hiroh Saji, and Shinya Yamanaka. 2011. 'A more efficient method to generate integration-free human iPS cells', *Nature methods*, 8: 409-12.

Olgiati, S., A. Thomas, M. Quadri, G. J. Breedveld, J. Graafland, H. Eussen, H. Douben, A. de Klein, M. Onofrj, and V. Bonifati. 2015. 'Early-onset parkinsonism caused by alpha-synuclein gene triplication: Clinical and genetic findings in a novel family', *Parkinsonism Relat Disord*, 21: 981-6.

Oliveira, L. M., L. J. Falomir-Lockhart, M. G. Botelho, K. H. Lin, P. Wales, J. C. Koch, E. Gerhardt, H. Taschenberger, T. F. Outeiro, P. Lingor, B. Schüle, D. J. Arndt-Jovin, and T. M. Jovin. 2015. 'Elevated α-synuclein caused by SNCA gene triplication impairs neuronal differentiation and maturation in Parkinson's patient-derived induced pluripotent stem cells', *Cell Death Dis*, 6: e1994.

Ono, Kenjiro, Tokuhei Ikeda, Jun-ichi Takasaki, and Masahito Yamada. 2011. 'Familial Parkinson disease mutations influence α-synuclein assembly', *Neurobiology of disease*, 43: 715-24.

Orenstein, Samantha J., Sheng-Han H. Kuo, Inmaculada Tasset, Esperanza Arias, Hiroshi Koga, Irene Fernandez-Carasa, Etty Cortes, Lawrence S. Honig, William Dauer, Antonella Consiglio, Angel Raya, David Sulzer, and Ana M. Cuervo. 2013. 'Interplay of LRRK2 with chaperone-mediated autophagy', *Nature neuroscience*, 16: 394-406.

Osafune, K., L. Caron, M. Borowiak, R. J. Martinez, C. S. Fitz-Gerald, Y. Sato, C. A. Cowan, K. R. Chien, and D. A. Melton. 2008. 'Marked differences in differentiation propensity among human embryonic stem cell lines', *Nat Biotechnol*, 26: 313-5.

Ostlund, C., E. S. Folker, J. C. Choi, E. R. Gomes, G. G. Gundersen, and H. J. Worman. 2009. 'Dynamics and molecular interactions of linker of nucleoskeleton and cytoskeleton (LINC) complex proteins', *J Cell Sci*, 122: 4099-108.

Ostrerova, N., L. Petrucelli, M. Farrer, N. Mehta, P. Choi, J. Hardy, and B. Wolozin. 1999. 'alpha-Synuclein shares physical and functional homology with 14-3-3 proteins', *The Journal of neuroscience*, 19: 5782-91.

Oueslati, Abid, Margot Fournier, and Hilal A. Lashuel. 2010. 'Role of post-translational modifications in modulating the structure, function and toxicity of alpha-synuclein: implications for Parkinson's disease pathogenesis and therapies', *Progress in brain research*, 183: 115-45.

Outeiro, T. F., P. Putcha, J. E. Tetzlaff, R. Spoelgen, M. Koker, F. Carvalho, B. T. Hyman, and P. J. McLean. 2008. 'Formation of toxic oligomeric alpha-synuclein species in living cells', *PLoS One*, 3: e1867.

Owada, Y., S. A. Abdelwahab, N. Kitanaka, H. Sakagami, H. Takano, Y. Sugitani, M. Sugawara, H. Kawashima, Y. Kiso, J. I. Mobarakeh, K. Yanai, K. Kaneko, H. Sasaki, H. Kato, S. Saino-Saito, N. Matsumoto, N. Akaike, T. Noda, and H. Kondo. 2006. 'Altered emotional behavioral responses in mice lacking brain-type fatty acid-binding protein gene', *Eur J Neurosci*, 24: 175-87.

Oyadomari, S., and M. Mori. 2004. 'Roles of CHOP/GADD153 in endoplasmic reticulum stress', *Cell Death Differ*, 11: 381-9.

Pacelli, C., N. Giguère, M. J. Bourque, M. Lévesque, R. S. Slack, and L. Trudeau. 2015. 'Elevated Mitochondrial Bioenergetics and Axonal Arborization Size Are Key Contributors to the Vulnerability of Dopamine Neurons', *Curr Biol*, 25: 2349-60.

Paddison, P. J., A. A. Caudy, E. Bernstein, G. J. Hannon, and D. S. Conklin. 2002. 'Short hairpin RNAs (shRNAs) induce sequence-specific silencing in mammalian cells', *Genes Dev*, 16: 948-58.

Paisan-Ruiz, C., K. P. Bhatia, A. Li, D. Hernandez, M. Davis, N. W. Wood, J. Hardy, H. Houlden, A. Singleton, and S. A. Schneider. 2009. 'Characterization of PLA2G6 as a locus for dystonia-parkinsonism', *Ann Neurol*, 65: 19-23.

Pankiv, S., T. H. Clausen, T. Lamark, A. Brech, J. A. Bruun, H. Outzen, A. Øvervatn, G. Bjørkøy, and T. Johansen. 2007. 'p62/SQSTM1 binds directly to Atg8/LC3 to facilitate degradation of ubiquitinated protein aggregates by autophagy', *J Biol Chem*, 282: 24131-45.

Pankratz, N., G. W. Beecham, A. L. DeStefano, T. M. Dawson, K. F. Doheny, S. A. Factor, T. H. Hamza, A. Y. Hung, B. T. Hyman, A. J. Ivinson, D. Krainc, J. C. Latourelle, L. N. Clark, K. Marder, E. R. Martin, R. Mayeux, O. A. Ross, C. R. Scherzer, D. K. Simon, C. Tanner, J. M. Vance, Z. K. Wszolek, C. P. Zabetian, R. H. Myers, H. Payami, W. K. Scott, T. Foroud, and PD GWAS Consortium. 2012. 'Meta-analysis of Parkinson's disease: identification of a novel locus, RIT2', *Ann Neurol*, 71: 370-84.

Parihar, M. S., A. Parihar, M. Fujita, M. Hashimoto, and P. Ghafourifar. 2008. 'Mitochondrial association of alpha-synuclein causes oxidative stress', *Cell Mol Life Sci*, 65: 1272-84.

Parker, W. D., J. K. Parks, and R. H. Swerdlow. 2008. 'Complex I deficiency in Parkinson's disease frontal cortex', *Brain Res*, 1189: 215-8.

Pasanen, P., L. Myllykangas, M. Siitonen, A. Raunio, S. Kaakkola, J. Lyytinen, P. J. Tienari, M. Pöyhönen, and A. Paetau. 2014. 'Novel α-synuclein mutation A53E associated with atypical multiple system atrophy and Parkinson's disease-type pathology', *Neurobiol Aging*, 35: 2180.e1-5.

Peng, Jun, Qiuyue Liu, Mahendra S. Rao, and Xianmin Zeng. 2013. 'Using human pluripotent stem cell-derived dopaminergic neurons to evaluate candidate Parkinson's disease therapeutic agents in MPP+ and Rotenone models', *Journal of biomolecular screening*, 18: 522-33.

Perez, Ruth G., Jack C. Waymire, Eva Lin, Jen J. Liu, Fengli Guo, and Michael J. Zigmond. 2002. 'A role for alpha-synuclein in the regulation of dopamine biosynthesis', *The Journal of neuroscience*, 22: 3090-99.

Perier, C., K. Tieu, C. Guégan, C. Caspersen, V. Jackson-Lewis, V. Carelli, A. Martinuzzi,

M. Hirano, S. Przedborski, and M. Vila. 2005. 'Complex I deficiency primes Bax-dependent neuronal apoptosis through mitochondrial oxidative damage', *Proceedings of the National Academy of Sciences of the United States of America*, 102: 19126-31.

Perrier, Anselme L., Viviane Tabar, Tiziano Barberi, Maria E. Rubio, Juan Bruses, Norbert Topf, Neil L. Harrison, and Lorenz Studer. 2004. 'Derivation of midbrain dopamine neurons from human embryonic stem cells', *Proceedings of the National Academy of Sciences of the United States of America*, 101: 12543-48.

Petra, Pasanen, Myllykangas Liisa, Siitonen Maija, Raunio Anna, Kaakkola Seppo, Lyytinen Jukka, J. Tienari Pentti, Pöyhönen Minna, and Paetau Anders. 2014. 'A novel α-synuclein mutation A53E associated with atypical multiple system atrophy and Parkinson's disease-type pathology', *Neurobiology of Aging*, 35: 21800-218000000.

Pfisterer, Ulrich, Agnete Kirkeby, Olof Torper, James Wood, Jenny Nelander, Audrey Dufour, Anders Björklund, Olle Lindvall, Johan Jakobsson, and Malin Parmar. 2011. 'Direct conversion of human fibroblasts to dopaminergic neurons', *Proceedings of the National Academy of Sciences of the United States of America*, 108: 10343-48.

Pissadaki, E. K., and J. P. Bolam. 2013. 'The energy cost of action potential propagation in dopamine neurons: clues to susceptibility in Parkinson's disease', *Front Comput Neurosci*, 7: 13.

Polymeropoulos, M. H., J. J. Higgins, L. I. Golbe, W. G. Johnson, S. E. Ide, G. Di Iorio, G. Sanges, E. S. Stenroos, L. T. Pho, A. A. Schaffer, A. M. Lazzarini, R. L. Nussbaum, and R. C. Duvoisin. 1996. 'Mapping of a gene for Parkinson's disease to chromosome 4q21-q23', *Science*, 274: 1197-9.

Polymeropoulos, M. H., C. Lavedan, E. Leroy, S. E. Ide, A. Dehejia, A. Dutra, B. Pike, H. Root, J. Rubenstein, R. Boyer, E. S. Stenroos, S. Chandrasekharappa, A. Athanassiadou, T. Papapetropoulos, W. G. Johnson, A. M. Lazzarini, R. C. Duvoisin, G. Di Iorio, L. I. Golbe, and R. L. Nussbaum. 1997. 'Mutation in the alpha-synuclein gene identified in families with Parkinson's disease', *Science (New York, N.Y.)*, 276: 2045-47.

Poole, A. C., R. E. Thomas, L. A. Andrews, H. M. McBride, A. J. Whitworth, and L. J. Pallanck. 2008. 'The PINK1/Parkin pathway regulates mitochondrial morphology', *Proceedings of the National Academy of Sciences of the United States of America*, 105: 1638-43.

Postuma, R. B., A. E. Lang, R. P. Munhoz, K. Charland, A. Pelletier, M. Moscovich, L. Filla, D. Zanatta, S. Rios Romenets, R. Altman, R. Chuang, and B. Shah. 2012. 'Caffeine for treatment of Parkinson disease: a randomized controlled trial', *Neurology*, 79: 651-8.

Prasanthi, J. R., A. Huls, S. Thomasson, A. Thompson, E. Schommer, and O. Ghribi. 2009. 'Differential effects of 24-hydroxycholesterol and 27-hydroxycholesterol on beta-amyloid precursor protein levels and processing in human neuroblastoma SH-SY5Y cells', *Mol Neurodegener*, 4: 1.

Pratt, A. J., and I. J. MacRae. 2009. 'The RNA-induced silencing complex: a versatile gene-silencing machine', *J Biol Chem*, 284: 17897-901.

Prediger, Rui D. 2010. 'Effects of caffeine in Parkinson's disease: from neuroprotection to the management of motor and non-motor symptoms', *Journal of Alzheimer's disease : JAD*, 20 Suppl 1: 20.

Proukakis, Christos, Christopher G. Dudzik, Timothy Brier, Donna S. MacKay, J. M. Cooper, Glenn L. Millhauser, Henry Houlden, and Anthony H. Schapira. 2013. 'A novel α-synuclein missense mutation in Parkinson disease', *Neurology*, 80: 1062-64.

Pu, L., U. Igbavboa, W. G. Wood, J. B. Roths, A. B. Kier, F. Spener, and F. Schroeder. 1999. 'Expression of fatty acid binding proteins is altered in aged mouse brain', *Mol Cell*

Biochem, 198: 69-78.

Qin, J. Y., L. Zhang, K. L. Clift, I. Hulur, A. P. Xiang, B. Z. Ren, and B. T. Lahn. 2010. 'Systematic comparison of constitutive promoters and the doxycycline-inducible promoter', *PLoS One*, 5: e10611.

Qing, H., W. Wong, E. G. McGeer, and P. L. McGeer. 2009. 'Lrrk2 phosphorylates alpha synuclein at serine 129: Parkinson disease implications', *Biochem Biophys Res Commun*, 387: 149-52.

Qing, H., Y. Zhang, Y. Deng, E. G. McGeer, and P. L. McGeer. 2009. 'Lrrk2 interaction with alpha-synuclein in diffuse Lewy body disease', *Biochem Biophys Res Commun*, 390: 1229-34.

Rahim, A. A., A. M. Wong, S. J. Howe, S. M. Buckley, A. D. Acosta-Saltos, K. E. Elston, N. J. Ward, N. J. Philpott, J. D. Cooper, P. N. Anderson, S. N. Waddington, A. J. Thrasher, and G. Raivich. 2009. 'Efficient gene delivery to the adult and fetal CNS using pseudotyped non-integrating lentiviral vectors', *Gene Ther*, 16: 509-20.

Ramirez, A., A. Heimbach, J. Gründemann, B. Stiller, D. Hampshire, L. P. Cid, I. Goebel, A. F. Mubaidin, A. L. Wriekat, J. Roeper, A. Al-Din, A. M. Hillmer, M. Karsak, B. Liss, C. G. Woods, M. I. Behrens, and C. Kubisch. 2006. 'Hereditary parkinsonism with dementia is caused by mutations in ATP13A2, encoding a lysosomal type 5 P-type ATPase', *Nat Genet*, 38: 1184-91.

Reeve, A. K., M. H. Ludtmann, P. R. Angelova, E. M. Simcox, M. H. Horrocks, D. Klenerman, S. Gandhi, D. M. Turnbull, and A. Y. Abramov. 2015. 'Aggregated α-synuclein and complex I deficiency: exploration of their relationship in differentiated neurons', *Cell death & disease*, 6.

Reeve, A., E. Simcox, and D. Turnbull. 2014. 'Ageing and Parkinson's disease: why is advancing age the biggest risk factor?', *Ageing Res Rev*, 14: 19-30.

Reinhardt, Peter, Benjamin Schmid, Lena F. Burbulla, David C. Schöndorf, Lydia Wagner, Michael Glatza, Susanne Höing, Gunnar Hargus, Susanna A. Heck, Ashutosh Dhingra, Guangming Wu, Stephan Müller, Kathrin Brockmann, Torsten Kluba, Martina Maisel, Rejko Krüger, Daniela Berg, Yaroslav Tsytsyura, Cora S. Thiel, Olympia-Ekaterini E. Psathaki, Jürgen Klingauf, Tanja Kuhlmann, Marlene Klewin, Heiko Müller, Thomas Gasser, Hans R. Schöler, and Jared Sterneckert. 2013. 'Genetic correction of a LRRK2 mutation in human iPSCs links parkinsonian neurodegeneration to ERK-dependent changes in gene expression', *Cell stem cell*, 12: 354-67.

Reubinoff, B. E., P. Itsykson, T. Turetsky, M. F. Pera, E. Reinhartz, A. Itzik, and T. Ben-Hur. 2001. 'Neural progenitors from human embryonic stem cells', *Nat Biotechnol*, 19: 1134-40.

Richardson, J. R., Y. Quan, T. B. Sherer, J. T. Greenamyre, and G. W. Miller. 2005. 'Paraquat neurotoxicity is distinct from that of MPTP and Rotenone', *Toxicol Sci*, 88: 193-201.

Rijk, De M. C., W. A. Rocca, D. W. Anderson, and M. O. Melcon. 1997. 'A population perspective on diagnostic criteria for Parkinson's disease', *Neurology*.

Ring, K. L., L. M. Tong, M. E. Balestra, R. Javier, Y. Andrews-Zwilling, G. Li, D. Walker, W. R. Zhang, A. C. Kreitzer, and Y. Huang. 2012. 'Direct reprogramming of mouse and human fibroblasts into multipotent neural stem cells with a single factor', *Cell Stem Cell*, 11: 100-9.

Rival-Gervier, Sylvie, Mandy Y. Lo, Shahryar Khattak, Peter Pasceri, Matthew C. Lorincz, and James Ellis. 2013. 'Kinetics and epigenetics of retroviral silencing in mouse embryonic stem cells defined by deletion of the D4Z4 element', *Molecular Therapy* 21: 1536-50.

Roberts, Rosalind F., Richard Wade-Martins, and Javier Alegre-Abarrategui. 2015b. 'Direct visualization of alpha-synuclein oligomers reveals previously undetected pathology in Parkinson's disease brain', *Brain : a journal of neurology*, 138: 1642-57.

Rogers, Jack T., Sohan Mikkilineni, Ippolita Cantuti-Castelvetri, Deborah H. Smith, Xudong Huang, Sanghamitra Bandyopadhyay, Catherine M. Cahill, Maria L. Maccecchini, Debomoy K. Lahiri, and Nigel H. Greig. 2011. 'The alpha-synuclein 5'untranslated region targeted translation blockers: anti-alpha synuclein efficacy of cardiac glycosides and Posiphen', *Journal of neural transmission (Vienna, Austria : 1996)*, 118: 493-507.

Roussa, E., M. Wiehle, N. Dünker, S. Becker-Katins, O. Oehlke, and K. Krieglstein. 2006. 'Transforming growth factor beta is required for differentiation of mouse mesencephalic progenitors into dopaminergic neurons in vitro and in vivo: ectopic induction in dorsal mesencephalon', *Stem Cells*, 24: 2120-9.

Ruepp, M. D., S. Vivarelli, R. S. Pillai, N. Kleinschmidt, T. N. Azzouz, S. M. Barabino, and D. Schümperli. 2010. 'The 68 kDa subunit of mammalian cleavage factor I interacts with the U7 small nuclear ribonucleoprotein and participates in 3'-end processing of animal histone mRNAs', *Nucleic Acids Res*, 38: 7637-50.

Rungsiwiwut, R., C. Manolertthewan, P. Numchaisrika, V. Ahnonkitpanit, P. Virutamasen, M. Techakumphu, and K. Pruksananonda. 2013. 'The ROCK inhibitor Y-26732 enhances the survival and proliferation of human embryonic stem cell-derived neural progenitor cells upon dissociation', *Cells Tissues Organs*, 198: 127-38.

Rutherford, Nicola J., Brenda D. Moore, Todd E. Golde, and Benoit I. Giasson. 2014. 'Divergent effects of the H50Q and G51D SNCA mutations on the aggregation of α-synuclein', *Journal of neurochemistry*, 131: 859-67.

Ryan, Brent J., Selim Hoek, Edward A. Fon, and Richard Wade-Martins. 2015. 'Mitochondrial dysfunction and mitophagy in Parkinson's: from familial to sporadic disease', *Trends in biochemical sciences*, 40: 200-10.

Ryan, Brent J., Lara L. Lourenço-Venda, Mark J. Crabtree, Ashley B. Hale, Keith M. Channon, and Richard Wade-Martins. 2014. 'α-Synuclein and mitochondrial bioenergetics regulate tetrahydrobiopterin levels in a human dopaminergic model of Parkinson disease', *Free radical biology & medicine*, 67: 58-68.

Ryan, Scott D., Nima Dolatabadi, Shing F. Chan, Xiaofei Zhang, Mohd W. Akhtar, James Parker, Frank Soldner, Carmen R. Sunico, Saumya Nagar, Maria Talantova, Brian Lee, Kevin Lopez, Anthony Nutter, Bing Shan, Elena Molokanova, Yaoyang Zhang, Xuemei Han, Tomohiro Nakamura, Eliezer Masliah, John R. Yates, Nobuki Nakanishi, Aleksander Y. Andreyev, Shu-ichi Okamoto, Rudolf Jaenisch, Rajesh Ambasudhan, and Stuart A. Lipton. 2013. 'Isogenic human iPSC Parkinson's model shows nitrosative stress-induced dysfunction in MEF2-PGC1α transcription', *Cell*, 155: 1351-64.

Samali, A., U. Fitzgerald, S. Deegan, and S. Gupta. 2010. 'Methods for monitoring endoplasmic reticulum stress and the unfolded protein response', *Int J Cell Biol*, 2010: 830307.

Sandor, C., P. Robertson, C. Lang, A. Heger, H. Booth, J. Vowles, L. Witty, R. Bowden, M. Hu, S. A. Cowley, R. Wade-Martins, and C. Webber. 2017. 'Transcriptomic profiling of purified patient-derived dopamine neurons identifies convergent perturbations and therapeutics for Parkinson's disease', *Hum Mol Genet*.

Sapru, Mohan K., Jonathan W. Yates, Shea Hogan, Lixin Jiang, Jeremy Halter, and Martha C. Bohn. 2006. 'Silencing of human alpha-synuclein in vitro and in rat brain using lentiviral-mediated RNAi', *Experimental neurology*, 198: 382-90.

Satake, W., Y. Nakabayashi, I. Mizuta, Y. Hirota, C. Ito, M. Kubo, T. Kawaguchi, T.

Tsunoda, M. Watanabe, A. Takeda, H. Tomiyama, K. Nakashima, K. Hasegawa, F. Obata, T. Yoshikawa, H. Kawakami, S. Sakoda, M. Yamamoto, N. Hattori, M. Murata, Y. Nakamura, and T. Toda. 2009. 'Genome-wide association study identifies common variants at four loci as genetic risk factors for Parkinson's disease', *Nat Genet*, 41: 1303-7.

Sato, Shigeto, Tomoki Chiba, Eri Sakata, Koichi Kato, Yoshikuni Mizuno, Nobutaka Hattori, and Keiji Tanaka. 2006. '14-3-3eta is a novel regulator of parkin ubiquitin ligase', *The EMBO journal*, 25: 211-21.

Schapira, A. H., J. M. Cooper, D. Dexter, P. Jenner, J. B. Clark, and C. D. Marsden. 1989. 'Mitochondrial complex I deficiency in Parkinson's disease', *Lancet*, 1: 1269.

Schrader, M., and H. D. Fahimi. 2006. 'Peroxisomes and oxidative stress', *Biochim Biophys Acta*, 1763: 1755-66.

Schöndorf, David C., Massimo Aureli, Fiona E. McAllister, Christopher J. Hindley, Florian Mayer, Benjamin Schmid, S. P. Sardi, Manuela Valsecchi, Susanna Hoffmann, Lukas K. Schwarz, Ulrike Hedrich, Daniela Berg, Lamya S. Shihabuddin, Jing Hu, Jan Pruszak, Steven P. Gygi, Sandro Sonnino, Thomas Gasser, and Michela Deleidi. 2014. 'iPSC-derived neurons from GBA1-associated Parkinson's disease patients show autophagic defects and impaired calcium homeostasis', *Nature communications*, 5: 4028.

Seibler, Philip, John Graziotto, Hyun Jeong, Filip Simunovic, Christine Klein, and Dimitri Krainc. 2011. 'Mitochondrial Parkin recruitment is impaired in neurons derived from mutant PINK1 induced pluripotent stem cells', *The Journal of neuroscience*, 31: 5970-76.

Selvaraj, S., Y. Sun, J. A. Watt, S. Wang, S. Lei, L. Birnbaumer, and B. B. Singh. 2012. 'Neurotoxin-induced ER stress in mouse dopaminergic neurons involves downregulation of TRPC1 and inhibition of AKT/mTOR signaling', *J Clin Invest*, 122: 1354-67.

Senior, Steven L., Natalia Ninkina, Robert Deacon, David Bannerman, Vladimir L. Buchman, Stephanie J. Cragg, and Richard Wade-Martins. 2008. 'Increased striatal dopamine release and hyperdopaminergic-like behaviour in mice lacking both alpha-synuclein and gamma-synuclein', *The European journal of neuroscience*, 27: 947-57.

Shaltouki, Atossa, Renuka Sivapatham, Ying Pei, Akos A. Gerencser, Olga Momčilović, Mahendra S. Rao, and Xianmin Zeng. 2015. 'Mitochondrial alterations by PARKIN in dopaminergic neurons using PARK2 patient-specific and PARK2 knockout isogenic iPSC lines', *Stem cell reports*, 4: 847-59.

Shannon, Kathleen M., Ali Keshavarzian, Ece Mutlu, Hemraj B. Dodiya, Delia Daian, Jean A. Jaglin, and Jeffrey H. Kordower. 2012. 'Alpha-synuclein in colonic submucosa in early untreated Parkinson's disease', *Movement disorders*, 27: 709-15.

Sharma, M., J. Burré, P. Bronk, Y. Zhang, W. Xu, and T. C. Südhof. 2012. 'CSPα knockout causes neurodegeneration by impairing SNAP-25 function', *EMBO J*, 31: 829-41.

Sharon, R., I. Bar-Joseph, G. E. Mirick, C. N. Serhan, and D. J. Selkoe. 2003. 'Altered fatty acid composition of dopaminergic neurons expressing alpha-synuclein and human brains with alpha-synucleinopathies', *J Biol Chem*, 278: 49874-81.

Sharon, R., M. S. Goldberg, I. Bar-Josef, R. A. Betensky, J. Shen, and D. J. Selkoe. 2001. 'alpha-Synuclein occurs in lipid-rich high molecular weight complexes, binds fatty acids, and shows homology to the fatty acid-binding proteins', *Proceedings of the National Academy of Sciences of the United States of America*, 98: 9110-15.

Shavali, S., H. M. Brown-Borg, M. Ebadi, and J. Porter. 2008. 'Mitochondrial localization of alpha-synuclein protein in alpha-synuclein overexpressing cells', *Neurosci Lett*, 439:

125-8.

Shen, J., X. Chen, L. Hendershot, and R. Prywes. 2002. 'ER stress regulation of ATF6 localization by dissociation of BiP/GRP78 binding and unmasking of Golgi localization signals', *Dev Cell*, 3: 99-111.

Shi, Y., P. Kirwan, J. Smith, H. P. Robinson, and F. J. Livesey. 2012. 'Human cerebral cortex development from pluripotent stem cells to functional excitatory synapses', *Nat Neurosci*, 15: 477-86, S1.

Shimizu, F., T. K. Watanabe, H. Shinomiya, Y. Nakamura, and T. Fujiwara. 1997. 'Isolation and expression of a cDNA for human brain fatty acid-binding protein (B-FABP)', *Biochim Biophys Acta*, 1354: 24-8.

Shioda, N., Y. Yabuki, Y. Kobayashi, M. Onozato, Y. Owada, and K. Fukunaga. 2014. 'FABP3 protein promotes α-synuclein oligomerization associated with 1-methyl-1,2,3,6-tetrahydropiridine-induced neurotoxicity', *J Biol Chem*, 289: 18957-65.

Shulman, J. M., P. L. De Jager, and M. B. Feany. 2011. 'Parkinson's disease: genetics and pathogenesis', *Annu Rev Pathol*, 6: 193-222.

Siddiqui, A., S. J. Chinta, J. K. Mallajosyula, S. Rajagopolan, I. Hanson, A. Rane, S. Melov, and J. K. Andersen. 2012. 'Selective binding of nuclear alpha-synuclein to the PGC1alpha promoter under conditions of oxidative stress may contribute to losses in mitochondrial function: implications for Parkinson's disease', *Free Radic Biol Med*, 53: 993-1003.

Sidransky, E., M. A. Nalls, J. O. Aasly, J. Aharon-Peretz, G. Annesi, E. R. Barbosa, A. Bar-Shira, D. Berg, J. Bras, A. Brice, C. M. Chen, L. N. Clark, C. Condroyer, E. V. De Marco, A. Dürr, M. J. Eblan, S. Fahn, M. J. Farrer, H. C. Fung, Z. Gan-Or, T. Gasser, R. Gershoni-Baruch, N. Giladi, A. Griffith, T. Gurevich, C. Januario, P. Kropp, A. E. Lang, G. J. Lee-Chen, S. Lesage, K. Marder, I. F. Mata, A. Mirelman, J. Mitsui, I. Mizuta, G. Nicoletti, C. Oliveira, R. Ottman, A. Orr-Urtreger, L. V. Pereira, A. Quattrone, E. Rogaeva, A. Rolfs, H. Rosenbaum, R. Rozenberg, A. Samii, T. Samaddar, C. Schulte, M. Sharma, A. Singleton, M. Spitz, E. K. Tan, N. Tayebi, T. Toda, A. R. Troiano, S. Tsuji, M. Wittstock, T. G. Wolfsberg, Y. R. Wu, C. P. Zabetian, Y. Zhao, and S. G. Ziegler. 2009. 'Multicenter analysis of glucocerebrosidase mutations in Parkinson's disease', *N Engl J Med*, 361: 1651-61.

Simón-Sánchez, J., C. Schulte, J. M. Bras, M. Sharma, J. R. Gibbs, D. Berg, C. Paisan-Ruiz, P. Lichtner, S. W. Scholz, D. G. Hernandez, R. Krüger, M. Federoff, C. Klein, A. Goate, J. Perlmutter, M. Bonin, M. A. Nalls, T. Illig, C. Gieger, H. Houlden, M. Steffens, M. S. Okun, B. A. Racette, M. R. Cookson, K. D. Foote, H. H. Fernandez, B. J. Traynor, S. Schreiber, S. Arepalli, R. Zonozi, K. Gwinn, M. van der Brug, G. Lopez, S. J. Chanock, A. Schatzkin, Y. Park, A. Hollenbeck, J. Gao, X. Huang, N. W. Wood, D. Lorenz, G. Deuschl, H. Chen, O. Riess, J. A. Hardy, A. B. Singleton, and T. Gasser. 2009. 'Genome-wide association study reveals genetic risk underlying Parkinson's disease', *Nat Genet*, 41: 1308-12.

Singleton, A. B., M. Farrer, J. Johnson, A. Singleton, S. Hague, J. Kachergus, M. Hulihan, T. Peuralinna, A. Dutra, R. Nussbaum, S. Lincoln, A. Crawley, M. Hanson, D. Maraganore, C. Adler, M. R. Cookson, M. Muenter, M. Baptista, D. Miller, J. Blancato, J. Hardy, and K. Gwinn-Hardy. 2003. 'alpha-Synuclein locus triplication causes Parkinson's disease', *Science (New York, N.Y.)*, 302: 841.

Slodzinski, H., L. B. Moran, G. J. Michael, B. Wang, S. Novoselov, M. E. Cheetham, R. K. Pearce, and M. B. Graeber. 2009. 'Homocysteine-induced endoplasmic reticulum protein (herp) is up-regulated in parkinsonian substantia nigra and present in the core of Lewy bodies', *Clin Neuropathol*, 28: 333-43.

Smith, Wanli W., Haibing Jiang, Zhong Pei, Yuji Tanaka, Hokuto Morita, Akira Sawa, Valina L. Dawson, Ted M. Dawson, and Christopher A. Ross. 2005b. 'Endoplasmic reticulum stress and mitochondrial cell death pathways mediate A53T mutant alpha-synuclein-induced toxicity', *Human molecular genetics*, 14: 3801-11.

Soldner, Frank, Dirk Hockemeyer, Caroline Beard, Qing Gao, George W. Bell, Elizabeth G. Cook, Gunnar Hargus, Alexandra Blak, Oliver Cooper, Maisam Mitalipova, Ole Isacson, and Rudolf Jaenisch. 2009. 'Parkinson's disease patient-derived induced pluripotent stem cells free of viral reprogramming factors', *Cell*, 136: 964-77.

Soldner, Frank, Josée Laganière, Albert W. Cheng, Dirk Hockemeyer, Qing Gao, Raaji Alagappan, Vikram Khurana, Lawrence I. Golbe, Richard H. Myers, Susan Lindquist, Lei Zhang, Dmitry Guschin, Lauren K. Fong, B. J. Vu, Xiangdong Meng, Fyodor D. Urnov, Edward J. Rebar, Philip D. Gregory, H. S. Zhang, and Rudolf Jaenisch. 2011. 'Generation of isogenic pluripotent stem cells differing exclusively at two early onset Parkinson point mutations', *Cell*, 146: 318-31.

Soldner, Frank, Yonatan Stelzer, Chikdu S. Shivalila, Brian J. Abraham, Jeanne C. Latourelle, M. I. Barrasa, Johanna Goldmann, Richard H. Myers, Richard A. Young, and Rudolf Jaenisch. 2016. 'Parkinson-associated risk variant in distal enhancer of α-synuclein modulates target gene expression', *Nature*, 533: 95-99.

Song, Z., H. Chen, M. Fiket, C. Alexander, and D. C. Chan. 2007. 'OPA1 processing controls mitochondrial fusion and is regulated by mRNA splicing, membrane potential, and Yme1L', *J Cell Biol*, 178: 749-55.

Spillantini, M. G., R. A. Crowther, R. Jakes, M. Hasegawa, and M. Goedert. 1998. 'alpha-Synuclein in filamentous inclusions of Lewy bodies from Parkinson's disease and dementia with lewy bodies', *Proceedings of the National Academy of Sciences of the United States of America*, 95: 6469-73.

Spillantini, M. G., and M. Goedert. 2000. 'The alpha-synucleinopathies: Parkinson's disease, dementia with Lewy bodies, and multiple system atrophy', *Annals of the New York Academy of Sciences*, 920: 16-27.

Spillantini, M. G., M. L. Schmidt, V. M. Lee, J. Q. Trojanowski, R. Jakes, and M. Goedert. 1997. 'Alpha-synuclein in Lewy bodies', *Nature*, 388: 839-40.

Stadtfeld, M., M. Nagaya, J. Utikal, G. Weir, and K. Hochedlinger. 2008. 'Induced pluripotent stem cells generated without viral integration', *Science*, 322: 945-9.

Su, X., Q. S. Tan, B. H. Parikh, A. Tan, M. N. Mehta, Y. Sia Wey, S. B. Tun, L. J. Li, X. Y. Han, T. Y. Wong, W. Hunziker, C. D. Luu, Y. Owada, V. A. Barathi, S. S. Zhang, and S. S. Chaurasia. 2016. 'Characterization of Fatty Acid Binding Protein 7 (FABP7) in the Murine Retina', *Invest Ophthalmol Vis Sci*, 57: 3397-408.

Sugii, S., Y. Kida, T. Kawamura, J. Suzuki, R. Vassena, Y. Q. Yin, M. K. Lutz, W. T. Berggren, J. C. Izpisúa Belmonte, and R. M. Evans. 2010. 'Human and mouse adipose-derived cells support feeder-independent induction of pluripotent stem cells', *Proceedings of the National Academy of Sciences of the United States of America*, 107: 3558-63.

Sui, D., Z. Sun, C. Xu, Y. Wu, M. R. Capecchi, S. Wu, and N. Li. 2014. 'Fine-tuning of iPSC derivation by an inducible reprogramming system at the protein level', *Stem Cell Reports*, 2: 721-33.

Sundberg, Maria, Helle Bogetofte, Tristan Lawson, Johan Jansson, Gaynor Smith, Arnar Astradsson, Michele Moore, Teresia Osborn, Oliver Cooper, Roger Spealman, Penelope Hallett, and Ole Isacson. 2013. 'Improved cell therapy protocols for Parkinson's disease based on differentiation efficiency and safety of hESC-, hiPSC-, and non-human primate iPSC-derived dopaminergic neurons', *Stem cells (Dayton, Ohio)*, 31: 1548-62.

Szegezdi, E., S. E. Logue, A. M. Gorman, and A. Samali. 2006. 'Mediators of endoplasmic reticulum stress-induced apoptosis', *EMBO Rep*, 7: 880-5.

Szulc, J., M. Wiznerowicz, M. O. Sauvain, D. Trono, and P. Aebischer. 2006. 'A versatile tool for conditional gene expression and knockdown', *Nat Methods*, 3: 109-16.

Sánchez-Danés, A., A. Consiglio, Y. Richaud, I. Rodríguez-Pizà, B. Dehay, M. Edel, J. Bové, M. Memo, M. Vila, A. Raya, and J. C. Izpisua Belmonte. 2012. 'Efficient generation of A9 midbrain dopaminergic neurons by lentiviral delivery of LMX1A in human embryonic stem cells and induced pluripotent stem cells', *Human gene therapy*, 23: 56-69.

Sánchez-Danés, Adriana, Yvonne Richaud-Patin, Iria Carballo-Carbajal, Senda Jiménez-Delgado, Carles Caig, Sergio Mora, Claudia Di Guglielmo, Mario Ezquerra, Bindiben Patel, Albert Giralt, Josep M. Canals, Maurizio Memo, Jordi Alberch, José López-Barneo, Miquel Vila, Ana M. Cuervo, Eduard Tolosa, Antonella Consiglio, and Angel Raya. 2012. 'Disease-specific phenotypes in dopamine neurons from human iPS-based models of genetic and sporadic Parkinson's disease', *EMBO molecular medicine*, 4: 380-95.

Taguchi, N., N. Ishihara, A. Jofuku, T. Oka, and K. Mihara. 2007. 'Mitotic phosphorylation of dynamin-related GTPase Drp1 participates in mitochondrial fission', *J Biol Chem*, 282: 11521-9.

Takahashi, Kazutoshi, Koji Tanabe, Mari Ohnuki, Megumi Narita, Tomoko Ichisaka, Kiichiro Tomoda, and Shinya Yamanaka. 2007. 'Induction of pluripotent stem cells from adult human fibroblasts by defined factors', *Cell*, 131: 861-72.

Takahashi, Kazutoshi, and Shinya Yamanaka. 2006. 'Induction of pluripotent stem cells from mouse embryonic and adult fibroblast cultures by defined factors', *Cell*, 126: 663-76.

Takaoka, N., T. Takayama, T. Teratani, T. Sugiyama, S. Mugiya, and S. Ozono. 2011. 'Analysis of the regulation of fatty acid binding protein 7 expression in human renal carcinoma cell lines', *BMC Mol Biol*, 12: 31.

Takeshige, K., M. Baba, S. Tsuboi, T. Noda, and Y. Ohsumi. 1992. 'Autophagy in yeast demonstrated with proteinase-deficient mutants and conditions for its induction', *J Cell Biol*, 119: 301-11.

Tanaka, Y., S. Engelender, S. Igarashi, R. K. Rao, T. Wanner, R. E. Tanzi, A. Sawa, V. L Dawson, T. M. Dawson, and C. A. Ross. 2001. 'Inducible expression of mutant alpha-synuclein decreases proteasome activity and increases sensitivity to mitochondria-dependent apoptosis', *Hum Mol Genet*, 10: 919-26.

Tanner, C. M., F. Kamel, G. W. Ross, J. A. Hoppin, S. M. Goldman, M. Korell, C. Marras, G. S. Bhudhikanok, M. Kasten, A. R. Chade, K. Comyns, M. B. Richards, C. Meng, B. Priestley, H. H. Fernandez, F. Cambi, D. M. Umbach, A. Blair, D. P. Sandler, and J. W. Langston. 2011. 'Rotenone, Paraquat, and Parkinson's disease', *Environ Health Perspect*, 119: 866-72.

Tatton, N. A., and S. J. Kish. 1997. 'In situ detection of apoptotic nuclei in the substantia nigra compacta of 1-methyl-4-phenyl-1,2,3,6-tetrahydropyridine-treated mice using terminal deoxynucleotidyl transferase labelling and acridine orange staining', *Neuroscience*, 77: 1037-48.

Tehranian, R., S. E. Montoya, A. D. Van Laar, T. G. Hastings, and R. G. Perez. 2006. 'Alpha-synuclein inhibits aromatic amino acid decarboxylase activity in dopaminergic cells', *J Neurochem*, 99: 1188-96.

Teunissen, C. E., R. Veerhuis, J. De Vente, F. R. Verhey, F. Vreeling, M. P. van Boxtel, J. F. Glatz, and M. A. Pelsers. 2011. 'Brain-specific fatty acid-binding protein is elevated in serum of patients with dementia-related diseases', *Eur J Neurol*, 18: 865-71.

Thanvi, B., N. Lo, and T. Robinson. 2007. 'Levodopa-induced dyskinesia in Parkinson's disease: clinical features, pathogenesis, prevention and treatment', *Postgrad Med J*, 83: 384-8.

Thomas, B., A. S. Mandir, N. West, Y. Liu, S. A. Andrabi, W. Stirling, V. L. Dawson, T. M. Dawson, and M. K. Lee. 2011. 'Resistance to MPTP-neurotoxicity in α-synuclein knockout mice is complemented by human α-synuclein and associated with increased β-synuclein and Akt activation', *PLoS One*, 6: e16706.

Tofaris, G. K., R. Layfield, and M. G. Spillantini. 2001. 'alpha-synuclein metabolism and aggregation is linked to ubiquitin-independent degradation by the proteasome', *FEBS letters*, 509: 22-26.

Tolmachov, O. Tolmachova, T. Al-Allaf, F. 2011. 'Viral Gene Therapy', *intech*.

Tomishima, Mark. 2012. 'Midbrain dopamine neurons from hESCs', *StemBook*, StemBook, ed. The Stem Cell Research Community.

Trinh, Joanne, and Matt Farrer. 2013. 'Advances in the genetics of Parkinson disease', *Nature reviews. Neurology*, 9: 445-54.

Tönges, Lars, Paul Lingor, Roman Egle, Gunnar P. Dietz, Alfred Fahr, and Mathias Bähr. 2006. 'Stearylated octaarginine and artificial virus-like particles for transfection of siRNA into primary rat neurons', *RNA (New York, N.Y.)*, 12: 1431-38.

Ubl, Andreas, Daniela Berg, Carsten Holzmann, Rejko Krüger, Klaus Berger, Thomas Arzberger, Antje Bornemann, and Olaf Riess. 2002. '14-3-3 protein is a component of Lewy bodies in Parkinson's disease-mutation analysis and association studies of 14-3-3 eta', *Brain research. Molecular brain research*, 108: 33-39.

Uehara, T., T. Nakamura, D. Yao, Z. Q. Shi, Z. Gu, Y. Ma, E. Masliah, Y. Nomura, and S. A. Lipton. 2006. 'S-nitrosylated protein-disulphide isomerase links protein misfolding to neurodegeneration', *Nature*, 441: 513-7.

Uhl, G. R., J. C. Hedreen, and D. L. Price. 1985. 'Parkinson's disease: loss of neurons from the ventral tegmental area contralateral to therapeutic surgical lesions', *Neurology*, 35: 1215-8.

Ulmer, Tobias S., Ad Bax, Nelson B. Cole, and Robert L. Nussbaum. 2005. 'Structure and dynamics of micelle-bound human alpha-synuclein', *The Journal of biological chemistry*, 280: 9595-603.

Uversky, V. N., and D. Eliezer. 2009. 'Biophysics of Parkinson's disease: structure and aggregation of alpha-synuclein', *Curr Protein Pept Sci*, 10: 483-99.

Uversky, Vladimir N., Jie Li, Pierre Souillac, Ian S. Millett, Sebastian Doniach, Ross Jakes, Michel Goedert, and Anthony L. Fink. 2002. 'Biophysical properties of the synucleins and their propensities to fibrillate: inhibition of alpha-synuclein assembly by beta- and gamma-synucleins', *The Journal of biological chemistry*, 277: 11970-78.

Uéda, K., H. Fukushima, E. Masliah, Y. Xia, A. Iwai, M. Yoshimoto, D. A. Otero, J. Kondo, Y. Ihara, and T. Saitoh. 1993. 'Molecular cloning of cDNA encoding an unrecognized component of amyloid in Alzheimer disease', *Proceedings of the National Academy of Sciences of the United States of America*, 90: 11282-86.

Valente, E. M., A. R. Bentivoglio, P. H. Dixon, A. Ferraris, T. Ialongo, M. Frontali, A. Albanese, and N. W. Wood. 2001. 'Localization of a novel locus for autosomal recessive early-onset parkinsonism, PARK6, on human chromosome 1p35-p36', *American journal of human genetics*, 68: 895-900.

van Wilgenburg, B., C. Browne, J. Vowles, and S. A. Cowley. 2013. 'Efficient, long term production of monocyte-derived macrophages from human pluripotent stem cells under partly-defined and fully-defined conditions', *PLoS One*, 8: e71098.

Vance, J. E. 2014. 'MAM (mitochondria-associated membranes) in mammalian cells: lipids and beyond', *Biochim Biophys Acta*, 1841: 595-609.

Vandrovcova, J., A. M. Pittman, E. Malzer, P. M. Abou-Sleiman, A. J. Lees, N. W. Wood, and R. de Silva. 2009. 'Association of MAPT haplotype-tagging SNPs with sporadic Parkinson's disease', *Neurobiol Aging*, 30: 1477-82.

Venda, Lara L., Stephanie J. Cragg, Vladimir L. Buchman, and Richard Wade-Martins. 2010. 'α-Synuclein and dopamine at the crossroads of Parkinson's disease', *Trends in neurosciences*, 33: 559-68.

Vilar, M., H. T. Chou, T. Lührs, S. K. Maji, D. Riek-Loher, R. Verel, G. Manning, H. Stahlberg, and R. Riek. 2008. 'The fold of alpha-synuclein fibrils', *Proceedings of the National Academy of Sciences of the United States of America*, 105: 8637-42.

Vilariño-Güell, C., C. Wider, O. A. Ross, J. C. Dachsel, J. M. Kachergus, S. J. Lincoln, A. I. Soto-Ortolaza, S. A. Cobb, G. J. Wilhoite, J. A. Bacon, B. Behrouz, H. L. Melrose, E. Hentati, A. Puschmann, D. M. Evans, E. Conibear, W. W. Wasserman, J. O. Aasly, P. R. Burkhard, R. Djaldetti, J. Ghika, F. Hentati, A. Krygowska-Wajs, T. Lynch, E. Melamed, A. Rajput, A. H. Rajput, A. Solida, R. M. Wu, R. J. Uitti, Z. K. Wszolek, F. Vingerhoets, and M. J. Farrer. 2011. 'VPS35 mutations in Parkinson disease', *Am J Hum Genet*, 89: 162-7.

Wang, W., I. Perovic, and J. Chittuluru. 2011. 'A soluble α-synuclein construct forms a dynamic tetramer', *Proceedings of the ….*

Warren, Luigi, Philip D. Manos, Tim Ahfeldt, Yuin-Han H. Loh, Hu Li, Frank Lau, Wataru Ebina, Pankaj K. Mandal, Zachary D. Smith, Alexander Meissner, George Q. Daley, Andrew S. Brack, James J. Collins, Chad Cowan, Thorsten M. Schlaeger, and Derrick J. Rossi. 2010. 'Highly efficient reprogramming to pluripotency and directed differentiation of human cells with synthetic modified mRNA', *Cell stem cell*, 7: 618-30.

Watanabe, Kiichi, Morio Ueno, Daisuke Kamiya, Ayaka Nishiyama, Michiru Matsumura, Takafumi Wataya, Jun B. Takahashi, Satomi Nishikawa, Shin-ichi Nishikawa, Keiko Muguruma, and Yoshiki Sasai. 2007. 'A ROCK inhibitor permits survival of dissociated human embryonic stem cells', *Nature biotechnology*, 25: 681-86.

Watanabe, Y., H. Tatebe, K. Taguchi, Y. Endo, T. Tokuda, T. Mizuno, M. Nakagawa, and M. Tanaka. 2012. 'p62/SQSTM1-dependent autophagy of Lewy body-like α-synuclein inclusions', *PLoS One*, 7: e52868.

Watmuff, B., B. J. Hartley, C. P. Hunt, S. A. Fabb, C. W. Pouton, and J. M. Haynes. 2015. 'Human pluripotent stem cell derived midbrain PITX3(eGFP/w) neurons: a versatile tool for pharmacological screening and neurodegenerative modeling', *Front Cell Neurosci*, 9: 104.

Webb, Julie L., Brinda Ravikumar, Jane Atkins, Jeremy N. Skepper, and David C. Rubinsztein. 2003. 'Alpha-Synuclein is degraded by both autophagy and the proteasome', *The Journal of biological chemistry*, 278: 25009-13.

Weinreb, P. H., W. Zhen, A. W. Poon, K. A. Conway, and P. T. Lansbury. 1996. 'NACP, a protein implicated in Alzheimer's disease and learning, is natively unfolded', *Biochemistry*, 35: 13709-15.

Westermann, B. 2010. 'Mitochondrial fusion and fission in cell life and death', *Nat Rev Mol Cell Biol*, 11: 872-84.

Wilmut, I., A. E. Schnieke, J. McWhir, A. J. Kind, and K. H. Campbell. 1997. 'Viable offspring derived from fetal and adult mammalian cells', *Nature*, 385: 810-3.

Winklhofer, K. F., and C. Haass. 2010. 'Mitochondrial dysfunction in Parkinson's disease', *Biochim Biophys Acta*, 1802: 29-44.

Winslow, Ashley R., Chien-Wen W. Chen, Silvia Corrochano, Abraham Acevedo-Arozena, David E. Gordon, Andrew A. Peden, Maike Lichtenberg, Fiona M. Menzies, Brinda Ravikumar, Sara Imarisio, Steve Brown, Cahir J. O'Kane, and David C.

Rubinsztein. 2010. 'α-Synuclein impairs macroautophagy: implications for Parkinson's disease', *The Journal of cell biology*, 190: 1023-37.

Woodard, Chris M., Brian A. Campos, Sheng-Han H. Kuo, Melissa J. Nirenberg, Michael W. Nestor, Matthew Zimmer, Eugene V. Mosharov, David Sulzer, Hongyan Zhou, Daniel Paull, Lorraine Clark, Eric E. Schadt, Sergio P. Sardi, Lee Rubin, Kevin Eggan, Mathew Brock, Scott Lipnick, Mahendra Rao, Stephen Chang, Aiqun Li, and Scott A. Noggle. 2014. 'iPSC-derived dopamine neurons reveal differences between monozygotic twins discordant for Parkinson's disease', *Cell reports*, 9: 1173-82.

Xi, Jiajie, Yan Liu, Huisheng Liu, Hong Chen, Marina E. Emborg, and Su-Chun C. Zhang. 2012. 'Specification of midbrain dopamine neurons from primate pluripotent stem cells', *Stem cells (Dayton, Ohio)*, 30: 1655-63.

Xia, Y., H. A. Rohan de Silva, B. L. Rosi, L. H. Yamaoka, J. B. Rimmler, M. A. Pericak-Vance, A. D. Roses, X. Chen, E. Masliah, R. DeTeresa, A. Iwai, M. Sundsmo, R. G. Thomas, C. R. Hofstetter, E. Gregory, L. A. Hansen, R. Katzman, L. J. Thal, and T. Saitoh. 1996. 'Genetic studies in Alzheimer's disease with an NACP/alpha-synuclein polymorphism', *Annals of neurology*, 40: 207-15.

Xia, Z., H. Dudek, C. K. Miranti, and M. E. Greenberg. 1996. 'Calcium influx via the NMDA receptor induces immediate early gene transcription by a MAP kinase/ERK-dependent mechanism', *J Neurosci*, 16: 5425-36.

Xu, Jin, Shyan-Yuan Y. Kao, Frank J. Lee, Weihong Song, Lee-Way W. Jin, and Bruce A. Yankner. 2002. 'Dopamine-dependent neurotoxicity of alpha-synuclein: a mechanism for selective neurodegeneration in Parkinson disease', *Nature medicine*, 8: 600-06.

Yamanaka, Shinya. 2012. 'Induced pluripotent stem cells: past, present, and future', *Cell stem cell*, 10: 678-84.

Yan, J., L. Studer, and R. D. McKay. 2001. 'Ascorbic acid increases the yield of dopaminergic neurons derived from basic fibroblast growth factor expanded mesencephalic precursors', *Journal of neurochemistry*, 76: 307-11.

Yang, D. J. J., X. L. L. Wang, A. Ismail, C. J. Ashman, C. F. Valori, G. Wang, S. Gao, A. Higginbottom, P. G. Ince, M. Azzouz, J. Xu, P. J. Shaw, and K. Ning. 2014. 'PTEN regulates AMPA receptor-mediated cell viability in iPS-derived motor neurons', *Cell death & disease*, 5.

Yang, D., Z. J. Zhang, M. Oldenburg, M. Ayala, and S. C. Zhang. 2008. 'Human embryonic stem cell-derived dopaminergic neurons reverse functional deficit in parkinsonian rats', *Stem Cells*, 26: 55-63.

Yap, T. L., J. M. Gruschus, A. Velayati, W. Westbroek, E. Goldin, N. Moaven, E. Sidransky, and J. C. Lee. 2011. 'Alpha-synuclein interacts with Glucocerebrosidase providing a molecular link between Parkinson and Gaucher diseases', *J Biol Chem*, 286: 28080-8.

Yu, J. Y., S. L. DeRuiter, and D. L. Turner. 2002. 'RNA interference by expression of short-interfering RNAs and hairpin RNAs in mammalian cells', *Proceedings of the National Academy of Sciences of the United States of America*, 99: 6047-52.

Zarranz, Juan J., Javier Alegre, Juan C. Gómez-Esteban, Elena Lezcano, Raquel Ros, Israel Ampuero, Lídice Vidal, Janet Hoenicka, Olga Rodriguez, Begoña Atarés, Verónica Llorens, Estrella Gomez Tortosa, Teodoro del Ser, David G. Muñoz, and Justo G. de Yebenes. 2004. 'The new mutation, E46K, of alpha-synuclein causes Parkinson and Lewy body dementia', *Annals of neurology*, 55: 164-73.

Zeitelhofer, M., J. P. Vessey, Y. Xie, F. Tübing, S. Thomas, M. Kiebler, and R. Dahm. 2007. 'High-efficiency transfection of mammalian neurons via nucleofection', *Nat Protoc*, 2: 1692-704.

Zhang, S. C., M. Wernig, I. D. Duncan, O. Brüstle, and J. A. Thomson. 2001. 'In vitro differentiation of transplantable neural precursors from human embryonic stem cells', *Nat Biotechnol*, 19: 1129-33.

Zhang, Y., K. Chen, S. A. Sloan, M. L. Bennett, A. R. Scholze, S. O'Keeffe, H. P. Phatnani, P. Guarnieri, C. Caneda, N. Ruderisch, S. Deng, S. A. Liddelow, C. Zhang, R. Daneman, T. Maniatis, B. A. Barres, and J. Q. Wu. 2014. 'An RNA-sequencing transcriptome and splicing database of glia, neurons, and vascular cells of the cerebral cortex', *J Neurosci*, 34: 11929-47.

Zhao, M., H. Yang, X. Jiang, W. Zhou, B. Zhu, Y. Zeng, K. Yao, and C. Ren. 2008. 'Lipofectamine RNAiMAX: an efficient siRNA transfection reagent in human embryonic stem cells', *Mol Biotechnol*, 40: 19-26.

Zheng, B., Z. Liao, J. J. Locascio, K. A. Lesniak, S. S. Roderick, M. L. Watt, A. C. Eklund, Y. Zhang-James, P. D. Kim, M. A. Hauser, E. Grünblatt, L. B. Moran, S. A. Mandel, P. Riederer, R. M. Miller, H. J. Federoff, U. Wüllner, S. Papapetropoulos, M. B. Youdim, I. Cantuti-Castelvetri, A. B. Young, J. M. Vance, R. L. Davis, J. C. Hedreen, C. H. Adler, T. G. Beach, M. B. Graeber, F. A. Middleton, J. C. Rochet, C. R. Scherzer, and Global PD Gene Expression (GPEX) Consortium. 2010. 'PGC-1α, a potential therapeutic target for early intervention in Parkinson's disease', *Sci Transl Med*, 2: 52ra73.

Zhou, P., L. Qian, M. D'Aurelio, S. Cho, G. Wang, G. Manfredi, V. Pickel, and C. Iadecola. 2012. 'Prohibitin reduces mitochondrial free radical production and protects brain cells from different injury modalities', *J Neurosci*, 32: 583-92.

Zimprich, Alexander, Saskia Biskup, Petra Leitner, Peter Lichtner, Matthew Farrer, Sarah Lincoln, Jennifer Kachergus, Mary Hulihan, Ryan J. Uitti, Donald B. Calne, A. J. Stoessl, Ronald F. Pfeiffer, Nadja Patenge, Iria C. Carbajal, Peter Vieregge, Friedrich Asmus, Bertram Müller-Myhsok, Dennis W. Dickson, Thomas Meitinger, Tim M. Strom, Zbigniew K. Wszolek, and Thomas Gasser. 2004. 'Mutations in LRRK2 cause autosomal-dominant parkinsonism with pleomorphic pathology', *Neuron*, 44: 601-07.